Molecular Functions of Histone Demethylase MERCK complex on Fungal Development and Secondary Metabolism in Filamentous Fungus *Aspergillus nidulans* and *Aspergillus flavus*

Mevlüt Ulaş BSc, MSc

Maynooth University
National University of Ireland Maynooth

Thesis submitted to Maynooth University
for the degree of Doctor of Philosophy

October 2018

Supervisor:
Dr. rer. nat. Özgür Bayram,
Fungal Genetics & Secondary Metabolism Laboratory (FGSM),
Department of Biology,
Maynooth University,
Maynooth, Co. Kildare,
Ireland

Head of Department
Prof. Paul Moynagh

To my family and Hacer…

Table of Contents

Declaration of Authorship

This thesis has not previously been submitted in whole or in part to this or any other University for any other degree. This thesis is the sole work of the author, apart from generation of *A. nidulans* HA-tagged *kdmA*, *cclA*, *ecmB*, *rstB* strains, which were generated by Betim Karahoda and the analysis of the Bioinformatics data of this study, which was performed by Dr. Chris, Koon Ho Wong.

Mevlut Ulas MSc.

Acknowledgements

First and foremost, I would like to express my very great appreciation to my supervisor Dr. Ozgur Bayram not only for his supervision, encouragement, advice, support, guidance and effort to build my skills but also for giving a family environment throughout my PhD course in Ireland. Thank you so much boss. I would also like to thank Dr. Ozlem Sarikaya-Bayram for her support, encouragement, help, priceless lab protocols with tips and delicious recipes. I highly appreciated all your help, time and advices.

I am grateful to my beautiful oversea collaborators Dr. Chris, Koon Ho Wong, Dr. Kealing Tan and all Chris' Lab members to host me for 8 months in their lab by providing such an amazing hospitality, enjoyable social and research environment and help. I have greatly appreciated your help, time and scientific experience you shared with me. It was a truly amazing experience.

I wish to thank my annual thesis committee members Prof. Paul Moynagh and Dr. Emmanuelle Graciet for their help, constructive comments and recommendations over my PhD course. I would like to acknowledge Science Foundation of Ireland for funding this PhD study. I would like to extend my thanks to all administrative and technical staff of Maynooth University Biology Department for their assistance, help, training and patience.

To all current and past members of FGSM Lab, Dr. Nadia Mohammed El Ramli, Dr. Leandro José de Assis, Dean Frawley, Betim Karahoda, thank you all for your help and for making the lab, science and life more enjoyable during this intense PhD. My special thanks to everyone in the department, for advice, chat when needed, parties and borrowing reagents. Doing PhD in the Callan Building would be such a nightmare without you. And, Marcela Johana Isaza Correa, my special thanks are extended to you for your friendship, warm chats sponsored by Starbucks or Lavazza and always listen to me and my complains regarding PhD.

A huge THANK YOU, individually, to each member of my amazing family, they had been supporting and believing me throughout my whole life. Lastly, my dearest friends Naci Öz (ekrembora07), Varol Güler (Ünalan Prensi) and Hacer Meral (second best intern), there is no word I can use in here to express my gratitude towards you, all I can say is that I would not have completed this PhD if I did not have you. Thank you, for never letting me feel alone, for always keeping me smiley and happy, for sacrificing your time and always being there for me. Life is beautiful with you…

Publications and Presentations

Research Publications

Manfiolli, A.O., Mattos, E.C., de Assis, L.J., Silva, L.P., **Ulas, M.**, Brown, N.A., Bayram, O., Goldman, G.H. (2018). *Aspergillus fumigatus* high osmolarity glycerol mitogen activated protein kinases SakA and MpkC physically interact during osmotic and cell wall stresses. *Front. Microbiol.* (In review).

Ribeiro, L.F.C., Chelius, C., Boppidi, K., Naik, N., Hossain, S., Ramsey, J.J.J.L., Kumar, J., Ribeiro, L.F., Ostermeier, M., Tran, B., Goo, Y.A., de Assis, L.J., **Ulas, M.**, Bayram, O., Goldman, G.H., Lincoln, S., Srivastava, R., Harris, S.D., Marten, M.R. (2018). Comprehensive analysis of *A. nidulans* PKA phosphorylome identifies a novel mode of CreA regulation. *mBio* (In revision).

Elramli, N., Karahoda, B., Sarikaya-Bayram, O., Frawley, D., **Ulas, M.**, Oakley, C.E., Oakley, B.R., Seiler, S., Bayram, O. (2018). Assembly of a heptameric STRIPAK complex is required for coordination of light-dependent multicellular fungal development with secondary metabolism in *Aspergillus nidulans*. *PLoS Genet.* (In revision).

de Assis, L.J., **Ulas, M.**, Ries, L.N.A., El Ramli, N.A.M., Sarikaya-Bayram, O., Braus, G.H., Bayram, O., Goldman, G.H. (2018). Regulation of *Aspergillus nidulans* CreA-mediated catabolite repression by the F-box proteins Fbx23 and Fbx47. *mBio* **9**: e00840-18.

Manfiolli, A.O., de Castro, P.A., Dos Reis, T.F., Dolan, S., Doyle, S., Jones, G., Riaño Pachón, D.M., **Ulaş, M.**, Noble, L.M., Mattern, D. J., *et al.* (2017). *Aspergillus fumigatus* protein phosphatase PpzA is involved in iron assimilation, secondary metabolite production, and virulence. *Cell. Microbiol.* **19**: e12770.

Oral Presentations

14th European Conference on Fungal Genetics (ECFG14), Haifa, Israel: Assis, L.J., **Ulas, M.**, Ries, L.N.A., El Ramli, N.A.M., Sarikaya-Bayram, O., Braus, G.H., Bayram, O., Goldman, G.H. Regulation of Aspergillus nidulans CreA-mediated catabolite repression by the F-box proteins Fbx23 and Fbx47. February 2018

Poster Presentations

Annual Irish Fungal Society Meeting, Maynooth, Co.Kildare, Ireland: Role of Histone Demethylase KdmA Complex in the Control of Fungal Development and Secondary Metabolite Production in Aspergillus nidulans and Aspergillus flavus. **Ulas, M.**, Karahoda, B., Sarikaya-Bayram, O., Bayram, O., June 2018

Irish Fungal Society, Austrian Society for Medical Mycology and British Society for Medical Mycology (joint meeting), Malahide, Co.Dublin, Ireland: Role of histone demethylase KMRCS complex in the control of fungal development and secondary metabolite production in Aspergillus nidulans and Aspergillus flavus. **Ulas, M.**, Karahoda, B., Sarikaya-Bayram, O., Bayram, O., March 2016

Abbreviations

A2MDB	Aspergillus Secondary Metabolites Database
AFs	Aflatoxins
AspGD	Aspergillus Genome Database
bZIP	Basic leucine zipper transcription factor.
C-terminus	Carboxy-terminus
CDP	Central Developmental Pathway
C_2H_2	Cys_2-His_2 zinc finger
CBP	Calmodulin binding peptide
ChIP	Chromatin Immunoprecipitation
COMPASS	Complex of Proteins Associated with Set1
CPA	Cyclopiazonic acid
DNA	Deoxyribonucleic Acid
DEL	Deletion
DIG	Digoxigenin
dH_2O	distilled water or deionized water
ddH_2O	double-distilled water or deionized water
DTT	DL-dithiothreitol
EDTA	Ethylenediamine teraacetic acid
EMS	Ethyl methanesulfonate

GFP	Green Fluorescent Protein
GMM	Glucose Minimal Medium
gDNA	Genomic Deoxyribonucleic Acid
g	Gram
H_2O_2	Hydrogen peroxide
HCl	Hydrochloric Acid
h	Hour
HA	Hemagglutinin
HATs	Histone acetyltransferases
HDACs	Histone deactylaseses
HU	Hydroxyurea
HREs	Hormone Response Elements
IgG	Immunoglobulin G
KDa	Kilo Dalton
kbp	Kilo base pair
L	Litre
Lac	Lactose
LB	Luria Bertani Broth
LC-MS	Liquid chromatography, tandem mass spectrometry
MACS	Model-based Analysis of ChIP-seq
MAPK	Mitogen-activated protein kinase

MERCK	McmA-EcmB-RstB-CclA-KdmA
Min	Minute
MAT	Mating type genes
MS	Mass Spectrometry
MMS	Methyl methanesulfonate
mRFP	Monomeric red fluorescent protein
mM	millimolar
mg	milligram
ml	millilitre
NLS	Nuclear localization signal
NRPS	Non-ribosomal peptides
N-terminus	(NH_2) Amino-terminus
natR	nourseothricin resistance gene
nm	nanometer
ORF	Open Reading Frame
NaCl	Sodium Chloride
NaOH	Sodium Hydroxide
P	Probability value
PCA	Principal Component analysis
PCR	Polymerase chain reaction
pH	Potential of hydrogen

PKS	Polyketides
PMSF	Phenylmethylsulfonyl fluoride
PN	ß-lactam Antibiotic Penicillin (Penicillin)
PTMs	Post translational modifications
ptrA	Pyrithiamine resistance gene A
qRT-PCR	Quantitative real-time polymerase chain reaction
qPCR	Quantitative polymerase chain reaction
RT	Room Temperature
RP-HPLC	Reversed phase-high performance liquid chromatography
ROS	Reactive Oxygen Species
RNA	Ribonucleic acid
SDS	Sodium dodecylsulfate
SMURF	Secondary Metabolite Unknown Region Finder
SMs	Secondary metabolites
SUMO	Small ubiquitin-like modifier protein
ST	Sterigmatocystin
TFIIB	Transcription factor II B
TAP	Tandem Affinity Purification
TBP	TATA binding protein
TFA	Tri Fluoroacetic Acid
TBS	Tris buffered saline

TBST	Tris-buffered saline tween
TES	Transcriptional end site
TFs	Transcription factors
Trp	Tryptophan
TSS	Transcriptional start site
UV	Ultraviolet radiation
UTR	Untranslated region
v/v	Volume per volume
WKM	Wickerham Medium
WT	Wild-type
w/v	Weight per volume
YES	Yeast Extract Sucrose Medium
YGT	Yeast Glucose Trace Medium
µm	Micrometre
µg	Microgram
Δ	Deletion

Summary

Fungi has ability to produce a wide range of natural products called secondary metabolites. The production of these metabolites is tightly related with fungal development. SM production and development were shown to be affected by environmental factors such as light, pH and CO_2 level. Many of studies reported that regulation of these two processes is carried out by regulatory heteromeric protein complexes. SM production has been also shown to be associated with post-translational modifications in *A.nidulans*. Recently reported histone demethylase KdmA effects development and SM mechanisms in *A.nidulans*. This research study demonstrates molecular role of KdmA as well as its interacting proteins in *A.nidulans* and plant pathogen *A.flavus*. Comparative affinity purification coupled-MS analysis of KdmA showed that it phiscally interacts with four proteins McmA, EcmB, RstB, CclA and lead to form a complex(MERCK). Complex formation was also confirmed by performing MS-based analysis of other members by using different tags TAP, GFP, HA and MYC in *A.nidulans* and *A.flavus*. Morphology analysis revealed that deletion of *cclA* and *ecmB* cause significant decrease on sexual and asexual growth structures production as well as colony size in *A.nidulans* and *A.flavus*. Individual single and double deletion mutants of complex members exhibited significant alterations on production of secondary metabolites in both organisms. In addition, subcellular localization of complex members was investigated by using laser confocal microscopy and they were found to be localized in the nucleus. MS-based analysis showed no physical interaction between complex members in the absence of KdmA in *A.nidulans*. Genome-wide binding analysis (ChIP-seq) of complex members indicated common targets on the genome in *A.nidulans* supporting the effects on development and SM production and complex formation analysis data. Further active gene expression analysis (RNA pol II ChIP-seq) of complex members presented downregulation of SM and fungal development related genes in *A.nidulans* particularly repressor role of CclA on SM. It was also found that KdmA and CclA play a critical role on PTMs. H3K4me3, H3K9me3 and H3K36me3 mark signals significantly influenced in the absence of *cclA* in *A.nidulans*. Overall, this study highlights molecular function of MERCK complex by facilitating molecular genetics and biochemical approaches.

Chapter 1

Introduction

1.1 Control of gene expression

The gene expression term is used to describe the producing of different gene products in order to attain desired cell functions. Although the majority of these gene products are proteins, there are also some genes encoding non-coding RNAs which have crucial roles. The gene expression is carried through the processes of transcription, post-transcriptional modifications (RNA splicing), translation and post-translational modifications. It starts by transcription of DNA fragments into primary RNA molecules and followed by RNA splicing to generate messenger RNA (mRNA). Once the mRNA is produced, it is transported to the cytoplasm where it is translated into targeted polypeptide chains. These crucial processes are regulated through different checkpoints within the cell (**Figure 1.1**). In both prokaryotes and eukaryotes, housekeeping genes are constitutively expressed under all growth conditions. However, in prokaryotes, many other genes are expressed in response to their environment. In prokaryotes, induction of transcription often occurs in response to stimuli such as autoinducer chemical molecules, light, temperature and substrates, however, this process occurs less often in eukaryotes (Vilar *et al.*, 2003; Klug *et al.*, 2006).

Additionally, in eukaryotes, the regulation of gene expression is required to maintain homeostasis in the cells. DNA methylation has critical roles for the regulation of gene expression in both prokaryotes and eukaryotes. Cytosine and adenine bases of DNA can be methylated by DNA methytransferases. The methylation of DNA is generally related to the silencing of transcription (Kako *et al.*, 2018).

The chromatin structure of eukaryotic DNA is associated with the regulation of transcription. Acetylation, ubiquitination, phosphorylation, SUMOylation and methylation of histone proteins are major post-translational modifications (PTMs) that play crucial roles in both activating and repressing gene expression (Gillette and Hill, 2015). DNA methylation and PTMs of histone proteins will be discussed further in [Chapter 1.2].

Transcription factors (TFs) are proteins, which have one or more DNA-binding domains (DBD), and they are necessary for the regulation of gene expression. (Zhang *et al.*, 2017). Binding to a specific DNA sequence, TFs can either activate or repress gene transcription. TFs can be classified as general or specific transcription factors. General transcription factors interact with the promoter regions of all genes, which are transcribed by

RNA polymerase II, while specific TFs allow the individual genes to be active or silent specifically (Sperling, 2007).

In eukaryotes, several modifications are required to produce functional mRNA, including 5' capping, splicing and polyadenylation. The 5' terminus of mRNA acquires a 7-methylguanylate-cap structure, which is critical for mRNA stability and translation. Cap-binding protein complex (CBC) binds to capped mRNA and regulates the nuclear export of mRNA. The eukaryotic genome is comprised of many non-coding sequences known as introns. RNA splicing is a modification that removes introns from precursor mRNA (pre-mRNA) to form mature mRNA. The spliceosome is a small nuclear ribonucleo protein (snRNPs) complex and splicing reactions are generally catalyzed by this enzyme. Addition of a poly(A) tail at the 3' end of mRNA is recognized as polyadenylation, which is also crucial for stability, nuclear export and translation of mRNA (Sperling, 2007; Lackner and Bahler, 2008).

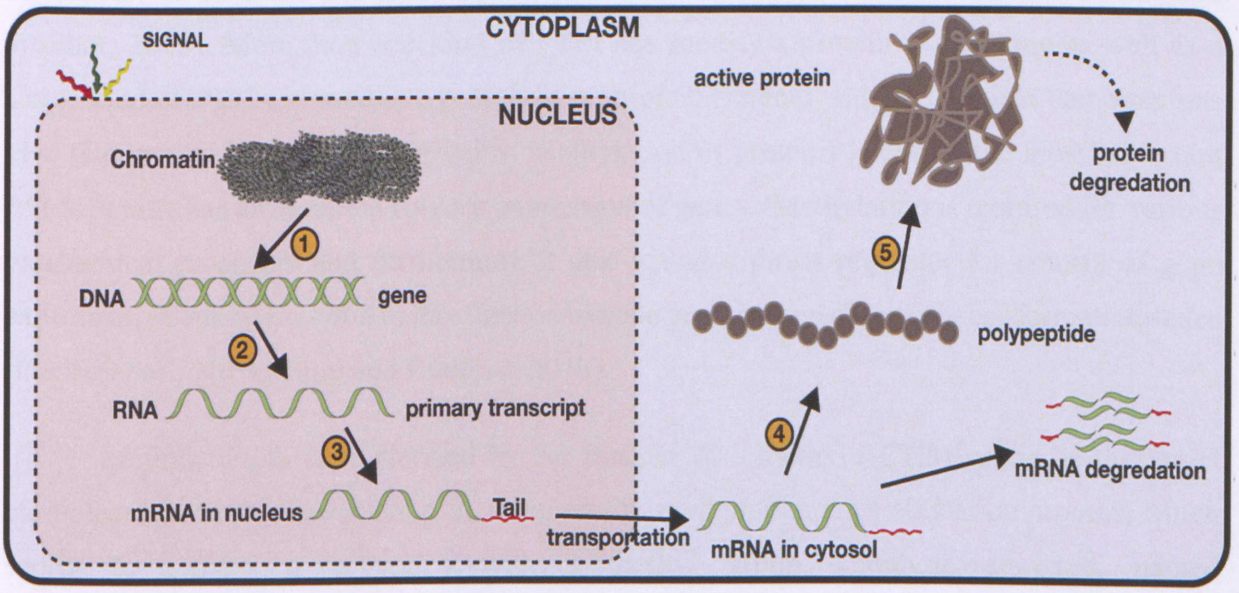

Figure 1.1 Main eukaryotic gene expression control levels. 1. Genome level includes amplification of DNA segments, chromatin condensation, DNA methylation, histone modifications. **2.** Transcription of primary RNA transcript. Mainly controlled by transcription factors. **3.** RNA processing (RNA splicing) and nuclear exportation to cytoplasm occur in this level. **4.** Translational level. Polypeptide synthesis and mRNA degradation take place. Translation is controlled by translation initiation factors and repressors including microRNAs. **5.** Posttranslational level. This level includes the control of protein folding and assembly,

possible polypeptide cleavages, modifications and transportation to organells. Adapted from *Pearson Education Inc.*

1.2 Post-translational modifications (PTMs)

Post-Translational Modifications (PTMs) are a regulatory mechanism of the cell that play critical roles in growth, development and reproduction. PTMs generally correspond with the attachment of a covalent group to amino acid residues in a protein, consequently modifying the protein's activity, function or localization and this modification is mostly reversible (Hochstrasser, 2009; Prabakaran *et al.*, 2012). Over 200 kinds of PTMs are identified to modify eukaryotic proteins. Several examples for prevalent modifications are phosphorylation, glycosylation, ubiquitination, SUMOylation, acetylation, methylation, disulfide bridge formation and lipidation that have enormous effects on numerous cellular processes, including the expression of genes and protein-protein interactions (Karve and Cheema, 2011; Duan and Walther, 2015). More than one kind of PTM can modify a protein at one time as well as a single kind of PTM can modify a protein at multiple different residues. Multiple combinations give rise to a wide variety for proteins. Methylation of proteins is one of the most important PTMs, which has an essential role for expression of genes. Methylation is required for various biochemical processes and furthermore it also act as a direct regulator for control of gene expression in eukaryotes due to its effect on histone proteins and chromatin conformation states (Deribe *et al.*, 2010; Yang and Bedford, 2013).

Methylation is characterized by the transfer of a methyl (-CH3) group on the target biomolecules via a covalent bond. In other words, methylation is an alkylation process, which serves to replace a hydrogen with a methyl group. Catalytic enzymes, named methyltransferases mediate the methylation reactions in cells. Methyltransferases methylate a variety of substrates such as proteins, DNA, RNA (mRNA, rRNA, tRNA, miRNA), lipids, carbohydrates, small organic molecules and heavy metals. The *S*-adenosyl-L-methionine (SAM), also named AdoMet, is generally a cofactor for methylation and is synthesized from ATP and amino acid L-methionine. (Smith and March, 2001; Struck *et al.*, 2012; Kako *et al.*, 2018). Chemically reactive SAM, as a methyl donor, is formed by bonding a methyl group to the sulphur atom of methionine. Methylation is one of the most prevalent PTMs in proteins. These modifications influence gene expression levels (phenotype), which is generally called epigenetics, but do not cause any change in the information encoded by DNA (Karve and Cheema, 2011; Sen and Keung 2018).

Methylation of DNA takes place in both prokaryotes and eukaryotes. Particularly, Cytosine-phosphate-Guanine (CpG) dinucleotide is methylated, which cause the 5-methylcytosine (5-mC) form. In prokaryotes, as well as cytosine, adenine residues are also methylated and this is required for postreplication repair mechanisms. In many prokaryotes, methylation of DNA acts as a part of the restriction modification system. Additionally, Dam adenine methyltransferase methylates the prokaryotic DNA at the adenine of a GATC motif. Methylation protects the host DNA from sequence specific restriction enzymes, which digest the foreign unmethylated DNA such as viral DNA (Low and Casadesus 2008; Brocato and Casto 2013). Methylation of DNA has been widely investigated in numerous eukaryotes including vertebrates, invertebrates, plants and fungi; furthermore, it is prevalent in plants and mammals while restricted in insects and fungi. For instance, *Aspergillus nidulans, Schizosaccharomyces pombe* and *Saccharomyces cerevisiae* have almost completely lost the capability of DNA methylation, however, *Neurospora crassa* has the DNA methylation capability (Selker *et al.*, 2003; Lee *et al.*, 2008; Kako *et al.*, 2018).

Methylation is a significant modification of DNA and plays a critical role in many processes such as cancer, regulation of gene expression, inactivation of X-chromosomes and repression of retroviral repetitive elements. In mammals, 60-80% of CpG dinucleotides are methylated. The unmethylated CpG sequences are often clustered and are named CpG islands (CGIs) that are generally found in the promoters of many genes including tissue-specific and housekeeping genes. In the promoters of tumor supressor genes, spontaneously hypermethylated CGIs lead to silencing of these genes which eventually triggers cancer growth (Brocato and Costa 2013; Smith and Meissner, 2013; Kako *et al.*, 2018).

1.3 Eukaryotic chromatin

In the nuclei of eukaryotic organisms, chromosomes are tightly packed together with histone and nonhistone proteins to form the complex called chromatin (**Figure 1.2**). It has been recorded that eukaryotic genomes contain five major histone groups; H2A, H2B, H3, H4, which form the histone core and H1/H5 which has a linker role between the cores. Each two copies of four histone types form the octamers. Around 147 base pairs (bp) of negatively charged DNA is wrapped around octamers containing the histone core roughly 1.65 times by positively charged side chains of histones (usually on lysine and arginine residues) (Luger *et al.*, 1997; Struhl and Segal, 2013; Lieleg *et al.*, 2015). This basic unit of packed DNA is known as the nucleosome, which represents the beads on a string (10 nm fiber) shape of chromatin.

Nucleosomes are connected to each other by a short segment of linker DNA. Binding of the histone H1 between the nucleosomes helps the establishment of helical chromatin structure. This binding equilibrates the interaction of DNA with the histone cores (Felsenfeld and Groudine 2003; Robinson *et al.*, 2006). Furthermore, condensed structure of these fibers are called metaphase chromosomes. As well as the role of packaging DNA in a very small volume of nucleus, chromatin also protects the DNA from damage (Chi *et al.*, 2010). Moreover, chromatin plays a crucial role in the replication of DNA and the expression of genes. In the nucleus, chromatin is divided into two forms: lightly packaged "euchromatin", which is highly active in gene transcription and more tightly packaged "heterochromatin", which is less active in gene transcription. During the S-phase of the cell cyle, heterochromatin slowly replicates. Under a microscope, heterochromatin regions appear darker than euchromatin regions. Heterochromatin can be partitioned into two categories, constitutive and facultative heterochromatin. Constantly packed, constitutive heterochromatin exists in all phases of the cell cycle and covers the genomes repetitive elements including telomeres, centromeres and transposable elements and it ensures genome stability. By contrast, more flexible facultative heterochromatin is cell cycle phase-specific and can be transformed into euchromatin.

Hence, depending on the cell cycle phase and environmental signals, genes in the facultative heterochromatin can be activated or silenced. Histone post-translational modifications (PTMs) control the interconversion of the facultative heterochromatin and euchromatin. These versions of post-translational modifications on histone proteins known as histone codes. (Grewal and Elgin, 2007; Saksouk *et al.*, 2015; Becker *et al.*, 2017).

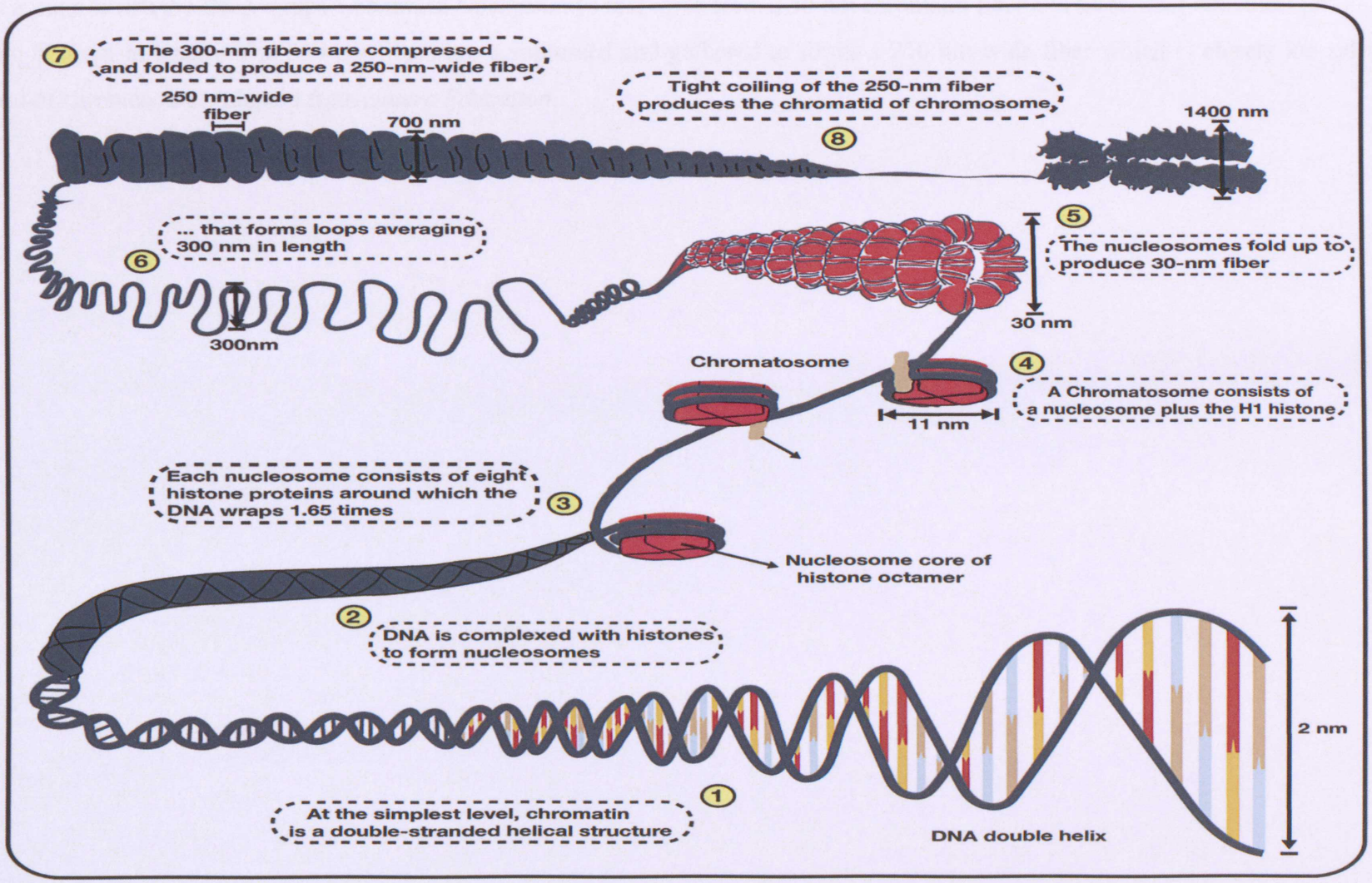

Figure 1.2: Eukaryotic chromosome structure. Chromosomes consist of packaged DNA which is tightly wrapped around histone proteins. Negatively charged DNA strongly bound around positively charged histones and make the nucleosomes. Each nucleosome consists of eight histone

proteins around which the DNA wraps 1.65 times. Nucleosomes fold up to form a 30-nm chromatin fiber and these fiber structures produce loops averaging 300-nm in length. The 300 nm fibers are compressed and gathered to forms a 250 nm-wide fiber which is closely looped into the chromatid of chromosome. Adapted from *Nature Education*.

1.4 PTMs of histone proteins

N-terminal tails of histone proteins are subjected to many post-translational modifications, which control the silencing or expression of genes. The role of some histone PTMs are described, but many of them are still unknown (Chi *et al.*, 2010; Gacek-Matthews *et al.*, 2015). The language of histone PTMs is very complex and is shaped by writer, eraser and reader enzymes. While writer enzymes add PTMs to histones, erasers remove specific PTMs from histones. Furthermore, reader enzymes recognize the PTM marks on histones (Fischle, 2012; Gillette and Hill, 2015). Five major PTMs of histones are acetylation, ubiquitination, phosphorylation, SUMOylation and methylation.

Acetylation is a very broadly studied PTM and is recognized as the addition of an acetyl group to the N-terminal tail of histones or to lysine residues. The acetylation of histone proteins is required for many processes; including silencing of heterochromatin, nucleosome assembly, condensation and folding of chromatin and gene expression, which is generally induced by acetylation. Histone acetylation and deacetylation are catalyzed by histone acetyltransferases (HATs) and histone deacetylases (HDACs). Acetylation positively regulates gene expression by decreasing the positive charge on lysine residues and consequently lessens the affinity between the histones and DNA (Shahbazian and Grunstein, 2007; Gillette and Hill, 2015).

Ubiquitination is one of the less well-understood PTM processes, characterized by the attachment of an 8.5kD ubiquitin protein to lysine residues. Ubiquitination and deubiquitination of histones are catalyzed by histone ubiquitin ligases and deubiquitinating enzymes, respectively. Histone ubiquitination is involved in diverse and essential cellular processes including DNA repair signaling, activation and regulation of gene expression (Cao and Yan, 2012; Alhamwe *et al.*, 2018).

Phosphorylation of histones is characterized by the attachment of phosphate groups to serine, threonine and tyrosine residues. Phosphorylation and dephosphorylation of histones are controlled by kinases and phosphatases, respectively. Histone phosphorylation has important roles in the regulation of transcription, chromatin compaction during cell division, apoptosis and DNA repair mechanism (Rossetto *et al.*, 2012).

Histone SUMOylation occurs at lysine residues via the attachment of the small ubiquitin-like modifier (SUMO) protein (10-kDa). SUMOylation of histones is a reversible modification that has roles in the DNA repair process and transcription. For example, SUMOylation of H4 results in the repression of transcription via recruiting HDAC, which removes acetyl groups. SUMOylation of H4, H2A and H2B in *Saccharomyces cerevisiae* leads to silencing of the transcription (Shiio and Eisenman, 2003; Nathan *et al.*, 2006; Harting *et al.*, 2013).

Acetylation and methylation are the most commonly studied histone PTMs, hence methylation will be discussed in detail (Bhaumik *et al.*, 2007). Methylation of histone proteins can take place on arginine, lysine and histidine residues. Lysine residues can be subjected to mono (me1), di (me2), or tri (me3) methylation and arginine residues can be subjected to mono or di methylation, however it has been reported that histidine residues can also be mono-methylated but this methylation is rare and it has not been well characterized. Dimethylation of arginine residues can be either symmetric or asymmetric (Greer and Shi, 2012). Methylation of histone proteins was thought to be an irreversible modification, however, the discovery of histone demethylases (HDMTs) has shown the reversibility of this modification (Shi *et al.*, 2004; Klose *et al.*, 2006). Regulation of histone methylation and demethylation are catalyzed by the histone methyl transferases (HMTs) and histone demethylases (HDMTs), respectively. However, any arginine residue catalyzed by HDMTs has not been reported. HMTs are usually divided into two groups: arginine N-methyltransferases and lysine N-methyltransferases. S-adenosylmethionine (SAM or AdoMet) is used as a cofactor by both HMTs. Methylation of histones is related to either repression or activation of gene expression. The position of the methylation and number of the transfered methyl groups both influence the functions of histone methylation (Araki and Mimura, 2017). There are several kinds of HDMs that specifically catalyze demethylation of lysine residues; the KDM1/LSD family, which contain the flavin adenine dinucleotide (FAD) dependent amine oxidases, KDM2-6 family (Jumonji C domain-containing HDM) and others (Labbe *et al.*, 2014, Araki and Mimura, 2017). Histone H3 and H4 proteins have the most widely studied methylation sites, but histone H1, H2A and H2B also have methylation sites (Greer and Shi, 2012).

Methylation of histone H3 at lysine 4 (H3K4), lysine 36 (H3K36) and lysine 79 (H3K79) is generally linked with active gene transcription. There are two kinds of HMTs that specifically catalyze lysine residues; one of them is Su(var)3-9, Enhancer of Zeste, Trithorax

(SET) domain HMT, which was identified in *Drosophila melanogaster*, and the other is non-SET domain HMT (Freitag, 2017). Mono-, di- and trimethylations of H3K4 (H3K4me1, H3K4me2, and H3K4me3) positively regulate transcription and H3K36me3 methylation takes place the active gene expression as well as these modifications are catalyzed by the SET domain HMTs. Moreover, H3K79me3 methylation is involved in active gene expression in yeast and is methylated by the non-SET domain HMTs. SET1 proteins create a complex named COMPASS (Complex of Proteins Associated with Set1), which catalyze H3K4 methylation and are conserved from yeast to human. On the other hand, SET2 HMT controls H3K36me3 methylation. Additionally, the KDM2 family, KDM4 family and NO66 HDMs demethylate the H3K36. H3K79 is methylated by the Non-SET domain Dot1 as well as demethylation of H3K79 is mediated by PHF8 (Strahl *et al.*, 2002; Gu and Lee, 2013; Araki and Mimura, 2017).

H3K9 m2 and H3K9 m3 methylations play important roles in the formation of constitutively silent heterochromatin while the level of H3K9 m1 is found to be increased in active promoters. Heterochromatin protein 1 (Swi6 in *S. pombe*, HepA in *A. nidulans*, HP1 in human) attaches to H3K9 m3 and accumulates in this mark, eventually resulting in silencing of the transcription (Barski *et al.*, 2007; Reyes-Dominguez *et al.*, 2010). H3K27 methylation is related to repression of transcription and controlled by PRC2 (polycomb repressive complex 2). Like H3K9, H3K27 m2 and H3K27 m3 levels are found to be increased in silenced promoters while H3K27 m1 levels are found to be elevated in active genes (Jiao and Liu, 2015; Araki and Mimura, 2017). Trimethylation of H4K20 is detected in heterochromatin and catalyzed by several SET domain HMTs (Freitag, 2017).

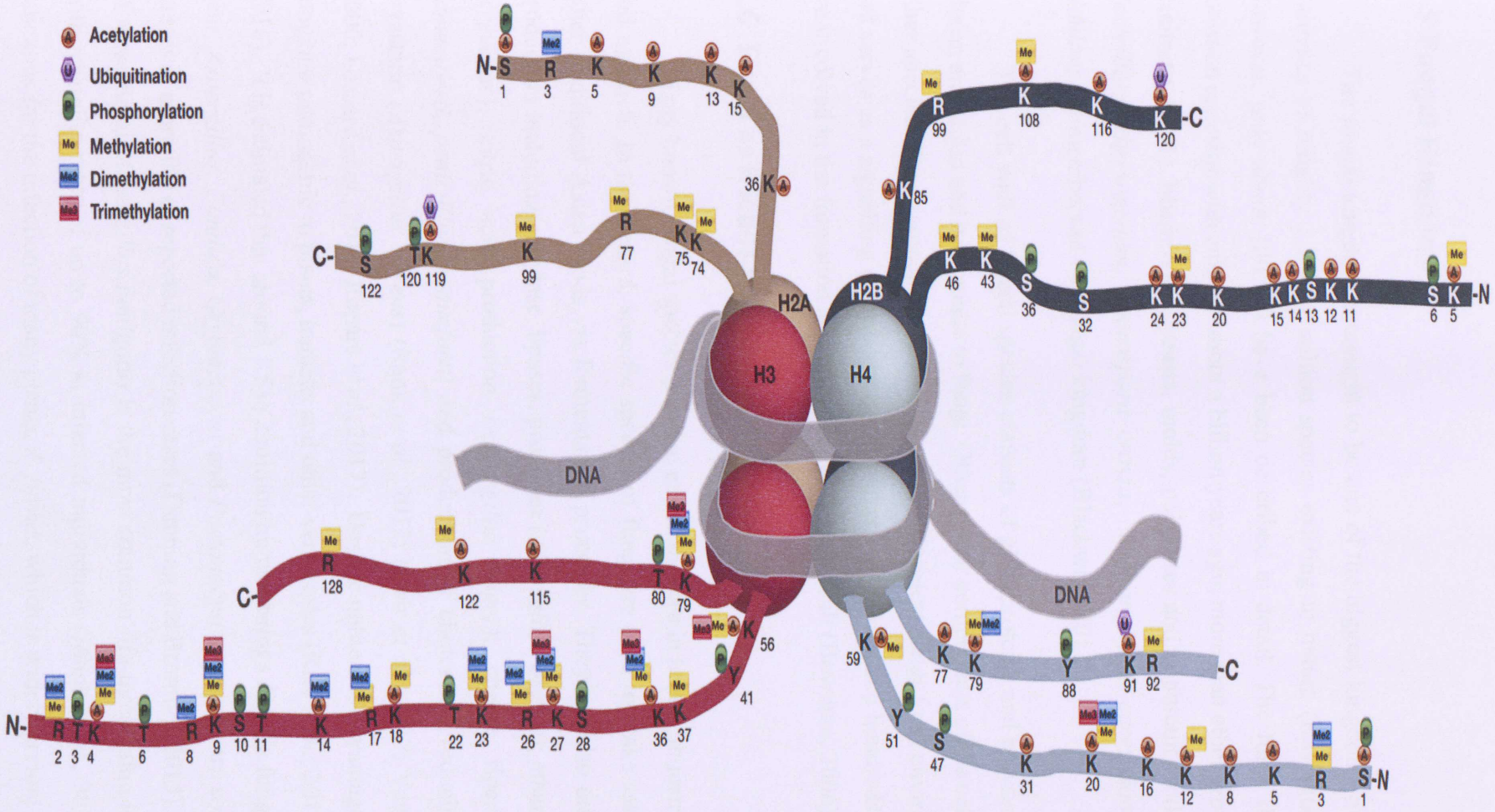

Figure 1.3: Detailed illustration of histone modifications. The known histone modifications sites are showed on each histone with different colours. One site can be modified more than once with different modifications. Only acetylation(orange), ubiquitination(purple), phosphorylation(green) and methylation (mono(yellow)-, di(blue)- and tri(red)) are illustrated in here. Adapted from *ReactionBiology* poster.

1.5 Fungal Kingdom

The fungal kingdom is thought to be one of the biggest kingdoms of organisms, with estimates of roughly 1.5 to 5 million species existing in nature (Kawaguchi *et al.*, 2013). However, only about 100,000 have been described in detail. The fungi descended from a common ancestor with animals about a billion years ago, more than other groups of eukaryotes (Heitman, 2011). Mushrooms, yeasts, molds, polypores and important model organisms like *Penicillium chrysogenum*, *Neurospora crassa*, *Saccharomyces cerevisiae* and *Aspergillus nidulans* are members of the fungal kingdom (Blackwell, 2011).

The cell wall of fungal species consists of glycoproteins and polysaccharides, mainly glucan and chitin and it is unique to fungi. Other minor components of the cell wall differ from other species. The presence of a cell wall serves to protect fungi from environmental stresses and serves as a signalling centre. Many biosynthetic pathways and hundreds of gene products are involved in the formation and reshaping of the cell wall (Bowman, 2006).

1.6 Fungi as friends and foes of mankind

Many known fungal species perform essential roles in health, industrial biotechnology and research. In this regard, specific species of fungi are used to make sake, soy sauce and other traditional Asian foods via fermentation processes. They are also utilised for enzyme production including; amylase, lipases, proteases (*Aspergillus oryzae*); ethanol production (*S. cerevisiae*); citric acid production (*Aspergillus niger*); cheese ripening (*penicillium camemberti, penicillium roqueforti*) and production of cholesterol reducing drugs such as lovastatin (*Aspergillus terreus*) (Rank *et al.*, 2012; Nasir *et al.*, 2017; Vandenberghe *et al.*, 2000; Lessard *et al.*, 2014; Ropars *et al.*, 2017). Despite numerous advantagous species, some fungi are pathogenic to plants, humans and other vertebrates (Ries *et al.*, 2017; Satterlee *et al.*, 2016). It is estimated that around 1.5 to 2 million human beings die of a fungal infection every year. *Aspergillus, Candida, Cryptococcus* and *Pneumocystis* generas are some of the highest causes of mortality of reported infection cases (Denning and Bromley, 2015). Among the range of these fungi, *Aspergillus fumigatus* is the most common life-threatening infectious species, with mortality rates of up to 90% in infected individuals (Jöhnk *et al.*, 2016). Fungi is also infamous for the infection of many plants. *A. flavus*, which is widely present on foodstuffs and

important crops, is a serious threat to both human and animal health due to the production of the carcinogenic mycotoxin, aflatoxin. Along with *A. flavus, A. parasiticus* also contaminates agricultural crops and produces aflatoxin. Contamination of crops with these fungi has caused enormous food shortages and agricultural economic losses all over the world (Amaike and Keller, 2011; Liang *et al.*, 2017).

1.7 *Aspergillus nidulans* as a eukaryotic model system

The obligate aerobe Aspergilli are members of filamentous ascomycetes. *Aspergillus* species are not selective to abiotic conditions and are among the most omnipresent fungi all over the world (Krijgsheld *et al.*, 2013). *A. nidulans* (*Emericella nidulans*) was introduced to science in 1953 (Pontecorvo *et al.*, 1953). *A. nidulans* can undergo three different methods of reproduction; vegetative, asexual and sexual and it is established as a model organism for genetics and cell biology (Todd *et al.*, 2007). *A. nidulans* has a 31 Mb genome, which is distributed over eight chromosomes, encodes around 11,000 genes and has been sequenced (Galagan *et al.*, 2005). Around 90% of these genes are still uncharacterized (Cerqueira *et al.*, 2014). Due to its haploid genome, the impact of genetic manipulations can be observed as phenotypes. Additionally, *A. nidulans* is a non-pathogenic fungus which minimizes the risks of use and it can be easily cultured in laboratory conditions (Casselton and Zolan, 2002). Research using *A. nidulans* has made significant contributions to our knowledge of the cell cycle, spore development, DNA repair, cell polarity, signalling, pH control, primary and secondary metabolism (Todd *et al.*, 2007).

1.7.1 Development of *A. nidulans*

Vegetative growth of *A. nidulans* starts with germination of a spore in a certain direction under appropriate conditions. Germination of spores can be easily affected by environmental factors such as light, conidial density or the presence of 8-carbon oxylipins (Oiartzabal-Arano *et al.*, 2016). Following germination, a germ tube (hypha) extends and grows in a polarized manner by apical extension. Hyphal growth, repeated branching and nuclear mitosis generate a multinucleate cellular network collectively known as the mycelium (Riquelme, 2013; Takeshita *et al.*, 2014). This basic form of fungal growth generates the enlargement of the plasma membrane, cell wall components biosynthesis and as the vesicle supply center the apical body of the Spitzenkörper. After 16-20 hours of growth, some of the hyphal cells cease normal growth and can be induced by environmental stimuli to undergo the

asexual or the sexual reproduction cycle (Bayram and Braus, 2012). Vegetative growth occurs only in submerged cultures, whereas asexual and sexual development requires an air-medium interface.

After a period of vegetative growth, *A. nidulans* cells become competent for reception of environmental signals and begin development asexually in the presence of light and a sufficient carbon dioxide/oxygen ratio (Adams *et al.*, 1998). Asexual development starts with differentiation of the mycelium to a thick-walled foot cell which extends to form the stalk. The stalk continues to grow and differentiate into a vesicle. This results in production of finger-like metulae and phialides. The phialides are mitotically highly active and produce mitotic asexual conidiospores that can produce new colonies. A complete asexual structure is known as a conidiophore (Adams *et al.*, 1998; Etxebeste *et al.*, 2010; Krijgsheld *et al.*, 2013).

Homothallic (self-fertility) fungi are capable of sexual reproduction with or without a mating partner while heterothallic (obligate out-crossing) fungi require a mating partner. The homothallic fungus *A. nidulans* can complete sexual reproduction by means of self-fertilisation (Braus *et al.*, 2002; Yun *et al.*, 2000). Competent *A. nidulans* cells begin development sexually when the conditions are favorable (in the dark and under elevated carbon dioxide concentrations). Sexual fruit body (cleistothecium) development starts with the formation of a dikaryon, which is the fusion of two ascogonial hyphae. This is followed by the creation of nest-like specialized tissue consisting of thick-walled Hülle cells that are responsible for protection and nourishment of the developing cleistothecium (Sarikaya-Bayram *et al.*, 2010). Within the nests, the primordium is formed which matures to produce a closed fruiting body, the cleistothecium where meiosis and nuclear fusion take place. Fusion of haploid nuclei leads to the formation of asci (Sohn and Yoon, 2002). This is followed by a meiotic and a mitotic cell division that generates eight haploid ascospores that contain eight nuclei. After an additional mitosis without cell division leads to mature binucleate ascospores. The ascospore wall accumulates the characteristic red pigment, asperthecin. The mature cleistothecium may harbour up to 80.000 viable ascospores with a diameter of approximately 150-200 µm (Braus *et al.*, 2002; Champe *et al.*, 1994; Szewczyk *et al*, 2008).

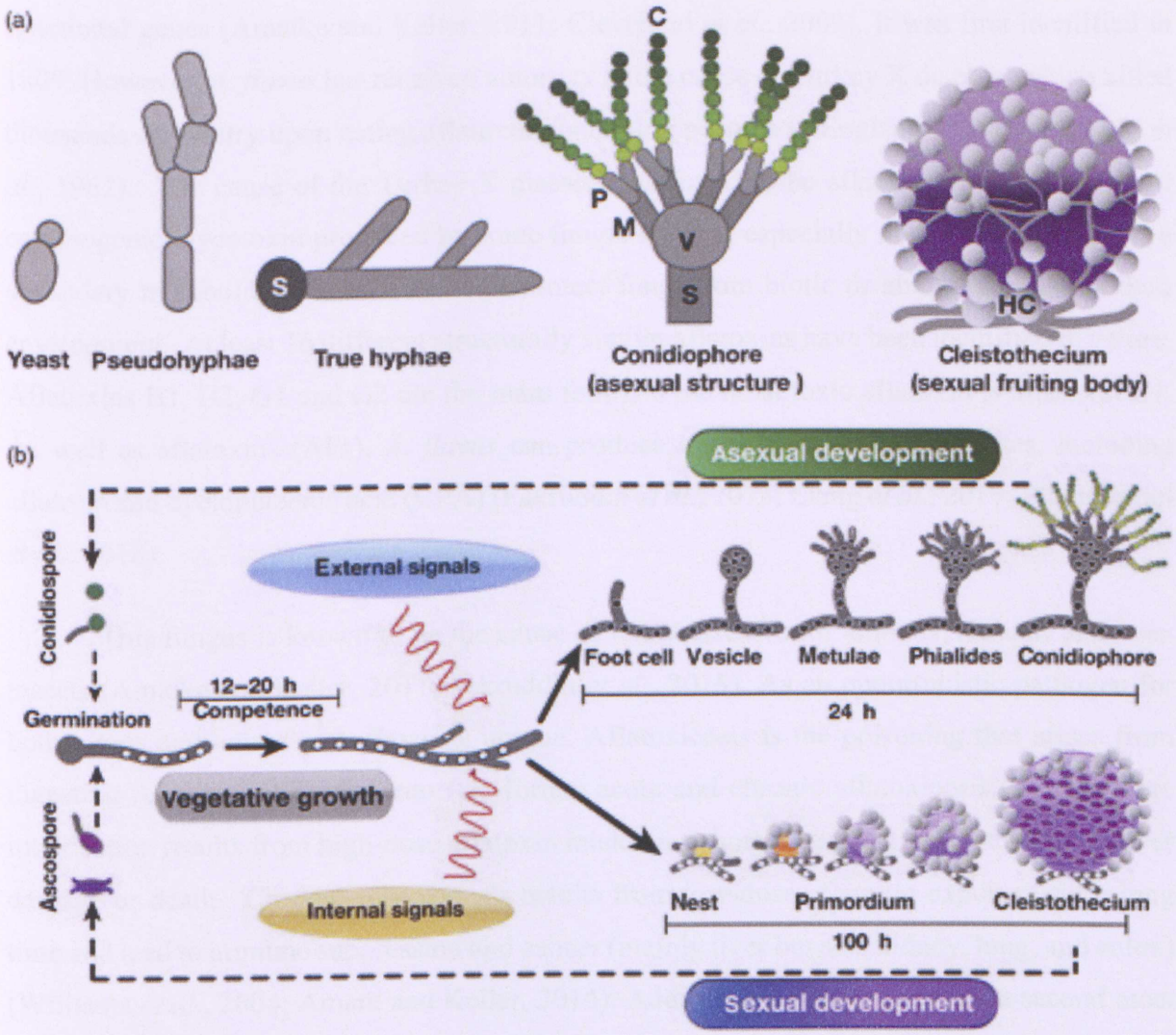

Figure 1.4 Fungal cell types and life cycle of model fungus *Aspergillus nidulans*. (a) Yeast form; pseudohyphae (prolonged cells); true hyphae; conidiophore; cleistothecium. S, stalk; V, vesicle; M, metulae; P, phialides; C, conidia; HC, Hülle cells. (b) Life cycle of the A. nidulans from vegetative growth to asexual or sexual alternatives of development. Briefly, A.nidulans forms hyphae structure in liquid media, undergoes asexual development and produce conidiophore structures in the presence of light. It forms cleisthothecium structures which includes ascospores inside through sexual development under dark conditions (Bayram and Braus, 2012).

1.8 Human and plant pathogen *Aspergillus flavus*

The ubiquitous fungus *Aspergillus flavus* is a saprophytic species present in soil as conidia or sclerotia and on plants as mycelia. Sclerotia helps fungi to survive in harsh environmental conditions and produce conidiospores under appropriate conditions. Like other *Aspergilli*, *A. flavus* has 8 chromosomes, a 36.8 Mb genome with roughly 12,000 predicted

functional genes (Amaike and Keller, 2011; Cleveland *et al.*, 2009). It was first identified in 1809. However, *A. flavus* has received notoriety as the cause of Turkey X disease, which killed thousands of poultry upon eating aflatoxin-containing peanuts in England in 1960. (Nesbitt *et al.*, 1962). The cause of the Turkey X disease was found to be aflatoxin which is the most carcinogenic mycotoxin produced by some fungal species, especially *A. flavus*. Aflatoxin is a secondary metabolite (SM) which helps protect fungi from biotic or abiotic stresses in their environment. At least 16 different structurally similar aflatoxins have been identified in nature. Aflatoxins B1, B2, G1 and G2 are the main four and the most toxic aflatoxin is aflatoxin B1. As well as aflatoxins (AFs), *A. flavus* can produce other secondary metabolites, including aflatrem and cyclopiazonic acid (CPA) (Fakruddin *et al.*, 2015; Liang *et al.*, 2017; Pfannenstiel *et al.*, 2018).

This fungus is known to be the cause of many diseases for animals, humans and even insects (Amaike and Keller, 2011; Fakruddin *et al.*, 2015). As an opportunistic pathogen for both plants and animals, *A. flavus* is unique. Aflatoxicosis is the poisoning that arises from ingesting AFs and is divided into two forms: acute and chronic aflatoxicosis. Acute severe intoxication results from high-dose aflatoxin intake in a short time and gives rise to direct liver damage or death. Chronic aflatoxicosis results from low-dose aflatoxin exposure for a long time and lead to immune suppression and cancer (mainly liver but also kidney, lung, and colon) (Williams *et al.*, 2004; Amare and Keller, 2014). Additionally, this fungus is the second most frequent cause of invasive and noninvasive aspergillosis after *A. fumigatus* in humans and other vertebrates. Aspergillosis is an infection that mostly emerges from the inhalation of fungal spores in immunocompromised individuals. As a serious source of infection for animals and humans and contaminant for agricultural crops, *A. flavus* and aflatoxin have caused tremendous economic losses all across the world (Amaike and Keller, 2011; Liang *et al.*, 2017). Thus, it is important to control contamination and secondary metabolite production of *A. flavus,* not only to reduce agricultural economic losses, but also to protect human and animal health.

1.9 Coordination of development and secondary metabolism

Fungal natural products like secondary metabolites (SMs) are low molecular weight compounds and are important for the health and pharmaceutical industries. Apart from their advantages, some secondary metabolites have harmful affects on agriculture and human health. SMs differ from primary metabolites in that they are not essential for fungal development. It is thought that SMs help fungi to protect themselves from biotic or abiotic stresses in their

ecological environments (Lim and Keller, 2014; Pfannenstiel *et al.*, 2018). According to their biosynthetic origin or enzyme classes, fungal SMs fall into five groups including polyketides (PKS), non-ribosomal peptides (NRPS), terpenes, indole alkaloids (dimethylallyl transferase, DMATS) and hybrid PK-NRPS. (Keller *et al.*, 2005). *A. nidulans* is related to *Aspergillus flavus* in that both species utilise components of the aflatoxin biosynthesis pathway (Chang *et al.*, 2012). According to Aspergillus Secondary Metabolites Database (A2MDB) catalogs, 675 *Aspergillus* species produce 807 unique non-redundant secondary metabolites (http://www.iictindia.org/A2MDB) (Vadlapudi *et al.*, 2017). Fungal development and secondary metabolism has a correlation recognized for a long time. At certain stages of development, production of the SMs takes place and developmental defects of cleistothecium distrupt SM production (Bayram and Braus, 2012). The regulatory protein complexes, transcriptional activators and epigenetic regulators coordinate fungal development and SM production.

Like other organisms, the life cycle of *A. nidulans* is regulated by light. To be aware of the changing environmental conditions, light signal detection is crucial. As a soil borne organism, whether it grows on or under the surface makes a significant difference in terms of abiotic and biotic factors such as light, oxygen/carbon dioxide ratio, humidity, osmotic stress, temperature and reactive oxygen species (ROS) (Rodríguez-Romero *et al.*, 2010; Jaimes-Arroyo *et al.*, 2015; Lind *et al.*, 2016). After cells become competent for reception of environmental signals, light signals induce asexual (conidiophore) development repress sexual (cleistothecia) development. Two different wavelength of light, red (650-680 nm) and blue (400-450 nm) affect fungal development. Different light receptor proteins mediate the light responses in *A. nidulans*. Phytochrome *fphA* is a sensor kinase that encodes the red light receptor which represses sexual development and induces asexual spore formation in red light. Cryptochromes *lreA* (light receptor A) and *lreB* encode the blue light receptors, which induce asexual development and interacts with *fphA*. In addition, CryA (Cryptochrome A) acts as a UVA-blue light receptor that stimulates asexual sporulation. Deletion of photolyase-like *cryA* results in Hülle cell formation in liquid culture and increases the number of cleistothecia under UV or blue-light. Similarly, deletion of *fphA* leads to an increase in the number of cleistothecia in red light (Blumenstein *et al.*, 2005; Purschwitz *et al.*, 2008; Bayram *et al.*, 2008a; Bayram *et al.*, 2010; Dasgupta *et al.*, 2016). Phytochrome FphA is associated with a variety of proteins, including a key protein known as VeA during regulation of light-dependent development of *A.*

nidulans (Sarikaya-Bayram *et al.*, 2015). It is suggested that, in *A. flavus*, a similar light dependent regulation mechanism is also conserved (Calvo and Cary, 2015).

During asexual development, all *Aspergillus* species produce mitotic spores called conidia, which are dispersed by the wind to allow for colonization of new habitats. The regulation of conidiation is coordinated by the genes belonging to the central developmental pathway (CDP) like *brlA*, *abaA* and *wetA* in *Aspergillus*. The master regulator BrlA is a C_2H_2 zinc finger transcription factor and functions as an essential activator for conidiation. Deletion of *brlA* in *A. nidulans* leads to bristle-like long aerial hyphae rather than conidiophores and blocks asexual development (Park and Yu, 2012; Yao *et al.*, 2017).

Early asexual development is induced by upstream regulators, *fluG, flbA*, *flbB*, *flbC*, *flbD*, and *flbE* that are known as *fluffy* genes (Wieser *et al.*, 1994; Wieser and Adams, 1995; Adams *et al.*, 1998; Kwon *et al.*, 2010a; Kwon *et al.*, 2010b). These genes encode signalling elements as well as various transcription factors necessary for *brlA* activation. The FluG protein is required for inhibiting vegetative growth and activating the FlbA protein, which regulates G-protein signalling. Knockout strains of *fluG* in *A. nidulans* lead to an aconidial and non-ST-producing phenotype. Despite that, deletion of *fluG* in *A. flavus* results in a delay and reduction in conidia production, elevated sclerotial production and no effect on aflatoxin biosynthesis. Based on this data, it is thought that signalling pathways related to conidiation and function of *fluG* are different in *A. flavus* and *A. nidulans*. A heterotrimeric G protein complex required for vegetative growth is attenuated by activated FlbA protein (Hicks *et al.*, 1997; Chang *et al.*, 2012; Park and Yu, 2012). Meanwhile, FluG activates the asexual development pathway FlbB/FlbC/FlbD and FlbE for the activation of *brlA*. FlbC, the putative transcription factor with two C_2H_2 zinc finger domains binds to the regulatory elements in the *brlA* promoter and with the help of the FlbB/FlbD/FlbE pathway, induces *brlA* expression (Etxebeste *et al.*, 2010; Kwon *et al.*, 2010).

Expression of *abaA* (abacus A) is induced by BrlA activity and is essential for differentiation of the finger-like phialide structures during the middle stages of conidiation in *Aspergillus*. Therefore, *abaA* mutants are incapable of conidia formation (Sewall *et al.*, 1990; Andrianopoulos and Timberlake, 1994; Yu, 2010). In addition, *yA* (yellow A) *A. nidulans* and *olgA* (homolog of *yA*) in *A. flavus* are responsible for spore color and *vosA* is necessary for spore maturation. Both *yA* and *vosA* are activated by AbaA transcription factors. VosA (viability of spores A), a velvet family fungal specific protein of *A. nidulans* is required for the

accumulation of trehalose, which is critical for the survival of asexual and sexual spores. It is suggested that both WetA and VosA of *A. flavus* regulate the trehalose production in conidia (Ni and Yu, 2007; Chang *et al.*, 2010; Wu *et al.*, 2017). *brlA* also induces expression of *wetA* (wet-white A), which is necessary for the formation of the cell walls of conidia in the late conidiophore differentiation stage in *Aspergillus*. Moreover, WetA ialso regulates the aflatoxin biosynthesis and vegetative growth in *A. flavus*. Further, it has been considered that *brlA, abaA* and *wetA* are cooperatively activated genes responsible for conidiophore production and spore maturation in *Aspergillus* (Sewall *et al.*, 1990; Marshall and Timberlake, 1991; Ni *et al.*, 2010; Wu *et al.*, 2017; Yao *et al.*, 2017).

The velvet family proteins, VeA, VelB, VelC and VosA are essential for coordination of fungal development and secondary metabolism in the presence or absence of light (Bayram and Braus, 2012). A key protein, VeA, is a conserved transcription factor that interacts with numerous proteins and shows light-dependent localization. In *A. nidulans,* VeA interacts with VelB to form a VeA-VelB heterodimer. Furthermore, VeA and VelB can migrate between the cytoplasm and the nucleus with the help of importin KapA. In dark conditions, VeA-VelB heterodimer migrates to the nucleus, while in the presence of light, it migrates to both the cytoplasm and the nucleus (Stinnett *et al.*, 2007; Ahmed *et al.*, 2013). The *A. nidulans* Velvet family domains of VeA, VelB, VelC and VosA reside in regions like those in the velvet proteins of *A. flavus* and these proteins act similar but have somewhat distinct roles in development and secondary metabolite production (Park and Yu, 2012; Chang *et al.*, 2013). Deletion of *veA* in *A. nidulans* leads to a loss of cleistothecia and reduction in the production of the aflatoxin precursor sterigmatocystin (ST) and the antibiotic penicillin (PN) (Kim *et al.*, 2002; Kato *et al.*, 2003). It is also stated that deletion of *veA* in *A. flavus* results in a loss of sclerotia, disruption of quorum sensing and a decrease in aflatoxin, aflatrem, and CPA production (Duran *et al.*, 2007; Amaike and Keller, 2009). Additionally, it is stated that VeA represses asexual development and CryA regulates *veA* expression in *A. nidulans* (Mooney and Yager, 1990; Bayram *et al.*, 2008a). In dark conditions, the VeA-VelB heteromimer interacts with histone methyltransferase LaeA (lack of *aflR* expression A) to form a trimeric velvet complex, which is essential for inducing sexual development and coordinating secondary metabolism in *A. nidulans*. İnteractions among the velvet components are the same in *A. flavus*. However, VelB and LaeA also interact with FluG. Consequently, velvet family proteins and FluG are critical for conidiation, sclerotial production and aflatoxin biosynthesis. The *velB* (velvet like B) deletion mutant in *A. nidulans* exhibits a lack of cleistothecia and reduced

secondary metabolite production. On the other hand, for *A. flavus,* VelB and VeA positively influence conidiation (Bayram *et al.*, 2008b; Amaike and Keller, 2009; Sarikaya-Bayram *et al.*, 2010; Bayram and Braus, 2012; Chang *et al.*, 2013). The VelB-VosA hetero-complex of *A. nidulans* is required for repression of asexual development and expression of important cell wall biosynthesis genes in the absence of light. The VelB-VosA hetero-complex of *A. flavus* is also required for asexual and sexual development (Sarikaya Bayram *et al.*, 2010; Chang *et al.*, 2013; Park *et al.*, 2015). Deletion of *velC* in *A. nidulans* results in decreased formation of cleistothecia and increased number of conidia, while overexpression of this gene promotes formation of cleistothecia. Sexual development is positively regulated by VelC in *A. nidulans* (Park *et al.*, 2014). However, Deletion of *velC* in *A. flavus* does not affect either development or toxin production (Chang *et al.*, 2013).

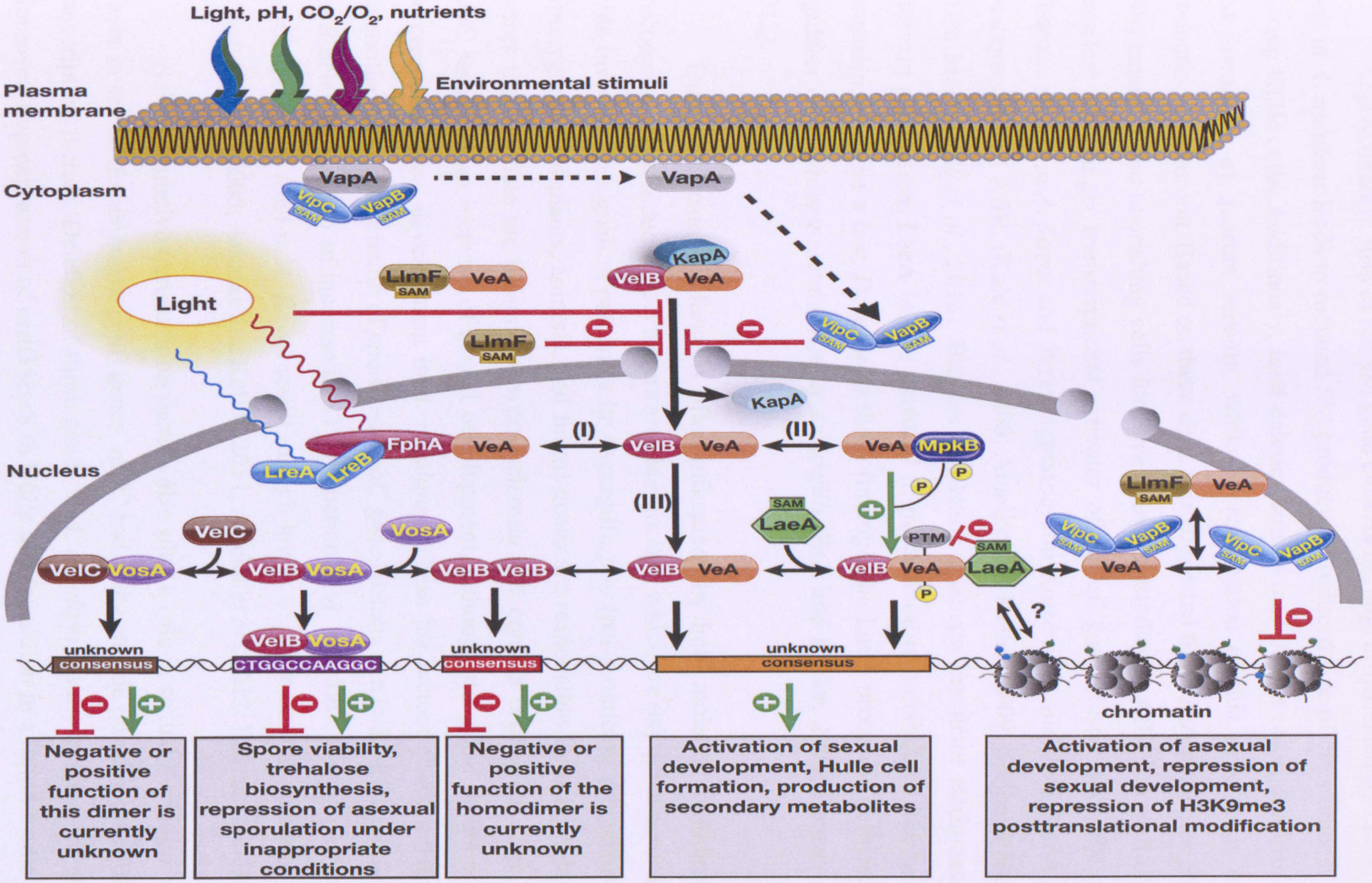

Figure 1.5: Molecular complexes formed by the velvet family proteins and the methyltransferases on the control of fungal development and secondary metabolite production. From Sarikaya-Bayram *et al*., 2015 and with the permission of author).

Approximately 50% of the SM gene clusters in fungi are affected by LaeA. Deletion of *laeA* in *A. nidulans* leads to reduced SM production, reduced size of cleistothecia and lack of nursing Hülle cells. Additionaly, *laeA* deletion strains in *A. flavus* result in a loss of sclerotia and disruption of quorum sensing, while overexpression of this gene leads to increased production of sclerotia. Based on these data, it is suggested that LaeA promotes production of SMs, sclerotia and nourishing cells for developing cleistothecia. AflR is a well-characterized binuclear zinc finger transcriptional activator of the *afl* gene cluster and *aflR* encodes the aflatoxin cluster in *A. flavus* and the sterigmatocystin cluster in *A. nidulans*. LaeA coordinates the expression of AflR. (Kale *et al.*, 2008; Amaike and Keller, 2009; Sarikaya Bayram *et al.*, 2010; Macheleidt *et al.*, 2016). Besides regulating aflatoxin precursor sterigmatocystin and aflatoxin production, LaeA is also essential to produce other metabolites like penicillin and lovastatin, to name a few. Because of these findings, the LaeA protein is defined as a global regulator of secondary metabolism in *Aspergilli* (Bok and Keller, 2004; Bayram and Braus, 2012).

Quorum Sensing in fungi is often influenced by lipid moieties including oxylipins. Precocious sexual inducer (*psi*) factors are pheromones, which are oxylipins derived from lipid acids involved in signaling pathways in Aspergilli. *ppo* (psi-producing oxygenases), and *lox* (lipoxygenases of plants, animals, and fungi) genes are responsible for the production of *psi* factors that regulate the balance between sclerotia and conidia production. The deletion of *ppoC* results in an increase of sexual development, although the *ppoA* deletion leads to an increase of asexual development in *A. nidulans*. These psi factors also regulate secondary metabolism. Double deletion of *ppoA* and *ppoC* genes results in a lack of ST production, while *ppoB* deletion leads to an increase in ST production in *A. nidulans*. Deletion of *ppoA, ppoB, ppoC, ppoD* and *loxA* in *A. flavus* result in high levels of aflatoxin and sclerotia production. (Yu and Keller, 2005; Amaike and Keller, 2011; Affeldt *et al.*, 2012; Bayram and Braus, 2012).

Several putative transcription factors also play a role in sexual development of fungi. Never in sexual development (*nsd*) genes, *nsdC* and *nsdD* encode putative zinc finger domain transcription factors. Deletion of these genes in *A. nidulans* results in a loss of cleistothecia. Moreover, overexpression of *nsdD* leads to Hülle cell formation in a liquid media (Han *et al.*, 2001; Kim *et al.*, 2009). Similarly, deletion of *nsdC* and *nsdD* in *A. flavus* lead to a reduction in conidiophore production, loss of sclerotia formation and loss of aflatoxin biosynthesis (Cary

et al., 2012). The Zn(II)(2)2Cys(6) transcription factor NosA (number of sexual spores) is critical for further development of cleistothecia and has been identified in both *A. flavus* and *A. nidulans*. Knockout strains of *nosA* in *A. nidulans* have small sized immature cleistothecia with little Hülle cells and no ascospores (Vienken and Fischer, 2006). Unlike the transcription factors mentioned above, putative basic helix-loop-helix (bHLH) type transcription factors of *A. nidulans*, encoded by *stuA* (Stunted A) and *wetA,* are necessary for both sexual and asexual development. Deletion of *stuA* and *wetA* in *A. nidulans* result in no cleistothecia and abnormal conidiophore production (Busby *et al.*, 1996; Wu and Miller, 1997). The *stuA* homolog of *A. flavus, AfStuA* is necessary for conidia and sclerotia development as well as aflatoxin production and CPA biosynthesis. Deletion of *AfStuA* leads to silencing of the aflatoxin gene cluster and blocks CPA production (Yao *et al.*, 2017). Another bHLH transcription factor of both *A. flavus* and *A. nidulans*, encoded by *devR*, plays a role in development (Tuncher *et al.*, 2004; Lv *et al.*, 2018).

As mentioned above, Velvet family proteins, VeA and VelB are neccesary for the formation of cleistothecia as well as the production of ST and PN. The *veA* and *velB* null mutants are not able to express the ST gene cluster. Light-dependent regulatory protein VeA plays a role as a bridge between VelB and global secondary metabolite regulator LaeA and collectively, the trimeric velvet complex regulates sexual development and SM production (Bok and Keller 2004; Bayram *et al.*, 2008b). MAP kinase pathways also play essential roles in secondary metabolism. In the nucleus, VeA interacts with the MAPK protein AnFus3, which phosphorylates the VeA protein in *vitro.* Mutants of the MAPK pathway downregulate the expression of both ST and PN genes (Bayram *et al.*, 2012a). VeA also interacts with a LaeA-like methyltransferase F (LlmF), which prevents the nuclear import of VeA. Knockout strains of *llmF* lead to nuclear accumulation of VeA, resulting in the elevation of sexual development and ST production (Palmer *et al.*, 2013). Additionally, a VeA-dependent secondary metabolism regulator MtfA (master transcription factor A) regulates ST, PN and terrequinone synthesis (Ramamoorthy *et al.*, 2013). Moreover, it has been shown that the VeA null mutant strains result in elevated transcripts of the orsellinic acid (OA) gene cluster. Consequently, OA and its derivatives F9775B/A, which has an anti-osteoporosis effect, can be produced by *veA*Δ mutants. Physical contact with the *Streptomyces rapamycinicus* bacterium leads to induction of the OA gene cluster, which is silenced under normal culture conditions. Deletion of COP9 in *A. nidulans* also results in upregulated transcripts of the OA gene cluster and OA production (Schroeckh *et al.*, 2009; Nahlik *et al.*, 2010; Bok *et al.*, 2013).

Many secondary metabolites, including aflatoxins produced by *A. flavus* have been found in sclerotia (Gloer, 1995). However, AFs have also been detected in mycelia and conidia (Wicklow and Cole, 1982; Wicklow and Shotwell, 1983). AF production occurs in the endosomes of mycelia and are then secreted outside of the cell (Chanda *et al.*, 2009). Based on the identification of core or "backbone" genes, the Secondary Metabolite Unknown Regions Finder (SMURF) software predicts that the *A. flavus* genome contains 18 nonribosomal peptide synthases (NRPS), 14 NRPS-like synthases, 25 polyketide synthases (PKS), 3 PKS-like synthases, 2 PKS-NRPS enzymes and 8 prenyltransferases as well as 55 secondary metabolite clusters (Amaike and Keller, 2011). As mentioned above, AF biosynthesis and sclerotial development are closely related. It was demonstrated that *veA* is necessary for AFs, CPA and aflatrem production in *A. flavus* (Calvo *et al.*, 2004; Duran *et al.*, 2007, Calvo and Cary, 2015). In addition to VeA, the global regulator of secondary metabolism LaeA interacts with VelB and predictedly with FluG. This complex controls SM production and sclerotial formation in *A. flavus* (Chang *et al.* 2013). Further, it has been shown that, deletion of *veA* and *laeA* lead to the reduction of pathogenicity on host seeds (Amaike and Keller, 2009). As well as *A. flavus* oxylipins, endogenous plant oxylipins, which interact with the infecting fungi, modulate the conidial and sclerotial development and secondary metabolism (Calvo and Cary, 2015). Knockout strains of *ppoA, ppoB, ppoC, ppoD* and *loxA* in *A. flavus* result in high levels of AFs and sclerotia production (Brown *et al.*, 2009). Never in sexual development (*nsd*) genes, *nsdC* and *nsdD* also affect the secondary metabolism in *A. flavus*. Deletion of both *nsdC* and *nsdD* results in an inability to produce aflatoxin (Cary *et al.*, 2012).

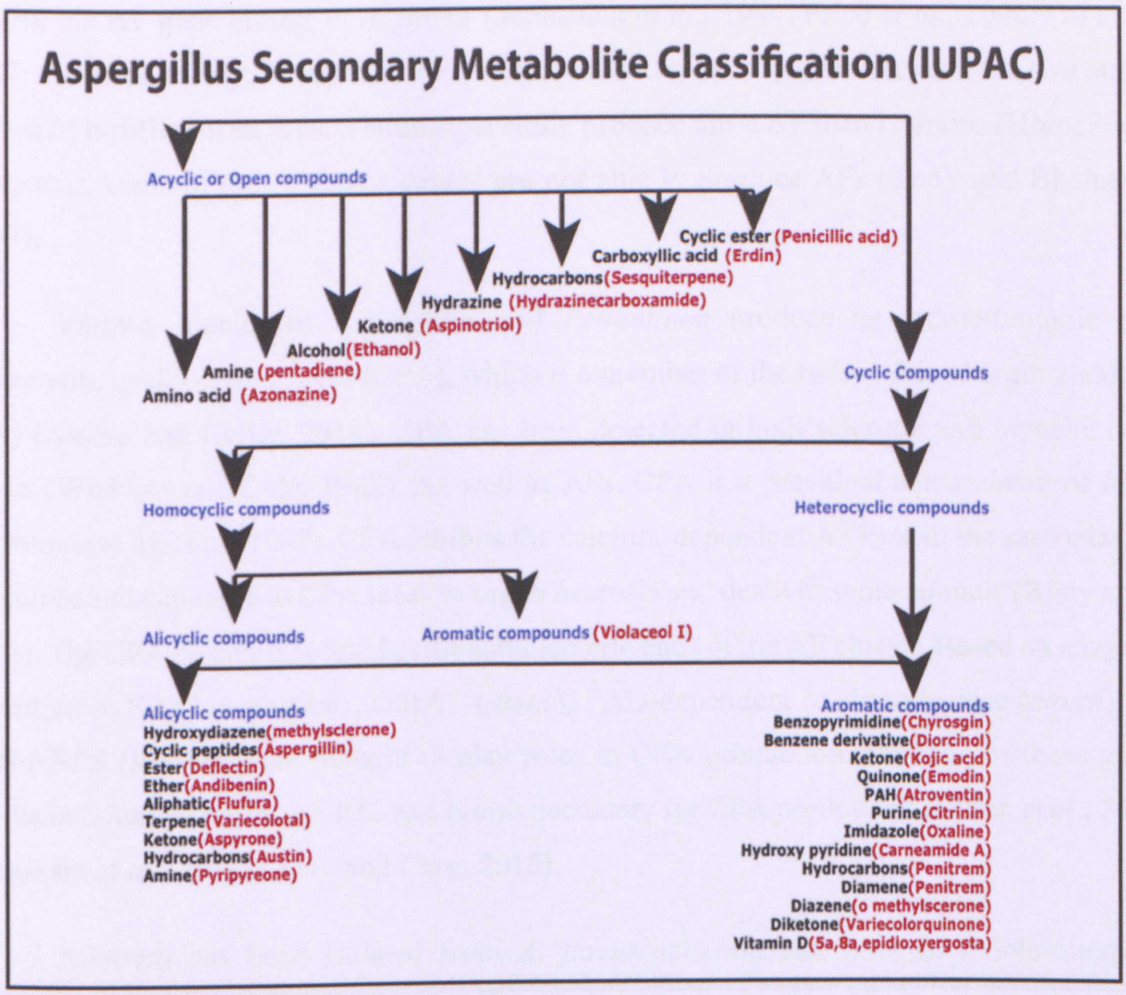

Figure 1.6: Secondary metabolite classification of Aspergillus. IUPAC based classification of each metabolite shown in various to chemical compounds with given examples under each category. From Vadlapudi *et al.*, 2017.

Polyketide-derived furanocoumarins, aflatoxins are synthesised from acetate. Fatty acid synthetases (AflA and AflB), a PKS (AflC) and a number of tailoring enzymes regulate AF production (Zeng *et al.*, 2011). Much of our knowledge of AF production and regulation come from ST biosynthesis, which is a precursor of AF, in model fungus *A. nidulans*. ST biosynthesis genes in *A. nidulans* are highly related to AF biosynthesis in *A. flavus*. The aflatoxin cluster of *A. flavus* spans a 70 kb DNA section and consists of 28 genes including two pathway-specific regulatory genes, *aflR* and a lesser extent *aflS* (*aflJ*). Zn(2)-Cys(6)-type protein AflR binds a palindromic sequence (5'-TCGN5CGA-3') in the promoter region of all aflatoxin biosynthetic genes and plays a role as a pathway-specific transcriptional activator. Deletion of *aflR* results in a complete loss of AF biosynthesis. AflS also regulates AF biosynthesis by interacting with AflR. The global regulators, VeA, NsdD, NsdC, and LaeA

control the AF gene cluster in *A. flavus* (Woloshuk *et al.*, 1994; Price *et al.*, 2006; Du *et al.*, 2007; Calvo and Cary, 2015). The AF production ability of *A. flavus* between the two strains (L and S) is different such as, S strains generally produce more AF than L strains (Horn, 2007). Moreover, some of the *A. flavus* strains are not able to produce AFs (Cotty and Bhatnagar, 1994).

Various species of *Aspergillus* and *Penicillium* produce an indole-tetramic acid mycotoxin, cyclopiazonic acid (CPA), which is a member of the indole-drived ergot alkaloids (EA) (Amare and Keller, 2014). CPA has been detected in both sclerotia and mycelia of *A. flavus* (Wicklow and Cole, 1982). As well as AFs, CPA is a prevalent contaminant of foods (Martins and Martins, 1999). CPA inhibits the calcium-dependent ATPase in the sarcoplasmic reticulum and exposure to CPA leads to organ necrosis and death in some animals (Riley *et al.*, 1992). The CPA cluster is located at the subtelemeric ends of the AF cluster. Based on enzymes identified in EAs biosynthesis, DMAT (*dmtA*), FAD-dependent oxido reductase (*moaA*) and PKS-NRPS (*pks-nrps*) are thought to play roles in CPA production. Deletion of these genes results in failure to produce CPA. *veA* is also necessary for CPA production (Duran *et al.*, 2007; Shinohara *et al.*, 2011; Calvo and Cary, 2015).

Aflatrem has been isolated from *A. flavus* sclerotia and it is an indole-diterpene mycotoxin. (TePaske *et al.*, 1992). Aflatrem is a tremorgenic mycotoxin, which causes neurological disorders (Gallagher and Wilson, 1979). Paxilline biosynthesis genes in *P. paxilli* are required for aflatrem biosynthesis in *A. flavus* (Zhang *et al.*, 2004; Nicholson *et al.*, 2009). Different from most other SM clusters, which exist at a single locus, the aflatrem cluster exists at two distinct loci on two distinct chromosomes. Eight genes; *atmA*, *atmB*, *atmC*, *atmD atmG*, *atmM*, *atmP* and *atmQ* are responsible for aflatrem production (Nicholson et al., 2009). Aflatrem biosynthesis is highly similar to paxilline, a mycotoxin in *Penicillium paxilli* (Parker and Scott, 2004). The global regulators, VeA and LaeA are also necessary for aflatrem production (Duran *et al.*, 2007; Georgianna *et al.*, 2010).

Recently, another SM known as the asparasone gene cluster was identified in *A. flavus*. Asparasone is a polyketide and it is responsible for dark brown pigmentation of sclerotia. Velvet complex proteins, VeA and LaeA, regulate the biosynthesis of asparasone. Deletion of the asparasone polyketide synthase (PKS) exhibits greyish-yellow sclerotia that are less resistant to insect predation and damage by UV and heat (Cary *et al.*, 2014).

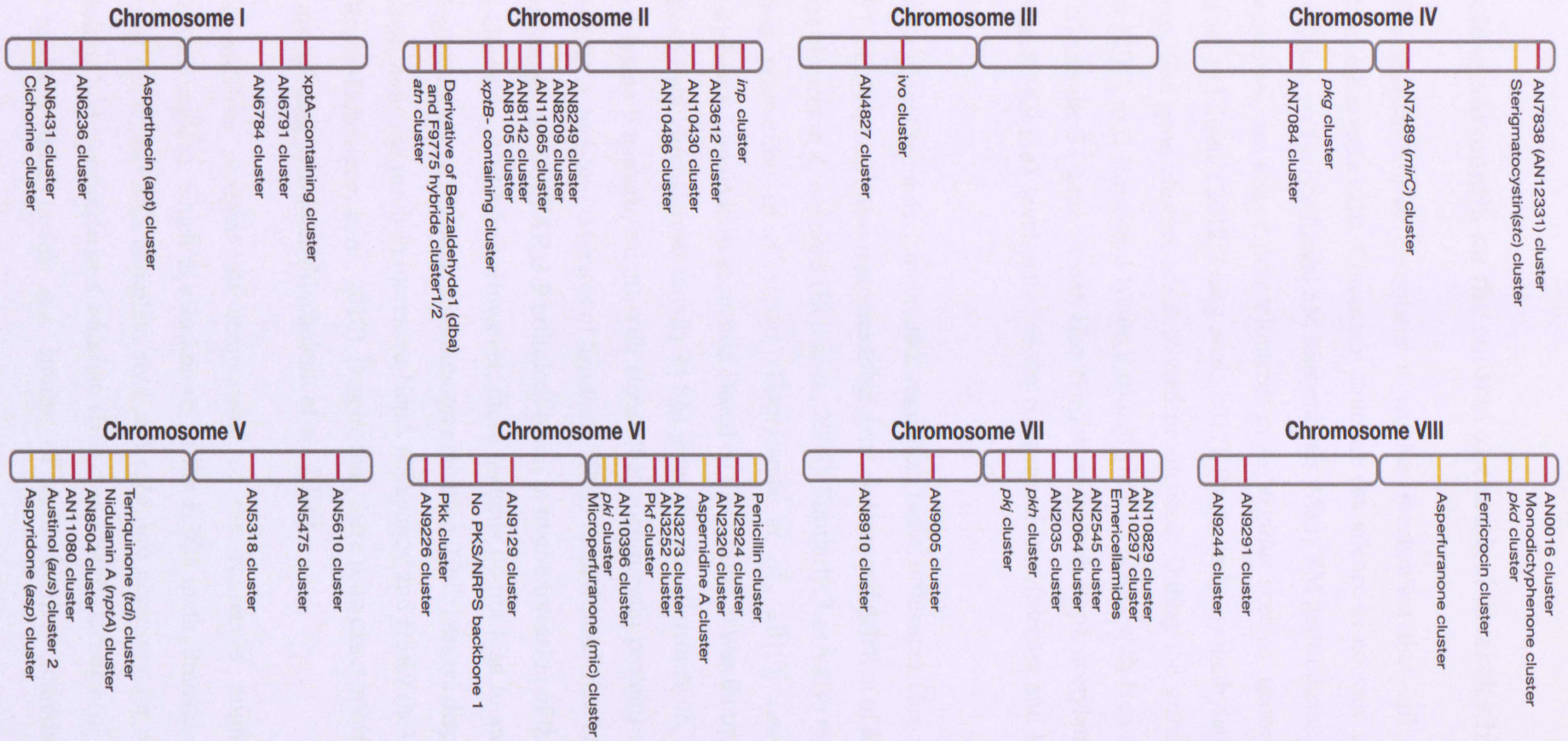

Figure 1.7: The chromosomal location of A.nidulans biosynthetic gene clusters with their known or predicted products on the genome through chromosomes (grey). All known products are shown in yellow together with the structure of compounds. Predicted clusters are displayed in pink. NRPS: nonribosomal peptide synthase, PKS: polyketide synthase. Adapted from Macheleidt *et al.,* 2016.

1.10 Role of chromatin on the control of chemical diversity in fungi

The remodelling of chromatin is another mechanism that influences the genetic processes in eukaryotic cells. Chromatin structure can silence or activate the transcription of genes and it can coregulate fungal SM biosynthesis. Many SM gene clusters, including ST and AF gene clusters, are placed near telomeres in *Aspergillus* species' genomes (Palmer *et al.*, 2010; Gacek and Strauss 2012; Liang *et al.*, 2017). Particularly, by methylation and acetylation of histones, SM gene clusters are activated or silenced. During the growth of *A. nidulans*, increased H3K9 me3 (histone 3 lysine 9 trimethylation) marks with HepA (heterochromatin protein) silence the ST gene cluster. However, when growth stops, acetylation of histones and a decreased H3K9 me3 level activates the ST gene cluster (Strauss and Reyes-Dominguez, 2010).

As a global secondary metabolite regulator, LaeA influences chromatin structure. As well as ST and PN, LaeA also regulates other gene clusters and deletion of *laeA* downregulates these gene clusters in *A. nidulans* (Bok *et al.*, 2006). Similarly, LaeA also regulates the AF and other SMs production in *A. flavus* (Georgianna *et al.*, 2010). LaeA protein has a methyltransferase domain in its sequence. Based on this feature, it was thought that LaeA might have histone methyltransferase activity in SM gene clusters (Perrin *et al.*, 2007). H3K9 me3 (histone 3 lysine 9 trimethylation) with HepA (heterochromatin protein) mark the silent ST gene cluster in *A. nidulans*. Mutants of *hepA* and H3K9 methyltransferase *clrD* (*S. pombe* Clr4 and *D. melanogaster* SU(VAR)3-9 ortholog) result in over-expression of the transcripts of the ST gene cluster in *A. nidulans*. However, these mutants do not lead to any physiological or morphological changes. Chromatin immunoprecipitation (ChIP) assays displayed that deletion of *laeA* in *A. nidulans* result in increased HepA occupancy and H3K9 me3 marks in ST gene cluster (Reyes-Dominguez *et al.*, 2010). Despite that, there is no exact information about LaeA directly methylating substrates (Macheleidt *et al.*, 2016).

A. nidulans contains all components of the conserved multi-subunit complex (COMPASS complex), which is also known as the H3K4 methyltransferase complex. Two members of the COMPASS complex, *setA* and *cclA,* are necessary for normal growth and sexual fruiting body formation in *A. nidulans* (Bok *et al.*, 2009; Harting *et al.*, 2013). Moreover, it was reported that, knock out strains of *cclA* produce emodines, which have

immunosuppressive, anti-inflammatory, anti-mutagenic and anti-cancer effects, and antimicrobial monodictyphenone as well as induce the production of the F9775A and F9775B (antiosteoporosis polyketides) (Bok *et al.*, 2009). In addition to this, deletion of *cclA* in *A. oryzae* (highly related to *A. flavus*) results in induction of the astellolide A and B (Shinohara *et al.*, 2011).

Generally, histone acetyltransferases (HATs) have an activating effect whereas histone deacetylases (HDACs) have an inhibiting effect on SM gene clusters. Both in *A. nidulans* and *A. flavus*, HAT enzymes are necessary for biosynthesis of ST and AF respectively. Treating *A. nidulans* with trichostatin, which is a HDAC inhibitor, results in significantly increased production of some metabolites as well as increased gene expression of telomere proximal gene clusters (Roze *et al.*, 2007; Shwab *et al.*, 2007). Similar to these effects, the *hdaA* (HDAC encoding gene) null mutant of *A. nidulans* leads to up-regulation of ST and PN gene clusters. Additionally, treating *A. nidulans* with suberoylanilide hydroxamic acid (SAHA), which is a HDAC inhibitor, results in activating the normaly silent orsellinic acid gene cluster. The SAGA-ADA histone acetlytransferase complex, containing GcnE and AdaB in *A. nidulans* is required for activation of the OA gene cluster by the bacteria *S. rapamycinicus*. Moreover, the SAGA-ADA complex is also responsible for activating some other gene clusters, such as ST, PN and terrequione (Nützmann *et al.*, 2011; Nützmann *et al.*, 2013).

Lately, it has been reported that the JMJD2/JHDM3 family H3K36me3 and H3K9me3 demethylase protein KdmA in *A. nidulans* has a critical role in the expression or repression of genes. While KdmA is necessary for full expression of several SM genes, it plays a role as a co-repressor of genes, which is involved in the production of primary metabolites (Gacek-Matthews *et al.*, 2015). In addition to that, JMJC family H3K4me3 demethylase KdmB, which is a member of the Jarid (JMJ–AT-rich interacting domain) group of enzymes is also involved in the regulation of SM biosynthesis in *A. nidulans*. Depending on the nutrient conditions, *kdmB* null mutants can increase the transcription of SM genes in limited nutrient conditions, whereas they increase the transcription of primary metabolism genes in nutrient-rich conditions. However, KdmB is necessary for full transcription of about 750 genes in *A. nidulans* (Gacek-Matthews *et al.*, 2016).

Recently, it was identified that the transcriptional regulator SntB, *S. cerevisiae* Snt2 homolog, is required for biosynthesis of ST and AF in *A. nidulans* and *A. flavus,* respectively. Deletion of *sntB* in *A. nidulans* results in failure to produce ST via downregulation of *aflR*.

Similarly, the *A. flavus ΔsntB* strain is also unable to synthesise AF. Moreover, Snt2 homologs of *Fusarium oxysporum f.sp. melonis* and *Neurospora crassa* are also required for pathogenicity and conidiation, respectively. (Denisov *et al.* 2011; Pfannenstiel et al., 2017; Pfannenstiel *et al.*, 2018). A more recent study points out that KdmB and histone deacetylase RpdA in *A. flavus* have crucial roles on development and secondary metabolism. Deletion of *kdmB* and *rpdA* lead to a decrease in sclerotia production and loss of AF biosynthesis. Further, it has been stated that KdmB, EcoA (putative cohesion acetyl transferase), RpdA and SntB form a tetrameric demethylase complex (KERS), which regulates fungal development, AF production and pathogenicity of *A. flavus*. (Karahoda *et al.*, in preparation).

1.11 Aim of this Study

Environmental dynamics are a constant challenge for all organisms to adapt or evolve in response to. Considering this, biotic and abiotic environmental factors play important roles in growth, development and genetic regulation. Studies indicate that fungal development and secondary metabolism processes are strongly affected by various environmental elements ranging from pH to nutrient levels to light to competition with other microorganisms. Fungi regulate development or produce small molecules known as secondary metabolites as a physiological response to these external factors. One very well-known cell response is the induction of asexual and sexual development in *A. nidulans* in response to light. Light controls the stimulation of asexual conidiation, while the absence of light induces sexual development. The significant correlation between fungal development and secondary metabolite production is also reported by previous studies (Bayram *et al.*, 2008a; Bayram and Braus, 2012).

There is a broad range of production of secondary metabolites and small bioactive molecules by filamentous fungi. These natural products can be detrimental (e.g Aflatoxin) or beneficial (e.g penicillin) to humankind. One noteworthy feature of genes that are responsible for the biosynthesis of fungal secondary metabolites is that they are clustered and behave as a single genetic locus for production of specific metabolites and this advantage eases their co-regulation (Yin and Keller, 2011). Some earlier studies have shown that SM biosynthetic gene clusters are located most often in sub-telomeric regions of chromosomes which are related with the heterochromatin state of chromatin and many of these clusters are silenced under laboratory conditions (Yu and Keller, 2005; Bayram *et al.*, 2008; Bok *et al.*, 2009). Having these findings has provided a convenient board to clarify the regulation mechanism of SM gene expression. Expression and regulation of fungal SM gene clusters are complex processes since they are

controlled in different regulatory levels which include pathway-specific, global regulators (*laeA*), heteromeric protein complexes (*velvet*) and epigenetic control factors (*cclA*) (Macheleidt *et al.*, 2016). Trimeric nuclear *velvet* complex which consist of VeA, VelB and LeaA methyltransferase controls the coordinated regulation of both fungal development and secondary metabolism (Bayram *et al.*, 2008). H3K9 methyltransferase *clrD* gene deletion causes expression of SM gene clusters in *A.nidulans* (Reyes-Domingues *et al.*, 2007). The chromatin modifying COMPASS complex subunit, H3K4 methyltransferase *cclA* gene is a repressor for SM gene clusters expression (Bok *et al.*, 2009). It has been recently reported that H3K36 and H3K9 demethylase KdmA is required for expression of some genes are involved in SM production (Gacek-Matthews *et al.*, 2015). Despite the current knowledge regarding relations between epigenetic regulation and fungal SM biosynthesis and development, the regulatory protein complexes for these processes still remain unclear.

- Therefore, first aim of this PhD study was to understand the nature of protein complexes involved in chromatin modification. Recently studied chromatin regulator KdmA was tagged with various epitope tags to reveal the protein complexes established by KdmA *in vivo*. Affinity purification studies coupled to mass spectrometry revealed McmA-EcmB-RstB-CclA-KdmA (MERCK) demethylase complex formed in *A. nidulans*.

- The second aim of the thesis was to examine how the MERCK protein complex influence fungal light, stress responses and secondary metabolite production.

- Since the MERCK complex contains chromatin binding proteins, third aim of the thesis was to reveal the genome wide binding profile of the complex and influence of the presence and absence of the KdmA in complex formation and genome wide binding. Since the MERCK complex has been conserved in eukaryotes and pathogenic fungi.

- The fourth aim of the thesis was to study the MERCK complex in plant pathogenic and aflatoxin producer fungus *A. flavus* to see how the MERCK complex controls fungal pathogenicity and aflatoxin production.

In summary, the MERCK complex represents an important chromatin regulatory complex which is conserved between *A. nidulans* and *A. flavus* and might represent an important protein complex to get crucial insights into the complex chromatin regulation of fungal development, pathogenicity and secondary metabolism.

Chapter 2

Materials and Methods

Chemicals used for solutions, buffers and media were purchased from Sigma-Aldrich Chemical Co. Ltd. (UK) and were of analytical grade, unless otherwise stated.

2.1 Strains Media and Cultivation Conditions

2.1.1 Fungal Strains Media and Cultivation Conditions

Aspergillus flavus and *Aspergillus nidulans* strains used in this study are shown in **Table 2.1.**, and **Table 2.2.**, respectively. *A. flavus* NRLL3357, *A.flavus* TJES19.1 and *A. nidulans* AGB551, *A. nidulans* FGSCA4 were used as wild-type hosts to transform deletion constructs, epitope tagging, complementation and H2A-mRFP fusion strains generation. *A. flavus* NRLL3357 and transformed *A. flavus* strains were cultivated on Glucose Minimal Medium (GMM). *A. nidulans* AGB551, *A. nidulans* FGSCA4 and transformed *A. nidulans* strains were cultivated on Glucose Minimal Medium (GMM) with 2% agar. For auxotroph strains, supplements such as Uridine (0.25g/L), Uracil (1g/L) and Pyridoxine (1mg/L) were added in appropriate amounts. For vegetative growth, Green Fluorescent Protein (GFP), Tandem Affinity Purification (TAP) and Hemagglutinin (HA) trap experiments of *A. flavus* strains were cultivated in Complete Media with appropriate supplements at 30°C for required cultivation time points; *A. nidulans* strains were cultivated in Glucose Minimal Medium (GMM) with appropriate supplements at 37°C for aimed incubation time points, in erlenmeyer flasks on a rotary shaker. Development was induced by filtering vegetative mycelia through miracloth and transferring on Complete Medium for *A. flavus* strains and on GMM with 2% Agar for *A. nidulans* strains.

To induce the strains asexually, plates containing the mycelia were incubated for 24, 48 hours during constant white light exposure. To induce the strains sexually, plates were incubated for 24, 48 hours in dark conditions.

Table 2.1 *A. flavus* strains used in this study

Strain	Genotype	Reference
NRRL3357	Wild type	Payne et al., 1993
TJES19.1	*nku70Δ, pyrG-*	Spraker and Keller unpublished
kdmAΔ	*kdmAΔ::AfpyrG, nku70Δ, pyrG-*	This study
cclAΔ	*cclAΔ::AfpyrG, nku70Δ, pyrG-*	This study
ecmBΔ	*ecmBΔ::AfpyrG, nku70Δ, pyrG-*	This study
rstBΔ	*rstBΔ::AfpyrG, nku70Δ, pyrG-*	This study
kdmA-GFP	*kdmA::sgfp::AfpyrG, nku70Δ, pyrG-*	This study

kdmA-3XHA	*kdmA::3XHA::AfpyrG, nku70Δ, pyrG-*	This study
kdmA $_{teton}$	*tetO7::Pmin::kdmA::AfpyrG, nku70Δ, pyrG-*	This study
kdmA comp.	*kdmAΔ::kdmA::phleoR, kdmAΔ::AfpyrG, nku70Δ, pyrG-*	This study
cclA comp.	*cclAΔ::cclA::phleoR, cclAΔ::AfpyrG, nku70Δ, pyrG-*	This study
ecmB comp.	*ecmBΔ::ecmB::phleoR, ecmBΔ::AfpyrG, nku70Δ, pyrG-*	This study
rstB comp.	*rstBΔ::rstB::phleoR, rstBΔ::AfpyrG, nku70Δ, pyrG-*	This study
cclA-3XHA	*cclA::3XHA::AfpyrG, nku70Δ, pyrG-*	This study
ecmB-3XHA	*ecmB::3XHA::AfpyrG, nku70Δ, pyrG-*	This study
rstB-3XHA	*rstB::3XHA::AfpyrG, nku70Δ, pyrG-*	This study
kdmA-GFP-mRFP	*gpdA::mrfp::H2A::phleo,kdmA::sgfp::AfpyrG, nku70Δ, pyrG-*	This study

Table 2.2 *A. nidulans* strains used in this study

Strain	Genotype	Reference
FGSCA4	*veA+*	FGSC*
AGB551	*nkuAΔ::argB, pyrG89, pyroA4, veA+*	Bayram et al., 2012
kdmA-TAP	*kdmA::ctap::natR;nkuAΔ::argB,pyrG89,pyroA4,veA+*	This study
cclA-TAP	*cclA::ctap::natR;nkuAΔ::argB,pyrG89,pyroA4,veA+*	This study
ecmB-TAP	*ecmB::ctap::natR;nkuAΔ::argB,pyrG89,pyroA4,veA+*	This study
rstB-TAP	*rstB::ctap::natR;nkuAΔ::argB,pyrG89,pyroA4,veA+*	This study
mcmA-TAP	*mcmA::ctap::natR;nkuAΔ::argB,pyrG89,pyroA4,veA+*	This study
kdmA-GFP	*kdmA::sgfp::natR;nkuAΔ::argB,pyrG89,pyroA4,veA+*	This study
cclA-GFP	*cclA::sgfp::natR;nkuAΔ::argB,pyrG89,pyroA4,veA+*	This study
ecmB-GFP	*ecmB::sgfp::natR;nkuAΔ::argB,pyrG89,pyroA4,veA+*	This study
rstB-GFP	*rstB::sgfp::natR;nkuAΔ::argB,pyrG89,pyroA4,veA+*	This study
mcmA-GFP	*mcmA::sgfp::natR;nkuAΔ::argB,pyrG89,pyroA4,veA+*	This study
kdmA-HA	*kdmA::3xHA::AfpyrG; nkuAΔ::argB, pyrG89,pyroA4,veA+*	This study
cclA-HA	*cclA::3xHA::AfpyrG; nkuAΔ::argB, pyrG89,pyroA4,veA+*	This study
ecmB-HA	*ecmB::3xHA::AfpyrG; nkuAΔ::argB, pyrG89,pyroA4,veA+*	This study
rstB-HA	*rstB::3xHA::AfpyrG; nkuAΔ::argB, pyrG89,pyroA4,veA+*	This study
mcmA-MYC	*mcmA::13xMYC::AfpyrG;nkuAΔ::argB,pyrG89,pyroA4,veA+*	This study
kdmA-GFP-mRFP	*gpdA::mrfp::h2A::pyroA;kdmA::sgfp::natR; nkuAΔ::argB, pyrG89,pyroA4,veA+*	This study
cclA-GFP-mRFP	*gpdA::mrfp::h2A::pyroA;cclA::sgfp::natR; nkuAΔ::argB, pyrG89,pyroA4,veA+*	This study
ecmB-GFP-mRFP	*gpdA::mrfp::h2A::pyroA;ecmB::sgfp::natR; nkuAΔ::argB, pyrG89,pyroA4,veA+*	This study
rstB-GFP-mRFP	*gpdA::mrfp::h2A::pyroA;rstB::sgfp::natR; nkuAΔ::argB, pyrG89,pyroA4,veA+*	This study
mcmA-GFP-mRFP	*gpdA::mrfp::h2A::pyroA;mcmA::sgfp::natR; nkuAΔ::argB, pyrG89,pyroA4,veA+*	This study
kdmAΔ	*kdmAΔ::prtA;nkuAΔ::argB,pyrG89,pyroA4,veA+*	This study
cclAΔ	*cclAΔ::prtA;nkuAΔ::argB,pyrG89,pyroA4,veA+*	This study
ecmBΔ	*ecmBΔ::prtA;nkuAΔ::argB,pyrG89,pyroA4,veA+*	This study
rstBΔ	*rstBΔ::prtA;nkuAΔ::argB,pyrG89,pyroA4,veA+*	This study
kdmA tetOn	*tetO7::Pmin::kdmA;nkuAΔ::argB,pyrG89,pyroA4,veA+*	This study
cclA tetOn	*tetO7::Pmin::cclA;nkuAΔ::argB,pyrG89,pyroA4,veA+*	This study
ecmB tetOn	*tetO7::Pmin::ecmB;nkuAΔ::argB,pyrG89,pyroA4,veA+*	This study
rstB tetOn	*tetO7::Pmin::rstB;nkuAΔ::argB,pyrG89,pyroA4,veA+*	This study
mcmA tetOn	*tetO7::Pmin::mcmA;nkuAΔ::argB,pyrG89,pyroA4,veA+*	This study

cclA-TAP,kdmAΔ	*kdmAD::AfpyrG;cclA::ctap::natR;nkuAΔ::argB,pyrG89, pyroA4,veA+*	This study
ecmB-TAP,kdmAΔ	*kdmAD::AfpyrG;ecmB::ctap::natR;nkuAΔ::argB,pyrG89, pyroA4,veA+*	This study
rstB-TAP, kdmAΔ	*kdmAD::AfpyrG;rstB::ctap::natR;nkuAΔ::argB,pyrG89, pyroA4,veA+*	This study
mcmA-TAP, kdmAΔ	*kdmAD::AfpyrG; mcmA::ctap::natR; nkuAΔ::argB,pyrG89, pyroA4,veA+*	This study
kdmAΔ,cclAΔ	*cclAΔ::AfpyrG; kdmAΔ::ptrA; nkuAΔ::argB, pyrG89, pyroA4,veA+*	This study
kdmAΔ,ecmBΔ	*ecmBΔ::AfpyrG; kdmAΔ::ptrA; nkuAΔ::argB ,pyrG89, pyroA4,veA^{+}*	This study
kdmAΔ,rstBΔ	*rstBΔ::AfpyrG; kdmAΔ::ptrA; nkuAΔ::argB, pyrG89, pyroA4,veA^{+}*	This study
rstBΔ,cclAΔ	*rstBΔ::AfpyrG; cclAΔ::ptrA; nkuAΔ::argB, pyrG89, pyroA4,veA^{+}*	This study
rstBΔ,ecmB	*rstBΔ::AfpyrG; ecmBΔ::ptrA; nkuAΔ::argB, pyrG89, pyroA4,veA^{+}*	This study
cclAΔ,ecmBΔ	*cclAΔ::AfpyrG; ecmBΔ::ptrA; nkuAΔ::argB, pyrG89, pyroA4,veA+*	This study
kdmA comp.	*^{p}kdmA::kdmA::kdmA^{t}-AfpyrG; kdmAΔ::prtA; nkuAΔ::argB, pyrG89, pyroA4, veA+*	This study
cclA comp.	*^{p}cclA::cclA::cclA^{t}-AfpyrG; cclAΔ::prtA; nkuAΔ::argB, pyrG89, pyroA4, veA+*	This study
ecmB comp.	*^{p}ecmB::ecmB::ecmB^{t}-AfpyrG; ecmBΔ::prtA; nkuAΔ::argB, pyrG89, pyroA4, veA+*	This study
rstB comp.	*^{p}rstB::rstB::rstB^{t}-AfpyrG; rstB::prtA; nkuAΔ::argB, pyrG89, pyroA4, veA+*	This study
cclA-HA, kdmAΔ	*cclA::3xHA::AfpyrG; kdmAD::prtA; nkuAΔ::argB, pyrG89, pyroA4,veA+*	This study
ecmB-HA, kdmAΔ	*ecmB::3xHA::AfpyrG; kdmAD::prtA; nkuAΔ::argB, pyrG89, pyroA4,veA+*	This study
rstB-HA, kdmAΔ	*rstB::3xHA::AfpyrG; kdmAD::prtA; nkuAΔ::argB, pyrG89, pyroA4,veA+*	This study
mcmA-MYC, kdmAΔ	*mcmA::13xMYC::AfpyrG; kdmAD::prtA; nkuAΔ::argB, pyrG89,pyroA4,veA+*	This study
cclA-GFP-mRFP, kdmAΔ	*kdmAΔ::AfpyrG; gpdA::mrfp::h2A::pyroA; cclA::sgfp::natR; nkuAΔ::argB, pyrG89, pyroA4,veA+*	This study
ecmB-GFP-mRFP, kdmAΔ	*kdmAΔ::AfpyrG; gpdA::mrfp::h2A::pyroA; ecmB::sgfp::natR; nkuAΔ::argB, pyrG89, pyroA4,veA+*	This study
rstB-GFP-mRFP, kdmAΔ	*kdmAΔ::AfpyrG; gpdA::mrfp::h2A::pyroA; rstB::sgfp::natR; nkuAΔ::argB, pyrG89, pyroA4,veA+*	This study
mcmA-GFP-mRFP, kdmAΔ	*kdmAΔ::AfpyrG; gpdA::mrfp::h2A::pyroA; mcmA::sgfp::natR; nkuAΔ::argB, pyrG89, pyroA4,veA+*	This study

kdmA truncated-*HA*	*AfpyroA::*$^{N\Delta1\text{-}793}$*kdmA::3xHA; nkuAΔ::argB, pyrG89,pyroA4,veA+*	*kdmA::3xHA::AfpyrG;*	This study

2.1.2 Bacterial Strains Media and Cultivation Conditions

The competent *Escherichia coli* strains used in this study were Stellar (Clontech) and MACH-1 (Invitrogen). *E. coli* strains were cultivated on or in LB medium supplemented with Ampicillin (100μg/ml) at 37°C for time interval 12-16 hours with shaking at 200 rpm.

2.2 Nucleic acid methods

2.2.1 Genomic DNA extraction

Genomic DNA of *A. flavus* and *A. nidulans* were extracted from frozen mycelia or conidia, using the ZR Fungal/Bacterial DNA Kit (Zymo Research, California, USA) according to the manufacturer's instructions.

2.2.2 Total RNA extraction

Total *A. flavus* and *A. nidulans* RNA was extracted from frozen mycelia using the Qiagene RNeasy Plant Mini Kit (Cat No:74104) according to the manufacturer's instructions.

2.2.3 Plasmid purification

Plasmid DNA from *E. coli* was isolated using Qiagen Mini-Prep Plasmid Purification Kit (Cat No: 27104) according to the manufacturer's instructions.

2.2.4 Agarose gel purification of DNA fragments

DNA fragments were extracted from agarose gel slices using Qiagen QIAquick Gel Extraction Kit (Cat No: 28706) according to the manufacturer's instructions.

2.3 Strain Creation

2.3.1 Plasmid construction

Oligonucleotides and plasmids used for the generation of *A. flavus* and *A. nidulans* strains are listed in **Table 2.3.**, **Table 2.4.**, **Table 2.5.** and **Table 2.6.**, respectively.

Table 2.3 Oligonucleotides utilized for *A.flavus* strains including experiments

Label	Sequence in 5'>3' direction	Size	Feature
BK97	TTCGAGCTCGGTACCCCCTTAAGAGGTATTGGCCTTACTT	40	*kdmA* 5 UTR pUC19 connector (del)
BK98	TCAGGCCATCGGCTAGCTTG	20	*kdmA* nested 5 UTR (del)
BK99	GAGCATTGTTTGAGGCCGTCTAGGCCCCATCGTCA	35	*kdmA* 5 UTR *pyrG* connector
BK100	GCCTCCTCTCAGACAGTGACACACACACTTGTTTTGTTGTG	41	*kdmA* 3 UTR *pyrG* connector
BK101	ACTCTAGAGGATCCCCAGCACTCTCCTGCTTATTATTTTCC	41	*kdmA* 3 UTR pUC19 connector (del)
BK102	AGCACTCTCCTGCTTATTATTTTCC	25	*kdmA* nested 3 UTR (del.)
BK103	TTCGAGCTCGGTACCCAGATGTTGTGAACCAGCACGATC	39	*cclA* 5 UTR pUC19 connector (del)
BK104	AGATGTTGTGAACCAGCACGATC	23	*cclA* nested 5 UTR (del)
BK105	GAGCATTGTTTGAGGCTTGCTTCGTTAGCCCGTATCAG	38	*cclA* 5 UTR *pyrG* connector
BK106	GCCTCCTCTCAGACAGGCTGAATTTGTTTCGTGGATGAGC	40	*cclA* 3 UTR *pyrG* connector
BK107	ACTCTAGAGGATCCCCGTCCTTTGCTCAGCAGCATCC	37	*cclA* 3 UTR pUC19 connector (del.)
BK108	GTCCTTTGCTCAGCAGCATCC	21	*cclA* nested 3 UTR (del)
BK109	TTCGAGCTCGGTACCCGTGGATTGCCCATCCATCCTAT	38	*mcmA* 5 UTR pUC19 connector (del)
BK110	GGTTTTGATCTACTCTATCGGGAC	24	*mcmA* nested 5 UTR (del)
BK111	GAGCATTGTTTGAGGCACGGTGGTCCTTGCTTCTGC	36	*mcmA* 5 UTR *pyrG* connector
BK112	GCCTCCTCTCAGACAGGGCTGGAACAAGGGTAGAACG	37	*mcmA* 3 UTR *pyrG* connector
BK113	ACTCTAGAGGATCCCCTGTGTACGGTACAGGGGGAG	36	*mcmA* 3 UTR pUC19 connector (del)
BK114	TGTGTACGGTACAGGGGGAG	20	*mcmA* nested 3 UTR (del)
BK115	TTCGAGCTCGGTACCCTCATCTACCATAACCGGCGACA	38	*ecmB* 5 UTR pUC19 connector (del)
BK116	TCATCTACCATAACCGGCGACA	22	*ecmB* nested 5 UTR (del)
BK117	GGTGAAGAGCATTGTTTGAGGCGTTATCGAGATATGTCTGACTTGCA	47	*ecmB* 5 UTR *pyrG* connector
BK118	ATCAGTGCCTCCTCTCAGACAGTCCTTGTGGTATGATCTTTGGAAAG	47	*ecmB* 3 UTR *pyrG* connector
BK119	ACTCTAGAGGATCCCCTTCCCCTTCCGTTGCAACTTTTG	39	*ecmB* 3 UTR pUC19 connector (del)
BK120	TTCCCCTTCCGTTGCAACTTTTG	23	*ecmB* nested 3 UTR (del)
BK121	TTCGAGCTCGGTACCCTTGGGGCCCAATGCGTTGTTG	37	*rstB* 5 UTR pUC19 connector (del)

BK122	TTGGGGCCCAATGCGTTGTTG	21	*rstB* nested 5 UTR (del)
BK123	GAGCATTGTTTGAGGCTTCTTAGAGACGGTGCAGCGAAA	39	*rstB* 5 UTR *pyrG* connector
BK124	GCCTCCTCTCAGACAGGCGATGAGTACGTCGGCTTC	36	*rstB* 3 UTR *pyrG* connector
BK125	ACTCTAGAGGATCCCCCAATTGAACTCCCCGCTCAAACA A	40	*rstB* 3 UTR pUC19 connector (del)
BK126	TACAGGGTACTACAACACAAAACC	24	*rstB* nested 3 UTR (del)
BK276	CGATGTTAGTCTTGCCTTGC	20	*skpA* 5'
BK277	GACCAGATGAAACTCAAGCTG	21	*skpA* 3'
BK260	GGATGACGGCATTCATTACTC	21	*kdmA* 5'
BK261	CCATCCGTTGAGCCGATTC	19	*kdmA* 3'
MUL23	GGTCCTTAAGGGAGGTGTGG	20	*cclA* 5'
MUL24	GGAGCCTACATTGCCGACAC	20	*cclA* 3'
MUL25	CAGTTAGCGCAACGATCGCTG	21	*ecmB* 5'
MUL26	GCAACGGCCAAGAGTATCGTC	21	*ecmB* 3'
MUL28	CTTTGGTAAACTCAGCTCCACTG	23	*rstB* 5'
MUL29	GCGAGTGAAGCTTGAACGATTC	22	*rstB* 3'
BK204	ACCAACACTGGCCGCATCTTC	21	*cclA* ORF 5'
BK205	TCAATGGACCTCTATCAGATACG	23	*cclA* ORF 3'
BK208	TTGGGCAACGTAGAGTTTAGCC	22	*ecmB* ORF 5'
BK209	AACCGATACGCTGGCTGCAC	20	*ecmB* ORF 3'
BK210	CAAGTGCCAGTTTTGCAATCGC	22	*rstB* ORF 5'
BK211	CCGACGCGCAATGAGTCTTC	20	*rstB* ORF 3'
MUL105	CCCAAGACCGACAAGGGCTGGTATCTGAACTGCATCTTC	39	*cclA* 5 UTR PAN8.1 connector
MUL106	GCGTTCTGGAGGGAGGCTCTTCTCTGCATCTCCGCC	36	*cclA* 3 UTR PAN8.1 connector
MUL107	CCCAAGACCGACAAGGCCGAGTCAATTATAGGTCACGC	38	*ecmB* 5 UTR PAN8.1 connector
MUL108	GCGTTCTGGAGGGAGGCTTCCAAGCTCGTTGAAGTACC	38	*ecmB* 3 UTR PAN8.1 connector
MUL109	CCCAAGACCGACAAGGCCGTAAGTGAGTGAGAGACCC	37	*rstB* 5 UTR PAN8.1 connector
MUL110	GCGTTCTGGAGGGAGGGCTGCTTCCTGCGTTACTATG	37	*rstB* 3 UTR PAN8.1 connector
MUL127	TTCGAGCTCGGTACCCCCTTGTCGGTAATGCTTGTCAC	38	*cclA* 5 UTR pUC19 connector (tag)
MUL128	GCTTTGCTACTAACGAATCTCTG	23	*cclA* nested 5 UTR (tag)
MUL129	CACCGCTACCACCTCCAGACATCTCGACATCATGGCC	37	*cclA HA&pyrG* connector
MUL130	GCCTCCTCTCAGACAGATTATACATTGTTCATCTAACTTG C	41	*cclA* 3 UTR *HA&pyrG* connector
MUL131	CATGTTATGTCTTACTCTACGCG	23	*cclA* nested 3 UTR (tag)
MUL132	ACTCTAGAGGATCCCCGTTCGCGATGTCTTCAGTACG	37	*cclA* 3 UTR pUC19 connector (tag)
MUL133	TTCGAGCTCGGTACCCGATCTCTGTTGTGCTACATGCC	38	*mcmA* 5 UTR pUC19 connector (tag)
MUL134	CGGATTGATCAGGTTCTGCC	20	*mcmA* nested 5 UTR (tag)
MUL135	CACCGCTACCACCTCCTGCAGTGGGTTGATGCTGGG	36	*mcmA HA&pyrG* connector

MUL136	GCCTCCTCTCAGACAGACGGTGGTCCTTGCTTCTGC	36	*mcmA* 3 UTR *HA&pyrG* connector
MUL137	CGGATACGGAACCCAGGAC	19	*mcmA* nested 3 UTR (tag)
MUL138	ACTCTAGAGGATCCCCCTTCGACATCTCTGGTCTCG	36	*mcmA* 3 UTR pUC19 connector (tag)
MUL139	TTCGAGCTCGGTACCCCAATCAGTCGCGTACAATACCC	38	*ecmB* 5 UTR pUC19 connector (tag)
MUL140	CTGGCTGAGTGTGATTTCTGG	21	*ecmB* nested 5 UTR (tag)
MUL141	CACCGCTACCACCTCCCTCCCGTGATACGAACCAGG	36	*ecmB HA&pyrG* connector
MUL142	GCCTCCTCTCAGACAGAAAGTTATCGAGATATGTCTGAC	39	*ecmB* 3 UTR *HA&pyrG* connector
MUL143	GTCGACGTTCACGCTTGCAG	20	*ecmB* nested 3 UTR (tag)
MUL144	ACTCTAGAGGATCCCCGTTGAAGTACCTAGCCCACTG	37	*ecmB* 3 UTR pUC19 connector (tag)
MUL145	TTCGAGCTCGGTACCCCTCACTGTCGCGATTCAGCG	36	*rstB* 5 UTR pUC19 connector (tag)
MUL146	GAATCTGCCATCGGCTTGTG	20	*rstB* nested 5 UTR (tag)
MUL147	CACCGCTACCACCTCCGTACGCCGTGCCTACACTAG	36	*rstB HA&pyrG* connector
MUL148	GCCTCCTCTCAGACAGGCGATGAGTACGTCGGCTTC	36	*rstB* 3 UTR *HA&pyrG* connector
MUL149	GCTATGACTTGCAGCATGTCG	21	*rstB* nested 3 UTR (tag)
MUL150	ACTCTAGAGGATCCCCGAACCATCATCCTCGCTATGTG	38	*rstB* 3 UTR pUC19 connector (tag)
MUL151	TTCGAGCTCGGTACCCCGCCACAGAAGAGCAGACATC	37	*kdmA* 5 UTR pUC19 connector (tag)
MUL152	CGCCACAGAAGAGCAGACATC	21	*kdmA* nested 5 UTR (tag)
MUL153	CACCGCTACCACCTCCAGGACTAAGAACGTTACAGAGATC	40	*kdmA HA&pyrG* connector
MUL154	GCCTCCTCTCAGACAGATCGAACTACCTTCCTCGAC	36	*kdmA* 3 UTR *HA&pyrG* connector
MUL155	CGCTCCACTGCATGACATGTC	21	*kdmA* nested 3 UTR (tag)
MUL156	ACTCTAGAGGATCCCCCGCTCCACTGCATGACATGTC	37	*kdmA* 3 UTR pUC19 connector (tag)
MUL157	CCCAAGACCGACAAGGCTGCATCGCTGGCGAACTAG	36	*kdmA* 3 UTR PAN8.1 connector
MUL158	GCGTTCTGGAGGGAGGCGGCTGCCACATCCGATG	34	*kdmA* 5 UTR PAN8.1 connector

Table 2.4 Oligonucleotides employed for *A. nidulans* strains

Label	Sequence in 5'>3' direction	Size	Feature
OZG916	GGAGGTGGTAGCGGTGGT	18	GGGSGG amplifier for all cassettes
OZG695	GCCTCAAACAATGCTCTTCA	20	*pyrG* stop
OZG694	CTGTCTGAGAGGAGGCACTGAT	22	*pyrG&pyroA* start
OSBRT20	CTCGAAGACATGCGAAATCAG		
OSBRT19	CAGGAGTTCGTTCGTACGTG		
MUL54	CTCTAGAGGATCCCCCGTTATCATCACGGGGTCTCTG	37	*rstB* 3 UTR pUC19 connector
MUL53	GCTTTATTGAGCCTGTCTGTGG	22	*rstB* nested 3 UTR
MUL52	GCCTCCTCTCAGACAGCTCACCGGCTTTTCATAGGGG	37	*rstB* 3 UTR *pyrG* connector
MUL51	GAGCATTGTTTGAGGCTTCTCAAGACGGGTTGTGTAGC	38	*rstB* 5 UTR *pyrG* connector
MUL50	GGAAAGGCTTGTCCCAATAGTG	22	*rstB* nested 5 UTR (del)
MUL49	TTCGAGCTCGGTACCCGGAGGTGATGAACCGTGAATC	37	*rstB* 5 UTR pUC19 connector
MUL48	CTCTAGAGGATCCCCACTCCGGAATTTCAACGCAGGC	37	*ecmB* 3 UTR pUC19 connector
MUL47	CCTGAGAATAAAGTCCTCGGC	21	*ecmB* nested 3 UTR
MUL46	GCCTCCTCTCAGACAGAGGCATCTTTGCCGTATGTTCTC	39	*ecmB* 3 UTR *pyrG* connector
MUL45	GAGCATTGTTTGAGGCTGTGGTAGCATCAGCGGCCA	36	*ecmB* 5 UTR *pyrG* connector
MUL44	GTGGTATTCAAGAAGCGCAAGC	22	*ecmB* nested 5 UTR
MUL43	TTCGAGCTCGGTACCCGAGTGATGAAGTGCCAGTGAAG	38	*ecmB* 5 UTR pUC19 connector
MUL42	ACTCTAGAGGATCCCCCGTCAGGAGGTAGAGATAAACA G	39	*kdmA* 3 UTR pUC19 connector
MUL41	CTCCAGATTAGTCCCATTCGG	21	*kdmA* nested 3 UTR
MUL40	GCCTCCTCTCAGACAGCTATGACTGCTTATAGACATGCC	39	*kdmA* 3 UTR *pyrG* connector
MUL39	GAGCATTGTTTGAGGCGAATGCCGTCGTCTATAAGTGC	38	*kdmA* 5 UTR *pyrG* connector
MUL38	GCAGTACGGTCCGGTTGATG	20	*kdmA* nested 5 UTR
MUL37	TTCGAGCTCGGTACCCGACTCATGCTCCTTCGTCTTC	37	*kdmA* 5 UTR pUC19 connector
MUL33	GAATGACTCGCCCATAAGCTTG	22	*rstB* 3' (cDNA)
MUL32	GACGATGATGCTGTCGACTCG	21	*rstB* 5' (cDNA)
MUL20	AAACAAAGATGCAAGAATGGGGTTGTACTTTCAGCTGC	38	*cclA* 3 UTR *ptrA* connector
MUL19	GATCCCGTAATCAATTAATGCGAATCCTTTGCGGATAGG	39	*cclA* 5 UTR *ptrA* connector
MUL18	ACTCTAGAGGATCCCCGAGTTTCAGTGGCTCGAGATG	37	*cclA* 3 UTR pUC19 connector
MUL17	CAGTTGTCCTAACCTGAGATACG	23	*cclA* nested 3 UTR
MUL16	GCCTCCTCTCAGACAGATGGGGTTGTACTTTCAGCTGC	38	*cclA* 3 UTR *pyrG* connector
MUL15	GAGCATTGTTTGAGGCAATGCGAATCCTTTGCGGATAG G	39	*cclA* 5 UTR *pyrG* connector
MUL14	CCACCTTGAATTATAGGCCCAG	22	*cclA* nested 5 UTR
MUL13	TTCGAGCTCGGTACCCGTATCTGAACCGCATCTTCGG	37	*cclA* 5 UTR pUC19 connector

MUL120	TTGAGGCGAATTATTTGGAACCTTCGCAGTGAATATCG	38	*rstB* 3 UTR pOSB113 connector
MUL119	AGCTCGGTACCCATTTGCTATGGAGCTGTCATCATGAC	38	*rstB* 5 UTR pOSB113 connector
MUL118	TTGAGGCGAATTATTTCTTCGACTCCGTCTCCATCAC	37	*ecmB* 3 UTR pOSB113 connector
MUL117	AGCTCGGTACCCATTTGAGGAGTATCGGAGTGATATGG	38	*ecmB* 5 UTR pOSB113 connector
MUL116	TTGAGGCGAATTATTTGTTCAATGCAACGGTAGTCCAG	38	*cclA* 3 UTR pOSB113 connector
MUL115	AGCTCGGTACCCATTTCGATGTGAGCTTCCCGTAGAG	37	*cclA* 5 UTR pOSB113 connector
MUL114	TTGAGGCGAATTATTTCAGACGACGGTTCACGAGTG	36	*kdmA* 3 UTR pOSB113 connector
MUL113	AGCTCGGTACCCATTTCGCAGGATCGAGTATTGACTAC	38	*kdmA* 5 UTR pOSB113 connector
BK51	GTGGCCCAATAAACCGTTGCTG	22	*rstB* nested 5 UTR
BK36	CCCATATAACGATCCACAAGTCG	23	*mcmA* nested 3 UTR
BK35	TCCACCGAGTCACTGTTTACTG	22	*mcmA* nested 5 UTR
BK281	GCATCTGGTCCTCAACCTC	19	*benA* qPCR F
BK280	GATGGCTGCCTCTGACTTC	19	*benA* qPCR R
BK245	GATCTGGTCCTCTTCCTCG	19	*sconC* 3'
BK244	CCAACTACCTTGACATCAAGC	21	*sconC* 5'
BK243	CAAGCGACTTCGTTGGCAC	19	*rstB* 3' (cDNA)
BK242	GGGTAACATCCTAGACGGTG	20	*rstB* 5' (cDNA)
BK241	CCCAGCTTCCTGTTCAAGG	19	*ecmB* 3'
BK240	CGAGACGTCATCTATTCAATCG	22	*ecmB* 5'
BK239	GCATCCGATTGCCTACAGG	19	*mcmA* 3'
BK238	CCTACATGACAAGCGAACAAC	21	*mcmA* 5'
BK237	GGTATCCTCCGGTTCTGG	18	*cclA* 3'
BK236	CGAGTATCAAGCTTGCCGAC	20	*cclA* 5'
BK235	GCTAAGAGCGGCACAGAG	18	*kdmA* 3'
BK234	CATGACTATGCTTCGTCTGAC	21	*kdmA* 5'
BK181	TGGTTGGTTGCCGTCCTTCAC	21	*rstB* nested 3 UTR (*tetO7)*
BK180	CTTGCTCACCATGTTTGCAAGATTCATCCTCAATCCACTC	40	*rstB* ORF *sgfp* connector
BK179	GCCTGAGTGGCCGTTTATGGCCCCGAGTGCATCAAGT	37	*rstB* ORF *tetO7* connector
BK178	CCTCTCAGACAGATTTTTCTCAAGACGGGTTGTGTAGC	38	*rstB* 5 UTR *pyrG/pyroA* connector
BK177	AAAGCTGGGTACATTTGCTTGAAGAATCGATGTTGTGTTG	40	*rstB* 5UTR pUC19 connector
BK174	TTGGCTGCAAGCCTCCGTC	19	*ecmB* nested 3 UTR (*tetO7)*
BK173	CTTGCTCACCATGTTTAGTTGTAGTTGTTGCGGGGTTC	38	*ecmB sgfp* connector
BK172	GCCTGAGTGGCCGTTTATGCCTTCCAAGACGCATACGG	38	*ecmB* ORF *tetO7* connector
BK171	CCTCTCAGACAGATTTTGTGGTAGCATCAGCGGCCA	36	*ecmB* 5 UTR *pyrG/pyroA* connector
BK170	AGTCGAGTATTCATAAAGCCACAAC	25	*ecmB* nested 5 UTR (*tetO7)*

BK169	AAAGCTGGGTACATTTGTGGTATTCAAGAAGCGCAAGC	38	*ecmB* 5 UTR pUC19 connector (*tetO7*)
BK168	AGGCACCAGAAACACCGCATC	21	*mcmA* nested 3 UTR (*tetO7*)
BK167	CTTGCTCACCATGTTTCCACATTCGCCAGTAAGTAGATG	39	*mcmA sgfp* connector
BK166	GCCTGAGTGGCCGTTTATGGCCGACATCACCGCCG	35	*mcmA* ORF *tetO7* connector
BK165	CCTCTCAGACAGATTTGATGGAAATAGAAACGAAGAGG CG	40	*mcmA* 5 UTR *pyrG/pyroA* connector
BK164	GGTGCTGGGATCGATTTGATAC	22	*mcmA* nested 5 UTR (*tetO7*)
BK163	AAAGCTGGGTACATTTGGGACTATCGCCTTCTATATCC	38	*mcmA* 5 UTR pUC19 connector (*tetO7*)
BK162	GACAATTTGCTCGTCGAAGCGC	22	*cclA* nested 3 UTR (*tetO7*)
BK161	CTTGCTCACCATGTTTTACAATATCGGCCAGTACGTCTT C	40	*cclA sgfp* connector
BK160	GCCTGAGTGGCCGTTTATGGCATCTACTCACGCAGCTG	38	*cclA* ORF *tetO7* connector
BK16	CACCGCTACCACCTCCAGCAGTGGGTTGGTGCTGG	35	*mcmA* 3'
BK159	CCTCTCAGACAGATTTAATGCGAATCCTTTGCGGATAGG	39	*cclA* 5 UTR *pyrG/pyroA* connector
BK158	TCGGATCTTCGTCTCCTCGAG	20	*cclA* nested 5 UTR (*tetO7*)
BK157	AAAGCTGGGTACATTTTGGTTTGACCGCTCGTCTCTG	37	*cclA* 5 UTR pUC19 connector (*tetO7*)
BK156	GTGGTTAGAGCTGCTGCCTG	20	*kdmA* nested 3 UTR (*tetO7*)
BK155	CTTGCTCACCATGTTTTTTGCATCACTAGGCCAGATACC	39	*kdmA sgfp* connector
BK154	GCCTGAGTGGCCGTTTATGGCTGCGACGATTGATCGC	37	*kdmA* ORF *tetO7* connector
BK153	CCTCTCAGACAGATTTCGCTATGAAGAGTATGGAAAAG AG	40	*kdmA* 5 UTR *pyrG/pyroA* connector
BK152	CGTCTGGATCGACTCATGCTC	21	*kdmA* nested 5 UTR (*tetO7*)
BK151	AAAGCTGGGTACATTTAGACTGTCAAGAAAGCCCCAGG	38	*kdmA* 5 UTR pUC19 connector (*tetO7*)
BK14	CCTCCTCTCAGACAGATTCGCGCTTAAGCGCTTGC	35	*mcmA* 3 UTR 5'

Table 2.5 Plasmids used for *A. flavus* strain generation

Plasmid	Description	Reference
pUC19	*E.coli* cloning plasmid	Thermo Scientific
PAN8.1	Phleomycin resistance cloning plasmid	Punt and van den Hondel, 1992
pOB536	*H2A mrfp* with *phleo* marker in *Sma*I pUC19	This study
pBK27	*kdmA*Δ by *pyr*G in *Sma*I pUC19	This study
pBK28	*cclA*Δ by *pyr*G in *Sma*I pUC19	This study
pBK30	*ecmB*Δ by *pyrG* in *Sma*I pUC19	This study
pBK31	*rstB*Δ by *pyrG* in *Sma*I pUC19	This study
pMU22	*cclA* comp in *Stu*I PAN8.1	This study

pMU23	*ecm*B comp in *Stu*I PAN8.1	This study
pMU24	*rst*B comp in *Stu*I PAN8.1	This study
pMU29	*cclA*-3xHA-*pyrG* in *Sma*I pUC19	This study
pMU31	*ecmB*-3xHA-*pyrG* in *Sma*I pUC19	This study
pMU32	*rstB*-3xHA-*pyrG* in *Sma*I pUC19	This study
pMU33	*kdmA*-3xHA-*pyrG* in *Sma*I pUC19	This study
pMU34	*kdmA*-GFP-*pyrG* in *Sma*I pUC19	This study
pMU35	*kdmA* comp in *Stu*I PAN8.1	This study

Table 2.6 Plasmids employed for the *A. nidulans* strain creation

Plasmid	Description	Reference
pUC19	*E.coli* cloning plasmid	Thermo Scientific
pOSB113	*pyrG*, *Swa*I and *Pme*I sites in pUC19	This study
pOB498	*ecmB* TAP *natR* cassette (with *Pme*I) in pUC19 *Sma*I	This study
pOB497	*ecmB* GFP *natR* cassette (with *Pme*I) in pUC19 *Sma*I	This study
pOB496	*mcmA* TAP *natR* cassette (with *Pme*I) in pUC19 *Sma*I	This study
pOB495	*mcmA* GFP *natR* cassette (with *Pme*I) in pUC19 *Sma*I	This study
pOB494	*rstB* TAP *natR* cassette (with *Pme*I) in pUC19 *Sma*I	This study
pOB493	*rstB* GFP *natR* cassette (with *Pme*I) in pUC19 *Sma*I	This study
pOB492	*cclA* TAP *natR* cassette (with *Pme*I) in pUC19 *Sma*I	This study
pOB491	*cclA* GFP *natR* cassette (with *Pme*I) in pUC19 *Sma*I	This study
pOB439	*H2A mRFP-pyroA* in pUC19 *Sma*I site	This study
pOB230	*rstB*Δ by *ptrA* in pUC19 *Sma*I site	This study
pOB228	*ecmB*Δ by *ptrA* in pJET vector	This study
pOB227	*kdmA*Δ by *ptrA* in pJET vector	This study
pMU7	*rstB*Δ by *pyrG* in pUC19 *Sma*I site	This study
pMU6	*ecmB*Δ by *pyrG* in pUC19 *Sma*I site	This study
pMU5	*kdmA*Δ by *pyrG* in pUC19 *Sma*I site	This study
pMU4	*cclA*Δ by *ptrA* in pUC19 *Sma*I site	This study
pMU3	*cclA*Δ by *pyrG* in pUC19 *Sma*I site	This study
pMU28	*rstB* comp. in pOSB113 *Swa*I site	This study
pMU27	*ecmB* comp. in pOSB113 *Swa*I site	This study
pMU26	*cclA* comp. in pOSB113 *Swa*I site	This study
pMU25	*kdmA* comp. in pOSB113 *Swa*I site	This study
PBK9	*rstB-3xHA-pyrG* in pUC19 *Sma*I site	This study
PBK7	*ecmB-3xHA-pyrG* in *Pme*I site	This study
pBK41	*mcmA-13xMYC-pyrG* in pUC19 *Sma*I site	This study
pBK40	*rstB-teton pyroA* in pOB549 *Swa*I site	This study
pBK4	*cclA-3xHA-pyrG* in *Pme*I site	This study
pBK39	*ecmB-teton pyroA* in pOB549 *Swa*I site	This study
pBK38	*mcmA-teton pyroA* in pOB549 *Swa*I site	This study
pBK37	*cclA-teton pyroA* in pOB549 *Swa*I site	This study
pBK36	*kdmA-teton pyroA* in pOB549 *Swa*I site	This study
pBK10	*kdmA-3xHA-pyrG* in pUC19 *Sma*I site	This study

2.3.2 Generation of deletion strains

The following section will describe how strains were contructed. To select for mutants prototrophic for pyrithiamine, uridine, uracil, pridoxine, phleomycin or nourseothricin; defined

medium plates were supplemented with pyrithiamine (1ml/L), uridine (5ml/L), uracil (1g/L), pyrodoxine(1ml/L) or nourseothricin (600µl/L) from their stock solutions as required.

To create the *kdmA, cclA, ecmB* and *rstB* deletion construct for *A. flavus*, the 5' UTR region of related gene was amplified from genomic DNA of either NRRL3357 or TJES19.1 using primers (Table 2.3) and 3' UTR with primers (Table 2.3) for *AfpyrG*. These three fragments were then fused and cloned in *Sma*I site of pUC19 by using in-fusion HD cloning kit (Clontech, Cat:638911) leading to the plasmids pBK27 (*kdmA*Δ::*AfpyrG*), pBK28 (*cclA*Δ::*AfpyrG*), pBK30 (*ecmB*Δ::*AfpyrG*), pBK31 (*rstB*Δ::*AfpyrG),* respectively. Linear deletion fragments were amplified from associated plasmid by using primers listed in **Table 2.3** and linear deletion fragments were transformed into TJES19.1 generating *kdmA, cclA, mcmA, ecmB* and *rstB* deletion mutants.

For the generation of the *kdmA, cclA, ecmB* and *rstB* deletion constructs for *A. nidulans*, the 5' and 3' UTR regions of linked gene were amplified from genomic DNA of either FGSCA4 or AGB551 using primers (Table 2.4) and same approach was applied for amplification of *ptrA* and *pyrG* fragments. The two fragments were fused to the *ptrA* and *pyrG* markers and amplified by a fusion PCR, using oligos (Table 2.4). Deletion cassettes were cloned in pJET vector heading to the plasmids pOB227 (*kdmA*Δ::*ptrA*), pOB228 (*ecmB*Δ::*ptrA*), pOB230 (*rstB*Δ::ptrA*)* and in *Sma*I site of pUC19 by using in-fusion HD cloning kit (Clontech, Cat:638911) leading plasmids pMU3 (*cclA*Δ::*pyrG*), pMU4 (*cclA*Δ::*ptrA*), pMU5 (*kdmA*Δ::*pyrG*), pMU6 (*ecmB*Δ::*pyrG*), pMU7 (*rstB*Δ::*pyrG)* respectively. Linear fragments were obtained from plasmids pOB227,pOB228 and pOB230 by digestion with *Pme*I (*Mss*I) and plasmids pMU3, pMU4, pMU5, pMU6, pMU7 by using oligonucteotides(Table2.4), then, were transformed into AGB551 generating *kdmA, cclA, ecmB* and *rstB* deletion strains.

For the generation of double deletions, deletion plasmids for *kdmA, cclA, ecmB* and *rstB* with *pyrG* marker were used. Briefly, linear deletion fragments (with *pyrG*) were provided by utilizing oligos from Table 2.4 and these cassettes were transformed to related gene deletion strain (with *ptrA*) to obtain double deletion mutant strain.

All deletions strains were confirmed by either Q-RT-PCR (**Figure 2.1**) or Southern blot analysis (**Figure 2.4 and 2.5)**

2.3.3 Generation of epitope tagged strains

For the creation of *kdmA::sgfp* and *kdmA::3xHA* fusions for *A. flavus*, the promoter and ORF (4.2kbp), and terminator sequences of *kdmA* were amplified using oligos (Table 2.3). These two fragments for each strain were fused to *sgfp::AfpyrG*, *3xHA::AfpyrG* cassettes in *Sma*I site of pUC19 by using in-fusion HD cloning kit (Clontech, Cat:638911) leading to plasmids pMU34 (*kdmA::sgfp*) and pMU33 (*kdmA:: 3xHA*). *kdmA::sgfp:: AfpyrG*, *kdmA::3xHA:: AfpyrG* fused cassettes were amplified by using primers (Table 2.3) and linear fragments were introduced into TJES19.1 strain. pMU29 (*cclA::3xHA*), pMU31 (*ecmB::3xHA*) and pMU32 (*rstB::3xHA*) plasmids, linear fragments were obtained in the same way as described for *kdmA* with the related primers(Table 2.3) and ORFs which are 1.9kbp, 2.7kbp and 2.6kbp respectively.

To replace the *kdmA* locus with *kdmA::sgfp*, *kdmA::ctap* and *kdmA::3xHA* fusions for *A. nidulans*, the promoter and ORF (4.5 kbp), and terminator sequences of *kdmA* were amplified using oligos (Table 2.4). *sgfp::natR*, *ctap::natR* and *3xHA::AfpyrG* cassettes were amplified from tool plasmids with suitable oligos (Table 2.4). *sgfp::natR*, *ctap::natR* and *3xHA::AfpyrG* cassettes were amplified from tool plasmids with suitable oligos (Table2.4). Then, *gfp* and *tap* fragments were fused to each other using a fusion PRC. *ha* fusion fragment cloned in *Sma*I site of pUC19 with adding *Pme*I cutting site by using in-fusion HD cloning kit (Clontech, Cat:638911) leading to plasmid pBK10 (*kdmA::3xHA*), respectively. These cassettes were released by *Pme*I digestion and linear cassettes were introduced into AGB551 strain. The same strategy was also applied for the other complex members by generating pOB491(*cclA::sgfp*), pOB492 (*cclA::ctap*), pBK4 (*cclA::3xHA*) plasmids for *cclA*(1.8 kbp), pOB497 (*ecmB::sgfp*), pOB498 (*ecmB::ctap*), pBK7 (*ecmB::3xHA*) plasmids for *ecmB*(2.4 kbp), pOB493 (*rstB::sgfp*), pOB494 (*rstB::ctap*),pBK9 (*rstB::3xHA*) plasmids for *rstB*(2.6 kbp) and pOB495 (*mcmA::sgfp*), pOB496 (*mcmA::ctap*), pBK41 (*mcmA::13xMYC*) for *mcmA*(0.9 kbp). Then, linear fragments were transformed to AGB551 strain. All epitope tagging were done under native promoter and endogenously. Epitope tagged strains were confirmed by doing functionality test with phenotype (**Figure 2.2**) and Western blot analysis (**Figure 3.2B** and **Figure 4.1E**).

2.3.4 Generation of complementation strains

For complementation of the *kdmA, cclA, ecmB* and *rstB* deletions for *A. flavus*; the *kdmA cclA, ecmB* and *rstB* genomic locus, containing 1,5 kbp promoter and terminator regions, were amplified from gDNA using primers (Table 2.3) and cloned into the *Stu*I site of PAN8.1, which yielded pMU35, pMU22, pMU23, pMU24, respectively. Then, pMU35, pMU22, pMU23, pMU24 circularly were introduced into *kdmA cclA, ecmB* and *rstB* deletion strains, respectively; for generating the complementation strains.

In order to generate complementation of the *kdmA, cclA, ecmB* and *rstB* deletions for *A. nidulans*; the *kdmA cclA, ecmB* and *rstB* genomic locus, containing 1,5 kbp promoter and terminator regions, were amplified from gDNA using primers (Table 2.4) and cloned into the *Swa*I site of pOSB113, which yielded pMU25, pMU26, pMU27, pMU28, respectively. Then, pMU25, pMU26, pMU27, pMU28 were introduced into *kdmA cclA, ecmB* and *rstB* deletion strains, respectively; to create the *kdmA, cclA, ecmB* and *rstB* complementation strains. All complementation strains were confirmed by the Q-RT-PCR (**Figure 2.1**).

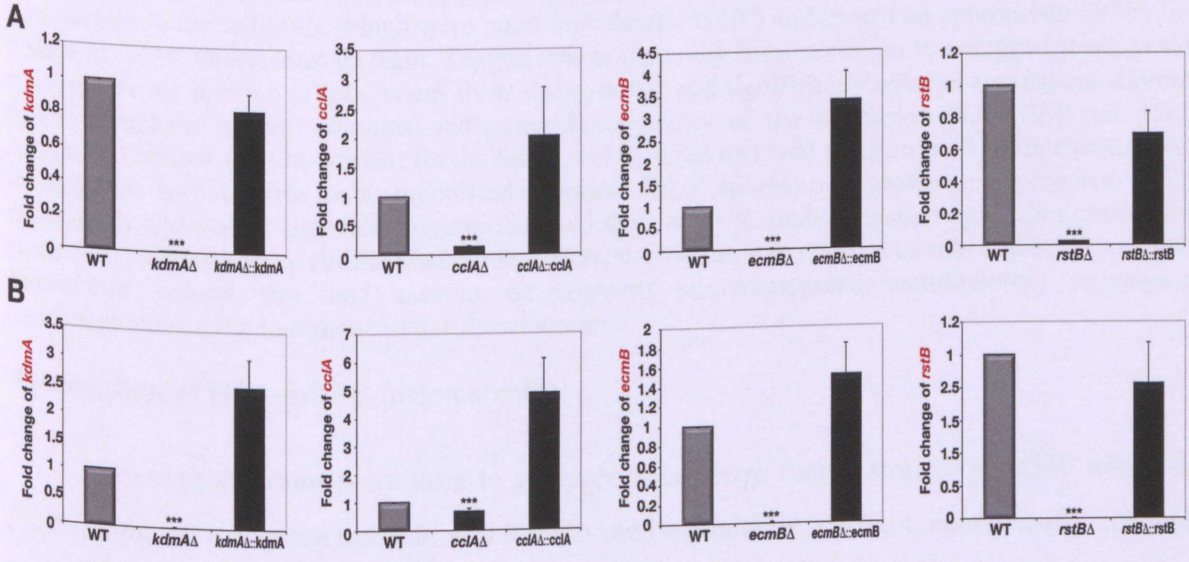

Figure 2.1 Relative expression levels of deletion and complementation strains. Expression level of *kdm*A, *ccl*A, *ecm*B and *rst*B deletions with *pyr*G marker and complementation strains compared to the *A. flavus* TJES19.1. Mutant strains and wild type were grown in appropriate Complete Media for 48 hours at 30°C vegetatively. **(B)** Expression level of *kdm*A, *ccl*A, *ecm*B and *rst*B deletions with ptrA and complementations strains compared to the *A. nidulans* AGB551. Mutant strains and wild type were grown in appropriate GMM for 48 hours at 37°C vegetatively. This experiment were performed three times and three biological repeats were performed per experiment. *ben*A was used as housekeeping gene. Error bars represent the standart deviation. Statistically significant difference, (*) $p<0.05$, (**) $p<0.001$, (***) $p<0.0001$ and (ns) $p>0.05$.

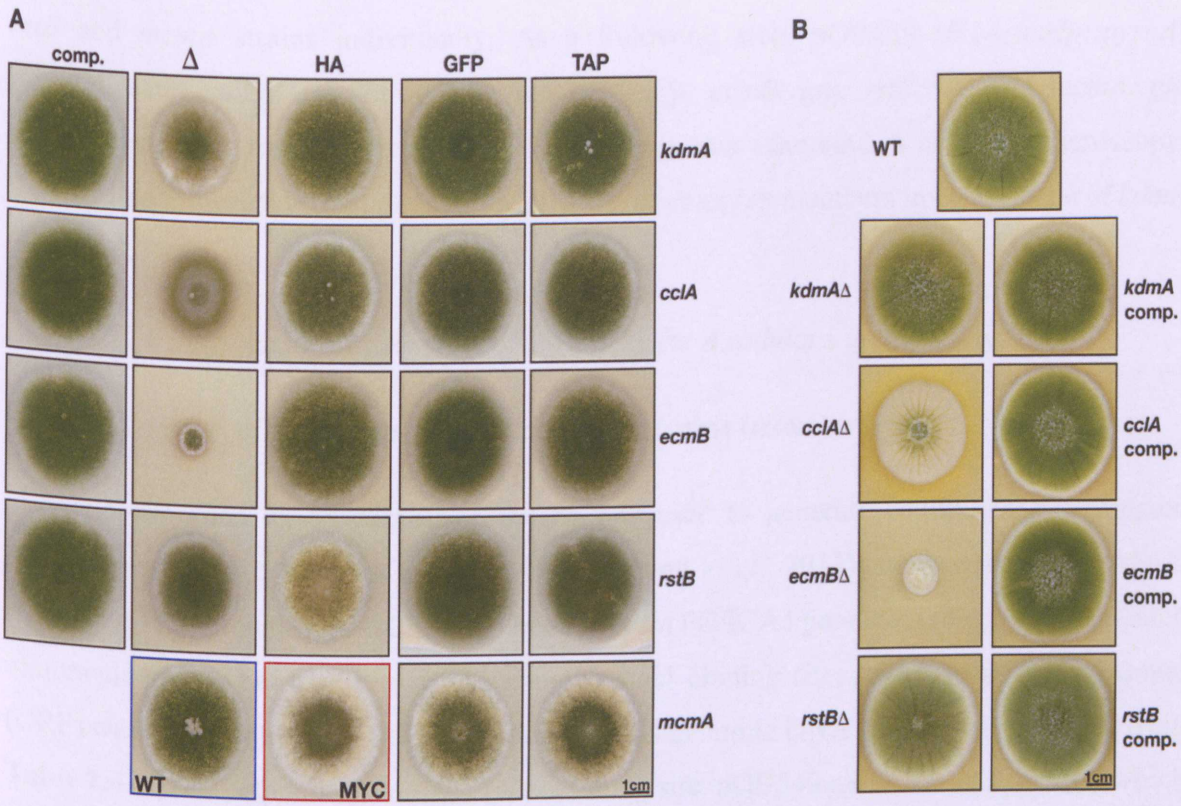

Figure 2.2 Growth test for the *A.nidulans* and *A.flavus* strains. (A) Growth test for the *kdm*A, *ccl*A, *ecm*B and *rst*B deletions and complementations in A.nidulans; HA, GFP and TAP fusions in comparison to the wild type which were point inoculated ($5x10^3$) and grown on appropriate GMM for 5 days at 37 °C under constant light. Tagged strains generally behave similar to untagged strain (wild type) where the deletion of *cclA*, *ecmB* show strong defect and significantly reduced asexual conidiation (green structures around colonies) indicating functionality of the tag-fusion (TAP,GFP and HA) *A.nidulans* strains. **(B)** Growth test for the *kdm*A, *ccl*A, *ecm*B and *rst*B deletions and complementations in A.flavus. Strains were point inoculated (approx. $5x10^3$ spores) and grown in appropriate YGT medium by addition of suppelements needed for 5 days at 30 °C under constant light. Complemented strains of *A.flavus* display similar phenotype with wild-type strain in contrast to *cclA* and *ecmB* mutants diminished colony size and asexual development structures(green conidiphores) suggesting confirmation of fully complemented *A.flavus* strains.

Generation of H2A-mRFP fusion strains

gfp-tagged strains were used to generate *H2A::mrfp* fusion strains. pOB439 which is *H2A::mrfp::pyroA* fusion plasmid was transformed ectopically to *kdmA*, *cclA*, *ecmB*, *rstB* and *mcmA* *gfp*-tagged strains resulting in *gfp* and *H2A::mrfp* fusions. Integration of fused strains *kdmA::gfp::H2A::mrfp*, *cclA::gfp::H2A::mrfp*, *ecmB::gfp::H2A::mrfp*, *rstB::gfp::H2A::mrfp*, *mcmA::gfp::H2A::mrfp* were checked under confocal microscopy which also show individual subcellular localizations (**Figure 3.1E**)

To create *H2A::mrfp* fusion of *cclA*, *ecmB*, *rstB*, *mcmA* strains in the absence of *kdmA*, firstly, *kdmA* deletion cassette was amplified from pMU5 (*kdmAΔ::pyrG*) with suitable primers from Table 2.4 and linear *kdmA* deletion fragment was transformed into *gfp*-tagged *cclA*, *ecmB*,

rstB and *mcmA* strains individually. As a following step, pOB439 (*H2A::mrfp::pyroA)* plasmid, ectopically, was introduced into *cclA::gfp*, *ecmB::gfp*, *rstB::gfp* and *mcmA::gfp* strains separately. Ectopic integration of *H2A::mrfp* was examined in confocal microscopy. Results also represent the subcellular localization of complex members in the absence of *kdmA* (**Figure 3.7D**).

H2A::mrfp fusion strains were created only for *A.nidulans* in this study.

2.3.5 Generation of tunable promoter replaced strains (*teton* strains)

A modified tet-on expression sytem was used to generate conditionally expressed *A.nidulans* strains of complex members (Helmschrott *et al.*, 2013). In order to create *kdmA-teton*, 5' UTR region of *kdmA*(1.3 kbp) obtained from FGSCA4 genomic DNA by using related oligonucleotides (**Table 2.4**) and according to *Swa*I cloning site. *kdmA* open reading frame (ORF) was also amplified by utilization of FGSCA4 genomic DNA with suitable primers from **Table 2.4** and corresponding with the *Pme*I cloning site. pOB549 modified tool plasmid which contains *pyroA* selective marker, ^{p}*tpiA*::rtTA2^{S}-M2::*tcgrA*::*tetO-*^{p}*min* fusion for tet-on sytem as well as *Swa*I and *Pme*I restriction site was digested by *Swa*I and *Pme*I. Previously amplified 5'UTR and ORF of *kdmA* were introduced into digested pOB549 by using in-phusion HD cloning kit (Clontech, Cat:638911) yielded to pBK36 plasmid. 5'UTR::*pyrG*::*teton*::*kdmA* fusion linear fragment was obtained from pBK36 with primers (**Table 2.4**) and linear fragment was transformed into AGB551 resulting in *kdmA-teton* strain. pBK37, pBK39, pBK40, pBK38 plasmids were created in the same way as explained above for *kdmA-teton* strain for *cclA*, *ecmB*, *rstB*, *mcmA*, respectively. Linear fragments were amplified from these plasmids by using primers (**Table 2.4**) and transferred to AGB551 giving rise to *cclA-teton*, *ecmB-teton*, *rstB-teton*, *mcmA-teton* strains. Strains were verified under different doxycycline concentrations (**Figure 2.3**).

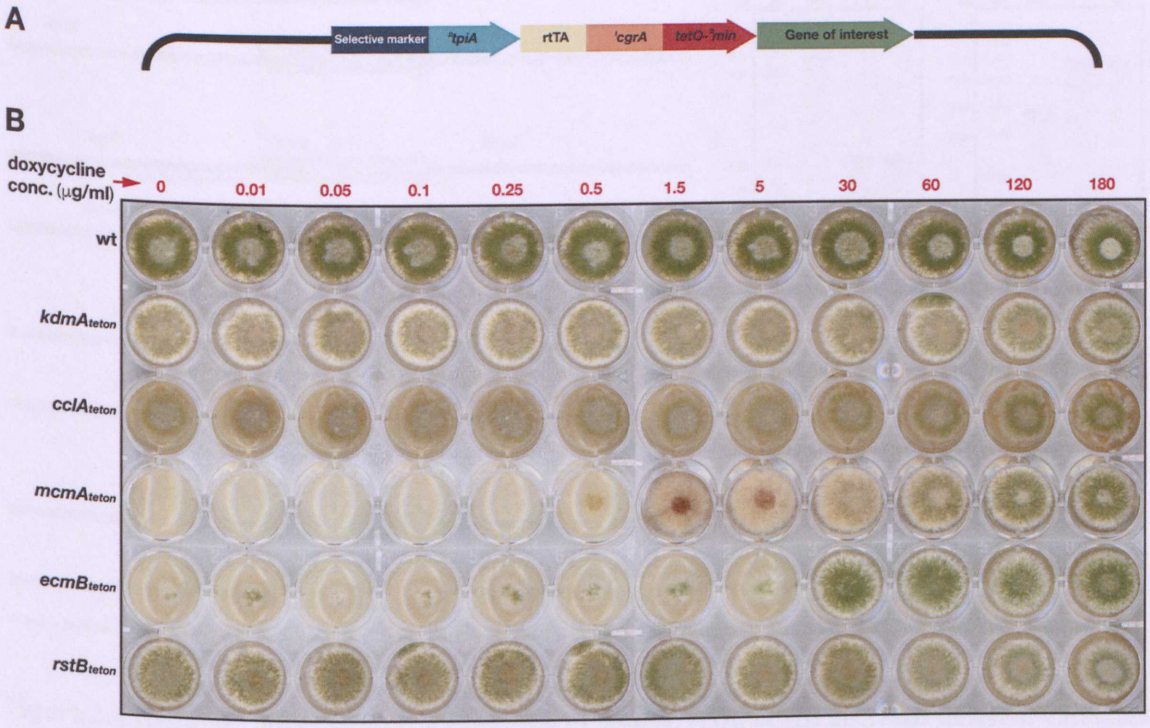

Figure 2.3 **(A)** teton expression linear fragment structure was obtained from plasmids for transformation **(B)** Doxycycline-dependent growth and verification of complex member's tetOn strains holding conditional promoter. $5x10^3$ conidia including 5 µl from each indicated strain's spore suspension were inoculated on AMM with required concentration of uridine, uracil ,agar supplemented and with the indicated amount of doxycycline and incubated at 37°C for 60 h under light condition.

2.4 Southern Blot Hybridization

Southern Blot Analysis was performed in order to confirm the deletion or replacement of a gene at a specific loci in *A. flavus* and *A. nidulans* genomic DNA (gDNA), and was carried out as described previously (Bayram *et al.*, 2008) with nonradioactively labeled probes. Genomic DNAs were digested with restriction enzymes and DNA-Probes were labelled with digoxigenin (DIG) using a DIG labeling kit (Roche). DIG labeled DNA probes were amplified by the PCR DIG Probe Synthesis kit (Roche, Cat:11277065910) as described in the manufacturer's protocol. Chemiluminescent signals were detected with G: BOX Chemi XRQ (Syngene) by using specific settings for CSPD (Roche) reagent.

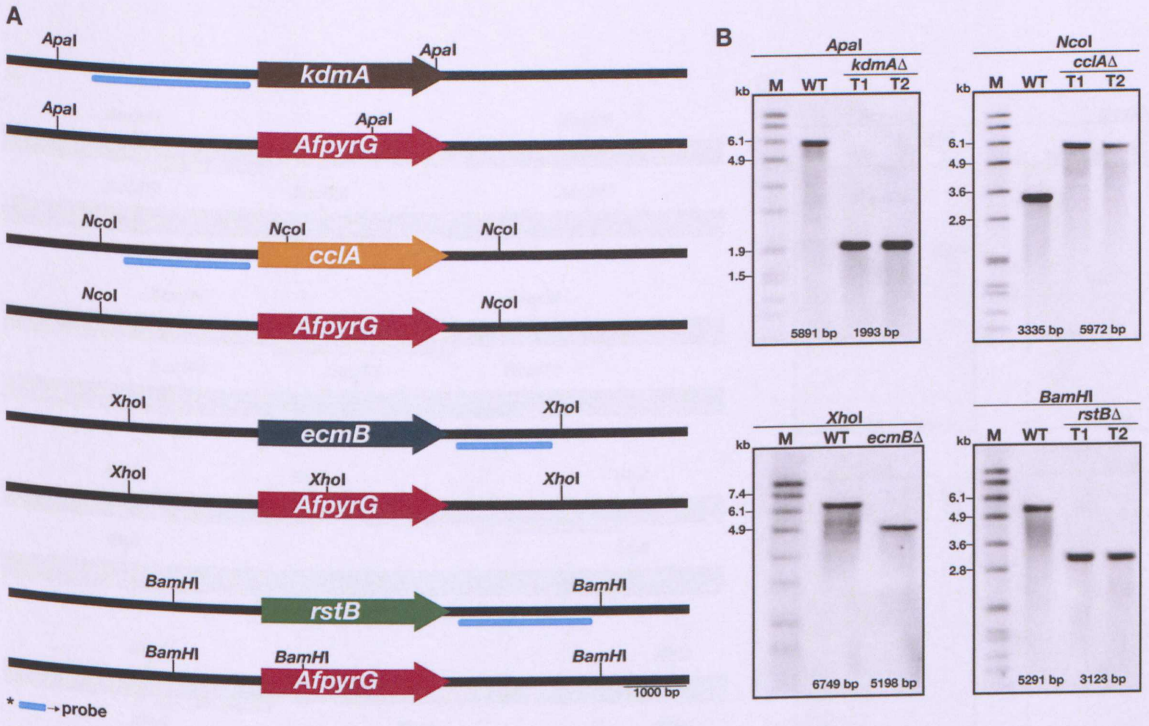

Figure 2.4 Genomic integration confirmation of *kdmA, cclA, ecmB* and *rstB* deletion cassettes in *A. nidulans*. **(A)** General depiction of the wild-type *kdm*A, *ccl*A, *ecm*B and *rst*B deletion loci. Scale bar (1000 bp), restriction enzymes and probes used for Southern Blot are shown in the figure. A small proportion of 5 5 UTR , 3 UTR or ORF were used as Southern probes. *Afpyr*G marker was used as deletion cassette. **(B)** Southern hybridizations of *kdm*A, *ccl*A, *ecm*B and *rst*B single deletions. Southern hybridizations confirm the replacement of endogenous loci by *Afpyr*G marker. Bands sizes are in agreement with theoretical maps shown in A.

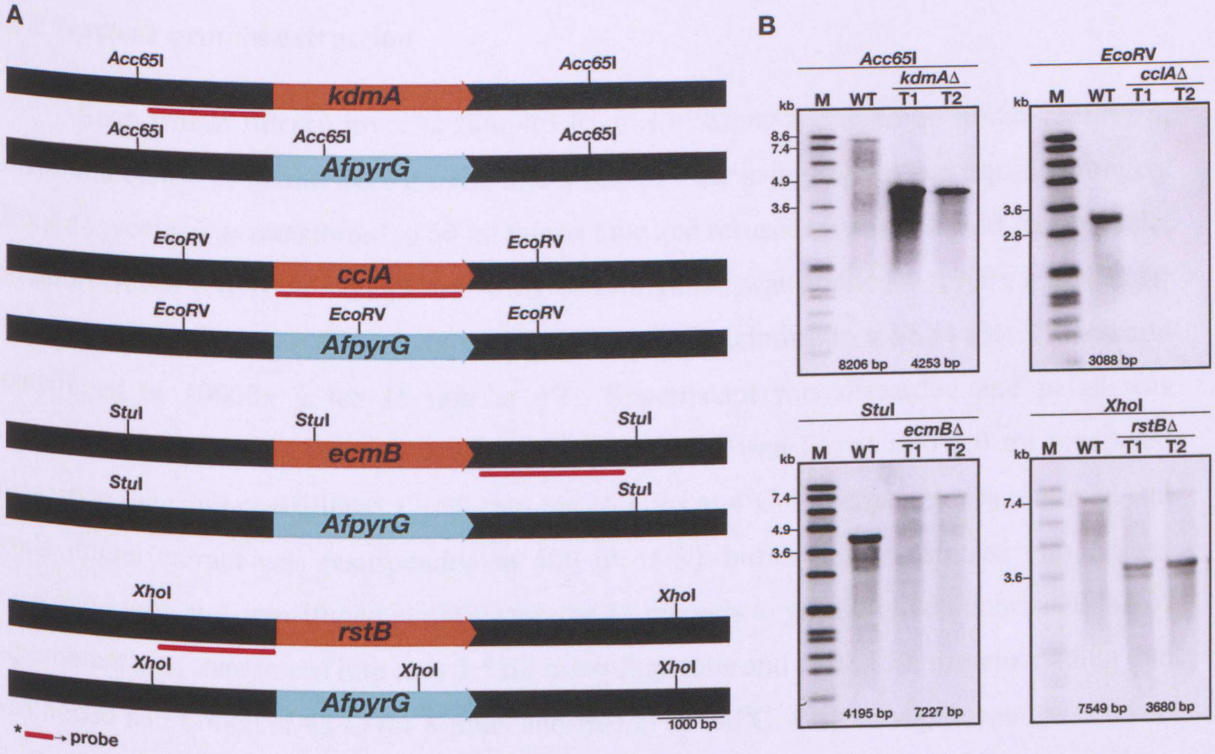

Figure 2.5 Genomic integration confirmation for *kdmA, cclA, ecmB* and *rstB* deletion cassettes in *A. flavus*. **(A)** General depiction of the wild-type *kdm*A, *ccl*A, *ecm*B and *rst*B deletion loci. Scale bar (1000 bp), restriction enzymes and probes used for Southern Blot are shown in the figure. A small proportion of 5 un-translated region (5 UTR), 3 UTR or ORF were used as Southern probes. *Afpyr*G marker was used as deletion cassette. **(B)** Southern hybridizations of *kdm*A, *ccl*A, *ecm*B and *rst*B single deletions. Southern hybridizations confirm the replacement of endogenous loci by *Afpyr*G marker. M: Molecular marker (kbp), T1&T2; Transformant 1&2, respectively. Bands sizes are in agreement with theoretical maps shown in A.

2.5 Protein Analysis

2.5.1 Total protein extraction

Mycelia from *A. flavus* and *A. nidulans* liquid cultures in Complete Media and GMM, respectively were harvested by filtering through miracloth, press dried and snap frozen in liquid nitrogen. The mycelia were ground into a fine powder using a mortar under liquid nitrogen. Around 1 mg of frozen mycelia were lysed in protein extraction buffer (B300 buffer) and added with 1 mM DTT, Protease inhibitor mix (Roche), 1.5 mM Benzamidine, 1x Phosphatase inhibitors mix (ROCHE) and 1 mM PMSF. Samples were then vortexed and were centrifuged

at 13,000 x g for 10 min at 4 °C. Protein concentrations were calculated according to the method described by Bradford (Bradford, 1976).

2.5.2 Nuclear protein extraction

Snap frozen filtered mycelia samples from *A.nidulans* and *A.flavus* liquid cultures in GMM and complete media were ground into a fine powder using mortar and liquid noitrogen. Ground mycelia was transferred to 50 ml falcon tube and resuspended in ice-cold 20 ml Nuclei Isolation Buffer (NIB) on ice and following centrifugation was applied at 1000x g at 4°C for 10 min. Supernatant was filtered through 2 layers of Miracloth into a SS34 (30ml) tube and centrifuged at 10000x g for 15 min at 4°C. Supernatant was discarded and pellet was resuspended with 1.5 ml Resuspension Buffer (RB) and transferred into 2.0 ml precooled microfuge tube and centrifuged 12000 rpm for 15 mins at 4°C. Supernatant was removed and crude nuclei extract was resuspended in 400 ul of ST buffer and transferred into 1.5 ml microfuge tube and centrifuged at 4800 rpm for 45 seconds to get rid of cell debris. 300 ul of supernatant was transferred into new 1.5 ml microfuge tube and 150 ul 3X protein loading dye was added and bolied at 95°C for 8 mins and frozen at -80°C. Rest of supernatant was taken for Bradford assay. According to Bradford results desired amount of nuclear protein was loaded 15% SDS-page gel.

2.5.3 SDS-PAGE electrophoresis and Western Blot

Stacking and separating SDS-PAGE gels were prepared according to **Table 2.7.** The gels were prepared using the Mini-Protean II gel casting apparatus (BioRad, CA, USA) according to the manufacturer's instructions. Protein exracts were prepared by adding one volume of 3X loading dye to every 2 volumes of sample and boil at 95 °C for 5-10 min. 100 µg of total protein extract was loaded onto the various percentages SDS gels as required (10% or 12%) and was separated at 120V until the dye front moved out of the gel. Proteins were transferred onto a nitrocellulose membrane (GE Healthcare) by electroblotting. The membrane was blocked with 5% w/v skim milk in TBS-T (blocking buffer) before the addition of primary antibody. After pouring the blocking buffer, primary antibody (For TAP tag: polyclonal rabbit α-calmodulin binding peptide (CBP) (1:1000 dilution in TBS with 5% milk), 05-932, EMD Millipore Corporation, and for GFP detection: α-GFP "mouse monoclonal IgG" (1:500 dilution in TBST with 5% milk), SC-9996, Santa Cruz Biotechnology) was added to the membrane for 1,5 h at room temperature on a shaker at 160 rpm. The primary antibody was poured and the

membranes were washed 3 X 5 min with TBS at 160 rpm. The secondary antibody (For TAP tag: goat α-rabbit (1:2000 dilution in TBS with 5% milk), G-21234, Life technologies, and for GFP detection: goat anti mouse (1:2000 dilution in TBST and 5% milk), 170-6516, Biorad) was added to the membranes for 1 h at room temperature and at 160 rpm. The secondary antibody was poured and the membranes were washed 3 X 5 min with TBS at 160 rpm. As detection reagent, the Enhanced Chemiluminescence (ECL) technology (Bio-Rad) products were used according to manufacturer's instructions. Chemiluminescent signals were detected with G: BOX Chemi XRQ (Syngene). Band intensities in the immunoblottings were normalized against rabbit polyclonal α-SkpA (Genescript) 1:2000 dilutions in TBS and 5% milk with 0.2% Tween-20 and goat α-rabbit was used as secondary antibody for SkpA.

Post-translation modifications immunoblot analysis were performed from nuclear protein extracts and 15% SDS-page gel was used for all analysis. α-H3K36me3(ab9050), α-H3K4me3(Active Motif; 39159), α-H3K9me3(Abcam; ab8899), α-H3K14Ac (Merck; 07-353) and α-H3(Abcam; ab1791) antibodies were used for modifications and loading control with 1:2000 dilution in TBS and 5% milk with 0.2% Tween-20. Goat α-rabbit was used as secondary antibody for all post-translation modifications analysis.

Table 2.7 Reagents composition for SDS-PAGE Stacking and Separating Gel

	Stacking Gel (Acrylamid 4 %)	**Separating Gel (Acrylamid 10 %)**	**Separating Gel (Acrylamid 12 %)**
H2O	3,67 ml	2,8 ml	3,2 ml
1 M Tris	650 µl (pH:6,8)	3,75 ml (pH:8,8)	2,6 ml (pH:8,8)
10 % SDS	50 µl	100 µl	100 µl
30 % Acrylamid, 0.8% Bis-Acrylamide	650 µl	3,3 ml	4 ml
TEMED	5 µl	10 µl	10 µl
10 % APS	25 µl	100 µl	100 µl

2.5.4 TAP (Tandem Affinity Purification) coupled mass spectrometry

Purification of TAP-tagged strains, preparation of the protein crude extracts and analysis of the proteins were performed with Tandem Affinity Purification (TAP) Protocol as described (Bayram *et al.*, 2008b). Briefly, mycelia samples were frozen and ground with liquid nitrogen. Ground mycelia was transferred into ice-cold SS34 tube and re-suspended with 15 ml B250 buffer which includes protease and phosphatase inhibitors and followed vortex vigorously. Re-suspended sample was centrifuged 16000 rpm at 4°C for 20 mins. Supernatant was transferred into new 15 ml tube and 100 ul IgG coupled magnetic beads added. Protein

and beads mixture was rotated at 4°C for 4 h. After beads treatment, protein extract was removed by using magnetic rack. Beads were washed with WB250, WB150 and TCB buffers, respectively by using magnetic rack. Beads were re-suspended with the 1.5 ml TCB buffer and transferred into new 1.5 ml microfuge tube. 20 ul TEV protease was added in sample and rotated at 4°C for O/N. After O/N incubation supernatant was transferred into new 1.5 ml tube and 200 ul equilibrated CAM (calmodulin affinity) magnetic beads solution was added and rotated at 4oC for 2 h. Rotated sample was placed on magnetic rack and supernatant was removed. Beads were washed down three times by using 1 ml CBB (calmodulin binding buffer). Then, trypsin digestion was performed on protein conjugated beads. By utilizing tryptic digest, proteins were digested into peptides and after that zip-tip process was applied. Zip-tipped peptides were run on LC-MS/MS.

Raw data from peptide analysis was run through the proteome discoverer software (*ThermoScientific*) against to *A.nidulans* protein database file (provided from AspGD) and *A.flavus* database file (obtained from NCBI). Detected protein list was generated by chosen with criteria of peptide confidence as 'high', minimum peptide number as 'two'. Extracted protein list for identified proteins were exported as excel file for *wt* and tagged strains. Tagged strains protein list was subtracted from *wt* list to get rid of unspecific binding proteins and unique interaction partners were presented for tagged strains.

2.5.5 GFP and HA affinity purification coupled mass spectrometry

Immunoprecipitation of GFP- or HA-tagged strains was performed as described in detail (Bayram *et al.*, 2012). Briefly, mycelia samples were frozen and ground with liquid nitrogen. Ground mycelia was transferred into ice-cold 1.5 ml tube and re-suspended with 1 ml GFP-trap buffer which includes protease and phosphatase inhibitors and followed vortex vigorously. Re-suspended sample was centrifuged 13000 rpm at 4°C for 10 mins. Supernatant was transferred into new 1.5 ml tube and 20 ul HA tag affinity magnetic beads added. Protein and beads mixture was rotated at 4°C for 2-3 h. After beads treatment, protein extract was removed by using magnetic rack. Beads were washed with GFP-trap buffer three times by using magnetic rack. Same further steps were performed on the protein conjugated beads here as explained in Section 2.5.4 for tryptic digest, zip-tip, running on the LC-MS/MS and generation of interaction protein lists.

2.6 Microscopy

2.6.1 Light Microscopy

A. flavus and A. nidulans colonies and quantification of sporulation were visualized using the Olympus szx16 microscope with Olympus sc30 camera. *A. flavus* and *A. nidulans* spores (approx. $5x10^3$) were point inoculated on GMM, which contains appropriate supplements. Plates were incubated during constant white light exposure (for asexual development) and in dark conditions (for sexual development) for 4-5 days at 30°C for *A. flavus* and at 37°C for *A. nidulans*. Sporulation was quantified with a hemocytometer and was performed in triplicate. Cell Sens Standard software (Olympus) were used for recording and processing of images.

The effect of genetic modification on sclerotial production in *A. flavus* and on fruiting body formation in *A. nidulans* were also assessed with the stereomicroscope (OLYMPUS, SZX16) by taking high magnification pictures. For sclerotia production, *A. flavus* strains were cultivated on Wickerham Medium (WKM), with appropriate supplements at 30°C for 14 days in dark conditions, and *A. nidulans* strains were cultivated on GMM with appropriate supplements at 37°C for 14 days in dark conditions. After incubation, plates were washed with 70% EtOH in order to improve visualization of sclerotia production.

2.6.2 Confocal microscopy

To assay the subcellular location pattern of Green fluorescent and monomeric red fluorescent protein (GFP and mRFP), strains were incubated in 500µl liquid GMM, with appropriate supplements in Lab-Tek Chambered Coverglass W/CVT (Thermo Scientific) for 12-16 hours at 25°C. Growth mycelial was analyzed using Olympus FluoView 1000 confocal microscope according to published method (Bayram *et al.*, 2012a).

2.7 Secondary metabolite Analysis

2.7.1 Organic extraction

For aflatoxin production, *A. flavus* wild type and mutant strains were point inoculated as 5µl (approx. 5000 conidia) in Yeast Extract Sucrose (YES) Medium, with appropriate supplements and agar plates at 30°C for 7 days in dark conditions. After incubation, approximately 1 cm sized punch of agar was taken from plate and chopped by scalpel and

transferred to tube followed by adding 4 ml of deionized H_2O and left on the shaker for 1h at RT. By the end of shaking, 4 ml Chloroform was added to each tube and put in the shaker for another 1h incubation at RT. Tubes were centrifugated for 10 mins at 5000 rpm to separate the two phases from each other and then all the Chloroform phase (about 4 ml) was transferred to another tube and dried in a speedy-vac concentrator (miVac DNA Concentrator).

A. nidulans samples were processed by the same method as described above for Sterigmatocystin production analysis, differently GMM agar medium with supplements was used and 10% groud oatmeal was added in media to induce the sterigmatocystin production. And also *A.nidulans* samples were incubated in the light conditions for 5 days at 37°C. Samples were extracted as triple biological replicates for both organisms.

2.7.2 Reverse Phase-High performance Liquid Chromatography (RP-HPLC)

The samples were resuspended in 200 µl methanol and run on a Shimadzu RP-HPLC with a photodiode array detector (PDA). Aflatoxin B2 (SIGMA, Cat: A9887) and sterigmatocystin (SIGMA,Cat:S3255) were used as standards from stock concentration which were dissolved in MetOH with 1mg/ml. For HPLC measurements, 20 µl of the concentrated samples or standards were injected onto a Luna®omega 5µm polar C18 column (LC column 150 x 4.6 mm) at a flow rate of 1 ml/min. Gradient elution was performed with HPLC grade water consisting of 0.1 % trifluoroacetic acid and acetonitrile consisting of 0.1 % trifluoroacetic acid was used. Gradient conditions of 5-100% acetonitrile over 30 min were used with PDA detection at 254 nm. For quantification of aflatoxin and sterigmatocystin, calibration curves were calculated from 6,25 µg/ml to 400 µg/ml.

2.7.3 LC-MS/MS

For the investigation of global secondary metabolite profile, $2x10^6$ spores/ml *A.nidulans* wild-type and mutant strains (single and double deletions) were inoculated in 50 ml GMM liquid media with needed supplements and incubated either 24h or 52h in shaker at 37^0C with 200 rpm shaking speed. After incubation time, 1ml of liquid culture sample was taken and frozen. This step was repeated as triple biological and 3 technical replicates for each strain as well as medium samples as negative control. Thawed 1ml culture samples were run on a QTrap 5500 LC-MS/MS System (Applied Biosystems, Foster City, CA, USA) equipped with a TurboIonSpray electrospray ionization (ESI) source and a 1290 Series HPLC System (Agilent, Waldbronn, Germany). Chromatographic separation was done at 25 °C on a Gemini® C18-

column, 150 × 4.6 mm i.d., 5 µm particle size, equipped with a C18 4 × 3 mm i.d. security guard cartridge (Phenomenex, Torrance, CA, USA). The chromatographic method, chromatographic and mass spectrometric parameters are described elsewhere (Malachová et al., 2014). Results were detected by running standard samples for each compound and were normalized according to wild-type 48h samples.

2.8 PCR methods

2.8.1 General PCR conditions

Standard PCR reactions were carried out to amplify fragments of DNA for cloning, transformation constructs, probes, and Colony PCR were carried out to test for recombinant plasmid presence in *E. coli*. Standart PCRs was generally carried out using Q5® High-Fidelity DNA polymerase (NEBioLabs, Cat: M0492S), and Colony PCR was generally carried out using Phusion® DNA polymerase (NEBbioLabs, Cat: M0530S). All PCR reactions were generally carried out with the following cycling parameters: initial denaturation at 98°C for 30 sec, 34 cycles of denaturation 98°C for 10 sec; annealing 63°C (or estimated melting temperature (Tm) of the primers used) for 20 sec; extension 72°C 20 sec/kb, and with final extension 72°C for 5 min. For Colony PCR reactions were generally carried out as described above with the exception that the initial denaturing step was increased to 95 °C for 5 min to allow the bacterial cells to rupture and release DNA for the PCR reaction. PCR reactions were performed in bench-top PCR machine (SENSOQUEST, Thermocycler48, Germany).

2.8.2 Q-RT-PCR

To monitor gene expression changes; *A. flavus* wild-type and mutant strains were cultivated in Complete Media with appropriate supplements in vegetative growth with aimed incubation time, and for developmental stage based expression (in sexual and asexual growth), basically, 20h vegetative stage growth mycelia were washed by autoclaved H_2O and shifted to Complete medium agar plate including needed supplements and incubated for aimed incubation time either under dark or light conditions at 30°C.

A.nidulans strains were cultivated in GMM liquid media with appropriate supplements at 37°C in different growth stages (Vegetative, Asexual, Sexual) for needed incubation time. For the developmental stages mycelia shift was processed as explained above and transfer to

GMM agar plates with the required supplements and incubated under dark or light conditions at 37°C.

After aimed incubations mycelia samples were washed by 1% DEPC (Diethyl pyrocarbonate) included and autoclaved H_2O and snap-freezed with liquid nitrogen. Total RNA was extracted from frozen mycelia by using the DNAse I (Cat.NO.79254, Qiagen) and was quantified by using Qubit RNA BR Assay Kit Protocol (Cat: Q10210) according to the manufacturer's instructions. About 1000 ng RNA was applied for cDNA synthesis by using the Transcriptor First Strand cDNA Synthesis Kit (Roche, Cat: 04896866001). qPCR reactions were performed by using LightCycler®480Sypr Green I Master (Roche). *skp*A and *benA* was used as house-keeping gene and for *A. flavus* and *A. nidulans*, respectively. Light Cycler® 480 Software was used for Relative Expression Analysis. The experiments were repeated as three biological followed by three technical replicates.

2.9 Transformation

2.9.1 Fungal Transformation

Transformation of *A. flavus* and *A. nidulans* were performed by polyethylene glycol mediated fusion of protoplasts as described previously (Punt and van den Hondel, 1992).

2.9.2 Bacterial Transformation

Competent *E. coli* Stellar (Clontech) and MACH-1 (Invitrogen) cells were prepared by the DMSO method as described (Inoue *et al.*, 1990). Transformation of competent *E. coli* cells was performed with SOB and SOC-media according to (Hanahan *et al.*, 1991). Colony PCR was performed to verify the presence of the desired insert in the plasmid of the sample clones.

2.10 Plant Pathogenicity Assays

The ability of the *Aspegillus flavus* strains to infect crop seeds was assayed as described.

2.10.1 Peanut Assay

Mature peanut seeds (*Arachis hypogaea*) were prepared by removing the brown exterior peanut layer (testa) by hand. The two cotyledons of each seed were separated and the embryo carefully removed without damaging any of the cotyledon tissue. Then, cotyledons

were surface sterilized by placing them in a tea ball infuser and dipping them in a beaker containing 0.05% sodium hypochlorite in sterile water for 3 min. The tea ball was transferred to a new beaker containing sterile distilled water for 30 s (wash step). Followed by a 5 s wash with 70% ethanol in a new beaker (additional sterilization step) and one more 30 s wash with sterile distilled water while shaking the tea ball. The cotyledons were drained completely were and placed in a petri dish until the time of infection. All the steps were aseptically performed in a biosafety hood. Peanut cotyledons were inoculated with a 10^5 spores/ml. Cotyledon treatments included water control (mock inoculation) and infection with fungal strains. For all treatments, 20 peanut cotyledons were immersed in 20 ml of sterile distilled water (control) or sterile distilled water with fungal conidia in 50 ml centrifuge tubes while shaking for 30 min in a rotary shaker at 100 rpm. Cotyledons were placed in petri dishes lined with three pieces of moist filter paper (to create a humidity chamber) and a water reservoir (lid of a 15 ml centrifuge tube containing 2 ml of sterile water) to maintain high humidity. Cotyledons were incubated for 4 days at 30 °C in dark conditions. The filter paper was moistened daily.

2.10.2 Aflatoxin Analysis from Peanut

Four days after infection, 4 pieces of peanut cotyledons were collected in 50 ml centrifuge tubes containing 3 ml 0.01% Tween 80 (v/v in ddH_2O) then tubes were vortexed vigorously and shaken at 150 rpm for 1 hour. For extraction, 5 ml of acetone was added to the tubes and shaken at 150 rpm for 10 minutes then 5 ml chloroform was added to each sample and shaken again at 150 rpm for 10 minutes. By the end of shaking, samples were centrifuged for 15 min at 2000 rpm to collect the organic lower phase. Samples were then dried out completely and were re-suspended in 5 ml of 0.1 M NaCl methanol:water (55:45 v/v) and 2.5 ml of hexane. Following the vortex for 1 min, tubes were centrifuged at 2000 rpm for 5 min. The hexane layer was collected and the fatty acid inter-phase layer was discarded. The remaining aqueous phase was washed an additional time with 2.5 ml hexane as described above. The hexane extracts were combined, allowed to dry and then re-suspended in 200 µl methanol and run on a Shimadzu RP-HPLC as described above (**Section 2.7.2**).

2.11 Stress tests

$5x10^3$ spores containing 5µl suspension of *A. flavus* and *A. nidulans* strains were spot inoculated on YGT and GMM with appropriate supplements and stress agents, respectively. *A. flavus* strains were incubated at 30°C for 72 hours, *A. nidulans* strains were incubated at 30°C

for 72 hours and each experiment was carried out in triplicate. Stress reagents and concentrations used in this study are shown in **Table 2.8.** For the determination of stress chemical concentration, three different concentrations were tried and minimum inhibition concentrations (MICs) were picked up and listed.

Table 2.8 Reagents and concentrations used for test stress process

Substance	Stock solution	Solvent	For 100 ml media
Hydroxyurea (HU)	50mg/ml	H_2O	197.6µl for 5.2mM
3-AT (3-amino1,2,4triazole)	100mg/ml	H_2O	83.3µl for 1mM final conc.
			250µl for 3mM final conc.
1M NaCl			5.84g
MMS (Methylmethanesulfonate)	Clear-liquid (100%)		30µl for 0.03%
Latrunculin B	1mg/ml	DMSO	20µl for 0.2µg/ml
4-NQO (4-Nitroquinoline *N*-oxide)	25mg/ml	Acetone	1µl for 0.25 µg/ml
CPT (Camptothecin)	10mg/ml (store 2-8°C)	DMSO	261µl for 75 µM final conc.
Benomyl	1mg/ml	DMSO	30µl for o.3g/ml
Caffeine			400µl for 2mM
SDS	10%	H_2O	50µl for 0.005%
EMS (Ethyl methanesulfonate)	Liquid (100%)		50µl for 0.05%
Congo Red			40µl for 20µm
H_2O_2	30%	H_2O	10µl for 1mM
			20µl for 2mM
Menadione sodium bisulfite (water soluble form of Menadione)	50mg/ml	H_2O	44.2µl for 0.08mM
Diamide (Tetramethylazodicarbox amide)	20mg/ml	H_2O	430.45µl for 0.5mM
Calcoflour			1ml for 5mg/ml
Nocodazole	5mg/ml	DMSO	2µl for 0.1µg/ml
1M KCl			7.45g

2.12 Nucleic acids Sequencing and Bioinformatics

2.12.1 Chromatin Immunoprecipitation (ChIP)

$2x10^6$ spores of, *A. nidulans* untagged AGB551 strain and *kdmA::3xHA, cclA::3xHA, ecmB::3xHA, mcmA::13xMYC* and *rstB::3xHA* tagged strains were cultivated in GMM with appropriate supplements at 37 °C for 20 and 48 hours at 200 rpm. After incubation, 3 ml of 37% formaldehyde (final conc. 1%) was added to the media to fix cells and cells were incubated

for 20 min at room temperature on a shaker at 90 rpm. For stop fixation, 25 ml of 2.5 M glycine was added on liquid cultures and were incubated for 20 min at room temperature on a shaker at 90 rpm. Cells were filtered to remove fixation buffer, washed by adding ddH_2O for 3 times and press dried. Following the snap frozen in liquid nitrogen, mycelia samples were measured as 30-40 mg aliqouts and were lyophilized in vacuum freeze dryer (Labconco Freezone 4.5) and kept at -80°C until chromatin preparation.

For the chromatin extraction, 100 µl zirconium oxide beads (0,5 mm diameter, ZROB05, NextAdvance) and 800 µl ice-cold FA lysis buffer (150mM NaCl) were added to 30-40 mg lyophilized mycelia containing tube. Samples were lysed for 3 min using Bullet Blender (NextAdvance, Storm24) for 5-8 times with a 3-min incubation on ice in between. Chromatin was pelleted by centrifugation at 15,000 r.p.m. for 20 min at 4 °C, re-suspended in 500 µl of FA (150mM NaCI) lysis buffer and fragmented in a sonicator (Qsonica Q800). Pellets were centrifuged at 15,000 r.p.m. for 30 min at 4°C, sonicated chromatin solution(supernatant) was transferred and kept at -80°C until use. To check chromatin quality, 25 µl chromatin solution and 75 µl Chip Elution Buffer were incubated at 65°C for overnight. Chromatin samples were purified by using Qiagen PCR Purification Kit (Cat No: 28106) according to the manufacturer's instructions and were run on 2% agarose gel. Optimum size of shredded chromatin was chosen around 200-400 bp otherwise all steps were repeated from chromatin extraction step.

Immuno-precipitation of *wild-type*, HA-tagged, MYC-tagged and mutant strains were carried out by first mixing 50 ml of chromatin extract with 450 ml of FA(150mM) lysis buffer and 2 µg of anti-HA (SantaCruz Biotechnology, Cat: sc-7392,) or 2 µg of anti-MYC (SantaCruz Biotechnology, sc-40(9E10)) or 2 µg of Anti-RNA polymerase II subunit B1(phospho-CTD Ser-5)(Milipore-MERCK, Cat: 04-1572) antibodies; for 1,5 h at room temperature on a rotator. Following incubation, 20 µl Protein A Sepharose (GE Healthcare) were added and mixed for another 1,5 h at room temperature on a rotator. Mixture was centrifuged at 3000 rpm for 2 min and supernatant was removed. Later Protein A Sepharose matrix was transferred to a Corning Costar SpinX centrifuge tube and was washed two times with FA (150mM NaCI) lysis buffer and once with FA (500mM NaCI) lysis buffer, then, once with ChIP wash buffer and once with TE wash buffer and centrifuged at 3000 rpm for 2 min. Immuno-precipitated chromatin DNA was eluted by incubation with 100 µl ChIP elution buffer at 65°C for 1 h and centrifuged at 3000 rpm for 2 min and SpinX filter discarded and eluted chromatin in tube was left at 65°C

overnight for decrosslinking. The following day, precipitated chromatin was purified by using Qiagen PCR Purification Kit (Cat No: 28106).

2.12.2 ChIP sequencing

Processing of ChIP-seq data and de-multiplexing were carried out as described previously (Wong *et al.*, 2013). Libraries were sequenced by the Illumina HiSeq2500 platform. The mitochondrial and nuclear genome sequences and General Feature File for *A. nidulans* AGB551 were downloaded from www.aspgd.org (GenBank project accession number: AACD00000000.1).

2.12.3 Bioinformatics analysis

Bioinformatics analysis of the data was processed as described previously (Xie *et al.*, 2017) by using *A. nidulans* genome sequence provided from AspGD.

2.13 Statistical Analysis

GraphPad Prism software (La Jolla, CA, United States) was used for statistical analysis. The significance of the data was tested with the Student's t-test and One-way ANOVA using a *p*-value (* means there is slight difference $p<0.05$, ** means more significant difference $p<0.005$ and *** means strong significant difference $p<0.0005$). The error bars in all figures indicate the standard deviation of the mean.

Chapter 3

The role of the MERCK complex in development and secondary metabolite production of *A. nidulans*

3.1 Identification of the MERCK demethylase complex and determination of its subcellular localization in *A. nidulans*

As outlined in the introduction section, fungal development and secondary metabolism processes are tightly connected to each other and the transcriptional control of biosynthetic SM gene clusters is mostly assisted by transcription factors or regulatory protein complexes (Bayram *et al.*, 2008a; Bok *et al.*, 2009; Yin and Keller, 2011). In a recent study, it was shown that KdmA (AN1060), a member of the KDM4 family of jumonji histone demethylase proteins, is involved in secondary metabolism and plays an important role in fungal development (Gacek-Mathew *et al.*, 2015). Since protein complexes and epigenetic regulations are critical for fungal growth and SM biosynthesis, KdmA complex formation was investigated experimentally. TAP coupled to MS revealed that KdmA which was endogenously expressed under its native promoter as TAP fusion interacts with some prominent proteins, including CclA (AN9399), EcmB (AN5533), RstB (AN12489) and McmA (AN8676).

In order to confirm the presence of the complex, KdmA and interacting proteins CclA, EcmB, RstB and McmA were individually epitope tagged with the following 4 different tags: TAP, GFP (Green Fluorescent Protein), HA (Hemagglutinin) and MYC tags. Functionalities of all tagged strains were checked by phenotype analysis and are shown in the material and methods section (**Figure 2.2**). Mycelia samples were taken from shaking cultures in 24h growth GMM medium and tag specific protein purification pulldown methods were applied and peptide samples were run on the MS (as described in Chapter 2). Individual unique peptide numbers for each tagged complex member can be seen in **Figure 3.1.C** by utilizing pulldown coupled MS analysis. Depending on TAP-tagged pulldowns, results (**Figure 3.1C**) were used to construct the interaction network of the complex that was generated by using the Cytoscape network analysis platform and identified unique peptide numbers were limited to three (**Figure 3.1D**). The network map shows protein-specific interacting proteins as well as common ones. Data shown in **Figure 3.1C** and **1D** strongly indicate that endogenously tagged and expressed KdmA, CclA, EcmB, RstB and McmA are reciprocally able to recruit each other, suggesting that there is indeed existence of MERCK complex formation in the cell. To survey the domain structure of the complex (**Figure 3.1A**) members and homology comparisons (**Figure 3.1B**), individual protein sequences of complex components were obtained from the Aspergillus Genome Database and domain analysis was performed by using Interpro and Pfam domain search online tools and NCBI pBLAST was used for homology map. As can be seen from the

interaction table in **Figure 3.1C**, only McmA is tagged with MYC, since a preliminary attempt of HA tagging was unsuccessful. A possible reason for this can be that tagging the gene causes disruption of gene function.

To understand the localization profile of the complex within the cell, a H2A::mRFP nuclear fusion cassette was transferred to functionally GFP tagged versions of each member individually by fungal transformation. 12h grown hyphal structure of individual H2A fused strains in chamber slides including GMM medium were examined using confocal laser microscopy (described in Chapter 2). Microscope images are shown in **Figure 3.1E**. The first row refers to a GFP filter signal whereas the second raw shows monomeric red fluorescent protein fused H2A where the nuclei is located and it can be seen that GFP and mRFP signals overlapped. Data from **Figure 3.1E** suggest that the MERCK complex members KdmA, CclA, EcmB, RstB and McmA are localized in the nucleus.

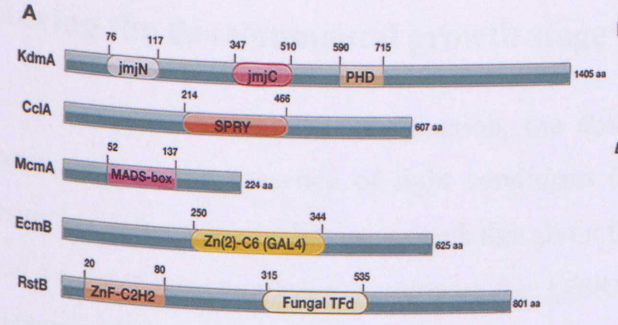

B

	kdmA	cclA	ecmB	rstB	mcmA
H.sapiens	KDM4	ASH2L			SRF
M.musculus	Kdm4	Ash2l			Srf
D.melanogaster	KDM4	ash2			CG3411-RB
A.thaliana	PKDM7	ASH2R			MAF4
C.elegans	jmjd-2	ash-2			unc-120
S.cerevisiae	RPH1	BRE2	ECM22	YGR067C	MCM1
N.crassa	NCU03505	NCU06993	NCU06993	NCU06993	NCU07430

ortholog present ortholog absent

C

		Unique Peptide Numbers				
		KdmA	CclA	EcmB	RstB	McmA
TAP- tagged	KdmA	58	20	18	24	1
	CclA	65	27	14	25	1
	EcmB	58	22	21	25	1
	RstB	52	21	14	26	1
	McmA	45	21	12	23	2
GFP- tagged	KdmA	43	18	13	18	1
	CclA	40	15	7	9	1
	EcmB	33	9	21	16	1
	RstB	45	13	11	21	1
	McmA	31	10	5	10	1
HA- tagged	KdmA	58	26	17	27	1
	CclA	65	28	13	26	2
	EcmB	51	17	21	20	1
	RstB	58	26	14	31	1
	McmA	54	22	9	17	5

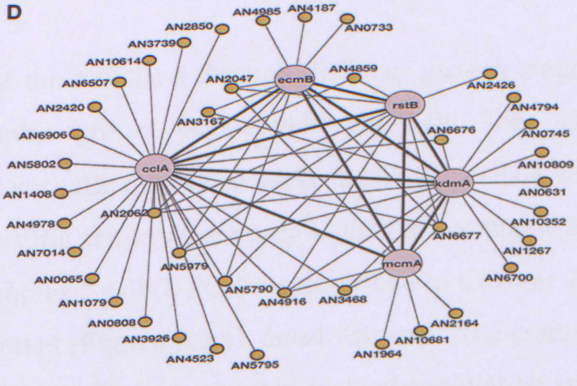

E

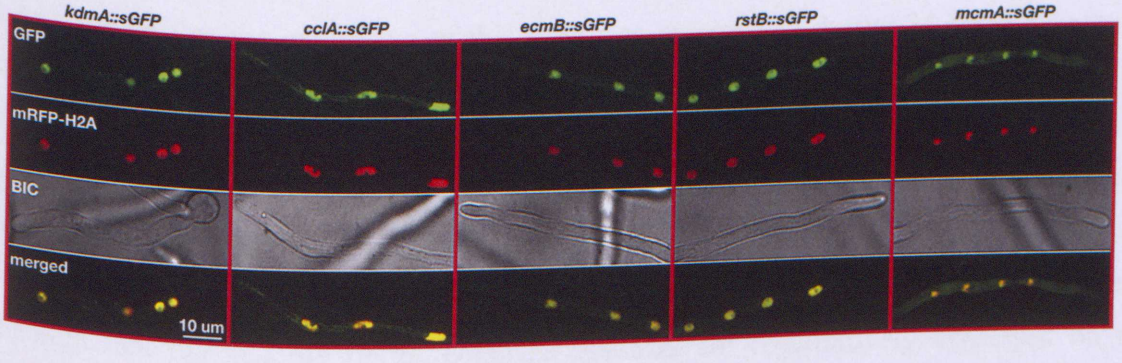

Figure 3.1 Domain map, identification and subcellular localization of MERCK complex components in *A. nidulans*. **(A)** An illustration of the domain architecture of the MERCK complex members. Amino acid numbers are indicated on the right side (C-terminus) of proteins. Domain annotation was accomplished by using InterPro (https://www.ebi.ac.uk/interpro/) and pfam database (https://pfam.xfam.org/). Protein sequences were taken from Aspergillus genome database (http://www.aspgd.org/) with individual accession numbers which are AN1060(*kdmA*), AN9399(*cclA*), AN5533(*ecmB*), AN12489(*rstB*) and AN8676(*mcmA*). **(B)** Ortholog table of MERCK complex members. NCBI Basic Local Alignment Tool (BLAST) was used to compare complex members protein sequences (from Aspergillus genome database). **(C)** Comparative mass spectrometry results table for complex members protein pull-downs. Each member was tagged with three different tags(TAP, GFP, HA or MYC) and purified by using three different methods. Unique peptide numbers refer to detected peptides by mass spectroscopy for each member's purification. **(D)** Interaction network of MERCK complex. Network was generated using a complex network analysis platform, Cytoscape (version 3.6.1) by using TAP-pulldown results for each member and interaction partners were set to have at least three unique peptide numbers. **(E)** Localization of complex members within living cells. GFP fused strains are localized in the nucleus which also matches with the mRFP fused H2A signal position in the nucleus.

3.2 Expression levels of the MERCK complex members are downregulated during the developmental growth stage in *A. nidulans*

As outlined in the introduction, the absence of *kdmA* was shown to give a blind phenotype in the presence of light conditions (Gacek-Mathew *et al.*, 2015). Showing the complex formation and having knowledge about the *kdmA*Δ response to environmental factors led to the gene expression pattern of the MERCK complex as well as protein expression patterns being investigated experimentally.

To examine gene expression levels of the members through different growth stages, mRNA was extracted from mycelia samples grown vegetatively for 24h, 36h, 48h (V24,V36,V48), asexually for 24h (A24), and sexually for 24h and 48h (S24,S48). cDNA was synthesized from mRNA samples and gene specific primers were used to gain the comparative transcriptional expression quantity for the complex by qRT-PCR (as described in Chapter 2). Amplification results were normalized and plotted (**Figure 3.2A**). *benA* was used as a control gene. It is known from the literature that *brlA* (AN0973) is involved in asexual conidiation and it was shown that the expression of this gene was upregulated during 24 hours of asexual induction. It was also shown that expression of *stcQ* (AN7810), a member of the sterigmatocystin gene cluster, is increased in the vegetative 36h stage. Having this knowledge created a chance to use both of these genes as reference genes to check the functionality and quality of cDNA. The top two plots in **Figure 3.2A** are significantly consistent with literature findings for *brlA* and *stcQ* and confirm the PCR products. Moreover, in **Figure 3.2A**, it is apparent that the majority of the complex members are constitutively expressed on the transcriptional level during the vegetative life cycle, whereas the expression considerably decreases during development growth (sexually and asexually). It can be also concluded from the plots that although there are slight differences, the expression patterns of all the complex members show similarity which supports the hypothesis that these proteins form a complex.

Protein extracts from fully functional 3XHA fused versions of KdmA (160 kDa), CclA (68 kDa), EcmB (72 kDa), RstB (93 kDa), 13XMYC fused version of McmA (40 kDa) and untagged *wt* strains were used to perform immunoblotting analysis. Protein extracts were isolated from cultures that had undergone vegetative growth in liquid (V24h,36h,48h), or had been induced in the presence of light asexually (A24) and in darkness sexually (S24,48). Grown mycelia were used to inspect the complex members' protein expression levels. HA and MYC

antibodies were employed to detect the signals and α-skpA antibody was used to detect SkpA, which served as a loading control for all samples (**Figure 3.2B**). In **Figure 3.2.1B**, most of the complex members show stronger signals during the vegetative stage than developmental stages where the protein expression reduces which is also in agreement with the gene expression results in panel **A** on the same figure. Individually speaking on the plots, two abundant bands were detected for the *kdmA::3XHA* blot and one is larger (~160 kDa) than the other(~80 kDa). One of the important findings of this study is that KdmA is expressed as two transcripts within the cell and this will be presented in further detail in **section 3.8** and this is the reason of these two separate signals from KdmA expression. As presented in the third blot of **Figure 3.2B,** there are two bands with different sizes, one is around 70 kDa (expected signal from EcmB) and the other is around 140 kDa. It should be noted that homodimer formation of EcmB was reported by a previous comparative biochemical analysis study of Upc2 (paralog of ecm22) and Ecm22 (EcmB homolog) in *S. cerevisiae.* Conserved domain analysis of Upc2 in comparison to its homologs from the same study stated that homodimerization is a general feature for these proteins (Yang *et al.*, 2014). This is can be the potential explanation for the higher size signal in the *ecmB::3XHA* immunoblotting image. Additionally, the same blot reveals that the homodimer form of EcmB disappears in the late phase of the sexual development stage (S48). Comparing **Figure 3.2A** and **3.2B** shows that transcriptional expression patterns of complex members is considerably in line with the protein expression profile.

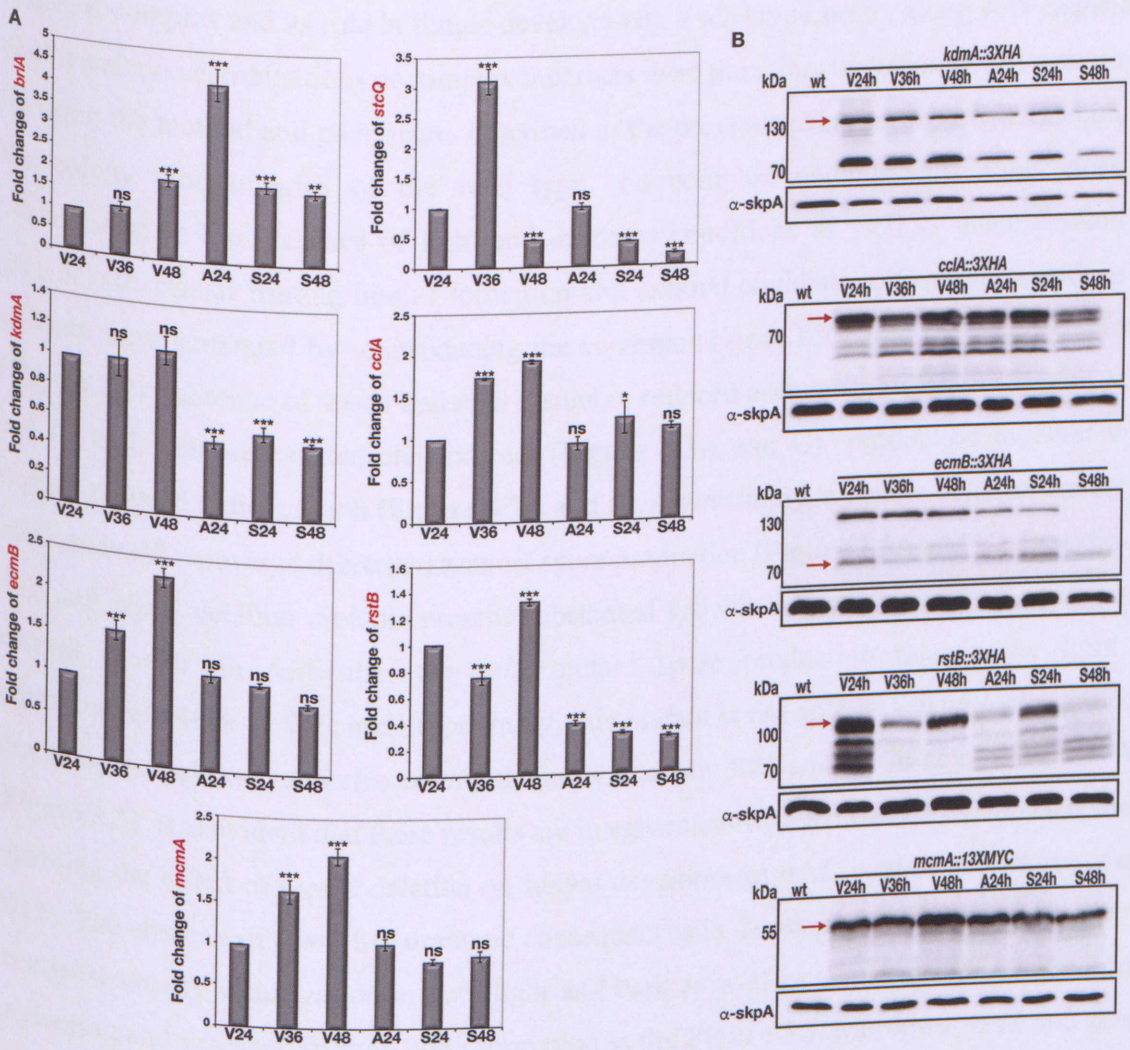

Figure 3.2 Expression analysis of the MERCK complex during vegetative and developmental growth (sexual and asexual) with different time points in *A. nidulans*. **(A)** Relative gene expression of *kdm*A, *ccl*A, *ecm*B, *rst*B and *mcm*A by qRT-PCR in different life stages and time points. *brl*A and stcQ were used as reference genes to check which are upregulated in asexual growth 24h and vegetative growth 36h, respectively. *ben*A was used as a housekeeping gene and results were normalized according to vegetative 24h samples. Graphs were obtained from three independent biological replicates and three technical replicates and bars represent standard deviations. The statistical significance is indicated as (*) $p < 0.05$, (**) $p < 0.001$, (***) $p < 0.0001$ and non-significant (ns) $p > 0.05$ compared with wild type. **(B)** Protein expression profile of epitope-tagged complex members during fungal development. 3XHA fusion strains of KdmA, CclA, EcmB, RstB and 13XMYC fused McmA were used to detect the signals in immunoblotting. Each signal for relevant protein was indicated with red arrow on blot. Molecular weights of KdmA, CclA, EcmB, RstB and McmA are 156.9 kDa, 65.4 kDa, 68.9 kDa, 89.7 kDa and 24.7 kDa, correspondingly. The sizes of 3XHA-tag and 13XMYC-tag are approximately 3 kDa and 15.6 kDa, respectively. 50 µg total protein was loaded into gels and α-SkpA antibody was used for loading control. Protein ladder (size as kDa) is stated on the left side of each blot.

Furthermore, in order to gain insight about the genetic interaction dynamics of the MERCK complex and its role in fungal development, a wild type strain, along with single and double deletion combinations of complex members were point inoculated on GMM agar plates by using the method and parameters described in the previous chapter. **Figure 3.2.2** contains the colony morphologies of the wild type and complex mutants with their close-up visualization in the presence of light and darkness conditions as well as quantification of growth rate, sexual fruiting bodies formation and asexual conidiation. Complementations of mutants were generated by reintroducing the correspond gene back into the deletion strains (**Figure 2.2**). Absence of *kdmA* and *rstB* results in reduced asexual conidiation (**Figure 3.3A** and **D**) and increased sexual cleistothecia (**Figure 3.3A** and **C**) production together with slightly reduced radial growth (**Figure 3.3A** and **B**). Interestingly, a double deletion mutant of *kdmA* and *rstB* recovered decreased asexual spore production (**Figure 3.3A** and **C**). In addition, *cclA* and *ecmB* deletion mutants present substantial growth deficiencies in both sexual and asexual growth. In particular, the *cclA* mutant spore production rate in the light is approximately 40% of WT, and surprisingly, this mutant is not able to generate cleistothecia structures in darkness and also colony diameter is about 40% smaller in comparison to WT (**Figure 3.3**). It is evident that these results are in agreement with a previously published study regarding the effect of a *cclA* deletion on fungal development in *A. fumigatus* (Palmer *et al.*, 2013). The absence of *ecmB* has dramatic consequences in development which can be clearly seen from colony visualization in both light and dark as well as almost disappeared conidia production and vanished fruiting body formation in the **Figure 3.3**. Moreover, *cclA* and *ecmB* mutants almost have lethal phenotype, suggesting that these two members have critical roles in fungal development. Another important observation from colony morphology analysis is that *cclA* and *ecmB* double deletion combination strains reveal a similar radial growth and conidia and cleisthotecia production pattern with their respective single deletion strains. Particularly, data in **Figure 3.3** suggest that *cclA* and *ecmB* have stronger epistatic effects than the other members of the complex.

In this section, the gene and protein expression profiles and growth effects of the MERCK complex components were investigated in depth. Empirically, it seems that complex members have important roles in fungal growth and light mediated development.

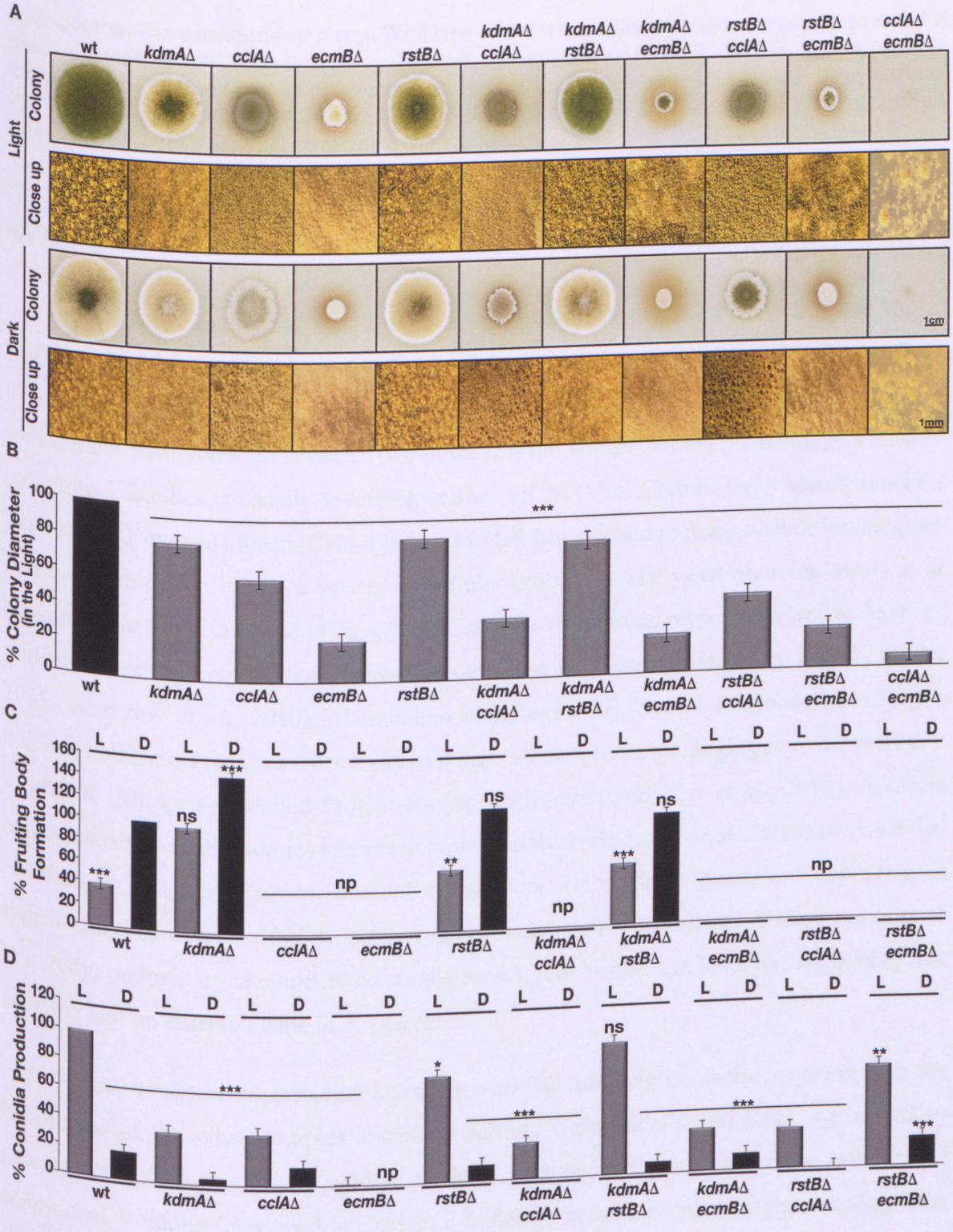

Figure 3.3 Phenotypical characterization of the MERCK complex in *A. nidulans*. **(A)** Colony morphologies and stereomicroscopic images of wild type, single and double mutant deletion combinations. Strains were point inoculated ($5x10^3$ spores) and grown on GMM agar plates at 37°C for 5 days sexually in dark and asexually in light conditions. **(B)** Colony diameter of each strain was measured from three independent plates and wild type colony size was used as a reference (100%). **(C)** Sexual fruiting bodies were quantified from approximately 5x10 mm^2 area of three independent sectors and from three independent plates. Wild type under constant dark condition was applied as a reference (100%). **(D)** Asexual conidiation quantification was performed from three different 5x10 mm^2 sized

cores and from three independent plates. Wild type under constant light condition was utilized as 100% standard. Standard deviations for colony diameter, cleistothecia and conidia formation were given on the bar graphs as error bar. Experiments were carried out in biological triplicates. The statistical significance is indicated as (*) $p < 0.05$, (**) $p < 0.001$, (***) $p < 0.0001$ and non-significant (ns) $p > 0.05$ compared with wild type. np refers to 'no production'.

3.3 Overexpression and carbon utilization profile of MERCK complex in *A. nidulans*

Detailed domain analysis of complex members (**Figure 3.1A**) showed that McmA contains a MADS-box sequence motif which is highly conserved in eukaryotes. This motif is 85 amino acids in length in *A. nidulans* and is found with slightly different lengths in the other well studied eukaryotes (Li *et al.*, 2016). Since it is not a large family, the naming of MADS-box protein families is usually species-specific: MCM (Mini Chromosome Maintenance) in yeast and SRF-type in human. DNA-binding MADS-box domain proteins include transcription factors which can influence a variety of cellular processes. The yeast homolog *mcm1* is an essential gene and is involved in the cell type specific pheromone response as well as having a critical role on the activator and repressor complexes in *S. cerevisiae* (Shore and Sharrocks, 1995; Gramzow *et al.*, 2010). Mammalian homologs SRF (Serum Response Factor) type transcription factors regulate the activity of many cellular processes ranging from the cell cycle to MAPK (Mitogen-Activated Protein Kinase) pathways (Gramzow *et al.*, 2010). A recent comprehensive transcriptomics and phenotypical analysis study (Li *et al.*, 2016) revealed that cellulase, sexual development, asexual conidiation and protease genes are expressed in significantly reduced levels in *A. nidulans* point mutated *mcmA* mutants. At the beginning of this study, preliminary attempts to delete the *mcmA* gene resulted in lethality, suggesting that *mcmA* is also an essential gene in *A. nidulans*.

Since evidence suggests that McmA is a critical transcription factor, together with the importance of the other complex members KdmA, CclA, EcmB and RstB, we aimed to generate modified promoter versions of these proteins by using the *tetOn* constitutive conditional promoter (described in Chapter 2 in detail) in order to gain insight on the cellular activities when the essential gene *mcmA* is overexpressed and expressed at low levels. Strains containing the inducible promoter were verified using different doxycycline concentrations morphologically (**Figure 2.3B**). Transcriptional verification of *tetOn* strains were confirmed by qRT-PCR and are demonstrated in **Figure 3.4B**. As shown in **Figure 3.4B**, gene expression levels of complex members which have the conditional promoter gradually increase as

doxycycline concentrations increase (given on the x-axis). Values were normalized according to the WT strain growth in the presence of 180 μg/ml doxycycline and *benA* was used as reference gene. By comparing figures **2.3B** and **3.4B,** it can be observed that the promoter altered strains in this study work sufficiently well.

To determine the minimum concentration of doxycycline required for expression of *mcmA* for further physiological and molecular analyses, the *mcmA-tetOn* strain was point inoculated on GMM agar plates in the absence and presence of different doxycycline concentrations (**Figure 3.4A**). It is observed from **Figure 3.4A** that the *mcmA* mutant strain cannot grow without doxycycline (dox) and has a strong defect in 1.5 μg/ml dox and it can survive under 5μl/ml doxycycline and starts to recover asexual conidiation and clesthotecia formation in the presence of 30 μg/ml dox. Deletion concentration was chosen as 5 μg/ml doxycycline for the *mcmA-tetOn* mutant by this observation.

tetOn strains of MERCK complex components were used to investigate the effects of individual overexpression of each within the cell. Data in **Figure 3.4B** showed that as the concentration increases, the expression also rises, however relative expression of *kdmA* and *mcmA* decrease when in the presence of 360 μg/ml doxycycline. Therefore, the concentration of doxycycline chosen for overexpression studies was determined to be 180 μg/ml. For the morphological examination of MERCK complex members, *tetOn* strain cultures were point inoculated on GMM agar plates in both the lack of dox and presence of 180 μg/ml dox under constant light and dark conditions for 5 days at 37°C. Images were taken of the plates and are displayed in **Figure 3.4C**. As can be seen from **Figure 3.3C**, in the absence of doxycycline, the *tetOn* mutant phenotypes of *kdmA*, *cclA*, *ecmB* and *rstB* are adequately similar with the knockout strains phenotype in the GMM medium (**Figure 3.3A**). Another important conclusion from the overexpression figure is that the radial size of the colonies in the existence of 180 μg/ml dox are smaller than the dox depletion condition. **Figure 3.4D** summarises the colony diameter quantifications and values of overexpressed strains in the light grown plates were normalized according to the WT colony size in the absence of doxycycline. Conidiation production of overexpression strains were also quantified and presented in **Figure 3.4E** and interestingly, asexual spore production is significantly affected when *mcmA* is expressed more than usual in the cell under light condition whereas high expressed *ecmB* slightly increase the asexual production in the both light and dark grown conditions.

In order to address whether any component of the MERCK complex is involved in carbon catabolism, single and double mutant strains of complex members were point inoculated in MM agar plates containing different carbon sources ranging from glucose to dextrose to K-acetate. After 4 days of growth plates were scanned and the images are displayed in **Figure 3.4.1**. A growth comparison was done in relation to phenotypes observed for GMM media (1% glucose). Overall, in **Figure 3.4.1** no significant difference was observed between the WT and knockouts, moreover, as it can be seen all the strains are unable to utilize galactose very well as it is expected since it is not usual to encounter in saprophytic fungi *A. nidulans* natural habitats. It is also observed that all mutants and WT strains revealed a slight increase in conidial production in comparison to the 1% glucose including medium.

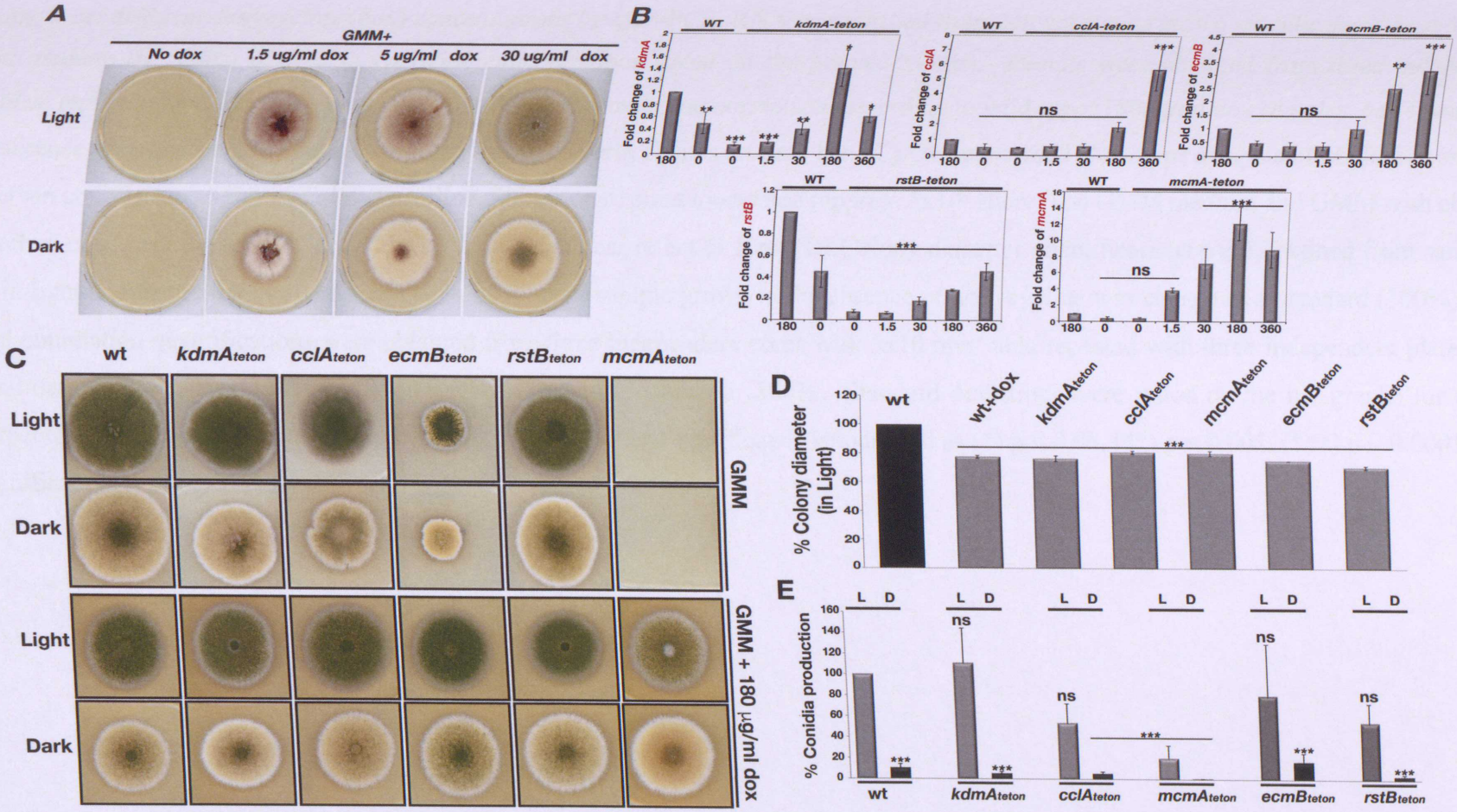

Figure 3.4: Characterization of teton conditional promoter replaced strains of MERCK complex in *A. nidulans*. **(A)** determination of doxycycline concentration for $mcmA_{tetOn}$ which is used as an *mcmA* deletion strain in our study. Strain was point inoculated on GMM agar plates, supplemented with varied doxycycline concentrations. Plates were incubated at 37 ^{o}C in either constant light or dark conditions for 5 days. Scale bar on the graph refers to 1 cm. **(B)** Determination of overexpression concentration for *kdmA, cclA, ecmB, rstB* and *mcmA* tetOn promoter replaced

strains under different doxycycline (dox) concentrations by qRT-PCR. RNA was purified from 24h vegetative grown mycelia samples at 37 °C in liquid medium by adding desired doxycycline concentrations stated on the graphs (x-axis). Results were obtained from three independent biological replicates and three technical replicates for each sample and normalized according to wild-type+180µg/ml dox samples. benA was used as a reference gene and standard deviations were shown as vertical lines on each bar. **(C)** *Overexpressed phenotype analysis of MERCK complex members in comparison to absence of doxycycline. Strains were point inoculated (approx. 5x10^3 spores) on GMM medium and GMM with chosen doxycycline concentration at 37 °C for 5 days. Shown scale bar refers to 1cm.* **(D)** Colony diameter quantifications were obtained from samples grown in light and from three independent plates. Wild-type sample grown in the absence of doxycycline was chosen as a standard (100%). **(E)** Asexual conidiation quantifications were obtained from three independent cores with 5x10 mm^2 area repeated with three independent plates for light and dark conditions. Wild-type in light was established as standard (100%). Standard deviations were stated on the bar graphs for both. Experiments were carried out in biological triplicates. The statistical significance is indicated as (*) $p < 0.05$, (**) $p < 0.001$, (***) $p < 0.0001$ and non-significant (ns) $p > 0.05$ compared with wild type.

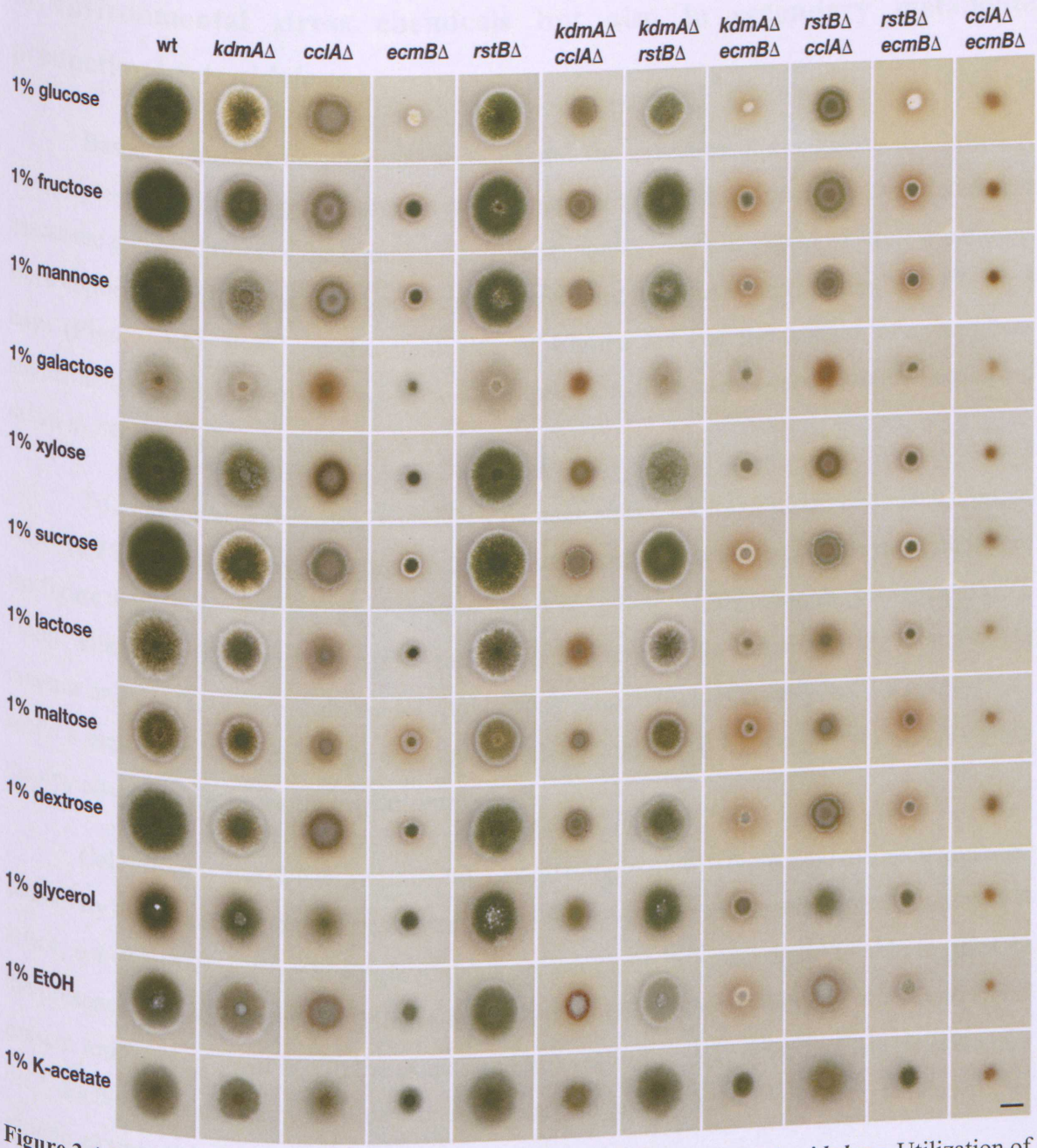

Figure 3.4.1: Carbon utilization profile of MERCK complex mutants in *A. nidulans*. Utilization of carbon sources for WT, single mutant and double mutant combinations. Point inoculated strains were grown on minimal media including desirable carbon sources plates at 37 °C under constant light source for 4 days. 1% glucose media refers to GMM media which was used as main media in the study and the other carbon sources percentage was determined accordingly. Scale bar size represents 1 cm.

3.4 The MERCK demethylase complex is not only involved in the responses to environmental stress chemicals but also in secondary metabolite production in *A. nidulans*

Based on data from previous sections and the evidence that suggests the MERCK demethylase complex plays important roles in many critical cellular processes, we decided to assess the potential roles of the complex in stress responses. Various chemical stress conditions were applied to GMM agar plates and strains were point inoculated and cultured at 37°C for 3 days (**Figure 3.5**). Panel on the right side of **Figure 3.5** has the images of agar plates supplemented with 5 μg/ml dox to induce low expression of the *mcmA-tetOn* mutant (explained detail in **Section 3.3**) in contrast to WT.

To monitor how they deal with DNA damage stress, CPT (75 μM) , EMS (0.05 %), 4-NQO (0.25 μg/ml), and hydroxyurea (5.2 mM) were utilized. It is also can be observed from the figure that single and double knockout mutants are strongly affected in the presence of CPT along with WT. Interestingly, *kdmA* and *ecmB* single mutants together with their double mutants and very low expressed *mcmA* show strong sensitivity particularly to CPT and 4-NQO while a lack of *cclA* in the single and double deletions and *rstB* knockout strain surprisingly display stronger resistance than wild-type.

Calcoflour white (CFW 5μg/ml) and Congo red (20 μg/ml) were used to check mutants' sensitivity to cell wall stressors. In **Figure 3.5**, CFW and Congo red panels explicitly show that *kdmA*, *ecmB* and *mcmA-tetOn* single mutants are seriously influenced and unable to grow in the presence of these chemicals. Moreover, double knockout combinations of *kdmA* and *ecmB* present total loss of growth. On the other hand, interestingly, WT, *cclA*, *rstB* single and *rstB-cclA* double deletion mutants illustrate significant resistance along with the reduced radial growth against abiotic this cell wall stress condition.

In order to obtain insight regarding the cytoskeleton stress response through the MERCK complex components, Benomyl (0.3 μg/ml) and an azole derivative antifungal agent Nocodazole (0.1 μg/ml) were employed in this study. As demonstrated in **Figure 3.5**, *ecmB* single and double and *mcmA-tetOn* mutant strains exhibit highly strong sensitivity by loss of growth. Surprisingly, deletion of *cclA* and *rstB* single mutants together with double mutants are able to grow and produce asexual conidia, although the WT strain also shows decreased growth rate and condiation.

MERCK complex component mutants were further tested by application of NaCI (1 M) as osmotic stress and H_2O_2 (1 mM) as oxidative stress agents to assess their responses in the presence of these two challenging environmental factors. *ecmB* and *mcmA-tetOn* mutants are mainly affected and nearly show lethal phenotype by having NaCI and H_2O_2 in their growth environment. Interestingly, *cclA* and *rstB* single knockout and double deletion mutants of these members display remarkable resistance against these tested stresses and can grow almost as same as in the absence of these chemicals (in the first panel), whereas wild-type has strong growth defect and diminished asexual spore production.

The data in **Figure 3.5** explicitly demonstrates that a lack of *kdmA*, *ecmB* (single and double mutants) and *mcmA* result in severe sensitivity to various different stress factors. Additionally, *cclA* and *rstB* mutants together with their double mutants show a clear strong resistance in the response to several different stress factors. These data clearly suggest that MERCK complex members are involved in stress responses to various chemicals and regulation of these pathways either as activator (*kdmA*, *ecmB*, *mcmA*) or repressor (*cclA* and *rstB*).

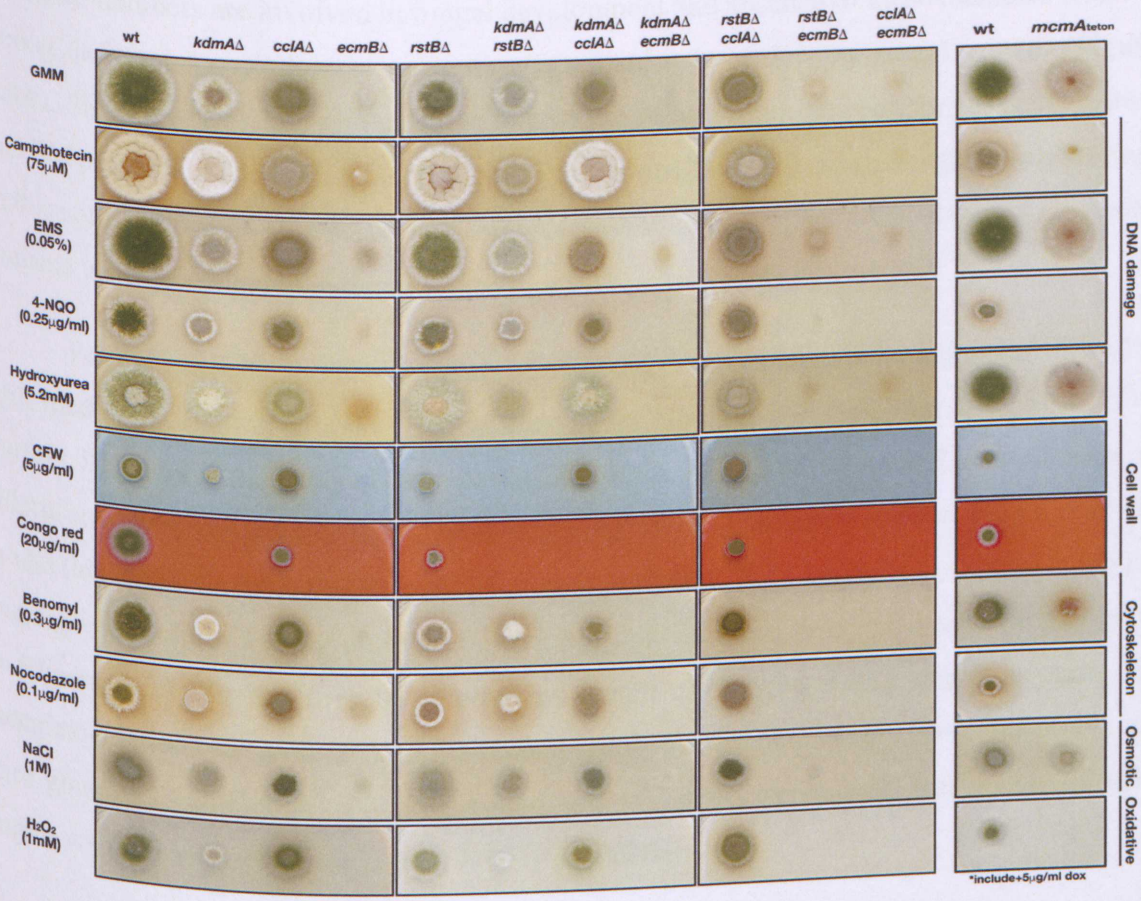

Figure 3.5: Comparison of growth responses to different stress chemicals for MERCK complex components in *A. nidulans*. Wild-type, single mutants, double mutant combinations and $mcmA_{tetOn}$ conditional strain cultures were point inoculated (approx. $5x10^3$ spores) on agar plates including GMM and supplemented DNA damage, Cell wall, Cytoskeleton, Osmotic and Oxidative stress chemicals and grown at 37°C for 3 days under constant light conditions. Plates on the right panel for $mcmA_{tetOn}$ strain include 5 μg/ml doxycycline concentration. Chemicals' concentrations used were shown on the image under their names. Scale bar refers to 1 cm.

It is important to reiterate that development is commonly associated with secondary metabolite production and they are co-ordinately regulated in microorganisms including fungi. A weakness or deficiency in developmental structures such as conidia and cleisthothecia is often correlated with an influence in SM production. It has also been reported that SM genes are clustered and co-regulated through transcriptional expression. Moreover, the co-regulation of these SM clusters can be in different ways such as by regulatory heteromeric protein complexes (*velvet* complex, *bZIPs*, *CCAAT* complex), pathway specific transcription factors (*aflR* in aflatoxin/sterigmatocystin production, *gliZ* in gliotoxin production and *lovE* in lovastatin production) (Bayram *et al.*, 2008b; Yin and Keller, 2011; Bayram and Braus, 2012).

Furthermore, in a previous section of this study, it was comprehensively shown that MERCK complex members are involved in fungal development and absence of these members result in strong deficient morphologies, suggesting a critical role in developmental growth (**Figure 3.3A**). Since it is well known that there is a strong relationship between fungal development and SM production and their transcriptional expressions are coregulated together with findings in this study, in this section secondary metabolite productions of MERCK complex members' mutants were investigated in detail.

For this purpose, initially, mutants of MERCK complex were point inoculated in GMM agar medium including ground oatmeal (for ST production induction) for 5 days at 37°C. Further ST extraction protocol was performed as described in Chapter 2 and samples in chloroform were run on the HPLC by comparing with ST standard profile. Results for ST production from three different biological replicates for WT, single and double mutants, overexpression (plus 180 µg/ml dox in agar plate) and complementation strains are presented in **Figure 3.6A**. In the first ST production graph of **Figure 3.6A,** single mutants and complementations are presented. In the second graph, double mutants are presented and in the third graph, ST production of overexpressed strains' results were given. Results on all three graphs were normalized according to WT ST production.

From the first graph, it can be clearly seen that the ST production rate is highest in the *rstB* mutant. Also, in *kdmA*, *cclA* and *ecmB* mutants, ST was produced more than WT. Surprisingly, *mcmA-tetOn* strain showed the lowest ST production rate among single deletion mutants. In the same plot, it is also displayed that the complemented strains of mutants presented acceptably decrease for *kdmA*, *cclA*, *ecmB* and *rstB* or increase for *mcmA-tetOn* in comparison to mutants which means they were complemented successfully by having similar production pattern with WT. Additionally, double knockouts of complex components also gave similar higher ST production rates than WT, with the exception of the *cclA-ecmB* double mutant which cannot produce ST. More surprisingly, the forced expression of *cclA*, *ecmB* and *rstB* by inducible promoters resulted in reduction on ST production unlike *kdmA* and *mcmA* overexpression produce higher ST than WT in the presence of 180 µg/ml doxycycline (**Figure 3.6A**). These data suggest that MERCK complex members individually and directly or indirectly influence sterigmatocystin biosynthesis.

In order to examine SM production for a broad range of metabolites, 1 ml liquid media of 24h (for primary metabolism which was not shown in this study) 52h grown culture samples

were taken and run on the LC-MS/MS system and detailed analysed results were given in **Figure 3.6B**. All the analyses were run in respect to their standards and were performed as triplicates. Left side of **Figure 3.6B** shows the metabolites and associated gene clusters of each metabolite production was given right side of the figure. Each row of pie charts refers to a metabolite, given on the left and each column indicates the strain (WT, single or double mutant). Each individual pie chart colour intensity shows the production rate for the metabolite is given on the row (e.g penicillin G was produced most by *rstB-cclA* double mutant).

Pathway specific comparative metabolite analysis of MERCK complex proteins (**Figure 3.6B**) indicated that only the deletion of *cclA* single and double mutant backgrounds are able to produce the penicillin G metabolite, suggesting that *cclA* acts as repressor for the AN2621 gene cluster. It can be clearly seen that identified peaks for ST production (AN7815 cluster) have the highest peaks in *rstB* and *mcmA* mutants. Investigation of the austionol biosynthesis pathway showed that *cclA* and *ecmB* mutants produce more austinol and its derivative compound than the other mutants as well as WT. Interestingly, in the absence of *cclA* and *mcmA*, Emericellamide synthesis reached peak levels, suggesting their leading role on the regulation of the AN2547 gene cluster. The final four rows of **Figure 3.6B** explicitly indicate that *cclA* and *ecmB* have critical influence in expression of the Monodictyphenone (AN0150) and Orsellinic acid (AN7909) SM biosynthetic gene clusters, whereas *cclA* and *ecmB* single mutants have the highest synthesis rate for the Citreoresin and Emodin and *cclA-ecmB* double mutant has the maximum production of FK 9775A, FK 9775B and Orsellinic acid. Overall, **Figure 3.4.2B** illustrates that in the absence of *kdmA,* metabolite production is mostly decreased in comparison to WT, with the exception of ST biosynthesis which is considerably consistent with one the bipartite function *kdmA* was reported previously (Gacek-Mathew *et al.*, 2015). On the other hand, *cclA* single and double deletion mutants showed drastic changes in expression of the majority of SM biosynthesis gene clusters, as presented in the figure. The data in this figure confirm the reported repressor function of *cclA* in SM production especially for Monodictyphenone and Orsellinic acid biosynthesis (Bok *et al.*, 2009) as well as the reflection of morphological growth defects on *ecmB* and *cclA* mutants on the SM production.

These given data suggest that complex members are essentially involved in regulation of the different SM biosynthesis pathways by acting individually in some and cooperating or

co-regulating in some others. In other words, MERCK complex proteins play an important role for SM production, exhibiting pathway-specific effects.

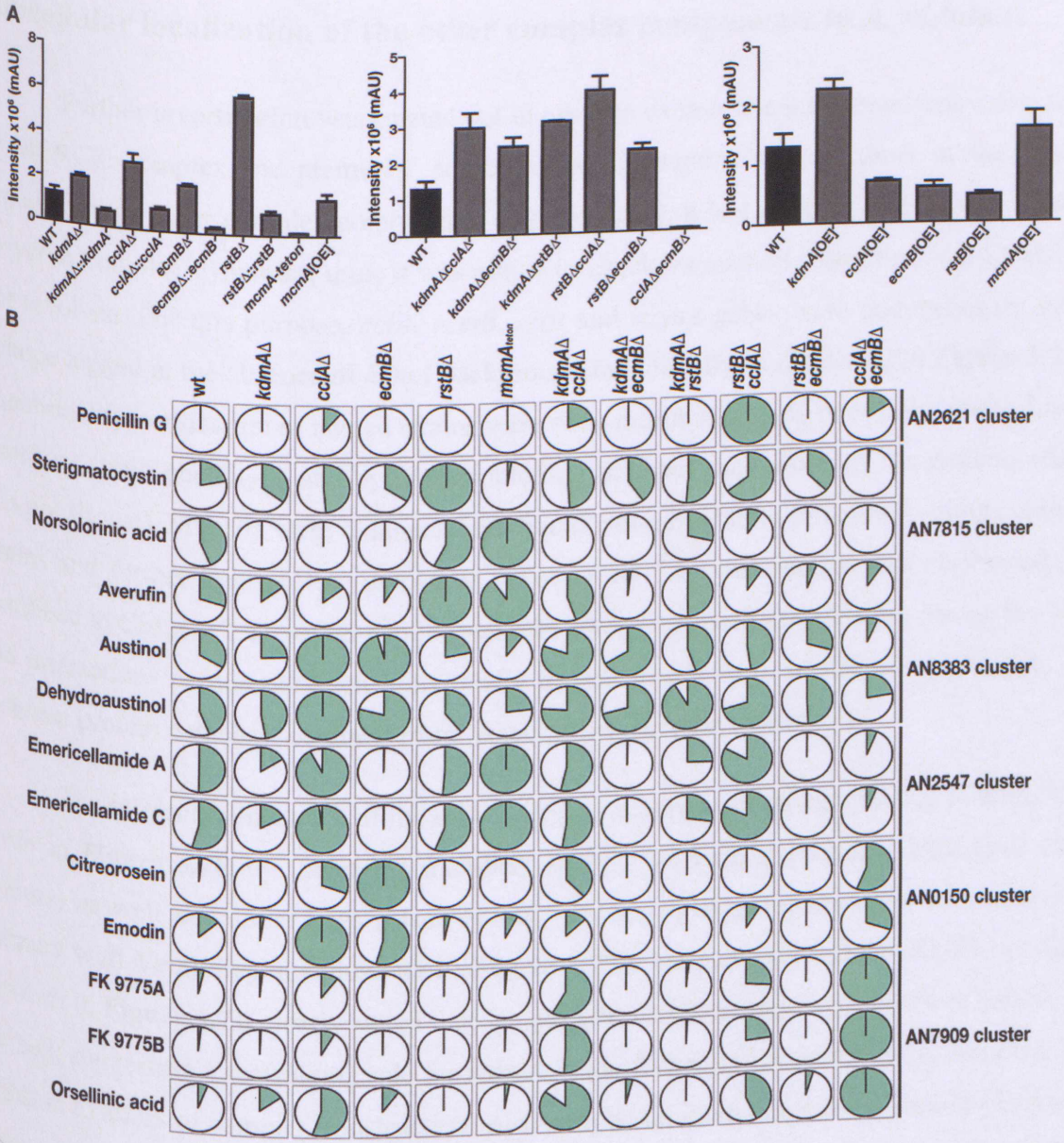

Figure 3.6: Secondary metabolite production profile of the MERCK complex in *A. nidulans*. **(A)** Sterigmatocystin (ST) production of complex members' single mutants, double mutant combinations, complementation strains and overexpression strains (include 180 µg/ml dox) in comparison to wild-type strain. Samples were taken from point inoculated (approx. $5x10^3$ spores) and grown at 37 °C under constant light for 5 days plates which include GMM and ground oatmeal (to induce ST production). Agar samples from plates were processed with organic extraction and then analysed with HPLC by using ST standard as reference. Values on the graphs are from three independent plates and error bars were also given on the bars. **(B)** Global secondary metabolite analysis for the WT, single mutants and double mutant combinations strains. The cultures were inoculated (approx. $2x10^6$ spores) in GMM liquid medium and grown at 37 °C shaking incubator for 52h. 1ml liquid medium samples were analysed by LC/MS from three replicates and filling the pie charts on the each row were arranged according to the strain which produced max amount of the stated metabolite (eg. max amount of penicillin G is produced by *rstB,cclA* double mutant strain). Gene clusters were defined on right side of the graph shows the stated metabolites production including cluster.

3.5 KdmA is a scaffold protein for the MERCK complex and does not affect subcellular localization of the other complex components in *A. nidulans*

Further investigation was carried out in order to explore the interdependency structure of MERCK complex and members' sub-complex interactions. Since KdmA is the largest protein among other complex components (**Figure 3.1A**), it has more potential to be a main player in complex dynamics, thus, it was aimed to check interaction relations when KdmA is not involved. For this purpose, *cclA*, *ecmB*, *rstB* and *mcmA* genes were endogenously TAP epitope tagged in the absence of *kdmA* background individually as illustrated in **Figure 3.7A**. Functionality verification of tagged strains were done morphologically in comparison to *kdmA* knockout strain phenotype and by immunoblotting to check expression of the proteins (data was not shown). Mycelia were obtained from liquid cultures of fully functional epitope tagged strains and further total protein extraction followed by TAP purification was performed, as described in Chapter 2. Digested peptide samples taken from each sample were run on the MS and interactions partners of each individually tagged strains were identified by using an *A. nidulans* protein database, obtained from 'Aspergillus Genome Database'.

The interaction network of the other complex components in the absence of KdmA is given in **Figure 3.7B** by indicating members specific interacting proteins (with their own colours) as well as mutual ones (black colour) and also giving the numbers of interaction partners with Venn-diagram illustration (**Figure 3.7C**). Interestingly, obtained collaboration network in **Figure 3.7B** clearly stated that the complex is not formed in the lack of KdmA in the cell, suggesting a scaffolding role for KdmA in the formation of the MERCK complex. In addition to a loss of complex construction, surprisingly, no intercommunication was observed among other complex members. MS-coupled proteomics approach analysis data indicate that KdmA plays a key role to form the complex and the other members behave complex-independent within the cell in the absence of KdmA.

Since it was shown that there is no complex formation when KdmA is not present in the cell, the subcellular localizations of CclA, EcmB, RstB and McmA were investigated experimentally in order to see whether a lack of KdmA influences the localisation patterns of the other complex members. To examine this, *kdmA* was deleted from genomic DNA in the GFP fused version strains of CclA, EcmB, RstB and McmA. Further, H2A::mRFP fusion was transformed to these strains (described in detail in Chapter 2). Strains cultured for 12-14h were

analysed using a laser confocal microscope and microscope pictures are presented in **Figure 3.7D**. In the first line of each image GFP signals, in second line mRFP signals and in the bottom line GFP and mRFP signals together were shown. It is clearly observed from **Figure 3.7D** that GFP tagged complex members have luminescence signal in same position where nucleic mRFPs are, suggesting that the rest of the complex members are localized within the nucleus and it is not dependant on KdmA existence in the cell.

In order to check how KdmA influences protein expression levels of the MERCK complex components, western blotting was performed. KdmA was removed from genomic DNA in HA tagged versions of CclA, EcmB, RstB and MYC tagged version of McmA and immunoblotting was performed by using related antibodies (were shown in blots as well) in comparison of KdmA positive strains. According to results given in **Figure 3.7E**, a lack of KdmA does not influence expression of CclA, it almost has the same signal intensity in both conditions. Interestingly, EcmB homodimer formation slightly decreases in the absence of KdmA while normal EcmB expression showed a small increase. Despite no considerable difference in protein expression levels between KdmA absence and presence states, interestingly, in the absence of KdmA, some posttranslational modification marks were observed on RstB and McmA (**Figure 3.7E**), suggesting that KdmA may be involved directly or indirectly in the regulation of posttranslational modifications of proteins.

All the data from **Figure 3.7** strongly indicate that as a scaffold protein KdmA recruits the other complex members and it is the key component for the MERCK complex along with the fact of no individual interaction between the other members, additionally, localization of complex components is independent from the KdmA presentation in the cell. Moreover, it also explained the suspicion of 'what if the decomposition of complex due to lower protein expression' which was indicated too.

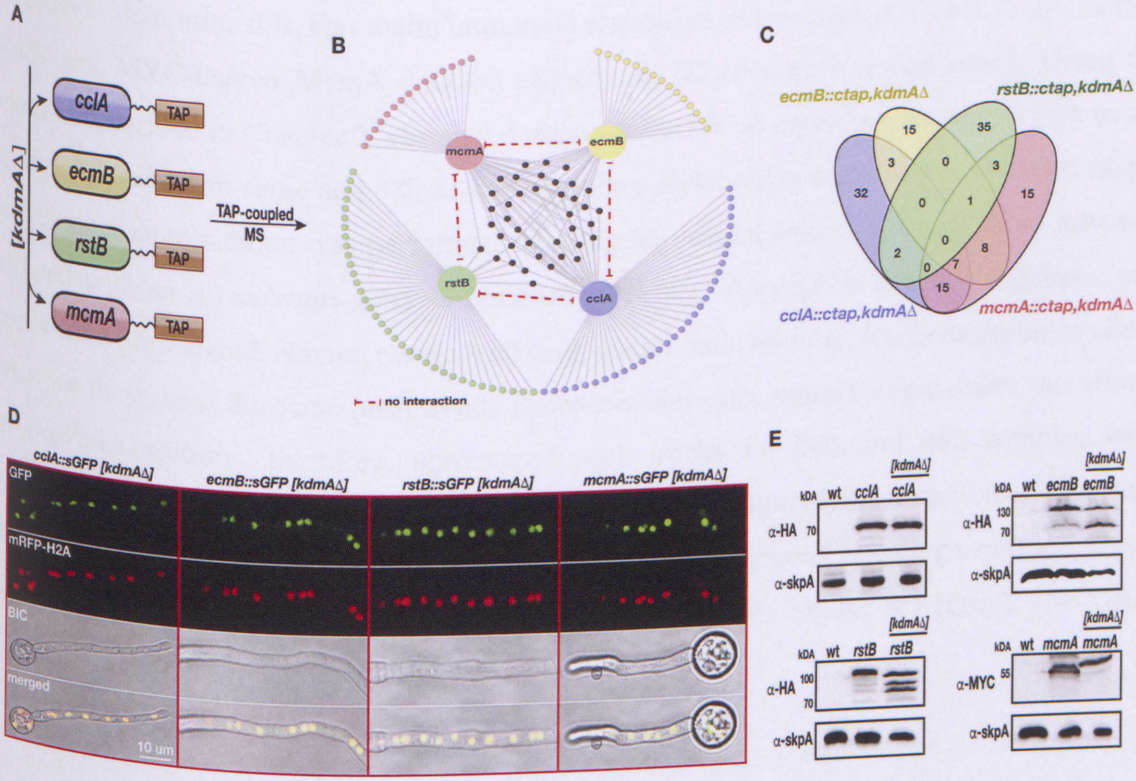

Figure 3.7: Mechanistic determination of the complex in the absence of *kdmA* in *A. nidulans*. **(A)** Schematic illustration of tagging approach for the complex members in *kdmA* deletion background. **(B)** Schematic presentation of interaction network among the other members of the complex in the absence of *kdmA*. Network was obtained from TAP coupled mass spectroscopy analysis results and interaction partners were limited with at least 3 unique peptide numbers. Cytoscape (version 3.6.1) was used to generate the network map. Each members' unique interacting proteins were coloured with their own specific colours, black coloured ones in the middle of network refer to more than one unique interaction with the other complex members. **(C)** Four-set Venn diagram of illustrated protein numbers by mass spectrometry as CclA, EcmB, RstB and McmA interaction partners in the deletion of *kdmA*. Each complex member was assigned with different colour. **(D)** In vivo visualization of complex members locations in the absence of *kdmA*. GFP tagged complex members show strong signals which are overlapped with *mRFP::Histone2A* fusion signals in the nucleus. **(E)** Protein expression comparison of CclA, EcmB, RstB and McmA in the presence and absence of KdmA. Antibodies used are shown on the figure. Molecular weights of KdmA, CclA, EcmB, RstB and McmA are 156.9 kDa, 65.4 kDa, 68.9 kDa, 89.7 kDa and 24.7 kDa, correspondingly. The sizes of 3XHA-tag and 13XMYC-tag are approximately 3 kDa and 15.6 kDa, respectively. 50 µg of protein was loaded on the gel. SkpA was used as a loading control.

3.6 Genome-wide binding profile of complex members in the presence and absence of *kdmA* in *A. nidulans*

Data from **section 3.5** provides evidence that the MERCK complex members play critical roles in the regulation of various cellular processes and metabolic pathways ranging from fungal development to secondary metabolism to stress responses. However, it is not clear

whether each protein binds or regulates the same target gene sets or if they behave dissimilarly. In order to determine this, chromatin immunoprecipitation of HA-tagged KdmA, CclA, EcmB, RstB and MYC-tagged McmA coupled sequencing (ChIP-seq) was performed. Using the method described in Chapter 2, chromatin was obtained from mycelia cultured for 20h to see primary metabolism stage and 48h to see secondary metabolism stage in liquid GMM media and immunoprecipitation was performed by using tag related antibody. Sequencing data was aligned with an *A. nidulans* genome obtained from the 'Aspergillus genome database' and reads were normalized. Having normalized peak counts data, initially, it was desirable to check whether they show the same peak trends genome-wide, since complex formation was shown in previous sections, therefore, normalized peak tracks for 20h and 48h samples were visualized by integrated genome viewer (IGV) platform (**Figure3.8**). It can clearly be seen from the figure that, either from narrow or larger view of the genome, binding peaks are almost identical for the complex members whereas there is no peak binding for WT (grey). This visual

data strongly suggests that the complex members are showing an intricate binding pattern throughout the *A. nidulans* genome.

To determine the targets and binding profile of complex members, a peak calling process, known as Model-based Analysis of ChIP-seq (MACS) was performed on their normalized data and binding peaks were determined and plotted by using R platform (https://www.r-project.org/) and results of genome-wide binding peaks were presented in **Figure 3.9** as heat-map. Data in this figure was presented in the order of KdmA target genes since it was shown as a scaffold protein of the complex. Target genes were categorized as 7 clusters (left sides of the figures with different colours) according to their binding location and peak strength. Heat-map display range was set as 5kb size from transcriptional start site (TSS) and 1kb from transcriptional end site (TES). Plots on the top of each heat-map show the signal

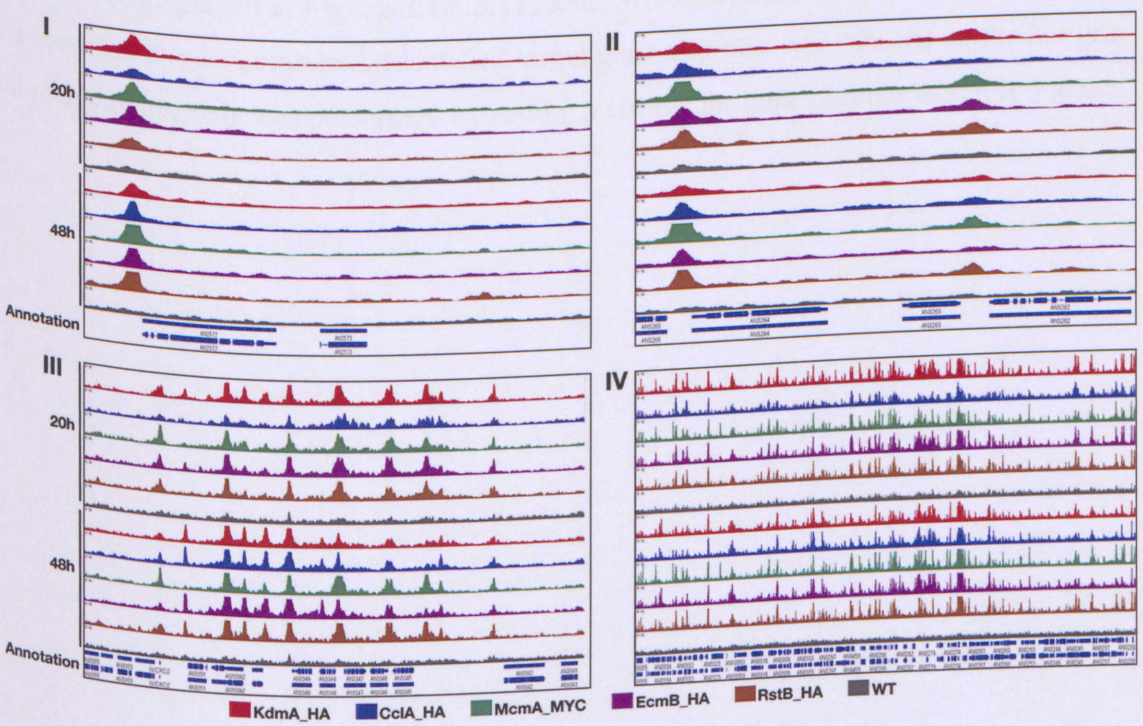

Figure 3.8: MERCK complex binding visualization with normalized ChIP-seq tracks on IGV. IGV screenshot images of individual complex member's HA or MYC ChIP-seq track peaks across the *A. nidulans* genome at 20h (in the primary metabolism stage) and 48h (in the secondary metabolism stage). "Annotation" part represents the genes on the genome. All ChIP-seq tracks were presented in same scale and screenshots were displayed with decreasing magnification (e.g I has the highest and IV has the lowest). Colours present the members which are KdmA (red), CclA (blue), McmA (green), EcmB (purple), RstB (light brown) and WT (grey). Time points were presented on the left side of the screenshots.

intensity and region for each cluster given on the left side and were shown with the cluster related colour for individual ChIP. H3 histone and pol II ChIP-seq (which will be explained in detail in further sections) binding profiles of WT nuclear extract also were presented on the figure for comparison.

As can be seen from **Figure 3.9**, the binding profiles of complex members at 20h and 48h were presented and they show almost identical patterns. It is apparent that these genome-wide ChIP-seq results consistently indicate that MERCK complex members' binding patterns are in parallel with the complex formation phenomena.

Although a significant majority of identified target genes were common, unique target genes were also found for each complex member. In order to individually categorize detected targets, identified genes processed by utilizing KEGG pathway based scheme on their functional annotations basis. Pathway related target analysis of KdmA, CclA, EcmB, RstB and McmA were displayed in **Figure 3.10**, **3.11**, **3.12**, **3.13** and **3.14** respectively, for 20h and 48h and common targets combined. Identified target gene numbers were shown on the bar graphs and pathway analysis was performed by setting a cut-off for gene number which is 5 genes.

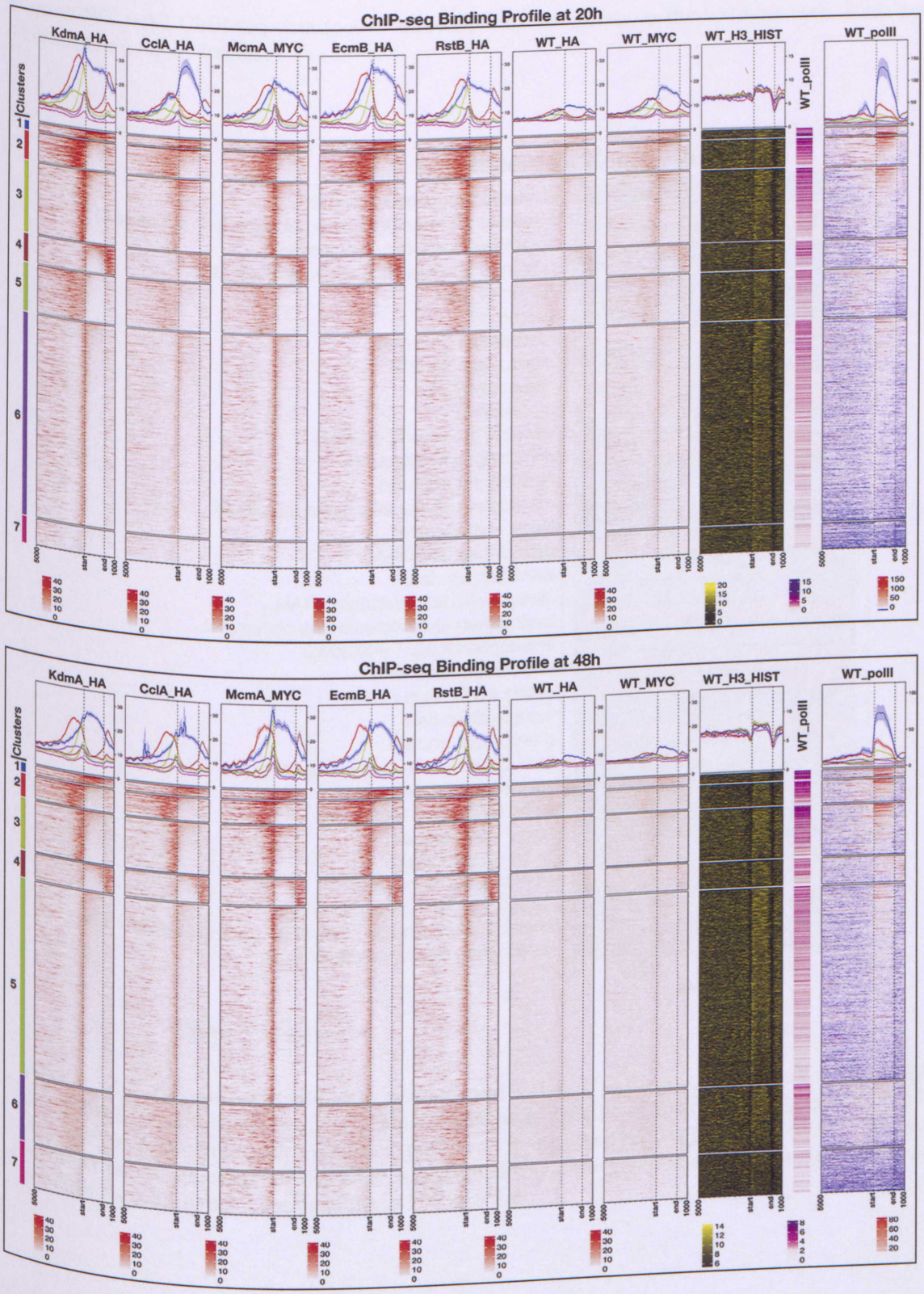

Figure 3.9: Genome-wide binding profile of MERCK complex members. Heat-map presentation of KdmA, CclA, McmA, EcmB, RstB and WT ChIP-seq binding respectively, with displaying 5kb distance from transcriptional start site (TSS) and 1 kb distance from transcriptional end site (TES) for all clustered (shown on left) and ranked genes. Scale of colours were given under each related heat map. WT H3 histone ChIP-seq data presented in the heat-map was shown with black and yellow colours

whereas WT polII ChIP-seq data (active transcription) was given on the last heat-map. Time points were stated on top of frames.

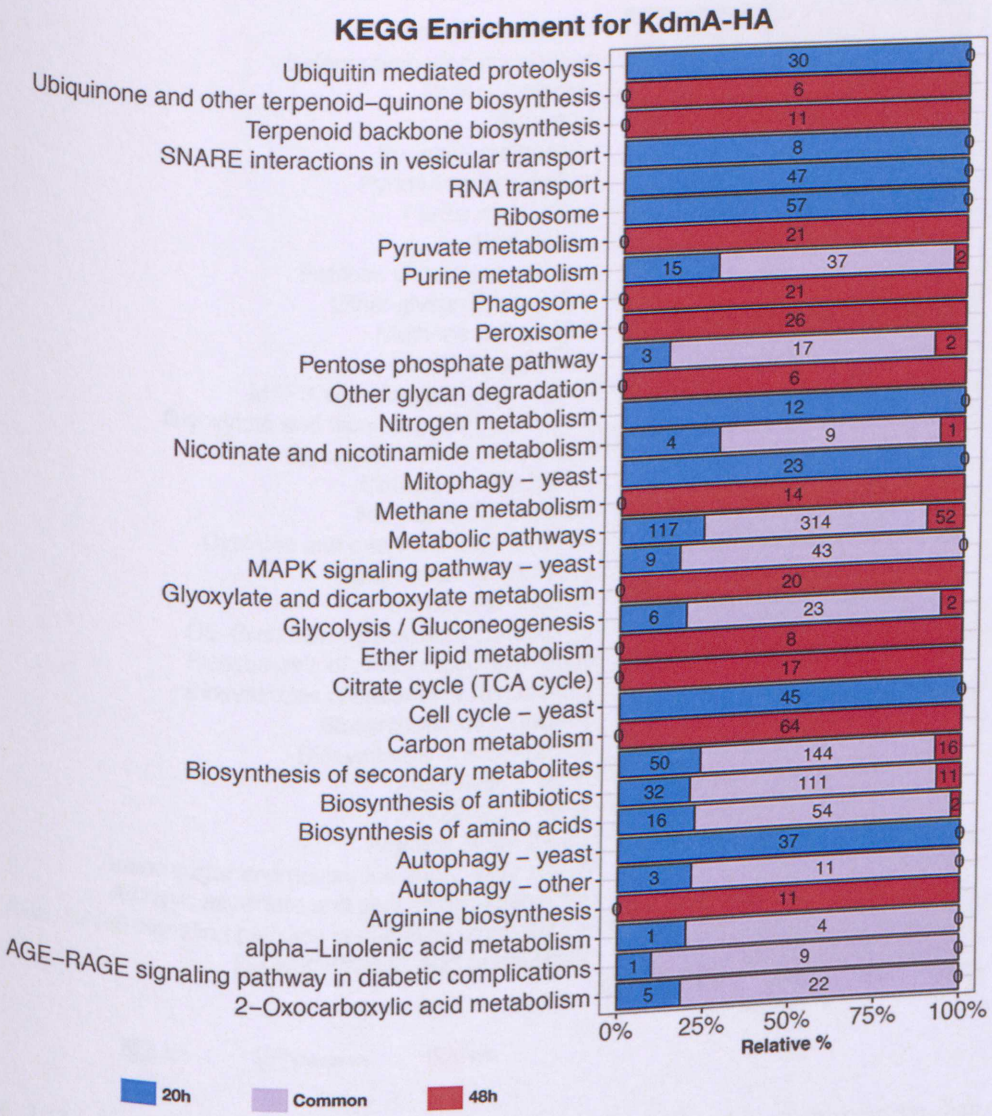

Figure 3.10: Genome-wide KdmA targets and related pathways. Comparative bar graph represents the relative percentage of KdmA target genes specific at 20h (blue bars), specific at 48h (red bars) or common to both conditions (pink bars) in the given KEGG pathways. KEGG pathway involved genes indicated on the bars. KEGG pathways are given based on the gene numbers enriched for KdmA-HA binding either at 20h or 48h.

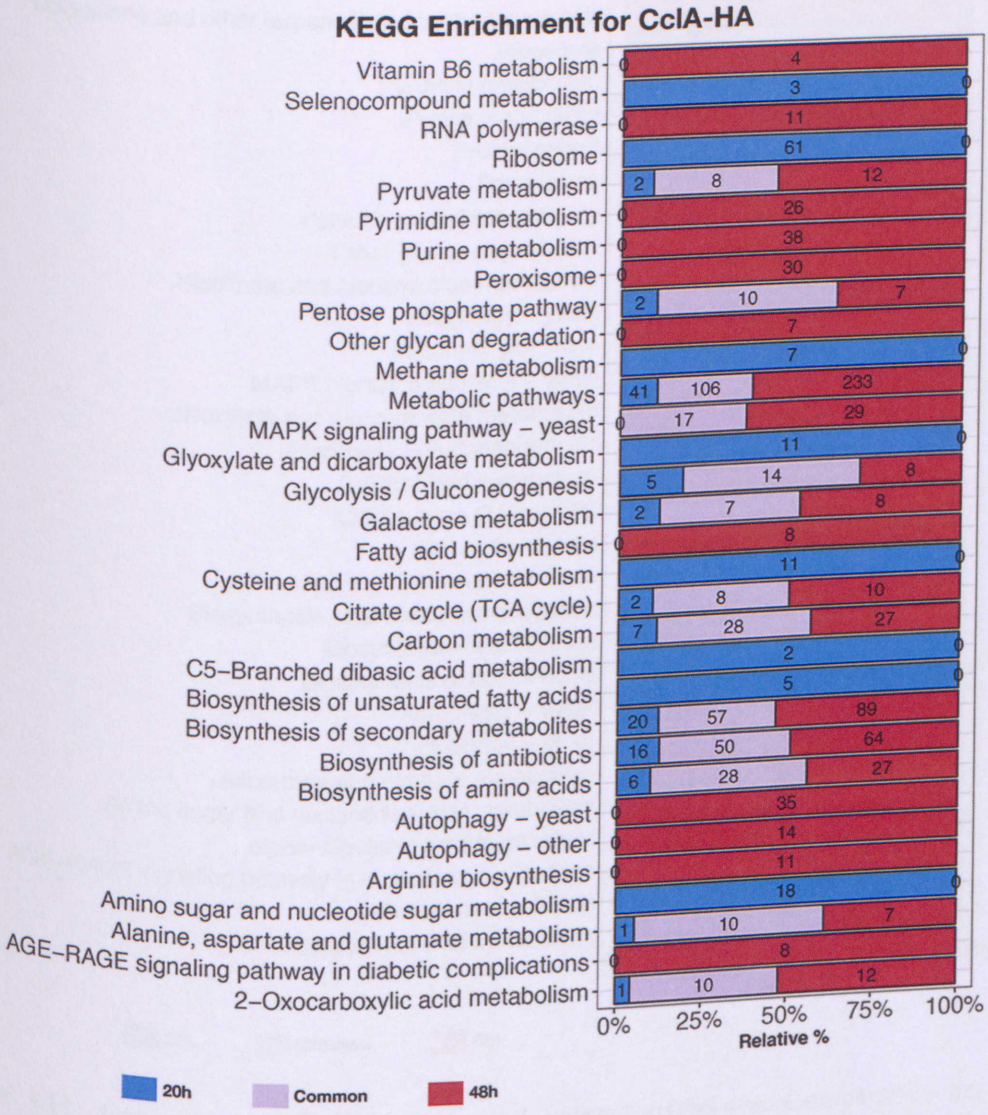

Figure 3.11: Genome-wide CclA targets and related pathways. Comparative bar graph represents the relative percentage of CclA target genes specific at 20h (blue bars), specific at 48h (red bars) or common to both conditions (pink bars) in the given KEGG pathways. KEGG pathway involved genes indicated on the bars. KEGG pathways are given based on the gene numbers enriched for CclA-HA binding either at 20h or 48h.

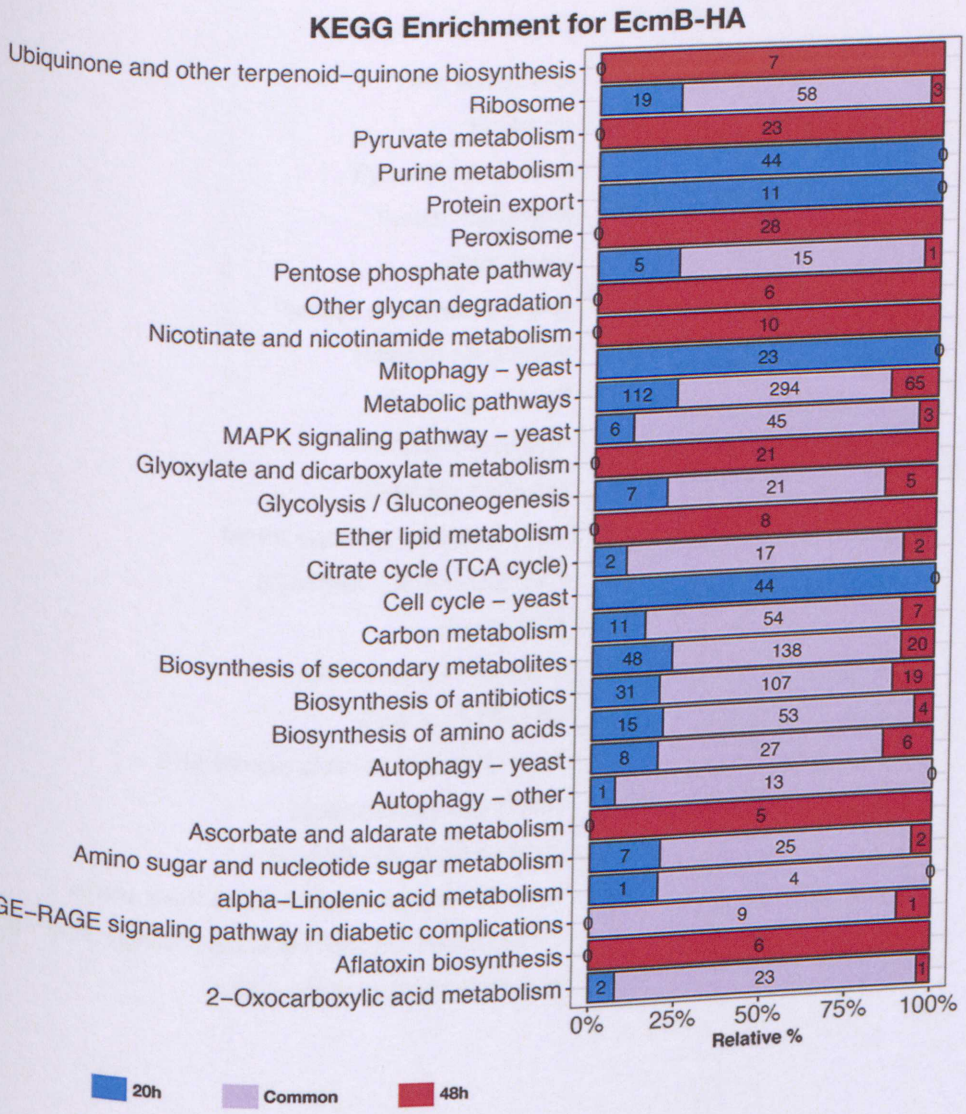

Figure 3.12: Genome-wide EcmB targets and related pathways. Comparative bar graph represents the relative percentage of EcmB target genes specific at 20h (blue bars), specific at 48h (red bars) or common to both conditions (pink bars) in the given KEGG pathways. KEGG pathway involved genes indicated on the bars. KEGG pathways are given based on the gene numbers enriched for EcmB-HA binding either at 20h or 48h.

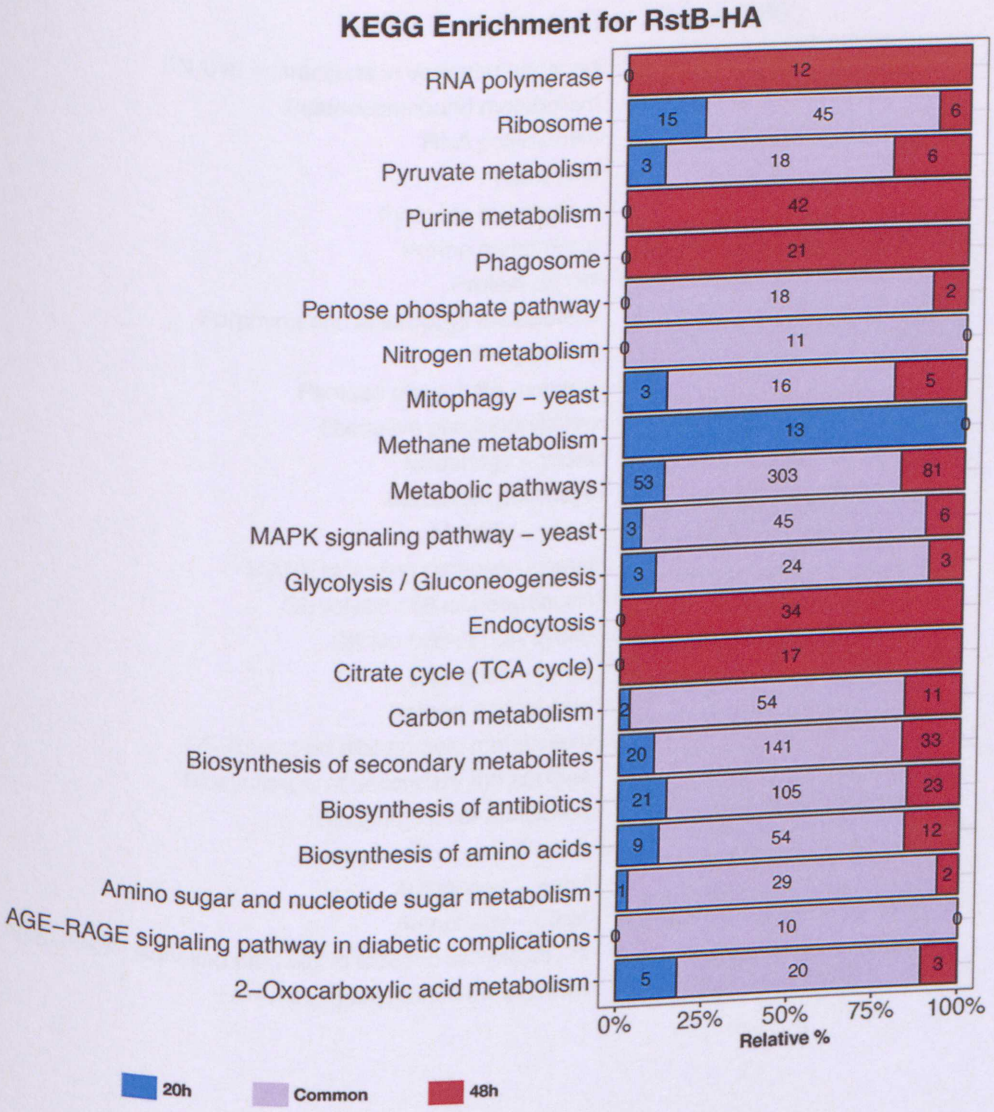

Figure 3.13: Genome-wide RstB targets and related pathways. Comparative bar graph represents the relative percentage of RstB target genes specific at 20h (blue bars), specific at 48h (red bars) or common to both conditions (pink bars) in the given KEGG pathways. KEGG pathway involved genes indicated on the bars. KEGG pathways are given based on the gene numbers enriched for RstB-HA binding either at 20h or 48h.

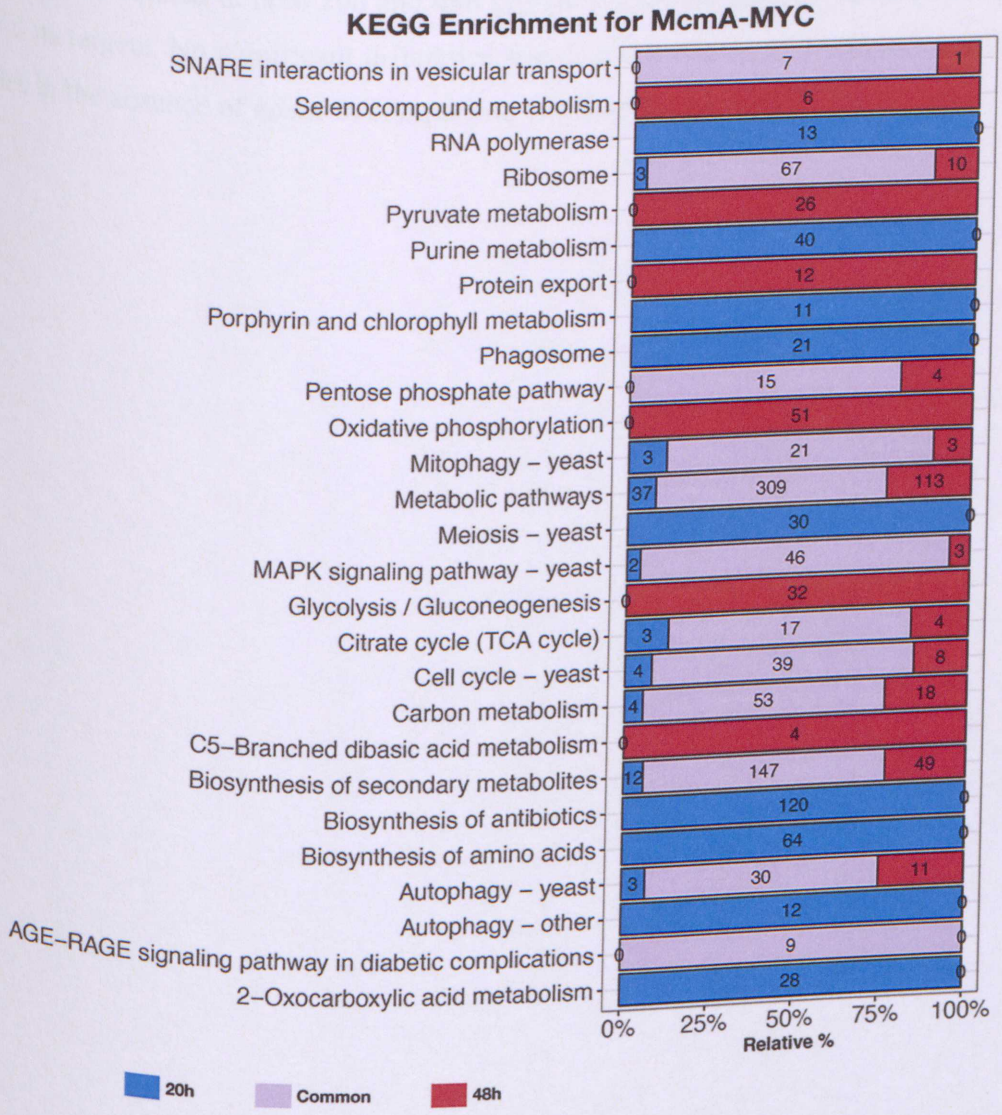

Figure 3.14: Genome-wide McmA targets and related pathways. Comparative bar graph represents the relative percentage of McmA target genes specific at 20h (blue bars), specific at 48h (red bars) or common to both conditions (pink bars) in the given KEGG pathways. KEGG pathway involved genes indicated on the bars. KEGG pathways are given based on the gene numbers enriched for McmA-MYC binding either at 20h or 48h.

As a part of this study, to display interdependency patterns of the MERCK complex, it was shown in **Section 3.5** that complex formation disappears in the absence of KdmA. Thus, it was aimed to investigate the genome-wide binding pattern of the other complex components in the *kdmA* deletion background. In order to assess that in *cclA*, *ecmB*, *rstB* HA-tagged and *mcmA* MYC-tagged strains, *kdmA* was deleted and ChIP-seq was performed on these strains. Normalized peaks were showed as heat-maps in **Figure 3.15** by comparing with their KdmA presented binding results. The order of ranked genes was presented as specific for each

member. From data in **Figure 3.15**, it is surprisingly apparent that *cclA* binding peaks disappear when *kdmA* is deleted in both 20h and 48h growth stages, suggesting that *kdmA* assigns *cclA* to bind its targets. No significant difference was found in the *ecmB*, *rstB* and *mcmA* binding profiles in the absence of *kdmA* in comparison to presented condition.

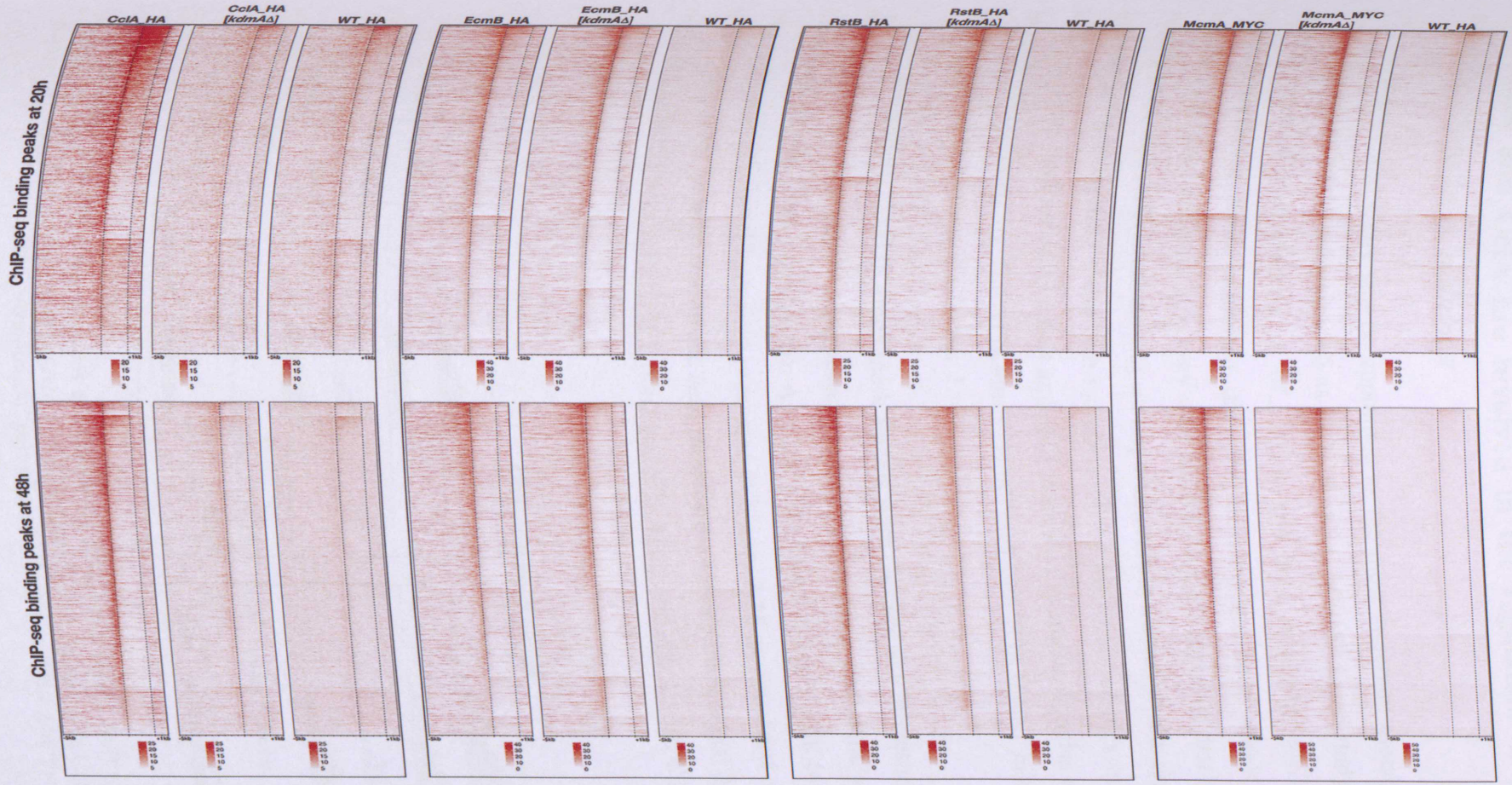

Figure 3.15: ChIP-seq analysis of MERCK complex members binding in the absence of KdmA. Peak density based heat-map presentation of CclA (HA), EcmB (HA), RstB (HA) and McmA (MYC) ChIP-seq binding in comparison to WT in the *kdmA* deletion background at 20h (upper heat-maps) and 48h (lower heat-maps). All ranked genes were presented according to the peak density shown with 5kb distance from transcriptional start site (TSS) and 1kb distance from transcriptional end site (TES). Peak density colour scales were shown under associated heat-map.

3.7 KdmA and CclA are involved in the regulation of posttranslational modifications in *A. nidulans*

KdmA and CclA can be appointed as the most important members of the MERCK complex since *kdmA* was reported as H3K36 by LC-MS/MS based study and H3K9 specific demethylase (Gacek-Mathew *et al.*, 2015) and *cclA* is a very well known H3K4me3 methyltransferase from published data but still has not been shown by comprehensive sequencing based analysis. It is very well known from the literature that both of these histone posttranslational modifications play an important role in transcriptional regulation. This raised interest in investigating these two members of the MERCK complex in this study. Histone ChIP-seq was performed on *kdmA* and *cclA* mutants. Chromatin samples of these mutants was immunoprecipitated by H3, H3K4me3, H3K9me3 and H3K36me3 histone antibodies and sequenced as described in Chapter 2.

Genome-wide H3K4me3 mark signals were checked and interestingly, on the majority of the genome this signal disappeared, except for on some vital cellular processes such as ribosomal genes (data not shown). As track peak based samples H3K4me3 mark disappear, two examples of signal loss were presented in **Figure 3.16** as visualized on IGB platform and it can obviously be seen that in the *cclA* mutants the histone mark signal disappeared although the signal clearly was seen in WT polII and H3K4me3 and *cclA*Δ polII ChIP binding results.

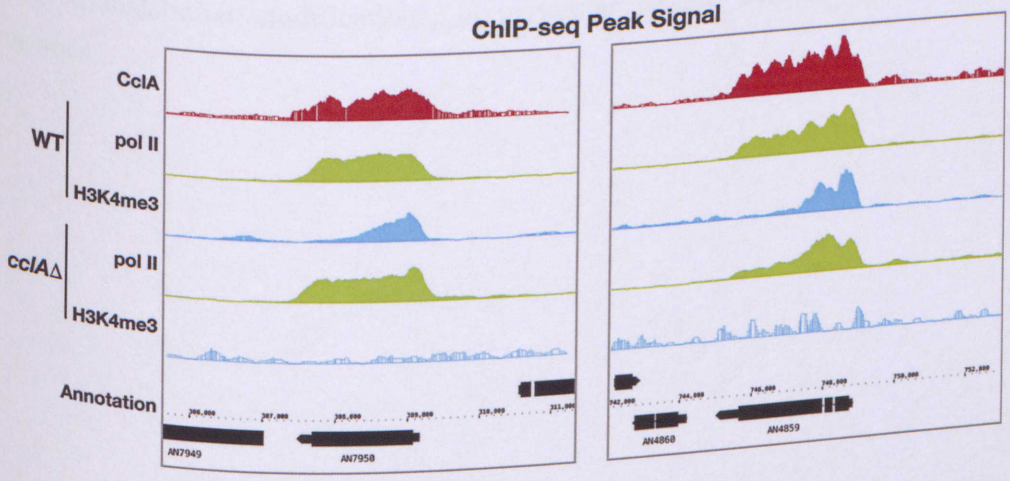

Figure 3.16: Loss of CclA reduces genome-wide H3K4me3 levels. IGB peak track examples shown for WT and *cclAΔ* pol II (green) and H3K4me3 (blue) signals with CclA-HA (red) signals across *A. nidulans* genome. 'Annotation' part refers to the genes in the genome.

To determine how H3, H3K9me3 and H3K36me3 levels change in the genome, five specific regions with 6 kb size were chosen from different part of chromosome I as shown in the **Figure 3.17** (according to the location on the chromosome, as percentage) and these regions were segmented by 20 sub-regions with 300bp size. Later expression values of mutants were divided by WT values and Log2 (fold change) heat-map in **Figure 3.17** was plotted subject to these values. What obviously stands out in the table is that H3K9me3 levels are significantly decreased in the *cclA* deletion mutant at both 20h and 48h and surprisingly, mostly in the telomeric regions of chromatin. In contrast to this reduction, the *kdmA* mutant showed an increase on the same histone modification and on similar region particularly at 20h. Moreover, interestingly, deletion of *cclA* resulted in a rise of H3K36me3 levels on the telomerase based regions and *kdmAΔ* not appeared to be affected importantly. No particular difference was observed on both mutants H3 levels.

To assess whether these differences would be observed on the other chromosomes as well, the whole chromosome IV was chosen for investigation and divided by 2 kb sized regions and expression analysed in comparison to WT (**Figure 3.18**). It is clear from **Figure 3.18** interestingly, there were also H3K9me3 signal reduction on the telomere regions and increment on chromosome body at both time points. Another interesting thing from this figure is that, chromosome-wide binding of H3K9me3 decreased in the *kdmA* deletion at 20h, oppositely increased at 48h.

Taken together, these results strongly demonstrate that *cclA* has an important role on histone posttranslational modifications, in particular around heterochromatic regions on chromosomes.

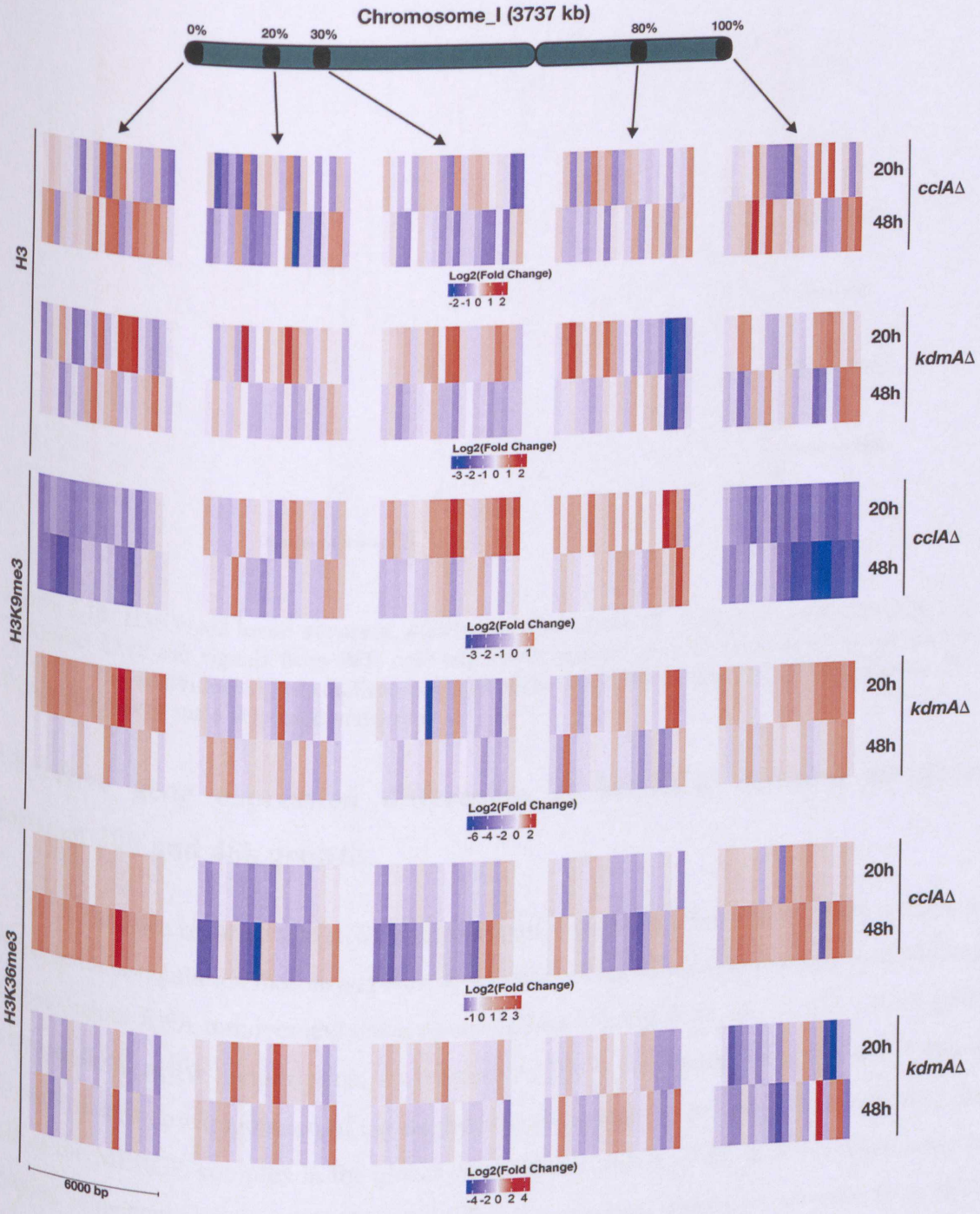

Figure 3.17: Histone modification levels in *cclA* and *kdmA* mutants at 20h and 48h. Heat-maps indicate the H3, H3K9me3 and H3K36me3 levels in the deletion of *cclA* and *kdmA* from 5 different regions of *A. nidulans* chromosome I. Shown each region is with 6000bp size and divided by 20 sub-regions (300bp). Region locations are presented as percentages on the chromosome. Log2 (fold change) colour scale of heat-maps which refers to expression level were shown below plot individually.

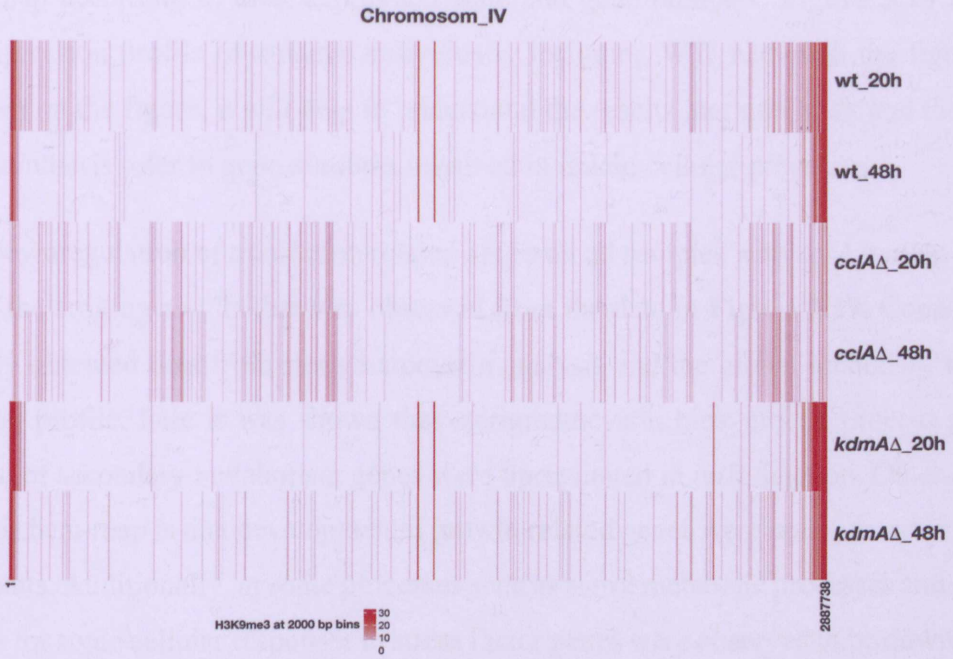

Figure 3.18: H3K9me3 levels across *A. nidulans* chromosome IV. Heat-map represents means of H3K9me3 ChIP-seq signals from WT, *cclA* and *kdmA* mutants at different time points of growth (20h and 48h). Individual signals on heat-map plot refers to a 2000bp region on the chromosome IV. Expression colour scale is located under map.

3.8 Active gene expression differences of MERCK complex members between 20h and 48h growth

It has been reported that RNA polII occupancy provides more precise determination of transcriptional regulation than steady state RNA level which differently depends on additional factors such as RNA turnover and transcription factors (Mokry *et al.*, 2011). Since RNA polII corresponds to active transcription, an increase of RNA polII refers to upregulation and a decrease means downregulation of expression. In order to get more insight with regard to the role of the MERCK complex in the global transcription profile, ChIP of RNA polymerase II coupled sequencing was used in this study. For this purpose, chromatin samples from WT, complex component mutants and WT grown in the presence of 5 µg/ml dox (as comparison for $mcmA_{tetOn}$ mutant) was utilized here.

Since it was kown that the expression values of WT and mutants are reliable (data not shown), regulated genes were identified by analysing differential bounding values at 20h and 48h for all samples, GO term enrichment analysis was performed by using DAVID Gene

Functional Classification tool from identified upregulated and downregulated genes and plotted on heat-map according to their expression state and gene numbers. **Figure 3.19** shows the active expression profile of mutants individually including WT. Although the figure legend was shown on the figure, it will help to understand the results that min, max and the numbers inside parenthesis refer to gene numbers involved in linked cellular processes.

Downregulation of translation related genes on all samples with *cclA* mutant exception is one of the striking results that was observed from the data in **Figure 3.19.** Consistent with previously obtained data from sterigmatocystin analysis and the global secondary metabolite production profile, here it was shown that sterigmatocystin biosynthetic process genes and regulation of secondary metabolism genes were upregulated in *rstB* deletion. Other consistent data in this heat-map is that developmental growth related genes were upregulated in *ecmB* and *cclA* mutants. Additionally, in some processes such as sterol metabolic processes and glycolytic processes for some cellular responses to stress factor genes were observed to be down regulated in all mutants and WT samples, but not in the *cclA* mutant. In summary, these results suggest an important role of the MERCK complex in transcriptional regulation.

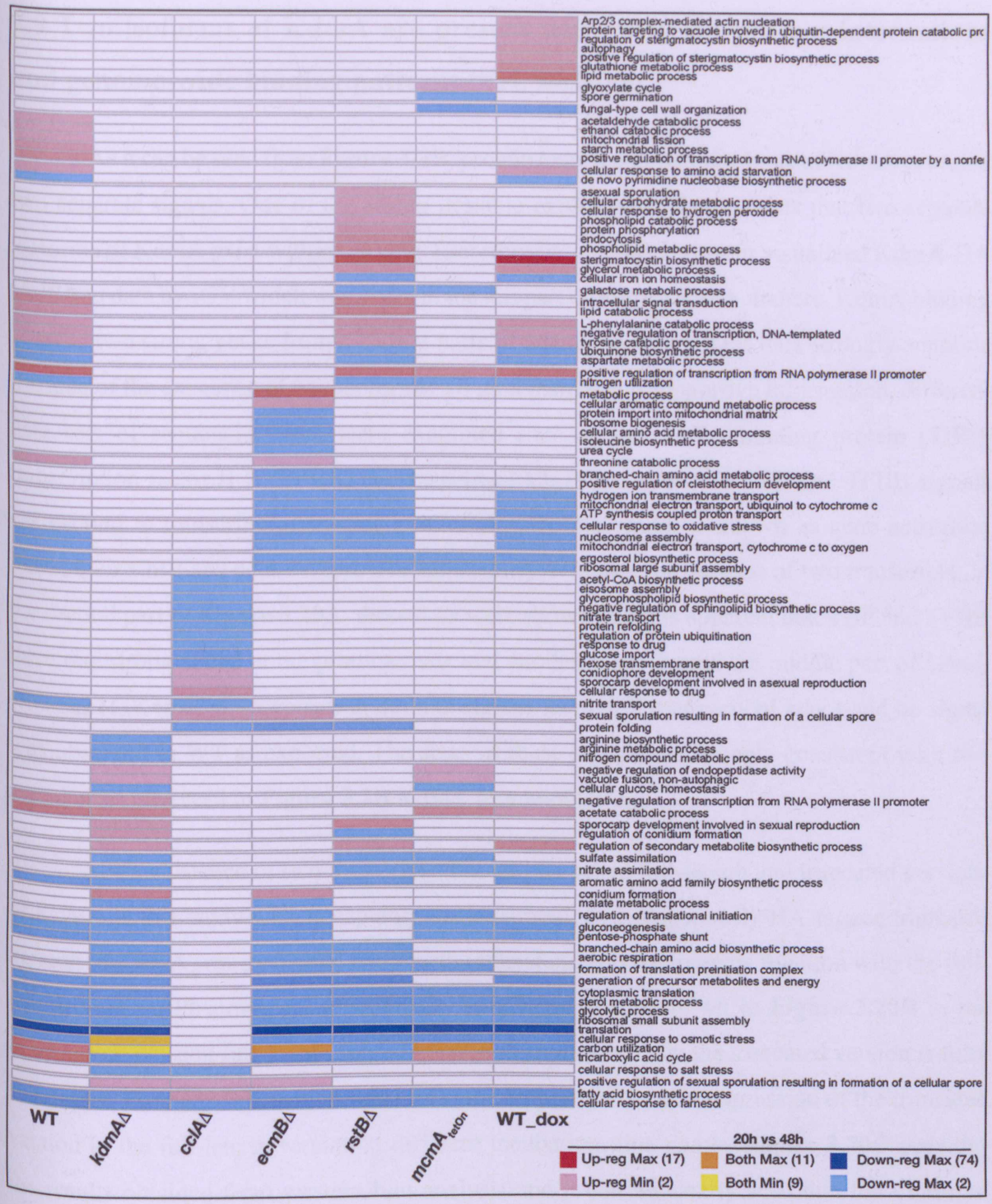

Figure 3.19: Comparison of MERCK complex members' active expression patterns. Heat-map illustrates differential expression levels of the genes which are involved in the cellular processes indicated on the right side of the plot for *A. nidulans* WT and mutant strains by comparing 20h and 48h growth stages. Colour scale descriptions were given on the figure according to their expression states (up-regulated, down regulated or both) and the number of the genes associated indicated the cellular process. Max refers to the highest annotated gene numbers detected from analysis (bracketed numbers), min represent the lowest annotated gene numbers (given in parenthesis) detected from analysis for the shown cellular process.

3.9 Two isoforms of KdmA are present with different protein interactions and genome-wide binding patterns in *A. nidulans*

As it can be seen from **Figure 3.2B**, protein expression western-blots of KdmA revealed two separate signals. One of the strong possible explanations for this was that two separate isoforms of KdmA exist within the cell. Therefore, it was checked from visualized KdmA-HA ChIP-seq data by IGV which was given in the left part of **Figure 3.20A**. In here, KdmA binding showed two strong peaks from different parts of annotated *kdmA*. This data strongly supports the idea of the existence of two isoforms. To gain insight and supportive information, different data sets of sequencing data were examined such as the TATA binding protein (TBP), transcription factor II B (TFIIB) and H3K4me3 ChIP data. Because TBP and TFIIB signals correspond to transcription starting point and H3K4me3 mark is known as gene activation mark, their ChIP-seq data will provide satisfactory evidence for the case of two transcripts. In the second part of **Figure 3.20A,** these data were shown and it is apparent that TBP and TFIIB have one strong signal at the promoter site and another peak around the middle part of *kdmA,* whereas H3K4me3 has two strong definite signals from different parts of *kdmA* and no signal was observed in WT as expected. The sizes of these signals are strongly consistent with two signal sizes observed in **Figure 3.2B** KdmA immunoblotting.

Since existence of two transcripts that will be called full-length and truncated versions of KdmA in this study were acceptably demonstrated, an endogenously HA-tagged truncated version of KdmA was generated in order to understand and compare its function with the full-length version. Phenotypical functionality confirmation was shown in **Figure 3.20B** in the presence of WT and full-length tagged version. It was shown that the truncated version is fully functional. Further confirmation was aimed to compare the protein expression of the truncated version to the full-length version at different incubation time points. **Figure 3.20C** provides the results obtained from western blot analysis and it can be clearly seen that the truncated version gave a single signal while full-length KdmA presented two signals with different sizes as expected. Having functionality and expression verification of truncated version of KdmA, it was further aimed to investigate what are the differences on the complex dynamics and interaction network with the other members. For the purpose of exploring the complex formation differences between the two, truncated versions' total protein was extracted and HA purification coupled MS was performed and surprisingly it was found that the truncated version

of KdmA was able to recruit only EcmB and RstB which are fungal specific transcription factors (**Figure 3.20D**) suggesting critical survival role of this isoform formation for fungi.

To determine whether there are any differences between these isoforms genome-wide targets, ChIP-seq was performed on a truncated HA-tagged version of KdmA at 20h and 48h growth and binding profiles of both versions were illustrated in **Figure 3.20E**. Data clearly showed that the truncated KdmA version could not bind as strong as full-length and there is a loss of binding at 20h while slightly stronger signal was observed at 48h than 20h for truncated version. Overall, these results strongly indicate the existence of two KdmA isoforms with different interaction partners and with different genome targets in the cell.

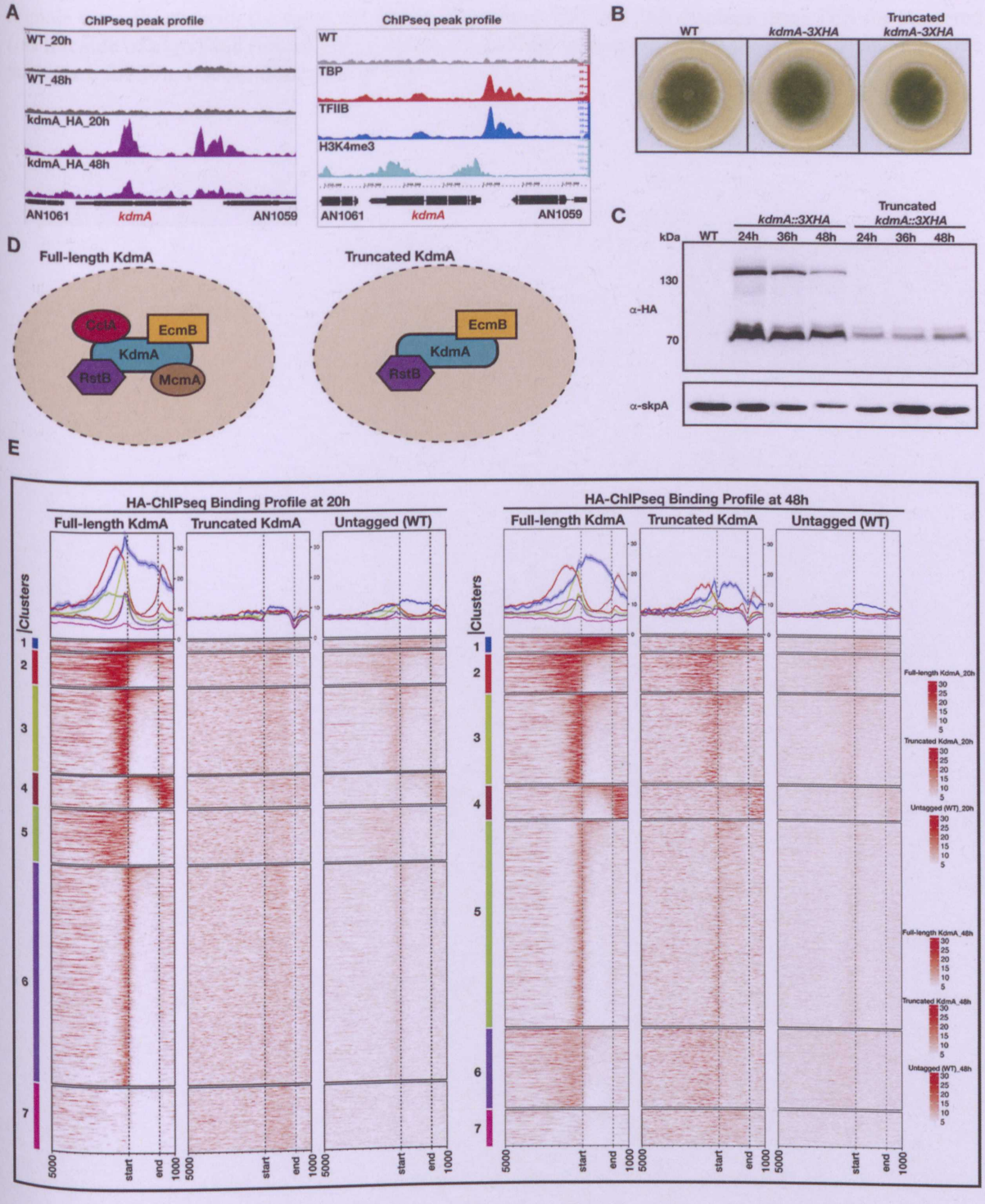

Figure 3.20: Different isoforms of KdmA are presented within the cell. (A) IGV browser view image of normalized KdmA ChIP-seq peaks, and IGB browser view image of normalized TATA box-binding protein (TBP), Transcription factor II B (TFIIB) and H3K4me3 signal peaks and their comparison. *kdmA* annotation is stated in bottom of images. **(B)** Morphological functionality analysis of HA tagged full-length and truncated versions of *kdmA*. **(C)** Western blot analysis of full-length (156.9 kDa) and truncated (~81 kDa) versions of KdmA. HA tagged strains were used and 50µg total protein was loaded on gel. α-SkpA was used as a loading control. **(D)** Illustration of interaction partners in the presence and absence of full-length KdmA. Illustration sketch is based on MS coupled protein purification analysis for both versions. **(E)** Heat-map demonstration of full-length and truncated versions of KdmA ChIP-seq binding profile in comparison to WT at 20h and 48h growth stages. Peak

signals were shown with the range of 5kb distance from TSS and 1kb distance from TES for clustered (on left side of plots) and ranked genes. Density colour scales were given on the right side and top three scales are for 20h, bottom three are for 48h.

Chapter 4

The role of the MERCK complex in development and secondary metabolism in *A. flavus*

4.1 Detection of the pentameric MERCK demethylase complex in *A. flavus*.

Comprehensive analysis of the MERCK complex was performed in *A. nidulans* as explained in detail in Chapter 3. Since *A. flavus* is a saprophytic and opportunistic pathogen fungus that produces highly carcinogenic aflatoxins as secondary metabolites, in this chapter it was aimed to particularly investigate the roles of the MERCK demethylase complex in this microorganism. Initially, complex members domain analysis was performed (**Figure 4.1A**). Protein sequences of members were obtained from NCBI with their gene IDs which are AFLA_067020 (*kdmA*-1), AFLA_067030 (*kdmA*-2), AFLA_089250 (*cclA*), AFLA_027860 (*ecmB*), AFLA_003630 (*rstB*) and AFLA_090910 (*mcmA*) and domain analysis was performed via the UniProt database. An interesting outcome of this analysis was that *kdmA* is annotated as two separate genes, most likely due to the presence of two isoforms within the cell, as is observed in *A. nidulans*. Having information of domain structure of members, further examination aimed to show conservation of these domains across different species by utilizing NCBI conserved domain search and a detailed table of results is given in **Figure 1.4B**. As it can be seen from the table, KdmA, CclA and McmA domains are found to be highly conserved whereas EcmB and RstB are fungal specific.

In order to assess complex formation in *A. flavus*, KdmA, CclA, EcmB and RstB were endogenously HA epitope tagged and KdmA was also GFP tagged. Functionality of these strains was confirmed morphologically in comparison to WT (data not shown) and HA affinity protein purification coupled MS was performed on them. By analysing MS results against an *A. flavus* proteome database (downloaded from NCBI), unique peptide numbers were obtained and are presented in **Figure 4.1C**. What is interesting about the data in this table is all tagged complex members reciprocally recruit each other, suggesting that there is indeed complex formation in *A. flavus*. Interestingly, the unique peptide numbers for KdmA were detected for two separately annotated proteins which are shown as KdmA-1 and KdmA-2. This data strongly complements earlier mentioned KdmA domain analysis and existence of two isoforms within the cell. The interaction network of the MERCK complex based on MS analysis is illustrated in **Figure 4.1D** and it is shown in the table on the same figure that the interaction network complex members interrelate with McmA, although tagging attempts for McmA were unsuccessful which is possibly due to protein disruption.

Observing complex formation raised the question of the protein expression level changes during vegetative and developmental growth stages. In order to answer this question,

fully functional HA tagged KdmA, CclA, EcmB and RstB strains were inoculated in liquid complete media for 24h, 36h, 48h (V24h, V36h, V48h) and 24h vegetative grown mycelia were shifted to complete media agar plate and incubated for 24h under constant light (A24h), 24h and 48h in darkness (S24h, S48h). Extracted total protein of each stage was loaded on SDS gel, and immunoblotting was performed. **Figure 4.1E** shows the results obtained from western blot analysis of complex members and their protein expression levels during different growth stages. The most striking observation to emerge from the western blot comparison was two different sized signals of KdmA, one is labelled as 'L' (~160 kDa) (shown with blue arrow) and another is labelled 'S' (~80 kDa) (shown with red arrow) which strongly suggests that there are two isoforms that exist in *A. flavus*. Besides, protein expression of KdmA shows decrease in 48h of sexual stage. From this data, it can also be seen that EcmB (~145 kDa) has approximately double size signal than it is expected as well as its expected expression signal suggesting that EcmB undergoes homodimerization in *A. flavus* which is also consistent with *A. nidulans* data from Chapter 3.

A further question that needed to be addressed was which compartment of the cell this complex is localized? In order to answer this question, a KdmA-GFP tagged strain was inoculated in liquid complete media and cultured for 12h. The hyphae of this strain were stained with nucleus specific stain DRAQ5 and location analysis was performed by using laser confocal microscopy after 30 min treatment. As presented in **Figure 4.1F**, the GFP signal shows the same position with the DRAQ5 red signal. signifying nuclear localisation of KdmA. Since it was shown that KdmA is a scaffold protein for the complex and all complex members localized in the nucleus in *A. nidulans*, as well as complex members possessing NLS (nucleus localization sequences) in *A. flavus*, the localization of other complex members were not checked in this study. However, all members of the MERCK complex were localized to nucleus in *A. nidulans*.

Taken together, these results provide sufficient insight into formation and interaction dynamics, as well as the protein expression profile and subcellular localization of the MERCK demethylase complex in *A. flavus*.

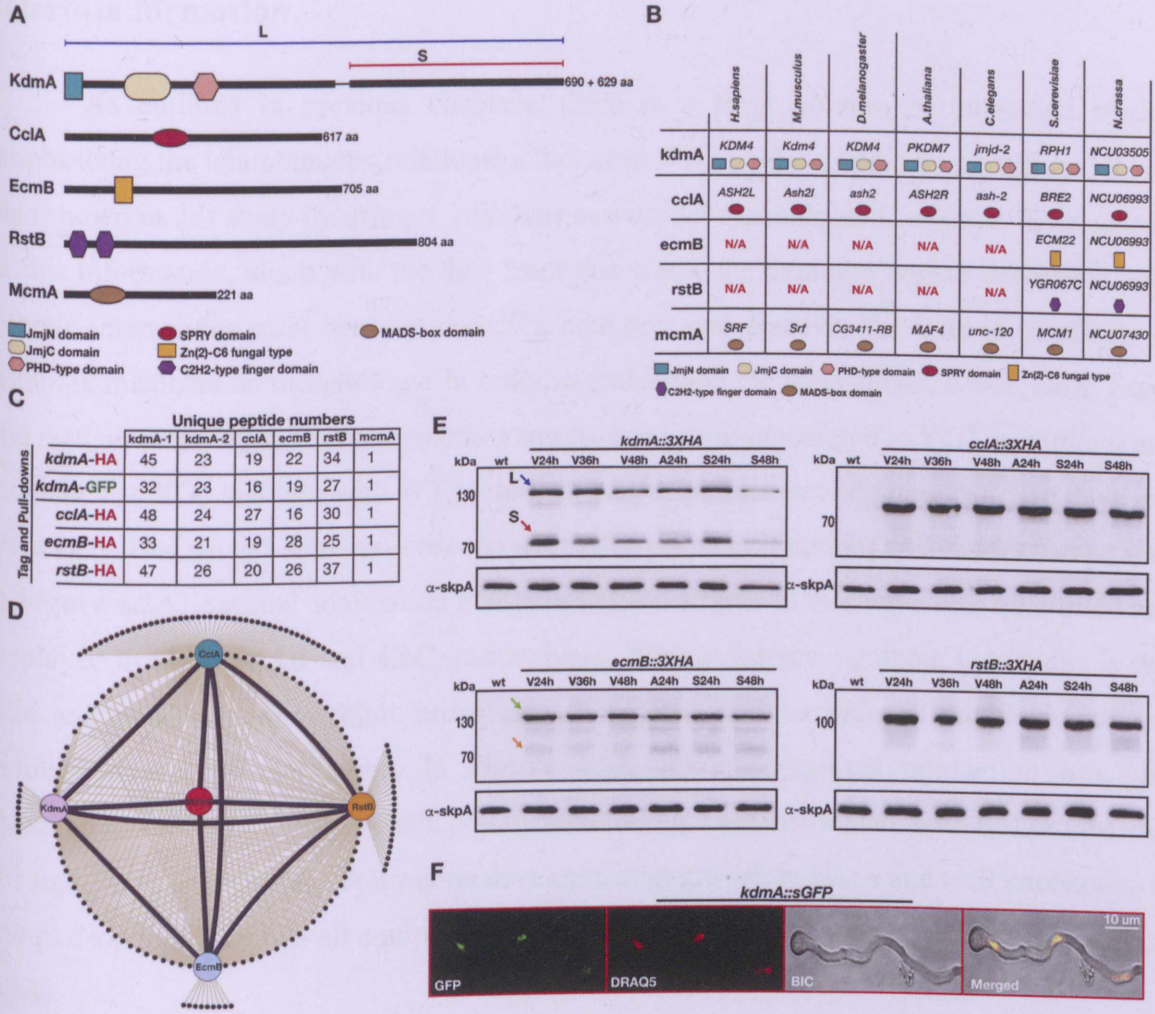

Figure 4.1 Protein domain diagrams, verification and protein expressions for the MERCK complex in *A. flavus*. **(A)** Individual domain structure of complex components. Protein sequences were provided from NCBI (https://www.ncbi.nlm.nih.gov/) with their gene symbols for AFLA_067020 (*kdmA*-1), AFLA_067030 (*kdmA*-2), AFLA_089250 (*cclA*), AFLA_027860 (*ecmB*), AFLA_003630 (*rstB*) and AFLA_090910 (*mcmA*) and domain analysis was performed on UniProt database (https://www.uniprot.org/). **(B)** Conserved domains and orthologues table of complex components among different species. BLAST analysis was done by using NCBI. N/A means that orthologue does not exist in that organism. **(C)** Interacting partners table for individual complex members presented with their specific pulldown and unique peptide numbers. Values were extracted from mass spectroscopy data. **(D)** Interaction network of the MERCK complex. Network was generated by summarizing MS data in Cytoscape software (version 3.6.1). Minimum limit was settled as three unique peptides for interaction partners. **(E)** protein expressions of KdmA, CclA, EcmB and RstB throughout vegetative and developmental (asexual and sexual) life stages in different growth time points. α-HA antibody was used for immunoblotting and 50 ug of protein was loaded on SDS-gel. α-SkpA antibody was used as a loading control. **(F)** Confocal visualization of KdmA subcellular localization. Red signals are a result of nuclear staining with the fluorescent far-red DNA stain DRAQ5. Merged signals represent overlapped red signals with GFP fused KdmA signals.

4.2 *cclA* and *ecmB* mutants show reduced conidial production and affect sclerotia formation.

As outlined in previous chapters, there is a large volume of published studies emphasizing the unambiguous relationship between SM and development in fungi and it was also shown in this study by using *A. nidulans* as a model organism in Chapter 3. With respect to this information, along with the data from this study, the next aim was to determine what genetic interactions exist between complex members and discover the individual effects of complex members on morphology. In order to understand the mechanism, *kdmA*, *cclA*, *ecmB* and *rstB* mutants and their complemented strains were point inoculated in YGT agar plates and incubated at 30°C together with WT in dark and light. Strains were cultured for five days and were visualized using a stereomicroscope with different magnifications and images can be seen in **Figure 4.2A**. Asexual conidiation numbers and radial growth rate were also quantified and displayed in **Figure 4.2B** and **4.2C**, respectively. What is interesting about the results is that *cclA* and *ecmB* mutants exhibit strong growth defects, such as reduced radial growth and diminished asexual sporulation. In **Figure 4.2A**, obvious pigment production was also observed around *cclA* deletion strain colony which is typically associated with SM production. No significant change was observed on developmental growth in *kdmA* and *rstB* knockouts, in comparison to WT, while all complex members showed a similar phenotype with *wt* (**Figure 4.2A**).

Together these results indicate that *cclA* and *ecmB* play important roles in fungal development and predictably in SM as well. The next investigation therefore sought to determine the roles of the complex members in the formation of developmental structures. *A. nidulans* reproduces via ascospores, which reside within cleistothecia structures for protection. Likewise, *A. flavus* has evolved to generate sclerotia structures to adapt to harsh environmental conditions. To gain insight of the MERCK complex's role in development, WT, mutant and complemented strains were point inoculated in WKM agar plates and incubated at 30 °C for 14 days in the dark. Plates were then scanned and asexual spores were washed with 70% EtOH to reveal underlying sclerotia formation, which was imaged using a stereomicroscope. Later, sclerotia numbers were quantified by counting one quarter of each plate and multiplying by four. The results obtained from this analysis are displayed in **Figure 4.2D and 4.2E**. What is striking about the images in the figure is that the absence of *cclA* causes loss of sclerotia production, suggesting a key role of *cclA* in this cellular process. Interestingly, the number of

sclerotia was strongly decreased in the *ecmB* deletion strain and sclerotia appeared to be immature. Additionally, from the images and plot, it can clearly be seen that in the absence of *kdmA* and *rstB,* sclerotia production rates were significantly decreased, whereas complemented strains showed similar production to the WT.

It has been demonstrated that *sclR* is a transcription factor that promotes sclerotial formation in *A. oryzae* (Jin *et al.*, 2011). In order to determine the transcriptional expression level of this gene in WT and mutant strains, mycelia from strains cultured vegetatively for 24h and shifted to WKM agar plates for 7 days in darkness was used to perform RNA extraction. Respective cDNA was tested via qRT-PCR and **Figure 4.2F** provides the results obtained from this experiment for WT and knockout strains. From the data in this figure, it is apparent that there is a decreasing in *sclR* expression in *cclA* and *ecmB* mutants. It is evident that the sclerotia production data in **Figure 4.2D** and **4.2E** are in agreement with transcriptional expression data of *sclR* in mutants. Overall, these results indicate that *cclA* and *ecmB* play an important role on *A. flavus* developmental growth.

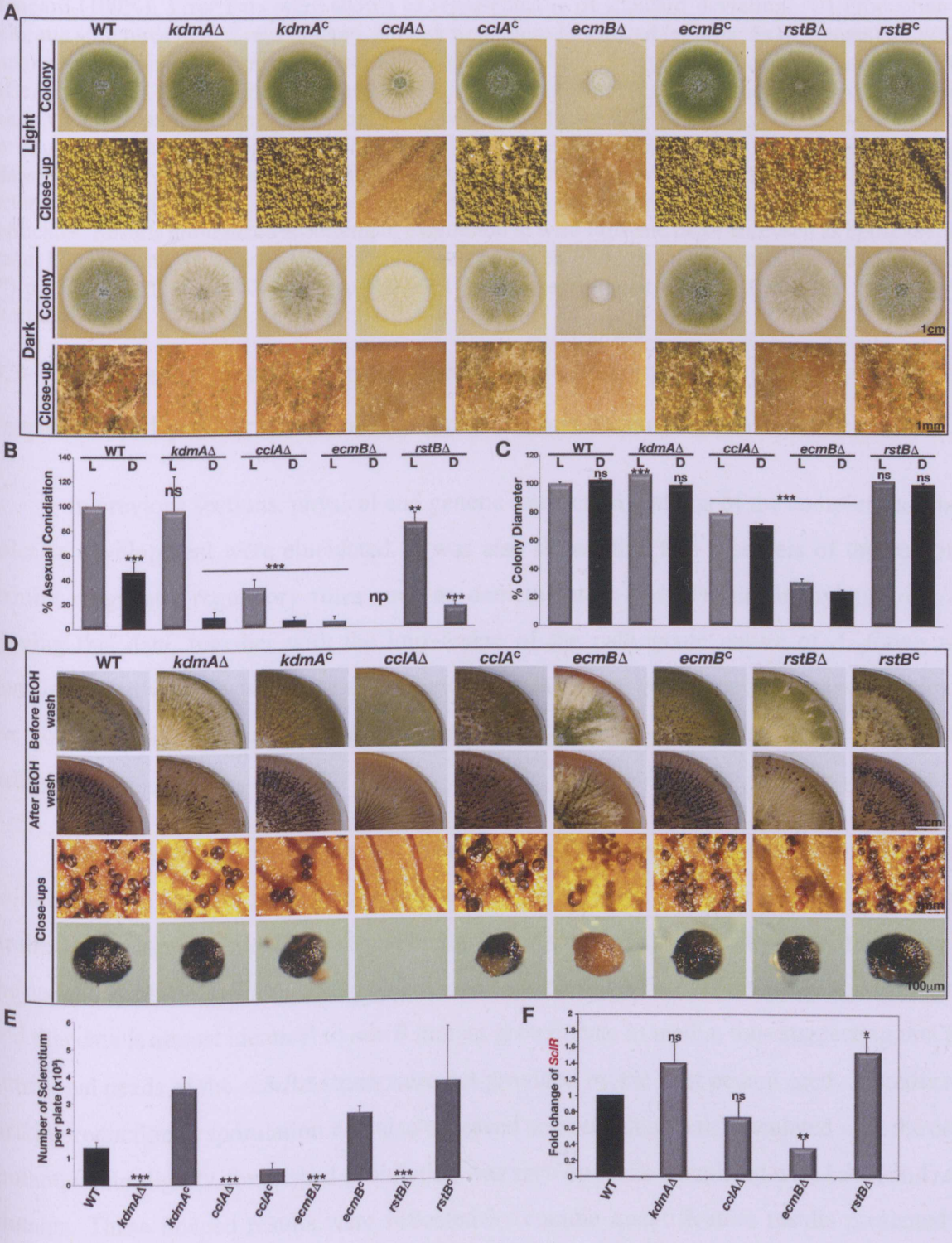

Figure 4.2 Morphology and sclerotia production analysis for complex member's mutants in *A. flavus*. **(A)** Stereomicroscopy colonies and close-up images of wild-type, mutants and complementation strains. Cultures were point inoculated (approx. $5x10^3$ spores) on YGT agar plate and grown at 30 °C for 5 days under constant light and dark conditions. **(B)** Asexual conidiation quantification values were obtained from three independent 5x10 mm^2 area cores and three different plates. Wild-type, cultured in light conditions was chosen to represent a 100% standard and the other values were presented relatively

to this value. Standard deviations are presented on the graph bars as vertical lines. **(C)** Colony diameters were measured from three independent plates and in the light grown wild-type size was considered as standard (100%). Error bars were shown as representative of standard deviation. **(D)** Production of sclerotia structures in *A. flavus* mutants. Strains were point inoculated (approx. $5x10^3$ spores) on WKM medium with required supplements and incubated at 30 °C for 14 days under constant dark conditions. After incubation, asexual conidiophores were washed away with 70% EtOH and close-up images were taken via a stereomicroscope. Scale bars are shown on the figure. **(E)** Sclerotia quantification was done by counting one quarter of a plate then multiplying by four. Values were taken from three independent plates and stated with their standard deviations as error bars on the graph. **(F)** Expression levels of *sclR* determined via qRT-PCR. Values are the mean of three independent biological and three technical replicates. Results normalized according to expression in wild-type and *benA* was used as housekeeping gene. Experiments were carried out in biological triplicates. The statistical significance is indicated as (*) $p < 0.05$, (**) $p < 0.001$, (***) $p < 0.0001$ and non-significant (ns) $p > 0.05$. 'np' refers to 'no production'.

4.3 The demethylase complex influences secondary metabolism, stress response and post translational modifications as well as host colonization.

In previous sections, physical and genetic interaction patterns of the complex and their roles in development were elucidated. It was also shown that two members of the complex exhibit epigenetic regulatory roles such as demethylation (*kdmA*) and methylation (*cclA*). Having this data, together with the knowledge of the pathogenic nature of *A. flavus* and correlation between development and secondary metabolism, we decided to assess the roles of the complex with respect to these significant cellular processes as well as stress response pathways.

The first step in this section was to determine the function of complex members in host colonization. In order to asses that, peanut seeds were infected with spores of WT and mutant strains, as described in the materials and methods section. As **Figure 4.3A** shows, interestingly, the capability of the *ecmB* mutant to colonize and sporulate on host peanut seeds was decreased and this data is almost identical to *ecmB* mutant growth data in media, thus suggesting that the nutritional needs of the *ecmBΔ* strain were not provided by the host peanut seed. Moreover, a striking reduction in sporulation was also observed on seeds that were inoculated with the *cclA* mutant, while slightly diminished conidiation was seen on seeds inoculated with *kdmA* and *rstB* mutants. These imaged results were reflected by conidia quantification results presented in **Figure 4.3B** which show clear significant decreases for *ecmB* and *cclA* mutants. To determine their virulence in terms of aflatoxin production on host seeds, aflatoxin was extracted from infected seeds and quantified via HPLC in comparison to an aflatoxin B1 standard. **Figure 4.3C** presents aflatoxin B1 levels produced by WT and mutants on peanut seeds and it is clear that the deletion of *cclA* results in a drastic increase of aflatoxin B1 production on host seeds.

Interestingly, it was observed that in the absence of *ecmB,* aflatoxin B1 production reached the lowest levels, while no significant differences were found for *kdmA* and *rstB* mutants. These results indicate that the deletion of *cclA* and *ecmB* affect virulence and aflatoxin production on host growth.

In order to gain insight on the roles of the complex components in SM, in particular, their individual aflatoxin production levels in growth media, strains were point inoculated in YES agar plates with required supplements and plates were incubated at 30°C for 7 days in dark conditions. Results are provided in **Figure 4.3D.** The most interesting aspect of this figure is that all mutants resulted in reduced aflatoxin B1 production in comparison to WT, particularly, the deletion of *ecmB* resulted in almost a complete loss of aflatoxin B1. Complemented strains showed an acceptable recovery in production in comparison to mutant strains. These data suggest *ecmB* and the other complex members play a key role in aflatoxin production.

To establish whether the MERCK complex is involved in stress response pathways, WT, mutants and complementation strains were point inoculated in the presence of various chemical stress factors with shown concentrations. Visual results were shown in **Figure 4.3E**. As it can be seen from the figure, *ecmB* was observed to be the most sensitive mutant to these stresses especially in the existence of DNA damage stress factor (0.02% MMS) and oxidative stress factor (6 mM H_2O_2). Although the other mutants showed sensitivity to some stress conditions, no significant effect was observed in the overall analysis.

A recent study demonstrated that *kdmA* is a H3K36me3 and H3K9me3 specific demethylase (Gacek-Mathew *et al.*, 2015) and H3K4 specific methyltransferase *cclA* is known as a subunit of the COMPASS complex which controls the regulation of H3K4 methylation. Moreover, in the previous chapter, the functions of *kdmA* and *cclA* on histone modifications were comprehensively shown by ChIP-seq analysis. Having this knowledge led us to investigate the role of the complex on posttranslational modifications. In order to understand more regarding that, nuclear extracts of WT and mutant strains were purified and immunoblotting was performed by using antibodies to detect specific histone modifications. Histone western-blot results are presented in **Figure 4.3F**. What is striking about the data in this figure is a significant decrease in the H3K4me3 level in the *cclA* mutant, which suggests its key role on this posttranslational modification. Interestingly, deletion of any complex members resulted in higher H3K36me3 mark signals than WT. Taken together, these results

strongly suggest that *kdmA* and *cclA* have critical functions on posttranslational modification marks of histones.

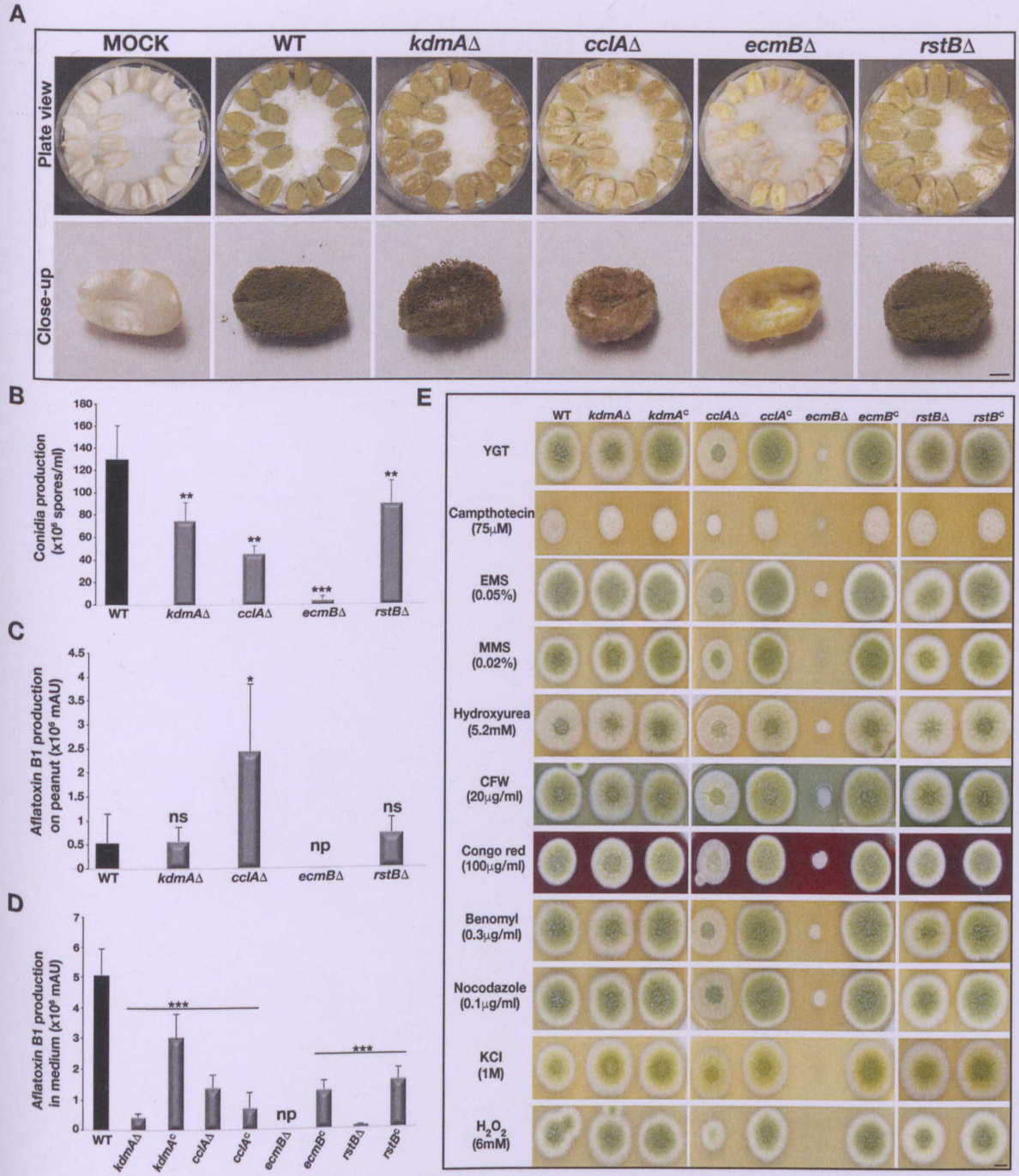

Figure 4.3: Host colonization, aflatoxin production, growth response to stress chemicals and histone modification expressions of MERCK complex members in A.flavus. **(A)** Peanut seeds infection by wt and mutant strains. Spores treated seed were incubated at 29°C for 5 days. Scale bar 10mm. **(B)** Conidia quantification values represent the mean of four independent peanuts quantification and from three different plates. **(C)** Aflatoxin production from spores peanuts. Quantification was assessed with three independent peanuts from three different plates. **(D)** Aflatoxin quantification from agar plate. Aflatoxin was extracted from Wt, mutant and complementation cultures were point inoculated (approx. $5x10^3$ spores) on YES agar plates which were incubated at 30°C in dark for 7 days. Values on the graph are corresponding to means of three independent biological replicates. Error bars were shown on the graph. **(E)** Phenotype characterization of complex members in response to chemical stress factors. Strains were point inoculated and incubated at 30°C for 65h under constant light condition. Chemical's concentrations are underlined on the figure. **(F)** Western blot analysis of wt and mutants' histone extracts for the checking histone modification level. α-corresponding histone antibody was used for each modification. 10 ug total nuclear extract was load on gel. α-H3 antibody was used for loading control check.

Chapter 5

Discussion

Lysine specific demethylase 1 (LSD1) and JMJC domain containing demethylase are two types of demethylase classes based on their demethylation mechanism. LSD1 type demethylases remove mono- and di- methylated lysine at lysine 9 and lysine 4 of H3 while JMJC type is also able to remove three-methylations and needs Fe^{+2} and oxygen as cofactor (D'Oto *et al.*, 2016). KdmA is a homolog of the highly conserved KDM4 family member of JMJC containing demethylases class. KDM4 family members was reported with regard to utilization of H3K9me2/me3 and H3K36me2/me3 histone marks and their association with various cancer types (Labbé *et al.*, 2014). It is yet not known whether KdmA presents as a complex within a cell, although much knowledge exists in the literature regarding it. This PhD study identified the formation of KdmA (AN1060) complex with its interaction members; which are McmA(AN8676)-EcmB(AN5533)-RstB(AN12489)-CclA(AN9399), here called MERCK complex.

Comprehensive and comparative protein domain, function, physical and genetic interactions, targets profile on the genome and transcriptional analysis of complex members were provided in detail through this research work. Extensive protein domain and homology analysis revealed that three members of complex KdmA (KDM4), CclA (ASH2L) and McmA (SRF type MADS-box TF) were found to be highly conserved through a wide range of organisms from fungi to humans whereas EcmB and RstB transcription factors were found to be presented only in the Fungal kingdom. Interestingly, the same complex formation was identified in the plant pathogen *A. flavus* with one difference, that KdmA is annotated by identifying two different genes AFLA_067020 and AFLA_067030. The gene IDs for MERCK complex are as follows; CclA (AFLA_089250), EcmB (AFLA_027860), RstB (AFLA_003630) and McmA (AFLA_090910).

5.1 MERCK complex role in *A.nidulans*

Growth and development

In *A.nidulans*, regulation of development and light response are commonly carried out by regulatory protein complexes such trimeric *velvet* complex or pathway specific transcription factors like *nosA* or *nsdD*. From the discovery of MERCK demethylase complex, presented in this study, it was shown that this complex regulates the fungal growth and development. In particular, *cclA* and *ecmB* mutants were found to exhibit strong growth deficiency as well as reduced asexual conidiation and clesthotecia formation. The same situation was observed for

their double deletion combinations suggesting that their stronger epistatic effect on morphology compared to other members and deletion of both members caused strong deficient phenotype. These results corroborate the findings of a great deal of previous work in *cclA* mutant phenotype analysis in *A.nidulans* (Bok *et al.*, 2009). Another important finding in this study was that although *kdmA* and *rstB* deletion strains were shown to have slightly reduced conidiophore production in comparison to *wt*, it interestingly produced more sexual fruiting bodies. Relative gene expression of complex members was shown to be downregulated at the developmental stages whereas they were constitutively expressed during the vegetative stage. Even though there was no change observed on CclA and McmA protein expression, protein amounts of KdmA, EcmB and RstB displayed reduced levels in sexual and asexual stages which is correlated with gene expression data. Additionally, genome-wide binding analysis of MERCK complex was also presented in this thesis by ChIP-seq analysis and target genes were also identified. Individual KEGG pathway analysis of complex members indicated that the majority of the targets are mostly common and are involved in some essential pathways such as carbon metabolism, cell cycle, MAPK signalling pathway, metabolic pathways and TCA cycle pathways. Previous studies were reported that some of these cellular pathways such as the fungal MAPK module is involved in the regulation of fungal development (Bayram *et al.*, 2012a). Moreover, in this research, RNA pol II occupancy analysis was also performed for mutants in order to investigate active transcriptional expression, since RNA pol II was shown to give a more precise profile than steady state RNA level (Mokry *et al.*, 2011). Differential expression data of mutants demonstrated that genes are involved in positive regulation of sexual development and sexual sporulation cellular processes. They were upregulated in *cclA* and *ecmB* mutants 48h growth in comparison to 20h. In addition, it also was found that asexual conidiation formation genes were upregulated at the late growth phase (48h). Deletion of subunit of H3K4 methyltransferase Set1C (COMPASS) complex yeast homolog BRE2 phenotype analysis showed diminished vegetative growth rate in *S.cereviasiae* (Yoshikawa *et al.*, 2011). In budding yeast, EcmB homolog ECM22 was shown as the regulator for the sterol biosynthesis pathway, together with its paralog UPC2 and reduction on vegetative growth rate (Yang *et al.*, 2014). Taken together, the findings of this research provide fundamental insights and critical role of the MERCK complex for fungal development.

Secondary metabolism

It is known from the literature that secondary metabolism is mostly co-regulated by pathway specific gene clusters and is related with subtelomeric regions of chromatin. Thus, another goal of the present study was to assess the role of MERCK demethylase complex on SM. The regulatory role of this complex was found on secondary metabolism in *A.nidulans* performing comprehensive analysis of SM by HPLC and LC/MS-MS. One of the interesting findings of this analysis was that complex members' single mutants showed significant increase in ST production, particularly, *rstB* mutant was found to produce the highest level. Although the double mutant combination of MERCK complex members were showed with higher amounts of produced ST, *cclA* and *ecmB* double and $mcmA_{tetOn}$ mutant strains indicated a lower ST production rate than *wt*. It is also interesting to note that the degree of ST production in the over expressed condition of complex members was opposite of mutants with the kdmA overexpression exception which still showed a higher amount. It has been suggested by previously published research in *A. nidulans* that deletion of *kdmA* resulted in a reduced ST level (Gacek-Mathew *et al.*, 2015), however, outcomes of the current study are in contrast to earlier findings. Since veA^{+} background strains were used in this study, the possible explanation for this conflict may be using the *veA1* background strain which has the partial loss of function mutation on *veA* which was shown to coordinate regulation between SM and development in response to light (Bayram *et al.*, 2008b). A more interesting outcome was observed in the global metabolite analysis that the production of different metabolites were based on different complex members, for example, ST and its biosynthesis side products indicated to have higher production rate in *rstB* and $mcmA_{teton}$ single and double mutants. In contrast, the austinol biosynthesis were more upregulated in the *cclA* and *ecmB* single and double knockout strains. Interestingly, orsellinic acid biostynthesis was shown to have increased production in the *cclA* and *ecmB* single mutants, and reached peak production in the double deletion of them. This finding also suggested that the regulation of these metabolite gene clusters are carried out by these complex members. KEGG enrichment analysis of genome-wide targets of the members was found to reflect the similar picture of SM profiles by having a big proportion of targeted genes in -biosynthesis of secondary metabolites- pathway, particularly with some more SM related pathway for *cclA* targets. *cclA* was shown to act as a repressor for SMs and in the biosynthesis of some metabolites, which revealed the increased trend such as monodictyphenone and orsellinic acid in the absence of *cclA* (Bok *et al.*, 2009). Outcomes of this study showed strong consistency with the published data. As transcriptional support, RNA

pol II occupancy of complex mutants also provided upregulated profile for secondary metabolism related genes at late vegetative growth phase. In particular, in the absence of *rstB* ST biosynthetic process included genes and in the absence of *cclA* fatty acid biosynthetic process genes were found to be upregulated. According to these, significant data was shown in this study strongly suggesting that MERCK complex plays a key role on secondary metabolism in *A. nidulans*.

Epigenetic regulation

Histone demethylase KdmA was reported with H3K36me3 and H3K9me3 specific demethylase activity by utilizing LC-MS based approach (Gacek-Mathew *et al.*, 2015) and CclA very-well known from literature as a subunit of histone methyltransferase SET1C (COMPASS) complex with H3K4 methylation function. This research study showed the nuclear function of the MERCK complex through PTMs on epigenetic regulation mechanism. Dynamic histone modification marks usually determine the state of chromatin and play an active role on gene expression. H3K4me2/me3 and H3K36me2/me3 are commonly known as transcriptionally active gene expression marks which is linked with euchromatin state while H3K9me2/me3 and H3K27me3 are broadly recognised as silent transcription marks referring to heterochromatin state. An extensive ChIP-seq based histone modification analysis was performed, indicating that H3K4me3 level in the *cclA* mutants were drastically diminished and signals were observed from some ribosomal genes only, suggesting the key role of *cclA* on the gene expression. Another interesting research outcome was that RNA pol II signal profile of *wt* which refers to active transcription was almost identical with *cclA* genome-wide binding profile suggesting that *cclA* strongly corresponds to the active gene expression. Furthermore, *cclA* mutant was also found to cause increased H3K9me3 mark signal on the central regions of the chromosome body but significantly reduced signal on the telomeric regions. Reduction of this methylation mark signal was also observed at telomeric regions in the absence of *kdmA*, particularly, in the early vegetative growth stage (20h). Although *kdmA* was reported as H3K36 specific demethylase, there was no significant change observed in this mutant, but surprisingly, substantial increase was found at the chromosomal ends in the *cclA* mutant. All data observed from PTMs analysis of this study so far clearly indicates the critical role of MERCK complex on the chromatin modification mechanisms.

Presentation of KdmA isophorms

KdmA is a homolog of human KDM4, a subfamily of JMJC-domain containing demethylases. As one of the largest members of the subfamily, KDM4 contains five functional members KDM4A-E with different domain structures (jmjC and jmjN domains are common for all), chromosomal locations and size differences. KDM4D was shown to form two clusters as KDM4E and F. Although these two were considered to be pseudogenes, the functionality of KDM4E was reported (Whetstine *et al.*, 2006; Katoh *et al.*, 2007) and in some of other highly eukaryotes this case was also reported. It was found that KdmA was annotated as two different genes in *A. flavus* by dividing it in two parts. Here, in this study, it was discover that KdmA is presented by two isophorms as two different transcripts within the cell. The truncated version of KdmA (short form) was generated to explore its role in the cell and its functionality and expression were confirmed. Domain structure comparison of the full-length and truncated versions of KdmA showed that the truncated version (short version of KdmA) does not include any specific domain whereas the other domains jmjC, jmjN and PHD domains were located on the earlier part of on full-length KdmA. The truncated version of KdmA was identified to have physical interactions with only EcmB and RstB as complex members by MS coupled protein pulldown analysis. It is important to reiterate that EcmB and RstB were found to be fungal specific members of the MERCK complex. Comparing genome-wide target profiles of both KdmA forms, interestingly, it was observed that the short version almost shows loss of binding at 20h while having slightly increased targets at 48h suggesting a possible role of the short form under limited conditions for the cell.

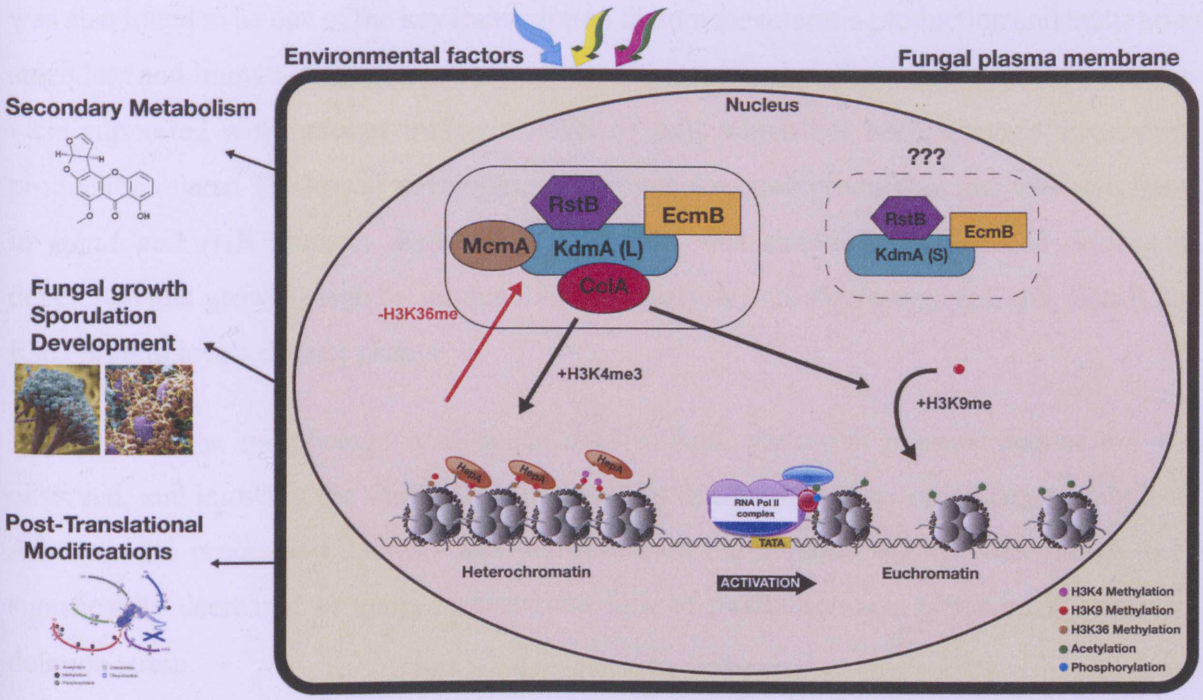

Figure 5.1: Schematic illustration of proposed model for MERCK complex and its function in *A.nidulans*. Pentameric MERCK complex is localized in the nucleus. Two isophorms of KdmA are presented in the cell which are called here short (S) and long (L) forms. Long form interacts with four interaction partners whereas short form interacts with RstB and EcmB. H3K4me3 level on the genome based on existence of histone methyltransferase CclA within the cell. Deletion of *cclA* also affects the genome-wide H3K9me3 and H3K36me3 level. Fully functional MERCK complex controls development and SM through TFs (EcmB and RstB) and utilizing post-translational modifications.

5.2 MERCK complex role in *A.flavus*

As mentioned earlier in this chapter, MERCK complex was found in AF producer fungus *A. flavus* by utilizing a proteomics approach and its function on development was also demonstrated by this research work. From the literature and following supportive strain creation attempt, it was shown that mcmA is an essential gene for *A. flavus* as well. *cclA* and *ecmB* mutants were found to show a reduction of their colony size as well as major decrease in asexual conidiation production in both dark and light conditions, in particular loss of conidiation in *ecmB* mutant. Interestingly, although there was no striking difference on the asexual sporulation under light conditions in the absence of *kdmA* and *rstB*, a substantial effect was observed in darkness. Findings of this study provided that *cclA* is essential for *A. flavus* sexual development structure sclerotia where there was no production observed. Besides, *ecmB*

was also found to be one of the key transcription factors for sclerotia production and maturation since less and immature sclerotia structure was observed in the absence of it. These outcomes were supported with reduced transcript level of sclR which has been reported as sclerotia production related TF. Lower developmental growth structure production rate was also found in *kdmA* and *rstB* mutants. Expression of KdmA was shown to be reduced during the developmental growth stage by immunoblotting analysis and, interestingly, CclA, EcmB and RstB protein levels did not change.

From the morphology analysis of *cclA* mutant, yellowish pigment production was observed, and knowing the strong relation between development and secondary metabolism, Aflatoxin B1 production analysis was performed on the mutants. AF B1 was shown to be significantly decreased in many mutants and lack of production was observed in the *ecmB* deletion strain.

A. flavus is a very well-known aggressive plant pathogen with a strong effect particularly on commercially important plants such a peanut and corn. The role of MERCK complex on the host colonization was assessed by infecting peanuts with mutant spores and the produced AF B1 level on peanut seeds were quantified. Findings of this investigation clearly showed that *cclA* mutant spores were able to grow well on seeds by giving a significant reduction on sporulation rate. In addition, *ecmB* deletion resulted in a loss of sporulation and making fluffy hyphae structures on the peanut. Although *cclA* could not produce more spores than *wt*, AF analysis showed that it has the highest AF production amount among the mutants whereas *ecmB* did not show any production. These findings strongly indicate the role of MERCK complex on host virulence.

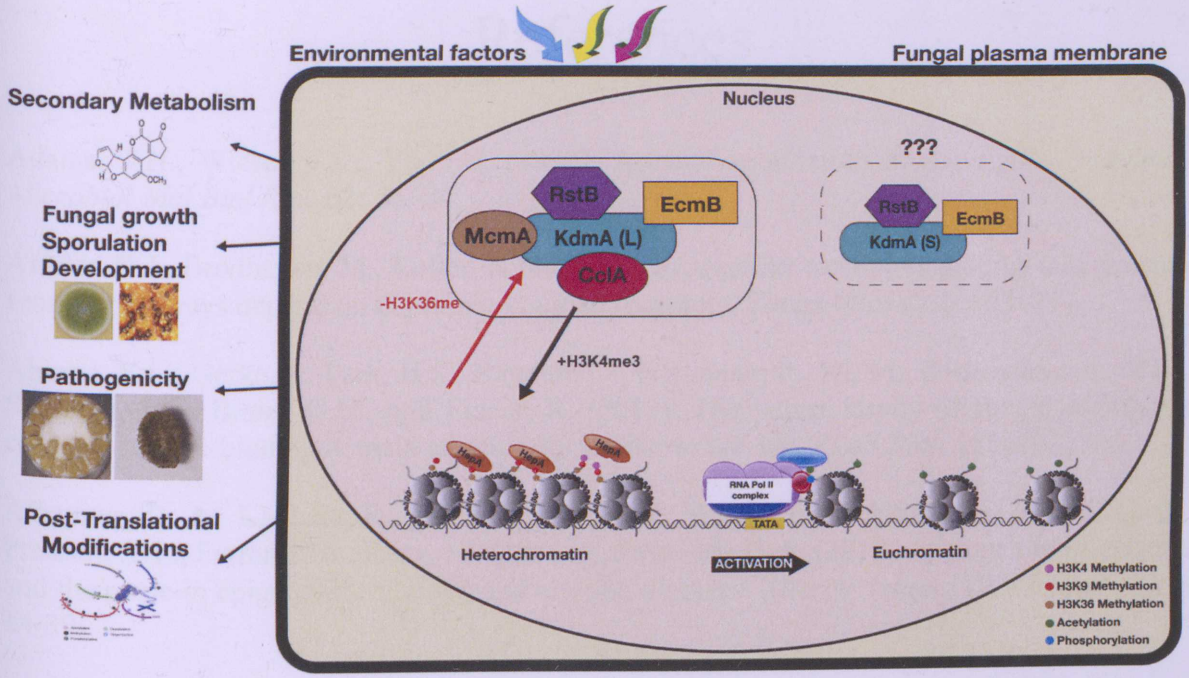

Figure 5.1: Schematic illustration of proposed model for MERCK complex and its function in *A.flavus*. Heteromeric MERCK protein complex is localized in the nucleus. Two isophorms of KdmA are presented in the cell which are called here short (S) and long (L) forms. H3K4me3 level based on existence of histone methyltransferase CclA within the cell where H3K36me3 levels relies on KdmA. CclA and EcmB influence host colonization. Fully functional MERCK complex controls development and SM through TFs (EcmB and RstB) and utilizing post-translational modifications.

In the previous chapter the role of MERCK complex was discussed in detail in relation to *A. nidulans*. In this section, the function of MERCK complex in PTMs mechanism was shown in *A. flavus*. Histone modification western blotting was performed on mutants and results indicated that H3K4me3 modification mark level significantly decreased in *cclA* mutant, whereas H3K36me3 mark shows increasing trend on mutants in comparison to *wt*. This is consistent with given *A. nidulans* data, which suggests the important role of MERCK complex in *A. flavus* epigenetic regulation mechanism.

To conclude, this study represents the formation of pentameric MERCK demethylase complex and its molecular functions within the cell in *A.nidulans* and *A.flavus*. It has provided deep information regarding with the complex on the fungal development and secondary metabolism as well as post-translation modifications. All together, this research contributes global characterization of MERCK complex and reveals interesting avenues for the future investigations.

References

Adams, T.H., Wieser, J.K., Yu, J.H. (1998). Asexual sporulation in *Aspergillus nidulans*. *Microbiol Mol Biol Rev.* **62:** 35–54.

Affeldt, K.J., Brodhagen, M., Keller, N.P. (2012). *Aspergillus* oxylipin signaling and quorum sensing pathways depend on G protein-coupled receptors. *Toxins (Basel)* **4**: 695–717.

Ahmed, Y.L., Gerke, J., Park, H.S., Bayram, O., Neumann, P., Ni, M., Dickmanns, A., Kim, S.C., Yu, J.H., Braus, G.H., and Ficner, R. (2013). The velvet family of fungal regulators contains a DNA-binding domain structurally similar to NF-kB. *PLoS Biol.* **11**: e1001750.

Alhamwe, B. A., Khalaila, R., Wolf, J., Bülow, V. V., Harb, H., Alhamdan, F., Hii, C. S., Prescott, S. L., Ferrante, A., Renz, H., Garn, H., Potaczek, D. P. (2018). Histone modifications and their role in epigenetics of atopy and allergic diseases. *Allergy Asthma Clin Immunol* **23:** 14-39.

Amaike, S., Keller, N.P. (2011). *Aspergillus flavus. Ann. Rev. Phytopathol.* **49**: 107–133.

Amaike, S., Keller, N.P. (2009). Distinct roles for VeA and LaeA in development and pathogenesis of *Aspergillus flavus*. *Eukaryot. Cell* **8**: 1051–1060.

Andrianopoulos, A., Timberlake, W.E. (1994). The Aspergillus nidulans *aba*A gene encodes a transcriptional activator that acts as a genetic switch to control development. *Mol Cell Biol*, **14**: 2503-2515.

Araki, Y., Mimura, T. (2017). The histone modification code in the pathogenesis of autoimmune diseases. *Mediators Inflamm.* 2608605.

Barski, A., Cuddapah, S., Cui, K., Roh, T.Y., Schones, D.E., Wang, Z., Wei, G., Chepelev, I., Zhao, K. (2007). High-resolution profiling of histone methylations in the human genome. *Cell* **129(4):** 823–837.

Bayram, Ö., Biesemann, C., Krappmann, S., Galland, P., Braus, G.H. (2008a). More than a repair enzyme: *Aspergillus nidulans* photolyase-like CryA is a regulator of sexual development. *Mol Biol Cell* **19**, 3254–3262.

Bayram, Ö., Krappmann, S., Ni, M., Bok, J.W., Helmstaedt, K., Valerius, O., Braus-Stromeyer, S., Kwon, N.J., Keller, N.P., Yu, J.H., Braus, G.H. (2008b). VelB/VeA/LaeA complex coordinates light signal with fungal development and secondary metabolism. *Science* **320:** 1504–1506.

Bayram, Ö., Braus, G.H., Fischer, R., Rodríguez-Romero, J. (2010). Spotlight on *Aspergillus nidulans* photosensory systems. *Fungal Genet Biol.* **47:** 900–908.

Bayram, Ö., Braus, G.H. (2012). Coordination of secondary metabolism and development in fungi: the velvet family of regulatory proteins. *FEMS Microbiol Rev* **36(1):** 1-24.

Bayram, Ö., Bayram, Ö.S., Ahmed, Y.L., Maruyama, J., Valerius, O., Rizzoli, S.O., Ficner, R., Irniger, S., Braus, G.H. (2012a). The *Aspergillus nidulans* MAPK module AnSte11-Ste50-Ste7-Fus3 controls development and secondary metabolism. *PLoS Genet,* **8:** e1002816.

Bayram Ö., Bayram, Ö. S., Valerius, O., Johnk, B., Braus, G.H. (2012b). Identification of protein complexes from filamentous fungi with tandem affinity purification. *Methods Mol Biol.* **9444**: 191-205.

Black, D. L., (2003). Mechanisms of Alternative Pre-Messenger RNA Splicing. *Annual Review of Biochemistry* **72**: 291-336.

Becker, J. S., Nicetto, D., Zaret, K. (2017). H3K9me3-Dependent Heterochromatin: Barrier to Cell Fate Changes. *Trends Genet.* **32(1):** 29–41.

Bhaumik, S.R., Smith, E., Shilatifard, A. (2007). Covalent modifications of histones during development and disease pathogenesis. *Nature structural & molecular biology* **14,** 1008-16.

Blackwell, M. (2011). The Fungi: 1, 2, 3 ... 5.1 Million Species? *American Journal of Botany* **98:** 426-438.

Blumenstein, A., Vienken, K., Tasler, R., Purschwitz, J., Veith, D., Frankenberg-Dinkel, N., Fischer, R., (2005). The *Aspergillus nidulans* phytochrome FphA represses sexual development in red light. *Curr Biol.* **15:** 1833–1838.

Bradford, M.M. (1976). A rapid and sensitive method for the quantitation of microgram quantities of protein utilizing the principle of protein-dye binding. *Anal Biochem* **72**: 248–254.

Braus, G., Krappmann, H.S., Eckert, S.E. (2002). Sexual development in ascomycetes: fruit body formation of *Aspergillus nidulans*. In: Molecular biology of fungal development. H. D. Osiewacz (ed). New York, Basel: Marcel Decker, Inc., pp. 215-244.

Brocato, J., Costa, M., (2013). Basic Mechanics of DNA Methylation and the Unique Landscape of the DNA Methylome in Metal-Induced Carcinogenesis. *Crit Rev Toxicol.* **43(6):** 1-38.

Brown, S.H., Scott, J.B., Bhaheetharan, J., Sharpee, W.C., Milde, L., Wilson, R.A., et al. (2009). Oxygenase coordination is required for morphological transition and the host-fungus interaction of *Aspergillus flavus*. *Mol.Plant Microbe Interact.* **22**: 882–894.

Bok, J.W., Keller, N.P. (2004). LaeA, a regulator of secondary metabolism in Aspergillus spp. Eukaryot Cell **3**: 527–535.

Bok, J. W., Hoffmeister, D., Maggio-Hall, L. A., Murillo, R., Glasner, J. D., Keller, N. P. (2006). Genomic mining for Aspergillus natural products. *Chem Biol.* **13:** 31-7.

Bok, J.W., Chiang, Y.M., Szewczyk, E., Reyes-Dominguez, Y., Davidson, A.D., Sanchez, J.F,, et al. 2009. Chromatin level regulation of biosynthetic gene clusters. *Nat Chem Biol.* **5(7)**: 462–4.

Bok, J.W., Soukup, A.A., Chadwick, E., Chiang, Y.M., Wang, C.C., Keller, N.P. (2013). VeA and MvlA repression of the cryptic orsellinic acid gene cluster in *Aspergillus nidulans* involves histone 3 acetylation. *Mol Microbiol* **89(5):** 963-74.

Bowman, S. M. (2006). The structure and synthesis of the fungal cell wall. *Bio Essays* **28(8):** 799-808.

Busby, T. M., Miller, K.Y., Miller, B.L. (1997). Suppression and enhancement of the *Aspergillus nidulans* medusa mutation by altered dosage of the bristle and stunted genes. *Genetics* **143:** 155-63.

Calvo, A.M., Bok, J.W., Brooks, W., Keller, N.P. (2004). VeA is required for toxin and sclerotial production in *Aspergillus parasiticus*. *Appl. Environ. Microbiol.* **70**, 4733–4739.

Calvo, A.M., Cary, J.W., 2015. Association of fungal secondary metabolism and sclerotial biology. *Frontiers in Microbiology* **6(62):** 1-15.

Cary, J.W., Harris-Coward, P.Y., Ehrlich, K.C., Mack, B.M., Kale, S.P., Larey, C., Calvo, A.M. (2012). NsdC and NsdD affect *Aspergillus flavus* morphogenesis and aflatoxin production. *Eukaryot. Cell* **11:** 1104–1111.

Cary, J.W., Harris-Coward, P.Y., Ehrlich, K.C., Di Mavungu, J.D., Malysheva, S.V., De Saeger, S., Dowd, P.F., Shantappa, S., Martens, S.L., Calvo, A.M. (2014). Functional characterization of a veA-dependent polyketide synthase gene in *Aspergillus flavus* necessary for the synthesis of asparasone, a sclerotium-specific pigment. *Fungal Genet. Biol.* **64:** 25–35.

Cao, J., Yan, Q., (2012). Histone ubiquitination and deubiquitination in transcription, DNA damage response, and cancer. *Front Oncol.* **2:** 26.

Casselton, L., Zolan, M. (2002). The art and design of genetic screens: filamentous fungi. *Nat Rev Genet* **3(9):** 683-697.

Cerqueira, G.C., Arnaud, M.B., Inglis, D.O., Skrzypek, M.S., Binkley, G., Simison, M., Miyasato, S.R., Binkley, J., Orvis, J., Shah, P., Wymore, F., Sherlock, G., Wortman, J.R. (2014). The Aspergillus Genome Database: multispecies curation and incorporation of RNA-Seq data to improve structural gene annotations. *Nucleic Acids Res.* **42:** D705–710

Champe, S.P., Nagle, D.L., and Yager, L.N. (1994). Sexual sporulation. *Prog Ind Microbiol* **29**: 429-454.

Chanda, A., Roze, L. V., Kang, S., Artymovich, K. A., Hicks, G. R., Raikhel, N. V., et al. (2009). A key role for vesicles in fungal secondary metabolism. *Proc.Natl. Acad.Sci.U.S.A.* **106**: 19533–19538.

Chang, P.K., Scharfenstein, L.L., Wei, Q., Bhatnagar, D. (2010). Development and refinement of a high-efficiency gene-targeting system for *Aspergillus flavus*. *Journal of Microbiological Methods* **81**: 240–246.

Chang, P.K., Scharfenstein, L.L., Mack, B., Ehrlich, K.C. (2012). Deletion of the *Aspergillus flavus* orthologue of *A. nidulans fluG* reduces conidiation and promotes production of sclerotia but does not abolish aflatoxin biosynthesis. *Appl. Environ. Microbio*l. **78**: 7557–7563.

Chang, P.K. Scharfenstein, L.L., Ehrlich, K.C. (2013). *Aspergillus flav*us VelB acts distinctly from VeA in conidiation and may coordinate with FluG to modulate sclerotial production. *Fungal Genet. Biol.* **58–59**, 71–79.

Chi, P., Allis, C.D, Wang, G.G. (2010). Covalent histone modifications--miswritten, misinterpreted and mis-erased in human cancers. *Nature reviews. Cancer* **10:** 457-69.

Cleveland, T.E., Yu, J., Fedorova, N.D., Bhatnagar, D., Payne, G.A., et al. (2009). Potential of *Aspergillus flavus* genomics for applications in biotechnology. *Trends Biotechnol.* **3**:151–57.

Cotty, P. J., Bhatnagar, D. (1994). Variability among atoxigenic *Aspergillus flavus* strains in ability to prevent aflatoxin contamination and production of aflatoxin biosynthetic pathway enzymes. *Appl. Environ. Microbiol.* **60**: 2248–2251.

Dasgupta, A., Fuller, K.K., Dunlap, J.C., Loros, J.J, (2016). Seeing the world differently: variability in the photosensory mechanisms of two model fungi. *Environ Microbiol.***18(1)**: 5-20

Denisov, Y., Freeman, S., Yarden, O. (2011). Inactivation of Snt2, a BAH/PHD-containing transcription factor, impairs pathogenicity and increases autophagosome abundance in *Fusarium oxysporum. Mol Plant Pathol.* **12(5)**: 449-61.

Denning, D.W, Bromley, M.J. (2015). Infectious Disease. How to bolster the antifungal pipeline. *Science* **347**: 1414–1416.

Deribe, Y.L., Pawson, T., Dikic, I. (2010). Post-translational modifications in signal integration. *Nat Struct Mol Biol.* **17**: 666–672.

Du, W., O'Brian, G.R., Payne, G.A. (2007). Function and regulation of *aflJ* in the accumulation of aflatoxin early pathway intermediate in *Aspergillus flavus*. *Food Addit. Contam.* **24**: 1043–50.

Duan, G., Walther, D. (2015). The Roles of Post-Translational Modifications in the Context of Protein Interaction Networks. *PLoS Comput Biol* **11(2).**

Duran, R.M., Cary, J.W., Calvo, A.M. (2007). Production of cyclopiazonic acid, aflatrem, and aflatoxin by *Aspergillus flav*us is regulated by *veA*, a gene necessary for sclerotial formation. *Appl. Microbiol. Biotechnol.* **73**: 1158–1168.

Dyer, P.S., O'Gorman, C.M. (2011). A fungal sexual revolution: Aspergillus and Penicillium show the way. *Curr Opin Microbiol.* **14**: 649–54.

Etxebeste, O., Garzia, A., Espeso, E. A., Ugalde, U. (2010). *Aspergillus nidulans* asexual development: making the most of cellular modules. *Trends Microbiol,* **18:** 569-76.

Fakruddin, M., Chowdhury, A., Hossain, M.N., Ahmed, M.M. (2015). Characterization of aflatoxin producing *Aspergillus flavus* from food and feed samples. *Springer Plus* **4**:159.

Fan, J., Krautkramer, K.A., Feldman, J.L., Denu, J.M. (2015). Metabolic Regulation of Histone Post-Translational Modifications. *ACS Chem. Biol.* **10(1):** 95–108.

Felsenfeld, G., Groudine, M. (2003). Controlling the double helix. Nature, **421**: 448-453.

Fischle, W. (2012). One, two, three: how histone methylation is read. *Epigenomics* **4:** 641-53.

Freitag, M. (2017). Histone Methylation by SET Domain Proteins in Fungi. *Annual Review of Microbiology.* **71**: 41-39.

Gacek, A., Strauss, J. (2012). The chromatin code of fungal secondary metabolite gene clusters. *Appl Microbiol Biotechnol,* **95**: 1389–1404.

Gacek-Matthews, A., Noble, L.M., Gruber, C., Berger, H., Sulyok, M., Marcos, A.T., Strauss, J., Andrianopoulos, A. (2015). Kdma, a histone h3 demethylase with bipartite function, differentially regulates primary and secondary metabolism in *Aspergillus nidulans. Mol. Microbiol.* **96**: 839–860.

Gacek-Matthews, A., Berger, H. (2016). Kdmb, a jumonji histone h3 demethylase, regulates genome-wide h3k4 trimethylation and is required for normal induction of secondary metabolism in *Aspergillus nidulans. PLoS Genet.* **12**: e1006222.

Galagan, J. E., Calvo, S. E., Cuomo, C., Ma, L. J., Wortman, J. R., Batzoglou, S., Lee, S. I., Basturkmen, M., Spevak, C. C., Clutterbuck, J., Kapitonov, V., Jurka, J., et al. (2005). Sequencing of *Aspergillus nidulans* and comparative analysis with *A. fumigatus* and *A. oryzae. Nature,* **438:** 1105-15.

Gallagher, R.T., Wilson, B.J. (1979). Aflatrem, the tremorgenic mycotoxin from *Aspergillus flavus. Mycopathologia* **66**: 183–185.

Georgianna, D.R., Fedorova, N.D., Burroughs, J.L., Dolezal, A.L., Bok, J., Horowitz-Brown, S., Woloshuk, C.P., Yu, J., Keller, N.P., Payne, G.A. (2010). Beyond aflatoxin: four distinct expression patterns and functional roles associated with *Aspergillus flavus* secondary metabolism gene clusters. *Mol. Plant Pathol.* **11:** 213–226.

Gillette, T.G., Hill, J.A. (2015). Readers, writers, and erasers: chromatin as the whiteboard of heart disease. *Circ Res.* **116(7):** 1245-53.

Gloer, J.B. (1995). Antiinsectan natural products from fungal sclerotia. *Acc.Chem. Res.* **28**: 343–350.

Gramzow, L., Ritz, M.S., Theißen, G. (2010). On the origin of MADS-domain transcription factors. *Trends in Genetics* **26(4):** 149-153.

Greer, E., Shi, Y. (2012). Histone methylation: a dynamic mark in health, disease and inheritance. *Nat Rev Genet.* **13(5)**: 343–357.

Grewal, S. I., Elgin, S.C. (2007). Transcription and RNA interference in the formation of heterochromatin. *Nature* **447,** 399-406.

Gu, B., Lee, M.G. (2013). Histone H3 lysine 4 methyltransferases and demethylases in self-renewal and differentiation of stem cells. *Cell & Bioscience* **3(1)**: 39.

Han, K. H., Han, K.Y., Yu, J.H., Chae, K.S., Jahng, K.Y., Han, D. M. (2001). The *nsdD* gene encodes a putative GATA-type transcription factor necessary for sexual development of *Aspergillus nidulans. Mol Microbiol* **41:** 299-309.

Hanahan D., Jessee J., Bloom F. R. (1991). Plasmid transformation of *Escherichia coli* and other bacteria. *Methods in Enzymology* **204**: 63-113.

Harting, Y., Bayram, O., Laubinger, K., Valerius, O., Braus, G.H. (2013). Interplay of the fungal sumoylation network for control of multicellular development. *Mol Microbiol.* **90(5)**: 1125–1145.

Helmschrott, C., Sasse, A., Samantaray, S., Krappmann, S., Wagener, J. (2013). Upgrading fungal gene expression on demand: improved systems for doxycycline-dependent silencing in *Aspergillus fumigatus*. *Appl. Environ. Microbiol.* **79**: 1751–1754.

Hicks, J. K., Yu, J. H., Keller, N. P., Adams, T.H. (1997). *Aspergillus* sporulation and mycotoxin production both require inactivation of the FadA G alpha protein-dependent signaling pathway. *EMBO J* **16**: 4916-4923.

Hochstrasser, M. (2009). Origin and function of ubiquitin-like proteins. *Nature* **458**: 422– 429.

Horn, B.W. (2007). Biodiversityof *Aspergillus* section *Flavi* in the United States: a review. *Food Addit. Contam.* 24: 1088–1101.

Horn, B.W., Moore, G.G., Carbone, I. (2009). Sexual reproduction in *Aspergillus flavus*. *Mycologia* **101**: 423–429.

Horn, B., Sorensen, R.B., Lamb, M.C., Sobolev, V.S., Olarte, R.A., Worthington, C.J., Carbone, I. (2014). Sexual reproduction in *Aspergillus flavus* sclerotia naturally produced in corn. *Phytopathology* **104:** 75-85.

Inoue, H., Nojima, H., Okayama, H. (1990). High efficiency transformation of *Escherichia coli* with plasmids. *Gene* **96 (1)**: 23-28.

Jaimes-Arroyo, R., Lara-Rojas, F., Bayram, Ö., Valerius, O., Braus, G.H., Aguirre, J. (2015). The SrkA Kinase Is Part of the SakA Mitogen-Activated Protein Kinase Interactome and Regulates Stress Responses and Development in *Aspergillus nidulans*. *Eukaryot Cell* **14:** 495–510.

Jiao, L., Liu, X. (2015). Structural basis of histone H3K27 trimethylation by an active polycomb repressive complex 2. *Science* **350 (6258)**: aac4383

Jin, F.J., Takahashi, T., Matsushima, K., Hara, S., Shinohara, Y., Maruyama, J., Kitamoto, K., Koyama, Y. (2011). SclR, a Basic Helix-Loop-Helix Transcription Factor, Regulates Hyphal Morphology and Promotes Sclerotial Formation in *Aspergillus oryzae*. *EUKARYOTIC CELL* **10(7):** 945–955.

Jöhnk, B., Bayram, Ö., Abelmann, A., Heinekamp, T., Mattern, D.J., Brakhage, A.A., et al. (2016). SCF Ubiquitin Ligase F-box Protein Fbx15 Controls Nuclear Co-Repressor Localization, Stress Response and Virulence of the Human Pathogen *Aspergillus fumigatus*. *PLoS Pathog* **12(9)**. e1005899

Kako, K., Kim J.D., Fukamizu A. (2018). Emerging impacts of biological methylation on genetic information, *The Journal of Biochemistry*. **165 (1)**: 9-18.

Kale, S.P., Milde, L., Trapp, M.K., Frisvad, J.C., Keller, N.P., et al. 2008. Requirement of LaeA for secondary metabolism and sclerotial production *Aspergillus flavus*. *Fungal Genet. Biol.* **45**: 1422–29.

Karve, T.M., Cheema, A.K. (2011). Small changes huge impact: the role of protein posttranslational modifications in cellular homeostasis and disease. *Journal of amino acids,* 207691.

Kato, N., Brooks, W., Calvo, A.M. (2003). The expression of sterigmatocystin and penicillin genes in *Aspergillus nidulans* is controlled by *veA*, a gene required for sexual development. *Eukaryot Cell* **2:** 1178–1186.

Katoh, Y., Katoh, M. (2007). Comparative integromics on JMJD2A, JMJD2B and JMJD2C: preferential expression of JMJD2C in undifferentiated ES cells. *Int J Mol Med* **20:** 269-273.

Kawaguchi, M., Nonaka, K., Masuma, R., Tomoda, H. (2013). New method for isolating antibiotic-producing fungi. *J Antibiot.* **66:** 17–21.

Keller, N. P., Turner, G., Bennett, J.W. (2005). Fungal secondary metabolism – from biochemistry to genomics. *Nat Rev Microbiol* **3:** 937-47.

Kim, H., Han, K., Kim, K., Han, D., Jahng, K., Chae, K., (2002). The *veA* gene activates sexual development in *Aspergillus nidulans. Fungal Genet Biol* **37**: 72–80.

Kim, H. R., Chae, K. S., Han, K. H., Han, D.M. (2009). The *nsdC* gene encoding a putative C_2H_2-type transcription factor is a key activator of sexual development in *Aspergillus nidulans*. *Genetics* **182:** 771-83.

Kim, J. H., Campbell, B. C., Yu, J., Mahoney, N., Chan, K. L., Molyneux, R. J., Bhatnagar, D., Cleveland, T. (2005). Examination of fungal stress response genes using *Saccharomyces cerevisiae* as a model system: targeting genes affecting aflatoxin biosynthesis by *Aspergillus flavus*. *Appl Microbiol Biotechnol* **67**: 807–815.

Klose, R. J., Yamane, K., Bae, Y., Zhang, D., Erdjument-Bromage, H., Tempst, P., Wong J., Zhang, Y. (2006). The transcriptional repressor JHDM3A demethylates trimethyl histone H3 lysine 9 and lysine 36. *Nature*, **442**: 312-316.

Klug, W., Cummings, M. R., Spencer C. A. (2006). Concepts of Genetics. 8th Ed. Pearson Education Inc, New Jersey: pg. 394-433

Krijgsheld, P., Bleichrodt, R.J., Veluw, G.J. van Wang, F., Müller, W.G., et al. (2013). Development in *Aspergillus*. *Studies in Mycology* **74**: 1–29.

Kwon, N.J., Garzia, A., Espeso, E.A., Ugalde, U., Yu, J.H. (2010a). FlbC is a putative nuclear C_2H_2 transcription factor regulating development in *Aspergillus nidulans. Mol Microbiol* **77**:1203-1219.

Kwon, N. J., Shin, K. S., Yu, J. H. (2010b). Characterization of the developmental regulator FlbE in Aspergillus fumigatus and *Aspergillus nidulans*. *Fungal Genet Biol* **47:** 981-93.

Labbé, R.M., Holowatyj, A., Yang, Z. (2014). Histone lysine demethylase (KDM) subfamily 4: structures, functions and therapeutic potential. *Am J Transl Res* **6(1):** 1-15.

Lackner, D.H., Bahler, J. (2008). Translational control of gene expression from transcripts to transcriptomes. *Int Rev Cell Mol Biol.* **271**: 199–251.

LabbE, R.M., Holowatyj, A., Yang, Z.Q. (2014). Histone lysine demethylase (KDM) subfamily 4: structures, functions and therapeutic potential. *Am J Transl Res.* **6(1)**: 1-15.

Lee, D. W., Freitag, M., Selker, E.U., Aramayo, R. (2008). A cytosine methyltransferase homologue is essential for sexual development in *Aspergillus nidulans*. *PLoS One* **3**: e2531

Lessard, M.H., Viel, C., Boyle, B., St-Gelais, D., Labrie, S. (2014). Metatranscriptome analysis of fungal strains *Penicillium camemberti* and *Geotrichum candidum* reveal cheese matrix breakdown and potential development of sensory properties of ripened Camembert-type cheese. *BMC Genomics* **15**:235.

Li, N., Kunitake, E., Aoyama, M., Ogawa, M., Kanamaru, K., Kimura, M., Koyama, Y., Kobayashi, T. (2016). McmA-dependent and -independent regulatory systems governing expression of ClrB-regulated cellulase and hemicellulase genes in *Aspergillus nidulans*. *Molecular Microbiology* **102(5):** 810–826.

Liang, L. Liu, Y., Yang, K., Lin, G., Xu, Z., Lan, H., Wang, X., Wang, Z. (2017). The Putative Histone Methyltransferase DOT1 Regulates Aflatoxin and Pathogenicity Attributes in *Aspergillus flavus*. *Toxins* **9 (7)**: E232.

Lieleg, C., Krietenstein, N., Walker, M., Korber, P. (2015). Nucleosome positioning in yeasts: methods, maps, and mechanisms. *Chromosoma* **124**: 131–151.

Lim, F.Y., Keller, N.P. (2014). Spatial and temporal control of fungal natural product synthesis. *Nat. Prod. Rep.* **31**: 1277–86.

Lind, A.L, Smith, T.D., Saterlee, T., Calvo, A.M., Rokas, A. (2016). Regulation of Secondary metabolism by the Velvet Complex Is Temperature-Responsive in Aspergillus. *G3 Genes Genomes Genetics* **6**: 4023-4033.

Low, D.A., Casadesus, J. (2008). Clocks and switches: bacterial gene regulation by DNA adenine methylation. *Curr Opin Microbiol* **11:** 106-12.

Luger, K., Mader, A.W., Richmond, R.K., Sargent, D.F., Richmond, T.J. (1997). Crystal structure of the nucleosome core particle at 2.8 A resolution. *Nature* **389:** 251-60.

Lv, Y., Lv, A., Zhai, H., Zhang, S., Li, L., Cai, J., Hu, Y. (2018). Insight into the global regulation of laeA in Aspergillus flavus based on proteomic profiling. *International Journal of Food Microbiology* **284**: 11–21.

Macheleidt, J., Mattern, D.J., Fischer, J., Netzker, T., Weber, J., Schroeckh, V., Valiante, V., Brakhage, A.A. (2016). Regulation and role of fungal secondary metabolites. *Annu. Rev. Genet.* **50**: 371–392.

Malachová, A., Sulyok, M., Beltrán, E., Berthiller, F., Krska, R. (2014). Optimization and validation of a quantitative liquid chromatography–tandem mass spectrometric method covering 295 bacterial and fungal metabolites including all regulated mycotoxins in four model food matrices. *J Chromatogr A.***1362**: 145–156.

Marshall, M.A., Timberlake, W.E. (1991). *Aspergillus nidulans* wetA activates spore-specific gene expression. *Mol Cell Biol* **11**: 55-62.

Martins, M. L., and Martins, H. M. (1999). Natural and invitro coproduction of cyclopiazonicacid and aflatoxins. *J. Food Prot.* **62**: 292–294.

Mokry, M., Hatzis, P., Schuijers, J., Lansu, N., Ruzius, F., Clevers, H., Cuppen, E. (2011). *Nucleic Acids Research* **40(1):** 148-158.

Mooney, J.L., Yager, L.N. (1990). Light is required for conidiation in *Aspergillus nidulans. Genes Dev.* **4(9)**: 1473-82.

Nahlik, K., Dumkow, M., Bayram, O., Helmstaedt, K., Busch, S., Valerius, O., Gerke, J., Hoppert, M., Schwier, E., Opitz, L., Westermann, et al. (2010). The COP9 signalosome mediates transcriptional and metabolic response to hormones, oxidative stress protection and cell wall rearrangement during fungal development. *Mol Microbiol* **78:** 964-79.

Nasir, A., Rahman, S.S., Hossain, M.M., Choudhury, N. (2017). Isolation of *Saccharomyces Cerevisiae* From Pineapple and Orange and Study Of Metal's Effectiveness on Ethanol Production. *European Journal of Microbiology and Immunology* **7(1):** 76–91.

Nathan, D., Ingvarsdottir, K., Sterner, D.E., Bylebyl, G.R., Dokmanovic, M., Dorsey, J.A., Whelan, K.A., Krsmanovic, M., Lane, W.S., Meluh, P.B., Johnson, E.S., et al. (2006). Histone sumoylation is a negative regulator in *Saccharomyces cerevisiae* and shows dynamic interplay with positive-acting histone modifications. *Genes Dev* **20:** 966-76.

Nesbitt, B.F. et al., 1962. *Aspergillus flavus* and Turkey X disease. Toxic metabolites of *Aspergillus flavus. Nature* **195**: 1062–1063.

Ni, M., Yu, J.H. (2007). A novel regulator couples sporogenesis and trehalose biogenesis in *Aspergillus nidulans. PLoS One* **2 (10):** e970.

Ni, M., Gao, N., Kwon, N.J., Shin, K.S., Yu, J.H. (2010). "Regulation of *Aspergillus* conidiation," in *Cellular and Molecular Biology of Filamentous Fungi*, eds K. Borkovich and D. Ebbole (Washington, DC: ASM Press), 559–576.

Nicholson, M.J. Koulman, A., Monahan, B. J., Pritchard, B. L., Payne, G. A., Scott, B., (2009). Identification of two aflatrem biosynthesis gene loci in Aspergillus flavus and metabolic engineering of Penicillium paxilli to elucidate their function. *Appl. Environ. Microbiol.* **75**: 7469–7481.

Nützmann, H.W., Fischer J., Scherlach K., Hertweck C., Brakhage A.A. (2013). Distinct amino acids of histone H3 control secondary metabolism in *Aspergillus nidulans*. *Appl. Environ. Microbiol.* **79**: 6102–9.

Nützmann, H.W., Reyes-Dominguez, Y., Scherlach, K., Schroeckh, V., Horn, F., et al. (2011). Bacteria-induced natural product formation in the fungus *Aspergillus nidulans* requires Saga/Ada-mediated histone acetylation. *PNAS* **108**: 14282–87.

Oiartzabal- Arano, E., Perez- de- Nanclares- Arregi, E., Espeso, E.A., Etxebeste, O. (2016). Apical control of conidiation in *Aspergillus nidulans. Curr Genet* **62**: 371–377.

Park, H.S., Yu, J.H. (2012). Genetic control of asexual sporulation in filamentous fungi. *Curr Opin Microbiol* **15:** 669-77.

Park, H.S., Nam, T.Y., Han, K.H., Kim, S.C., Yu, J.H. (2014). VelC positively controls sexual development in *Aspergillus nidulans*. *PloS One*. **9(2)**. e89883.

Park, H.S., Yu, Y.M., Lee, M.K., Maeng, P.J., Kim, S.C., Yu, J.H. (2015). Velvet-mediated repression of β-glucan synthesis in *Aspergillus nidulans spores*. *Sci Rep* **5**: 10199.

Palmer, J.M., Mallaredy, S., Perry, D.W., Sanchez, J.F., Theisen, J.M., Szewczyk, E., Oakley, B.R., Wang, C.C., Kelle, N.P., Mirabito, P.M. (2010). Telomere position effect is regulated by heterochromatin-associated proteins and NkuA in *Aspergillus nidulans*. *Microbiology* **156:**3522–3531.

Palmer, J.M., Theisen, J. M., Duran, R. M., Grayburn, W. S., Calvo, A. M., Keller, N. P. (2013). Secondary metabolism and development is mediated by LlmF control of VeA subcellular localization in *Aspergillus nidulans*. *PLoS Genet* **9(1):** e1003193.

Palmer, J.M., Bok, J.W., Lee, S., Dagenais, T.R.T., Andes, D.R., Kontoyiannis, D.P., Keller, N.P. (2013). Loss of CclA, required for histone 3 lysine 4 methylation, decreases growth but increases secondary metabolite production in *Aspergillus fumigatus*. *PeerJ* **1**: e4.

Parker, E. J., Scott, D. B. 2004. Indole-diterpene biosynthesis in ascomycetous fungi, in *Handbook of Industrial Mycology*, ed. Z. An (New York, NY: Marcel Dekker), 405–426.

Perrin, R.M., Fedorova, N.D., Bok, J.W., Cramer, R.A., Wortman, J.R., Kim, H.S., Nierman, W.C., Keller, N.P. (2007). Transcriptional regulation of chemical diversity in *Aspergillus fumigatus* by LaeA. *PLoS Pathog* **3 (4):** e50.

Pfannenstiel, B.T., Zhao, X., Wortman, J., Wiemann, P., Throckmorton, K., Spraker, J.E., et al. (2017). Revitalization of a Forward Genetic Screen Identifies Three New Regulators of Fungal Secondary Metabolism in the Genus Aspergillus. *MBio.* **8(5):** e01246-17.

Pfannenstiel, B.T., Greco, C., Sukowaty, A.T., Keller, N.P. (2018). The epigenetic reader SntB regulates secondary metabolism, development and global histone modifications in *Aspergillus flavus*. *Fungal Genet Biol.* **120**: 9-18.

Pontecorvo G, Roper JA, Hemmons LM, MacDonald KD & Bufton AW (1953) The genetics of *Aspergillus nidulans*. *Adv Genet.* **5:** 141–238

Prabakaran, S., Lippens, G., Steen, H., Gunawardena, J. (2012). Post-translational modification: nature's escape from genetic imprisonment and the basis for dynamic information encoding. *Wiley interdisciplinary reviews. Systems biology and medicine* **4:** 565-83.

Price, M.S., Nierman, W.C., Kim, H.S., Pritchard, B., Jacobus, C.A., et al. (2006). The aflatoxin pathway regulator AflR induces gene transcription inside and outside of the aflatoxin biosynthetic cluster. *FEMS Microbiol. Lett.* **255**: 275–79.

Punt, P.J., Van Den Hondel, C.A. (1992). Transformation of filamentous fungi based on hygromycin B and phleomycin resistance markers. *Methods Enzymol* **216:** 447-57.

Purschwitz, J., Müller, S., Kastner, C., Schöser, M., Haas, H., Espeso, E.A., Atoui, A., Calvo, A.M., Fischer, R. (2008) .Functional and physical interaction of blue- and red-light sensors in *Aspergillus nidulans*. *Curr Biol.* **18:** 255–259

Ramamoorthy, V., Dhingra, S., Kincaid, A., Shantappa, S., Feng, X., et al. (2013). The Putative C_2H_2 Transcription Factor MtfA Is a Novel Regulator of Secondary Metabolism and Morphogenesis in *Aspergillus nidulans*. *PLoS ONE* **8(9):** e74122.

Rank, C., Klejnstrup, M.L., Petersen, L.M., Kildgaard, S., Frisvad, J.C., Gotfredsen, C.H., Larsen, T.O. (2012). Comparative chemistry of *Aspergillus oryzae* (RIB40) and *A. flavus* (NRRL 3357). *Metabolites* **2:** 39-56.

Reyes-Dominguez, Y., Bok, J.W., Berger, H., Shwab, E.K., Basheer, A., Gallmetzer, A., Scazzocchio, C., Keller, N.P., Strauss, J. (2010). Heterochromatic marks are associated with the repression of secondary metabolism clusters in *Aspergillus nidulans*. *Mol Microbiol* **76:** 1376-86.

Ries, L.N.A., Rocha, M.C., de Castro, P.A., Silva-Rocha, R., Silva, R.N., Freitas, F.Z., de Assis, L.J., Bertolini, M.C., Malavazi, I., Goldman, G.H. (2017). The *Aspergillus fumigatus* CrzA transcription factor activates chitin synthase gene expression during the caspofungin paradoxical effect. *mBio* **8(3)**: e00705-17.

Riley, R. T., Goeger, D. E., Yoo, H., and Showker, J. L. (1992). Comparison of three tetramic acids and their ability to alter membrane functionin cultured skeletal muscle cells and sarcoplasmic reticulum vesicles. *Toxicol. Appl. Pharmacol.* **114**: 261–267.

Riquelme, M. (2013). Tip growth in flamentous fungi: a road trip to the apex. *Annu Rev Microbiol* **67**: 587–609.

Robinson, P. J., Fairall, L., Huynh, V. A., Rhodes, D. (2006). EM measurements define the dimensions of the "30-nm" chromatin fiber: evidence for a compact, interdigitated structure. *Proceedings of the National Academy of Sciences of the United States of America,* **103:** 6506-11.

Rodríguez-Romero, J., Hedtke, M., Kastner, C., Müller, S., Fischer, R. (2010). Fungi, hidden in soil or up in the air: light makes a difference. *Annu Rev Microbiol.* **64**: 585–610.

Ropars, J., Lopez-Villavicencio, M., Snirc, A., Lacoste, S., Giraud, T. (2017). Blue cheese-making has shaped the population genetic structure of the mould *Penicillium roqueforti*. *PLoS ONE* **12(3):** e0171387.

Rossetto, D., Avvakumov, N., Côté, J. (2012). Histone phosphorylation: a chromatin modification involved in diverse nuclear events. *Epigenetics.* **7**: 1098–108.

Roze, L.V., Arthur, A.E., Hong, S.Y., Chanda, A., Linz, J.E. (2007). The initiation and pattern of spread of histone H4 acetylation parallel the order of transcriptional activation of genes in the aflatoxin cluster. *Mol Microbiol.* **66(3):** 713-26.

Saksouk, N., Simboeck, E., Déjardin, J. (2015). Constitutive heterochromatin formation and transcription in mammals. *Epigenetics & Chromatin* **8(3):** 1-17.

Sarikaya-Bayram, Ö., Bayram, Ö., Valerius, O., Park, H.S., Irniger, S., Gerke, J., Ni, M., Han, K.H., Yu, J.H., Braus, G.H. (2010). LaeA control of velvet family regulatory proteins for light-dependent development and fungal cell-type specificity. *PLoS Genet.* **6(12):** 1-17.

Sarikaya-Bayram, Ö., Palmer, J.M., Keller, N.P., Braus, G.H., Bayram, Ö. (2015). One Juliet and four Romeos: VeA and its methyltransferases. *Front Microbiol.* **6(1).**

Satterlee, T., Cary, J.W., Calvo, A.M. (2016). RmtA, a Putative Arginine Methyltransferase, Regulates Secondary Metabolism and Development in *Aspergillus flavus*. *PLoS ONE* **11(5)**: e0155575.

Schroeckh, V., Scherlach, K., Nutzmann, H.W., Shelest, E., Schmidt-Heck, W., Schuemann, J., Martin, K., Hertweck, C., Brakhage, A.A. (2009). Intimate bacterial-fungal interaction triggers biosynthesis of archetypal polyketides in *Aspergillus nidulans*. *Proc Natl Acad Sci U S A* **106:** 14558-63.

Selker, E.U., Tountas, N.A., Cross, S.H., Margolin, B.S., Murphy, J.G., Bird, A.P., Freitag, M. (2003). The methylated component of the *Neurospora crassa* genome. *Nature,* **422:** 893-7.

Sen, D., Keung, A.J., (2018). Designing Epigenome Editors: Considerations of Biochemical and Locus Specificities. *Methods Mol Biol.* **1767**: 65–87.

Sewall, T.C., Mims, C.W., Timberlake, W.E. (1990). abaA controls phialide differentiation in *Aspergillus nidulans. Plant Cell* **2**: 731-739.

Shahbazian, M.D., Grunstein, M. (2007). Functions of site-specific histone acetylation and deacetylation. *Annu. Rev. Biochem.* **76**: 75–100.

Shi, Y., Lan, F., Matson, C., Mulligan, P., Whetstine, J.R., Cole, P.A., Casero, R.A., Shi, Y. (2004). Histone Demethylation Mediated by the Nuclear Amine Oxidase Homolog LSD1. *Cell*,**119**: 941–953.

Shiio, Y., Eisenman, R.N. (2003). Histone sumoylation is associated with transcriptional repression. *Proc Natl Acad Sci U S A,* **100:**13225-30.

Shinohara, Y., Kawatani, M., Futamura, Y., Osada, H., Koyama, Y. (2016). An overproduction of astellolides induced by genetic disruption of chromatin-remodeling factors in *Aspergillus oryzae*. *J Antibiot*. **69(1)**: 4–8.

Shore, P., Sharrocks, A.D. (1995). The MADS-Box Family of Transcription Factors. *Eur. J. Biochem.* **229:** 1-13.

Shwab, E. K., Bok, J.W., Tribus, M., Galehr, J., Graessle, S., Keller, N.P. (2007). Histone deacetylase activity regulates chemical diversity in Aspergillus. *Eukaryot Cell* **6:** 1656-64.

Smith, M., March, J. (2001). March's advanced organic chemistry: reactions, mechanisms, and structure, New York, John Wiley & Sons.

Smith, Z.D., Meissner, A. (2013). DNA methylation: roles in mammalian development. *Nature reviews. Genetics* **14:** 204-20.

Sperling, S. (2007). Transcriptional regulation at a glance. *BMC Bioinformatics* **8**: 1–6.

Sohn, K.T., Yoon, K.S. (2002). Ultrastructural Study on the Cleistothecium Development in *Aspergillus nidulans*. *Mycobiology* **30:** 117-127.

Stinnett, S.M., Espeso, E.A., Cobeno, L., Araujo-Bazan, L., Calvo, A.M. (2007). *Aspergillus nidulans* VeA subcellular localization is dependent on the importin alpha carrier and on light. *Mol Microbiol* **63**: 242–255.

Strauss, J., Reyes-Dominguez, Y. (2010). Regulation of secondary metabolism by chromatin structure and epigenetic codes. *Fungal Genet Biol* **48** 62-9.

Struck, A.W., Thompson, M.L., Wong, L.S., Micklefield, J. (2012). S-adenosylmethionine-dependent methyltransferases: highly versatile enzymes in biocatalysis, biosynthesis and other biotechnological applications. *Chembiochem: a European journal of chemical biology* **13:** 2642-55.

Strahl, B.D., Grant, P.A., Briggs, S.D., Sun, Z.W., Bone, J.R., Caldwell, J.A., Mollah, S., Cook, R.G., Shabanowitz, J., Hunt, D.F., Allis, C.D. (2002). Set2 is a nucleosomal histone H3-selective methyltransferase that mediates transcriptional repression. *Mol Cell Biol* **22:** 1298-306.

Struhl, K., Segal, E. (2013). Determinants of nucleosome positioning. *Nature structural & molecular biology* **20:** 267-73.

Szewczyk, E., Chiang, Y.M., Oakley, C.E., Davidson, A.D., Wang, C.C.C., Oakley, B.R. (2008). Identification and Characterization of the Asperthecin Gene Cluster of *Aspergillus nidulans*. *Appl Environ Microb*. **74**: 7607–7612.

Takeshita, N., Manck, R., Grun, N., de Vega, S.H., Fischer, R. (2014). Inter- dependence of the actin and the microtubule cytoskeleton during fungal growth. *Curr Opin Microbiol* **20C**: 34–41.

TePaske, M.R., Gloer, J.B., Wicklow, D.T., Dowd, P.F. (1992). Aflavarin and beta-aflatrem: new anti-insectan metabolites from the sclerotia of *Aspergillus flavus*. *J. Nat. Prod.* **55**: 1080–1086.

Todd, R.B., Davis, M.A., Hynes, M.J. (2007). Genetic manipulation of *Aspergillus nidulans*: meiotic progeny for genetic analysis and strain construction. *Nature Protocols* **2 (4)**: 811-821.

Cruz-Topete, D., Cidlowski, J. A. (2014). One Hormone, Two Actions: Anti- and Pro-Inflammatory Effects of Glucocorticoids. *Neuroimmunomodulation* **22**: 20–32.

Tuncher, A., Reinke, H., Martic, G., Caruso, M. L., Brakhage, A.A. (2004). A basicregion helix-loop-helix protein-encoding gene (*devR*) involved in the development of *Aspergillus nidulans*. *Mol Microbiol* **52:** 227-41.

Vadlapudi, V., Borah, N., Yellusani, K.R., Gade, S., Reddy, P., Rajamanikyam, M., Vempati, L.N.S., Gubbala, S.P., Chopra, P., Upadhyayula, S.M., Amanchy, R. (2017). *Aspergillus* Secondary Metabolite Database, a resource to understand the secondary metabolome of *Aspergillus* genus. *Sci Rep.* **7(1):** 7325.

Vandenberghe, L.P.S., Soccol, C.R., Pandey, A., Lebeault, J.M. (2000). Solid-state fermentation for the synthesis of citric acid by *Aspergillus niger*. *Bioresource Technology* **74:** 175-178.

Vienken, K., Fischer, R. (2006). The Zn(II)2Cys6 putative transcription factor NosA controls fruiting body formation in *Aspergillus nidulans*. *Mol Microbiol* **61:** 544-54.

Vilar, J. M. G., Guet, L. C., Leibler, S. (2003). Modeling network dynamics: the lac operon, a case study. *The Journal of Cell Biology*, **161(3):** 471-476.

Whetstine, J.R., Nottke, A., Lan, F., Huarte, M., Smolikov, S., Chen, Z., Spooner, E., Li, E., Zhang, G., Colaiacovo, M., et al. (2006). Reversal of histone lysine trimethylation by the JMJD2 family of histone demethylases. *Cell* **125:** 467-481.

Wieser, J., Adams, T.H. (1995). *flbD* encodes a Myb-like DNA-binding protein that coordinates initiation of *Aspergillus nidulans* conidiophore development. *Genes Dev* **9:** 491-502.

Wieser, J., Lee, B.N., Fondon, J., 3rd and Adams, T.H. (1994). Genetic requirements for initiating asexual development in *Aspergillus nidulans*. *Curr Genet* **27:** 62-9.

Wicklow, D. T., and Cole, R. J. (1982).Tremoragenic indole metabolites and aflatoxins in sclerotia of *Aspergillusflavus* link: an evolutionary perspective. *Can. J. Bot.* **60**, 525–528.

Wicklow, D.T., and Shotwell, O.L. (1983). Intrafungal distribution of aflatoxins among conidia and sclerotia of *Aspergillus flavus* and *Aspergillus parasiticus*. *Can. J. Microbiol.* **29**: 1–5.

Williams, J.H., Phillips, T.D., Jolly, P.E., Stiles, J.K., Jolly, C.M., Aggarwal, D., (2004). Human aflatoxicosis in developing countries: a review of toxicology, exposure, potential health consequences, and interventions. *Am. J. Clin. Nutr.* **80**: 1106– 1122.

Woloshuk C.P., Foutz K.R., Brewer J.F., Bhatnagar D., Cleveland T.E., et al. (1994). Molecular characterization of *aflR*, a regulatory locus for aflatoxin biosynthesis. *Appl. Environ. Microbiol.* **60**: 2408–14.

Wong K. H., Jin Y., Moqtaderi Z., (2013). Multiplex Illumina sequencing using DNA barcoding. *Current Protocols in Molecular Biology*. Chapter 7: Unit 7.11.

Wu, J., Miller, B. L. (1997). Aspergillus asexual reproduction and sexual reproduction are differentially affected by transcriptional and translational mechanisms regulating stunted gene expression. *Mol Cell Biol* **17:** 6191-201.

Wu, M.Y., Mead, M.E., Kim, S.C., Rokas, A., Yu, J.H. (2017). WetA bridges cellular and chemical development in *Aspergillus flavus*. *PLoS ONE* **12 (6)**: e0179571.

Xie, J. L., Qin, L., Miao, Z., Grys, B. T., Diaz, J. C., Ting, K., *et al.* (2017). The *Candida albicans* transcription factor Cas5 couples stress responses, drug resistance and cell cycle regulation. *Nat. Commun.* **8(1):** 499.

Yang, Y., Bedford, M.T. (2013). Protein arginine methyltransferases and cancer. *Nat Rev Cancer* **13:** 37-50.

Yang, H., Tong, J., Lee, C.W., Ha, S., Eom, S.H., Im, Y.J. (2014). Structural mechanism of ergosterol regulation by fungal sterol transcription factor Upc2. *Nat. Commun.* **6:** 6129.

Yao, G., Zhang, F., Nie, X., Wang, X., Yuan, J., Zhuang, Z. and Wang, S. (2017). Essential APSES Transcription Factors for Mycotoxin Synthesis, Fungal Development, and Pathogenicity in *Aspergillus flavus*. *Front. Microbiol.* **8**: 2277.

Yin, W., Keller, N.P. (2011). Transcriptional Regulatory Elements in Fungal Secondary Methabolism. The Journal of Microbiology **49(3):** 329-339.

Yoshikawa, K., Tanaka, T., Ida, Y., Furusawa, C., Hirasawa, T., Shimizu, H. (2011). Comprehensive phenotypic analysis of single-gene deletion and overexpression strains of *Saccharomyces cerevisiae. Yeast* **28:** 349–361.

Yu, J.H., Keller, N.P. (2005). Regulation of secondary metabolism in filamentous fungi. *Annu Rev Phytopathol* **43:** 437–458.

Yun, S.H., Arie, T., Kaneko, I., Yoder, O.C., Turgeon, B.G. (2000). Molecular organization of mating type loci in heterothallic, homothallic, and asexual. *Fungal Genet Biol* **31:** 7-20.

Zeng, H., Hatabayashi, H., Nakagawa, H., Cai, J., Suzuki, R., Sakuno, E., et al. (2011). Conversion of 11-hydroxy-O-methyl sterigmatocystin to aflatoxin G1 in *Aspergillus parasiticus*. *Appl. Microbiol. Biotechnol.* **90**: 635–650.

Zhang, S. Monahan, B. J., Tkacz, J S., Scott, B., (2004). Indole-diterpene gene cluster from *Aspergillus flavus*. *Appl. Environ. Microbiol.* **70**: 6875–6883.

Zhang Y., Ge F., Hou F., Sun W., Zheng Q., Zhang X., et al. (2017). Transcription factors responding to Pb stress in maize. *Genes* **8(9)**: 231.

Supplemented Materials

Fungal media and Reagents

50x *Aspergillus* Salt Solution

$NaNO_3$ (300 g), KCl (26g), KH_2PO_4 (76 g) were dissolved in 1 L distilled water (dH_2O). The solution pH was adjusted to pH 5.5 with addition of 5M KOH, and was autoclaved at 121 °C for 20 min. The solution was stored at room temperature (RT).

1000x *Aspergillus* Trace Elemets

$FeSO_4.7H_2O$ (1.0 g), and EDTA (10.0 g) were dissolved in 80 ml of dH_2O in the order indicated and then pH was adjusted to around 5,5 with addition of KOH pellets until obtain a golden yellow solution (solution 1). $ZnSO_4$. $7H_2O$ (4.4 g), H_3BO_3 (2.2 g), $MnCl_2.4H_2O$ (1.0 g), $CoCl_2.6H_2O$ (0.32 g), $CuSO_4.5H_2O$ (0.32 g), $(NH_4)6Mo_7O_{24}.4H_2O$ (0.22 g) were dissolved in 80 ml of dH_2O in the order indicated (solution 2). Solution 1 and solution 2 were combined and pH was re-adjusted to pH 6.5 using KOH pellets and then KOH solutions of decreasing concentration. Final volume was brought to 200 ml with dH_2O. The solution was filter sterilised and was stored at 4-8 °C.

1M $MgSO_4$

120.36 g/mol $MgSO_4$ was dissolved in 1 L dH_2O and autoclaved at 121 °C for 20 min. The solution was stored at RT.

50% Glucose

250 g glucose was dissolved in 500 ml dH_2O. The solution was autoclaved at 121 °C for 20 min and was stored at RT.

Glucose Minimal Media (GMM)

50x *Aspergillus* Salt Solution (16 ml), 50% Glucose (16 ml) and 1M $MgSO_4$ (1.6 ml) were added to 800 ml dH_2O. The solution was autoclaved at 121°C for 20 min and was cooled around~50°C. 1000x Trace Elements (800 µl) and supplementary material that was needed for strains (uridine, prydx) were added to the solution. The media was stored at 4°C.

Glucose Minimal Media Agar

50x *Aspergillus* Salt Solution (16 ml), 50% Glucose (16 ml), 1M $MgSO_4$ (1,6 ml) and agar (16g) were added to 800 ml dH_2O. The solution was autoclaved at 121°C for 20 min and was cooled around~ 50°C. 1000x Trace Elements (800 µl) and supplementary material that was needed for strains (uridine, prydx) were added to the solution. The media was poured into 90 mm sterile petri dishes. Plates were allowed to set and were stored at 4 °C.

Complete Media:

Yeast extract (1 g), peptone (2 g), tryptone (1 g), 50x *Aspergillus* Salt Solution (20 ml), 50% Glucose (20 ml), 1M $MgSO_4$ (2 ml) and agar (20 g) were added to 1L dH_2O. The solution was autoclaved at 121°C for 20 min and was cooled around~50°C. 1000x Trace Elements (1000 µl) and supplementary material that was needed for strains (uridine, prydx) were added to the solution. The media was poured into 90 mm sterile petri dishes. Plates were allowed to set and were stored at 4 °C.

Yeast Extract Sucrose (YES) Medium:

Yeast Extract (16 g), sucrose (120 g), $MgSO_4.7H_2O$ (800 mg) and agar (16 g) were added to 800 ml dH_2O then autoclaved at 121°C for 20 min. After cooling around~ 50°C media was poured into 90 mm sterile petri dishes. Plates were allowed to set and were stored at 4 °C.

Wickerham Medium (WKM):

Yeast Extract (2 g), peptone (3 g), corn steep solids (5 g), dextrose (2 g), sucrose (30 g), $NaNO_3$ (2 g), $K_2HPO_4.3H_2O$ (1 g), $MgSO_4.7H_2O$ (0.5 g), KCl (0.2 g), $FeSO_4.7H_2O$ (0.1 g), and agar (15 g) were added to 1 L dH_2O. The solution was autoclaved at 121°C for 20 min and was cooled around~50°C. Supplementary material that was needed for strains (uridine, prydx) were added to the media and stored at 4°C.

Yeast Glucose Trace (YGT) Medium:

0.5 % Yeast Extract (w/v) (4 g), 2 % glucose (16 g), and agar (16 g) were added to 800 ml dH_2O. The solution was autoclaved at 121°C for 20 min and was cooled around~50°C. 1000x Trace Elements (800 µl) and supplementary material that was needed for strains (uridine, prydx) were added to the solution. The media was stored at 4°C.

Uridine 5% (0.25g/l):

To prepare 5% Uridine solution, 5 g of Uridine was dissolved in 100 ml double distilled water (ddH2O). The solution was stored at 4°C.

Uracil (1g/l):

1 g Uracil dissolved in related media before autoclaved.

Pyridoxine 0.1% (1mg/l):

To prepare 0.1% Pyridoxine solution, 1g of Pyridoxine-HCL was dissolved in 1000 ml of ddH2O. The solution was stored at 4°C.

GMM Oatmeal Media:

To prepare GMM Oatmeal media, 10 g of grinded Oatmeal was added to 1 L of GMM agar before autoclaved.

Bacterial media

Luria-Bertani Broth (LB)

Luria Bertani Broth (25 g) (SIGMA) was dissolved in 1 L dH_2O. The liquid media was autoclaved at 121°C for 20 min. After cooling, 1 ml Ampicillin was added and was stored at 4 °C.

Luria-Bertani Agar (LB Agar)

Luria-Bertani Broth with Agar (35g) was dissolved in 1L dH_2O and autoclaved at 121 °C for 20 min. After cooling around ~50°C 1ml Ampicillin was added to media then media was poured into 90 mm sterile petri dishes. Plates were allowed to set and were stored at 4 °C.

Antibiotics

Ampicillin (100µg/ml)

1 g Ampicillin was dissolved in 10 ml ddH_2O and filter sterilized. The solution was stored at -20 °C.

Pyrithiamine (1ml/L)

1 g pyrithiamine hydrobromide (Sigma) was dissolved in 10 ml ddH2O and filter sterilized. The solution was stored at -20 °C.

Nourseothricin (600µl/L)

1 g Nourseothricin (Jena bioscience) was dissolved in 10 ml ddH2O and then filter sterilized. The solution was stored at -20 °C.

Agarose Gel Electrophoresis Reagents

2% Agarose gel:

4.0 g of Ultra pure™ Agarose (Invitrogen) was dissolved in 1x TAE electrophoresis buffer (200 ml) using microwaves for 2 min and then 8 µl of a SYBR®Safe(Invitrogen) DNA gel stain (10.000x concentrate in DMSO) was added. After cooling step, the solution was poured into a casting rig.

50x TAE Buffer:

242 g of Tris-Base and 18.6 g of EDTA were dissolved in 800 ml ddH_2O then 57.1 ml Glacial acetic acid added to the solution. The final volume was brought up to 1 L with ddH_2O and autoclaved at 121°C for 20 min.

Southern Blot Hybridization Reagents

1.5 M Sodium Hydroxide (NaOH):

40 g of Sodium Hydroxide was dissolved in 2 L dH_2O then autoclaved at 121°C for 20 mins. The solution was stored at RT.

0.25 M Hydrochloric Acid (HCl):

15.2 ml of Hydrochloric acid was slowly added to 2 L dH_2O then autoclaved at 121°C for 20 mins. The solution was stored at RT.

0.5 M Sodium Chloride (NaCl):

175.32 g of Sodium chloride was dissolved in 2 L dH_2O then autoclaved at 121°C for 20 mins. The solution was stored at RT.

20x SSC (Saline Sodium Citrate) Buffer:

350 g of Sodium Chloride and 176 g of Na-Citrate were dissolved in 1800 ml dH_2O then the pH of the solution was adjusted to 7 by using 5 M HCl. The final volume was brought up to 2 L with dH_2O and autoclaved at 121°C for 20 min. The solution was stored at RT.

Prehybridization Buffer:

20x SSC (75 ml), 10% Block Solution (60 ml), 10% SDS (3 ml), ddH_2O (6 ml) and Pure Formamide (150 ml) were mixed and dissolved at 68 °C. The solution was stored at -20 °C.

10x DIG Buffer1:

88 g of Sodium Chloride and 116 g of Maleic Acid were dissolved in 1 L dH_2O then the pH of the solution was adjusted to 7.5 using NaOH. The solution was autoclaved at 121°C for 20 mins and stored at RT.

DIG Buffer3:

6.05 g of 100 mM Tris-Base, 2.29 g of 100 mM NaCl and 5.08 g of 50 mM Magnesium Chloride ($MgCl_2$) were dissolved in 500 ml dH_2O then the pH of the solution was adjusted to 9.5 with HCl. The solution was autoclaved at 121°C for 20 mins and stored at RT.

SDS-PAGE Electrophoresis and Western Blot Reagents

10x TBS (Tris-Buffered Saline):

24 g of Tris base and 88 g of NaCl were dissolved in 900 ml of dH_2O then the pH was adjusted to 7.6 using 12 N HCl. The final volume was adjusted to 1 L with dH_2O. The solution was autoclaved and stored at RT.

5% Milk Solution:

5 g dried skimmed milk was dissolved in 100 ml 1x TBS. The solution was prepared fresh on day of use.

TBST (Tris-Buffer Saline and 0.1% Tween-20):

100 ml of 10x TBS and 1 ml of Tween-20 were added to 900 ml of dH_2O for 1 L solution. The solution was autoclaved and stored at RT.

1M Trizma-hydrochloride (Tris-HCl) pH 7.5:

157.6 g Tris-HCl was dissolved in 500 ml dH_2O and the pH was adjusted to 7.5 by using 1M NaOH. Final volume of the solution was adjusted to 1 L and stored at RT.

1mM EDTA:

Ethylenediaminetetraacetic acid dipotassium salt dehydrate (4.0445 mg) was added to 8 ml of dH_2O. The pH was adjusted to 8.0 in order to dissolve the salt. The solution was stored at -20°C.

Protease inhibitor mix (Roche):

Two Roche tablets were dissolved in 1 ml dH_2O. The solution was stored at -20°C.

100 mM PMSF:

1 g of Phenylmethylsulfonyl fluoride was dissolved in 60 ml ethanol (100%). The solution was stored at 4°C.

Protein extraction buffer (B300 buffer):

The 300 mM NaCl (17,53 g), 1 M pH: 7.5 Tris-HCl (50 ml), 10% Glycerol (10 ml), 1 mM EDTA (2 ml) and 0.1% NP-40 (1 ml) were dissolved in 1 L dH_2O. The solution was autoclaved and stored at 4°C. Immediately prior to use, the 1 M DTT (15µl), Protease inhibitor mix (Roche) (100 µl), 0.5 mM Benzamidine (30 µl), 1x Phosphatase inhibitors mix (4-(2-Aminoethyl benzenesulfony Fluoride Hydrochloride"CAS30827-99-7" ROCHE) (100 µl) and 100 mM PMSF (100 µl) were added to the solution.

10% (w/v) Sodium Dodecyl Sulfate (SDS):

SDS (10 g) was dissolved in 100 ml dH_2O and the solution was stored at RT.

0.5 M Tris-HCl pH 6.8:

Trizma hydrochloride (7.8 g) was dissolved in 80 ml dH_2O then pH was adjusted to 6.8 using 4 M NaOH. Final volume of the solution was adjusted to 100 ml with dH_2O and stored at RT.

10% (w/v) Ammonium Persulfate (APS):

Ammonium persulfate (100 mg) was dissolved in 1 ml dH_2O. The solution was stored at -20°C.

Chromatin Immunoprecipitation (ChIP) Reagents

FA Lysis Buffer1 (0.1% SDS and 150 mM NaCl):

1 M HEPES-KOH (50 ml, pH 7.5), 5 M NaCl (30 ml), 1 mM EDTA (2 ml pH 8.0), Triton X-100 (10 ml), 5% Sodium deoxycholate (20 ml) and 10% SDS (10 ml) were mixed then final volume of the solution was adjusted to 1 L with ddH_2O. The solution was stored at RT.

FA Lysis Buffer2 (0.1% SDS and 500 mM NaCl):

1 M HEPES-KOH (50 ml, pH 7.5), 5 M NaCl (100 ml), 1 mM EDTA (2 ml pH 8.0), Triton X-100 (10 ml), 5% Sodium deoxycholate (20 ml) and 10% SDS (10 ml) were mixed then final volume of the solution was adjusted to 1 L with ddH_2O. The solution was stored at RT.

ChIP Elution Buffer (2x Pronase Buffer):

1 M Tris-HCl (50 ml pH 7.5), 0.5 M EDTA (20 ml) and 20% SDS (50 ml) were mixed with 880 ml ddH_2O. (Total volume 1 L). The solution was stored at RT.

Tris-Buffered Saline (TBS):

1 M Tris-HCl (20 ml, pH 7.5) and 5 M NaCl (30 ml) were dissolved in 900 ml of ddH_2O. Final volume of the solution was adjusted to 1 L with ddH_2O. The solution was stored at RT.

100 mM PMSF:

1 g of Phenylmethylsulfonyl fluoride was dissolved in 60 ml ethanol (100%). The solution was stored at -20°C.

Pronase:

20 mg Pronase was dissolved in 20 ml TBS. The solution was stored at -20°C.

2.5 M Glycine:

187.68 g Glycine was dissolved in 1 L ddH_2O. The solution was heated to dissolve the glycine and autoclaved. The solution was stored at RT.

Wash Buffer:

2 M Tris-HCl (5 ml, pH 8.0), 4 M LiCl (62.5 ml), 0.5 M EDTA (2 ml), Igepal CA-630 (5 ml) and 5% Sodium deoxycholate (100 ml) were dissolved in 825.5 ml ddH_2O. The solution was stored at RT.

Tris-EDTA (TE) Buffer:

2 M Tris-HCl (5 ml, pH 8.0) and 0.5 M EDTA (2 ml) were dissolved in 993 ml ddH_2O. The solution was stored at RT.

Table S1: KdmA affinity purification-coupled MS results for TAP, GFP and HA tagged strains in *A.nidulans*.

Accession	Score	Coverage	# Proteins	# Unique Peptides	# Peptides	# PSMs	# AAs	MW [kDa]	calc. pI	
KdmA	346.52	58.22	1	58	58	98	1405	156.8	7.42	
RstB	134.60	37.95	1	24	24	42	801	89.7	7.20	
EcmB	115.88	42.24	1	18	18	33	625	68.9	6.42	KdmA-TAP
CclA	105.30	50.58	1	20	20	32	607	65.3	5.47	
McmA	5.06	4.91	1	1	1	2	224	24.7	5.66	
KdmA	82.20	41.49	1	43	43	55	1405	156.8	7.42	
RstB	54.29	30.34	1	18	18	24	801	89.7	7.20	
EcmB	47.94	29.12	1	13	13	19	625	68.9	6.42	KdmA-GFP
CclA	33.16	41.68	1	18	18	21	607	65.3	5.47	
AN8676	0.00	4.91	1	1	1	2	224	24.7	5.66	
AN1060	256.51	54.23	1	58	58	103	1405	156.8	7.42	
RstB	124.48	43.57	1	27	27	51	801	89.7	7.20	
CclA	115.70	61.94	1	26	26	40	607	65.3	5.47	KdmA-HA
EcmB	94.03	34.72	1	17	17	30	625	68.9	6.42	
McmA	5.27	4.91	1	1	1	2	224	24.7	5.66	

Table S2: CclA affinity purification-coupled MS results for TAP, GFP and HA tagged strains in *A.nidulans*.

Accession	Score	Coverage	# Proteins	# Unique Peptides	# Peptides	# PSMs	# AAs	MW [kDa]	calc. pI	
KdmA	310.96	62.85	1	65	65	103	1405	156.8	7.42	
CclA	135.57	60.63	1	27	27	46	607	65.3	5.47	
RstB	104.04	35.96	1	25	25	36	801	89.7	7.20	CclA-TAP
EcmB	59.21	33.12	1	14	14	21	625	68.9	6.42	
McmA	4.80	4.91	1	1	1	2	224	24.7	5.66	
KdmA	127.15	34.45	1	40	40	55	1405	156.8	7.42	
CclA	47.12	35.42	1	15	15	18	607	65.3	5.47	
RstB	26.41	13.98	1	9	9	12	801	89.7	7.20	CclA-GFP
EcmB	18.76	15.04	1	7	7	8	625	68.9	6.42	
McmA	4.29	4.91	1	1	1	2	224	24.7	5.66	
KdmA	300.66	61.35	1	65	65	108	1405	156.8	7.42	
CclA	167.34	61.78	1	28	28	57	607	65.3	5.47	
RstB	97.58	44.69	1	26	26	33	801	89.7	7.20	CclA-HA
EcmB	60.69	34.24	1	13	13	19	625	68.9	6.42	
McmA	6.91	8.93	1	2	2	4	224	24.7	5.66	

Table S3: EcmB affinity purification-coupled MS results for TAP, GFP and HA tagged strains in *A.nidulans*.

Accession	Score	Coverage	# Proteins	# Unique Peptides	# Peptides	# PSMs	# AAs	MW [kDa]	calc. pI	
KdmA	283.62	52.46	1	58	58	93	1405	156.8	7.42	
EcmB	221.28	43.84	1	21	21	70	625	68.9	6.42	
RstB	170.61	42.57	1	25	25	53	801	89.7	7.20	EcmB-TAP
CclA	96.95	51.40	1	22	22	33	607	65.3	5.47	
McmA	4.39	4.91	1	1	1	2	224	24.7	5.66	
EcmB	69.92	42.08	1	21	21	37	625	68.9	6.42	
KdmA	59.01	34.52	1	33	33	42	1405	156.8	7.42	
RstB	41.25	24.47	1	16	16	22	801	89.7	7.20	EcmB-GFP
CclA	20.73	24.05	1	9	9	10	607	65.3	5.47	
McmA	1.90	4.91	1	1	1	2	224	24.7	5.66	
KdmA	165.34	50.39	1	51	51	71	1405	156.8	7.42	
EcmB	162.84	39.20	1	21	21	57	625	68.9	6.42	
RstB	70.23	31.09	1	20	20	26	801	89.7	7.20	EcmB-HA
CclA	60.07	44.98	1	17	17	21	607	65.3	5.47	
McmA	4.85	4.91	1	1	1	2	224	24.7	5.66	

Table S4: RstB affinity purification-coupled MS results for TAP, GFP and HA tagged strains in *A.nidulans*.

Accession	Score	Coverage	# Proteins	# Unique Peptides	# Peptides	# PSMs	# AAs	MW [kDa]	calc. pI	
KdmA	199.94	52.88	1	52	52	71	1405	156.8	7.42	
RstB	135.78	45.32	1	26	26	48	801	89.7	7.20	
CclA	81.29	52.88	1	21	21	30	607	65.3	5.47	RstB-TAP
EcmB	59.88	32.00	1	14	14	19	625	68.9	6.42	
McmA	4.44	4.91	1	1	1	2	224	24.7	5.66	
KdmA	132.12	41.92	1	45	45	68	1405	156.8	7.42	
RstB	71.99	30.46	1	21	21	29	801	89.7	7.20	
EcmB	38.11	27.68	1	11	11	15	625	68.9	6.42	RstB-GFP
CclA	25.22	31.63	1	13	13	16	607	65.3	5.47	
McmA	3.94	4.91	1	1	1	2	224	24.7	5.66	
KdmA	246.10	52.38	1	58	58	86	1405	156.8	7.42	
RstB	161.48	49.56	1	31	31	58	801	89.7	7.20	
EcmB	96.12	32.32	1	14	14	29	625	68.9	6.42	RstB-HA
CclA	91.58	59.14	1	26	26	36	607	65.3	5.47	
McmA	4.83	4.91	1	1	1	2	224	24.7	5.66	

Table S5: McmA affinity purification-coupled MS results for TAP, GFP and MYC tagged strains in *A.nidulans*.

Accession	Score	Coverage	# Proteins	# Unique Peptides	# Peptides	# PSMs	# AAs	MW [kDa]	calc. pI	
KdmA	163.62	43.84	1	45	45	59	1405	156.8	7.42	
CclA	73.56	51.24	1	21	21	28	607	65.3	5.47	
RstB	55.55	32.33	1	23	23	29	801	89.7	7.20	McmA-TAP
EcmB	42.73	26.08	1	12	12	14	625	68.9	6.42	
McmA	7.70	18.30	1	2	2	4	224	24.7	5.66	
KdmA	67.94	25.20	1	31	31	38	1405	156.8	7.42	
CclA	21.59	23.23	1	10	10	11	607	65.3	5.47	
RstB	18.39	15.11	1	10	10	10	801	89.7	7.20	McmA-GFP
EcmB	9.04	9.44	1	5	5	6	625	68.9	6.42	
McmA	5.00	4.91	1	1	1	4	224	24.7	5.66	
KdmA	282.17	50.75	1	54	54	70	1405	156.8	7.42	
CclA	133.05	51.73	1	22	22	33	607	65.3	5.47	
RstB	66.55	27.72	1	17	17	20	801	89.7	7.20	McmA-MYC
EcmB	32.46	19.52	1	9	9	9	625	68.9	6.42	
McmA	27.89	29.46	1	5	5	11	224	24.7	5.66	

Table S6: Stress chemicals were utilized in this study and their effects in the cell.

Substance	Action
CPT (Camptothecin)	binds to DNA-topoisomerase I complexes and disrupts DNA-processing
EMS (Ethyl methanesulfonate)	DNA-ethylating mutagenic substance
4-NQO (4-Nitroquinoline *N*-oxide)	causes base substitutions mainly on guanine
Hydroxyurea (HU)	inhibits ribonucleoside reductase, blocks synthesis of deoxynucleotids
CFW (Calcoflour White)	cell wall stress (binds to cellulose and chitin)
Congo red	cell wall stress (binds β-D glucans)
Benomyl	Microtubule destabilizing
Nocodazole	inhibits microtubule polymerisation
NaCl	osmotic stress
H_2O_2	oxidative stress